N° d'ordre : **2017LYSEC59**

THESE de DOCTORAT DE L'UNIVERSITE DE LYON

délivrée par **l'Ecole centrale de Lyon**

Spécialité : **Matériaux** de l'Ecole Doctorale **EDML N° 34**

Soutenu le 29 Novembre 2017 à Lyon par

Pushkar DESHPANDE

préparée au Laboratoire de Tribologie et Dynamique des Systèmes en collaboration avec TOTAL Marketing Services

---

Interaction of MoDTC additive on TiO_2 APS coating under mixed/boundary lubrication conditions: A tribocatalytic process

---

'Intéraction de l'additif MoDTC avec un revêtement APS de TiO_2 en condition de lubrification mixte/limite : un processus tribocatalytique'

Composition du jury :

Dr. Ali **ERDEMIR**	Argonne National Laboratory	Examinateur
Prof. Antonella **ROSSI**	Università di Cagliari & ETH Zurich	Rapporteur
D.R. Pierre **MONTMITONNET**	Cemef MINES Paristech	Rapporteur
Prof. Mitjan **KALIN**	University of Ljubljana	Examinateur
Prof. Fabrice **DASSENOY**	Ecole Centrale de Lyon	Directeur
MCF HDR Clotilde **MINFRAY**	Ecole Centrale de Lyon	Co-Encadrante
Mr. Benoit **THIEBAUT**	TOTAL Marketing Services	Invitée

Acknowledgement

This study was funded by the FP 7 MC-ITN program titled Engineering Tribochemistry of Internal Combustion Engines (ENTICE) [290077] and sponsored by TOTAL Marketing Services through CIFRE. It was carried out in Laboratory of Tribology and System Dynamics, Ecole Centrale de Lyon and Centre de Recherche de Solaize, Total Marketing Services, France.

I would like to thank Total Marketing Services as well as LTDS for giving me this wonderful opportunity to work in the European project ENTICE. Secondly, I would like to thank my supervisors from the lab Clotilde and Fabrice as well as those from Total, Benoit and Frederic for their guidance throughout the duration of this thesis. I would also like to thank all the ENTICE fellows as well as the supervisors from various companies and universities for the fruitful discussions we had during ENTICE meetings.

I appreciate the help provided by Thierry Le Mogne for XPS analysis and Istvan Jenei as well as Beatrice Vacher for the TEM analysis. I would also like to thank the technicians from Total for their help to use all the tribometers in the tribology laboratory of CReS. I would also like to acknowledge the support given by all my colleagues and other fellow PhD students from the lab.

I would like to thank University of Leeds for allowing the use of Raman Spectroscopy. The authors would also like to thank CLYM in INSA de Lyon for the use of JEOL TEM. The authors would like to thank Oerlikon Surface Solutions segment (Mr. Frederic Meunier and Peter Ernst) for providing the appropriate coatings for this project.

Résumé de la thèse

Le nombre croissant de véhicules dans le monde est une source de préoccupation majeure car ils sont responsables d'une grande partie de la pollution atmosphérique et acoustique. La plupart de ces véhicules utilisent des moteurs thermiques (« Internal Combustion Engine ») à l'origine d'émissions de gaz polluants tels que les NO_x et SO_x. De nos jours, les nouvelles tendances en matière de conception des moteurs ont pour objectif de réduire leur poids, de permettre une faible consommation en carburant, une réduction des émissions polluantes ainsi qu'une durée de vie accrue des pièces mécaniques. Après avoir analysé les phénomènes à l'origine de la consommation énergétique des véhicules particuliers, Holmberg *et al.* [1] ont conclu que :

(a) un tiers de l'énergie (carburant) est utilisé pour vaincre les forces de frottement dans le moteur. Ainsi, les pertes par frottement représentent 28% de l'énergie totale consommée.

(b) la réduction des pertes par frottement entraînerait à termes une réduction globale de la consommation d'énergie car elle permettra de réduire par la même occasion les pertes d'échappement et de refroidissement.

(c) les nouveaux développements technologiques mis en place pour la réduction du frottement dans les voitures particulières pourraient réduire les frottements de 18% à court terme et de 61% à plus long terme [1].

Ces nouveaux développements ont conduit à l'utilisation de l'aluminium et de ses alliages comme composants du moteur, en lieu et place de l'acier et de la fonte, traditionnellement utilisés. Cependant, les surfaces en aluminium sont difficiles à protéger en raison de la corrosion et du comportement vis-à-vis de l'usure dans les contacts tribologiques. Des systèmes de protection sont utilisés comme des bagues, des structures poreuses ou des revêtements galvaniques. Pour augmenter l'efficacité et la longévité des composants du moteur, un procédé flexible de revêtement par pulvérisation thermique, à faible coût et facile à mettre en œuvre est actuellement utilisé sur les alliages de métaux légers comme l'aluminium mais aussi sur les aciers. Les principaux procédés de revêtement par projection thermique à usages commerciaux pour les composants du moteur sont la pulvérisation thermique par plasma d'arc soufflé sous pression atmosphérique (APS), le procédé de projection par flamme supersonique (HVOF) et les procédés à arc électrique. Une large gamme de matériaux peut être revêtue. Généralement, pour le contact segment - chemise d'un moteur, c'est le procédé APS qui est utilisé.

Ce travail de thèse nous a permis d'étudier le comportement tribologique de différents revêtements obtenus par pulvérisation thermique (APS) pour des contacts lubrifiés en régime limite. Plusieurs propriétés de ces revêtements comme la porosité, la rugosité, la microstructure, la dureté vont jouer un rôle important sur leurs comportements tribologiques. Par conséquent, ces paramètres ont été pris en compte et leurs effets sur le comportement tribologique ont été discutés. Les mécanismes à l'origine de la réponse tribologique ont également été étudiés et discutés.

L'objectif principal de ce travail a été d'étudier le comportement tribologique des revêtements APS en présence d'additif modificateur de frottement. Notre choix en termes d'additif modificateur de frottement s'est porté sur le MoDTC (Molybdenum Dialkyl - dithio Carbamate - MoDTC). Notre choix en termes de revêtement APS s'est porté sur : un acier, un acier contenant du Mo et un revêtement de TiO_2. L'influence de divers paramètres comme la rugosité, la concentration en MoDTC, la température, la pression de contact, la combinaison avec d'autres additifs et le changement du matériau antagoniste sur le comportement tribologique des revêtements APS a été étudiée.

La première partie de chapitre 1 présente les bases de la lubrification, les différents régimes de lubrification ainsi que les additifs couramment utilisés dans les lubrifiants automobiles. Leurs fonctions sont explicitées. Un focus particulier est fait sur un additif anti-usure très largement utilisé (le dithiophopshate de zinc - ZDDP) ainsi que sur un additif réducteur de frottement lui aussi très largement utilisé (le dithiocarbamate de molybdène - MoDTC).
Les divers contacts rencontrés dans les moteurs thermiques sont ensuite présentés et discutés avec un intérêt particulier pour le contact segment-chemise du moteur où les additifs de lubrification jouent un rôle important. Les matériaux classiquement utilisés pour les segments ainsi que les revêtements employés sur les chemises des cylindres sont ensuite présentés. Coté lubrifiant, il est à noter que la tendance actuelle est au lubrifiant à faible viscosité, ainsi qu'aux lubrifiants à faibles taux en cendres et présentant donc des teneurs en phosphore et soufre réduites, comme pour les lubrifiants « Low SAPS ». La nécessité d'optimiser l'action des additifs de lubrification pour les nouveaux matériaux utilisés sur les chemises des moteurs (typiquement les couches APS) est soulignée.

La deuxième partie passe en revue les différents processus thermiques utilisés lors de la fabrication des revêtements pour les chemises des moteurs ainsi que les différents types de matériaux utilisés. Le comportement tribologique en conditions lubrifiées de ces revêtements

est ensuite discuté au regard de la littérature sur le sujet. On peut conclure que les différents revêtements présentent un comportement tribologique intéressant dans des conditions lubrifiées en présence d'additifs tels que le ZDDP ou le MoDTC. Cependant, les propriétés du revêtement comme la nature chimique, la dureté, le module élastique, l'épaisseur, la rugosité de surface, la porosité, et l'adhérence du revêtement sur le substrat doivent être prise en compte. Ainsi, une mauvaise adhérence entre le revêtement et le substrat peut entrainer des fissures et de l'écaillage. Les contraintes résiduelles présentes dans les revêtements affectent également considérablement les propriétés de la couche. De plus, la plupart des revêtements obtenus par pulvérisation thermique présentent une forte rugosité de surface initiale entrainant souvent une usure élevée. La porosité de ces revêtements est aussi l'une de leur caractéristique. Dans certains cas, les pores sont bénéfiques pour la réduction de l'usure car ils agissent comme des réservoirs de lubrifiant favorisant ainsi la rétention du film fluide dans la zone de contact.

Il est à noter que certaines couches à base d'oxydes tels que le TiO_2 ou MoO_3 font apparaitre durant le frottement la formation d'oxydes non stœchiométriques appelés « phases Magneli » particulièrement résistantes à l'usure. Cela peut constituer un avantage lorsque les revêtements sont soumis à des conditions de sollicitations sévères car la formation de ces phases est favorisée à hautes température et pression.

En considérant les études menées sur l'interaction des additifs tels que le ZDDP et le MoDTC avec les revêtements obtenus par pulvérisation thermique, nous pouvons conclure que les phénomènes tribochimiques mis en jeu ne sont à ce jour que peu explicités dans la littérature. Il est par conséquent primordial d'étudier la tribochimie mise en jeu dans les contacts faisant intervenir les revêtements obtenus par pulvérisation thermique et les additifs à action tribologique les plus utilisés actuellement, à savoir le MoDTC et le ZDDP.

Ce travail porte donc sur l'étude de l'interaction entre le MoDTC et différents revêtements APS (à base d'acier et de TiO_2) ainsi que sur les performances tribologiques de ces revêtements en condition de lubrification limite en présence de MoDTC.

Dans le chapitre 2, les matériaux ainsi que les lubrifiants utilisés pour les essais tribologiques sont présentés. Le comportement tribologique de trois couches APS a été étudié en plus de celui d'un acier de référence. Les trois couches APS étudiées sont : un acier nommé « acier APS », un acier contenant 30%at de Mo nommé « acier Mo APS » et une couche à base de TiO_2 nommée « TiO_2 APS ». La bille est en acier 100Cr6. Concernant les lubrifiants, une huile

de base minérale groupe III a été utilisée avec ou sans MoDTC. Dans certains cas, un additif anti-usure a également été utilisé, le ZDDP.

Les différents tribomètres employés pour simuler le contact segment-chemise sont également présentés. Il s'agit :

- d'un tribomètre alternatif TE 77 dans une configuration spécifique « ring-on-liner » permettant d'utiliser de « vrais » chemises et segments ; l'idée étant de rester dans des conditions proches du contact segment-chemise réel.

- d'un tribomètre alternatif bille-plan, de manière à simplifier le contact tout en ayant des résultats d'usure quantifiables.

- du tribomètre Mini-Traction-Machine (MTM), afin d'étudier l'influence du taux de roulement-glissement sur la réponse tribologique.

Dans une seconde partie, les techniques de caractérisation utilisées avant et après frottement pour analyser la topographie des surfaces, leur composition chimique ainsi que leurs propriétés mécaniques sont présentées. Il s'agit des techniques de caractérisation telles que la microscopie optique, la microscopie électronique à balayage (MEB), la Microscopie Electronique en Transmission (MET), la Spectroscopie des Photoélectrons (XPS) et la spectroscopie Raman. L'interférométrie a également été utilisée pour accéder à la rugosité de surface ainsi qu'à l'usure. La technique de micro-indentation a permis la mesure des propriétés mécaniques des matériaux comme la dureté et le module élastique.

Chaque revêtement a fait l'objet d'une caractérisation fine avant frottement. De même, les tribofilms obtenus à l'issu du frottement ont fait l'objet d'une caractérisation chimique, structurale, et morphologique détaillées.

Chapitre 3 présente les résultats tribologiques obtenus dans les différentes configurations présentées au chapitre 2 telles qu'un test « ring-on-liner », un test alternatif bille-plan, et des tests sur la MTM. L'objectif principal de ce chapitre est de déterminer lequel, parmi les différents revêtements testés, présente les meilleures performances tribologiques en milieu lubrifié sous conditions limites. Les contacts ont donc été lubrifiés d'abord avec de l'huile de base seule, puis avec de l'huile de base et du MoDTC. L'effet du ZDDP, avec ou sans MoDTC a également été étudié. Les résultats obtenus dans les différentes configurations ont été comparés. Il a ainsi été constaté que toutes les configurations donnaient le même classement en termes de propriétés tribologiques des couches APS. En effet, le revêtement TiO_2 APS

présente les meilleures propriétés tribologiques lorsqu'il est lubrifié avec de l'huile de base et du MoDTC.

Les résultats obtenus ont permis de tirer les conclusions suivantes :

(1) Le contact acier - TiO_2 APS présente le meilleur comportement tribologique lorsqu'il est lubrifié avec de l'huile de base et du MoDTC. Il a par ailleurs été constaté une usure identique sur le revêtement TiO_2 APS lorsque celui-ci était lubrifié avec l'huile de base seule ou en présence d'additif MoDTC.

(2) Les tests tribologiques effectués avec le tribomètre MTM en présence d'huile de base et de MoDTC ont montré que le contact acier - TiO_2 APS était à l'origine d'une cinétique plus rapide de croissance du tribofilm comparé à l'acier de référence, à l'acier APS et à l'acier Mo APS. De plus, l'usure obtenue était la plus faible dans le cas du contact acier - TiO_2 APS.

Les résultats obtenus au chapitre 3 ont permis de conclure que le contact acier - TiO_2 APS offrait le meilleur comportement tribologique quelle que soit la configuration utilisée. Chapitre 4 se focalise désormais sur l'étude du comportement tribologique du revêtement TiO_2 APS en condition de lubrification mixte / limite et en présence d'huile de base contenant du MoDTC. Une comparaison est effectuée avec l'acier conventionnel non revêtu. Des essais MTM ont été réalisés afin d'étudier la cinétique de formation et de croissance du tribofilm. L'effet de l'ajout de ZDDP sur le comportement tribologique du système a également été étudié. La morphologie et la chimie du tribofilm ont été étudiées par le biais du MEB, de l'XPS, de la spectroscopie Raman et du MET.

Les conclusions suivantes ont été obtenues:

(1) Une réduction de 15 à 20% du frottement a été observée dans le cas d'un contact acier - TiO_2 APS en présence de MoDTC, par rapport au contact acier - acier.

(2) Cette réduction de frottement est possiblement due à deux facteurs:

(a) La présence d'un mélange constitué uniquement de MoS_2 et de MoO_3 dans le cas d'un contact acier - TiO_2 APS comparé au cas du contact acier - acier ou un mélange de MoS_2, MoO_3 et MoO_xS_y a été trouvé.

(b) La morphologie du tribofilm – de longs feuillets cristallins directement attachés à la surface de TiO_2 ont été observés dans le cas du contact acier - TiO_2 APS alors que des feuillets plus courts ont été observés, dans une matrice à base de Fe, Mo, S, C, O, dans le cas du contact acier - acier.

(3) Une faible usure a été obtenue dans le cas du contact acier - TiO_2 APS même lorsque ce dernier est lubrifié avec de l'huile de base; cela a été attribué à la transformation lors du frottement de la phase rutile en un oxyde substoichiométrique (Ti_nO_{2n-1}), appelé phase Magneli, connue pour être particulièrement résistante à l'usure. L'ajout de ZDDP dans le lubrifiant n'a d'ailleurs aucun effet supplémentaire sur la réduction de l'usure.

Dans le chapitre précédent, le comportement tribologique du contact acier - TiO_2 APS a été présenté.

Dans le chapitre 5, l'influence de divers paramètres tels que la rugosité, la réduction de la concentration de MoDTC, la température d'essai, la pression de contact et le changement du matériau antagoniste sur le comportement tribologique du système acier - TiO_2 APS a été étudié. Des comparaisons ont été effectuées avec l'acier de référence. Les principales conclusions tirées de ce chapitre sont les suivantes:

(1) Les études sur l'effet de la rugosité, dans le cas du contact acier - TiO_2 APS, ont montré que le comportement tribologique se révèle être similaire pour les échantillons ayant une rugosité de surface moyenne (Ra) similaire et donc pour un même lambda.

(2) Du MoS_2 est formé dans le cas du contact acier - TiO_2 APS lorsque la concentration en MoDTC dans l'huile de base est abaissée jusqu'à 0,01% en poids. Cette formation de MoS_2 s'accompagne d'une baisse du frottement significative. Dans le cas d'un contact acier - acier, la formation de MoS_2 n'a pas été observée à de si faibles concentrations.

(3) Les études sur l'effet de la température montrent que même à basse température, la formation de MoS_2 reste possible en présence de TiO_2 APS. Cela n'est pas le cas dans le cas d'un contact acier - acier.

(4) Les études sur l'effet de la pression ont montré que dans le cas du contact acier - TiO_2 APS, un bas frottement pouvait être obtenu même à de relativement basses pressions (0,4 GPa) comparé au contact acier - acier de référence où des pressions importantes sont nécessaires pour activer l'additif. La baisse du frottement est toujours liée à la formation de MoS_2. Il apparait donc que le contact acier - TiO_2 APS lubrifié avec du MoDTC est moins sensible à la pression que le contact acier - acier.

(5) Une étude de l'influence de la nature du matériau antagoniste avec le revêtement de TiO_2 APS a également été réalisée, la bille en acier ayant été remplacée par des billes en céramique (zircone et alumine). Les résultats ont montré une augmentation de la quantité de conversion

de MoDTC en espèces à base de Mo où le degré d'oxydation du molybdène est réduit par rapport à la molécule de MoDTC (Mo+V dans le MoDTC). Du MoS_2 (+IV), du Mo métallique (0) ainsi que des carbures (MoC, Mo_2C - +II ou +IV) sont ainsi détectés en plus d'oxydes de molybdène (+VI). Ces résultats montrent que le TiO_2 favorise la décomposition du MoDTC.

Nous avons montré lors des précédents chapitres que de meilleurs résultats tribologiques avaient été obtenus pour un contact acier - TiO_2 APS lorsque ce dernier était lubrifié avec un mélange huile de base et de MoDTC ; ceci, par rapport au contact acier - acier de référence. Compte tenu de ces résultats et de la littérature sur les propriétés tribologiques des nanoparticules, des essais tribologiques supplémentaires ont été réalisés en considérant une dispersion constituée de nanoparticules de TiO_2 (anatase ou rutile) mélangées avec du MoDTC dans de l'huile de base. Les tests de frottement ont été réalisés pour un contact acier - acier de référence et à l'aide d'un tribomètre linéaire bille - plan. La caractérisation des tribofilms a été réalisée par XPS et TEM. L'influence de la rugosité du plan en acier a été étudiée en comparant un revêtement APS en acier brut rugueux et notre acier de référence.

Les principaux résultats obtenus sont les suivants :

(1) Une dispersion stable (huile de base + MoDTC + nanoparticules de TiO_2) est obtenue dans le cas de nanoparticules de TiO_2 de 25 nm de diamètre et de structure anatase ainsi que dans le cas de particules de rutile de 100 nm de diamètre.

(2) Le comportement tribologique du contact acier - acier de référence lubrifié avec ces dispersions est particulièrement intéressant. Les mêmes niveaux de frottement que ceux obtenus dans le cas du contact acier - TiO_2 lubrifié par le MoDTC sont obtenus ($\mu \approx 0.04$).

(3) Le mélange de 0,5% en poids de particules de TiO_2 (de structure anatase et de 25 nm de diamètre) et de 0,5% en poids de MoDTC dans l'huile de base présente le coefficient de frottement le plus bas par rapport à toutes les autres dispersions réalisées à partir de particules de TiO_2 de différentes phases et tailles.

(4) L'analyse TEM a montré la formation d'un tribofilm d'environ 30 nm d'épaisseur constitué de longs feuillets de MoS_2 cristallins mélangés à des particules de TiO_2.

Le bas niveau de frottement obtenu s'explique donc par :

(a) la tribochimie du tribofilm :

Du MoS_2 et du MoO_3 purs sont formés sur les surfaces en acier. Aucune trace d'oxysulfures et de sulfates n'est détectée.

(b) la morphologie des feuillets de MoS_2 générés qui sont particulièrement longs.

(5) La réduction de la concentration en particules de TiO_2 (anatase 25 nm) et du MoDTC (de 0,5% à 0,1% en poids) montre que la dispersion est encore efficace pour abaisser le coefficient de frottement contrairement à la dispersion constituée uniquement de 0,1% de MoDTC dans l'huile de base (long temps d'induction observé). Cela suggère que l'ajout d'une petite quantité de nanoparticules de TiO_2 (anatase - 25 nm) ajoutée au MoDTC dans l'huile de base aide à la décomposition complète du MoDTC pour former du MoS_2 et conduire à un bas coefficient de frottement.

(6) avec une surface encore plus rugueuse que l'acier de référence (revêtement acier APS) une réduction encore plus importante du coefficient de frottement a été observée ($\mu \approx 0.03$) lors d'essais effectués avec cette même dispersion (huile de base + 0,5% en poids de MoDTC + 0,5% en poids de particules de TiO_2 anatase à 25 nm).

Les chapitres précédents ont présentés des résultats de frottement particulièrement bas obtenus μ autour de 0,04) pour un contact acier - TiO_2 APS lubrifié avec du MoDTC (chapitre 4 et 5) et pour un contact acier - acier lubrifié avec un mélange de nanoparticules de TiO_2 (anatase) et de MoDTC (chapitre 6). Les résultats sont résumés sur la figure 1.

a) MoDTC – contact acier –TiO_2 APS :

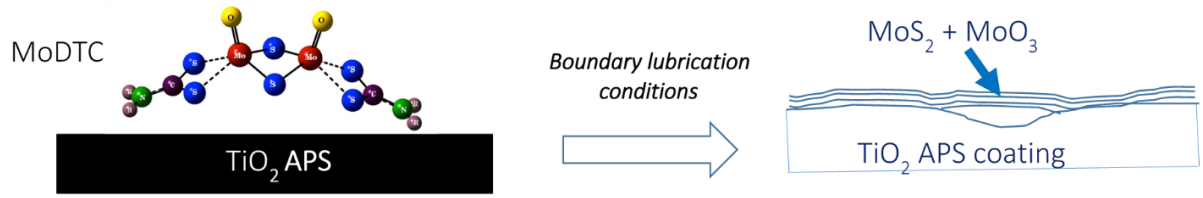

b) Nanoparticule de TiO_2 + MoDTC – contact acier-acier

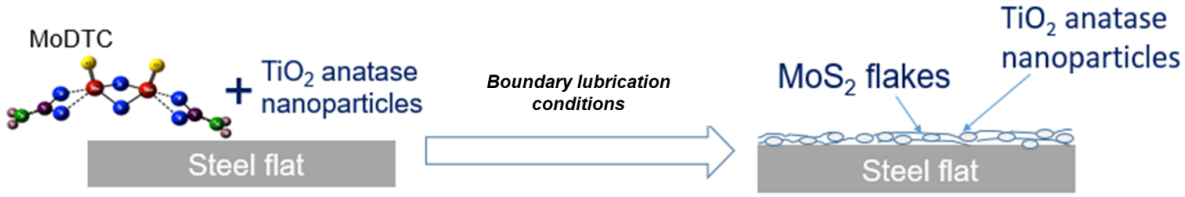

Figure 1 : Résumé des résultats principaux obtenus dans la thèse

Dans ces deux cas, les bas frottements observés sont dus à la présence de MoS_2 sans oxysulfure dans le tribofilm. Cela suggère que la décomposition tribochimique du MoDTC est facilitée par la présence du TiO_2 dans le contact. Chapitre 7 traite des mécanismes proposés pour expliquer cette décomposition du MoDTC pour former des feuillets de MoS_2 dans des contacts impliquant du TiO_2 sous forme de revêtement APS ou de nanoparticules.

Deux mécanismes sont discutés : la photocatalyse et la tribocatalyse. Différents tests sont effectués pour prouver / éliminer chacune des hypothèses.

Voici les conclusions obtenues :

(1) Aucune preuve n'a été trouvée en faveur du comportement photocatalytique et ce mécanisme a donc été rejeté.

(2) La tribocatalyse est considéré comme le mécanisme le plus probable pour expliquer la décomposition complète du MoDTC en présence de TiO_2 dans un contact lubrifié sévère. Le revêtement ou les nanoparticules deTiO_2 ne réagissent pas directement avec le MoDTC mais contribuent à la décomposition complète de l'additif en MoS_2. On parle donc de catalyse, et comme ce phénomène a lieu sous condition de frottement, il s'agit de tribocatalyse. La présence d'espèces Mo réduites dans le tribofilm (degré d'oxydation du Mo plus faible que dans la molécule MoDTC +V) suggère fortement la génération de particules chargées négativement dans le contact. Cette étape a été identifiée comme nécessaire dans une étude théorique précédente sur le mécanisme de conversion du MoDTC en MoS_2. Suivant les cas, la source de particules chargées négativement pourrait être due à un phénomène de triboémission ou à la formation de phases Magneli dans le contact, phase sous-stœchiométrique Ti_xO_{2-x} présentant des lacunes d'oxygène dans lesquelles sont piégées des charges négatives.

L'objectif principal de ce travail était d'étudier le comportement tribologique en régime de lubrification mixte/limite de différents revêtements APS en présence de MoDTC. Des travaux plus spécifiques avec le revêtement TiO_2 APS ont été réalisés ainsi qu'avec des nanoparticules de TiO_2 dans un contact acier-acier.

Ce travail nous a permis de mieux comprendre l'interaction du MoDTC avec le TiO_2 dans un contact tribologique lubrifié en régime limite. En effet, il a été mis en évidence que le TiO_2 favorise la formation de feuillets de MoS_2 sans pour autant participer à la réaction : on parle de processus tribocatalytique. Ceci semble possible, via la formation de charges négatives dans le contact qui aident à la décomposition du MoDTC. Ces charges négatives ont été mises en

évidence indirectement puisque des composés à base de molybdène « réduits » i.e. où le molybdène a un degré d'oxydation réduit par rapport à la molécule initiale de MoDTC, sont détectés dans le contact (Mo métal et carbures de molybdène). Afin de confirmer cela, il faudrait réaliser des expériences supplémentaires.

Ces travaux de thèse ont mis en évidence que la présence de TiO_2 dans un contact tribologique fonctionnant sous régime limite en présence de MoDTC permet d'obtenir des coefficients de frottement extrêmement bas même avec des surfaces relativement rugueuses et en conditions sévères de lubrification. Les résultats de ces travaux de thèse ont des retombées industrielles directes puisqu'il est ainsi possible d'optimiser l'action du MoDTC et de formuler des lubrifiants avec de faibles teneurs en MoDTC tout aussi performants qu'avant. Cette thèse a d'ailleurs fait l'objet de deux brevets.

Table of Contents

Abstract 1

General Introduction 3

Chapter 1 Literature review 7

1.1 Lubrication 8

1.1.1 Lubricants – Composition and Functions 10

1.1.1.1 Lubricant additives 10

1.1.1.2 Decomposition behaviour of additives 11

1.1.1.2.1 MoDTC (Molybdenum Dithiocabamate) 12

1.1.1.2.2 ZDDP (Zinc Dialkyl DithioPhosphate) 13

1.1.2 Lubrication in engine contacts 14

1.1.2.1 Piston ring – cylinder liner contact 15

1.1.2.1.1 Piston rings 16

1.1.2.1.2 Cylinder liners 16

1.1.3 Need for optimisation of additives for new materials used for piston ring – cylinder liner contact 17

1.2 Thermal spray coatings in tribological applications 18

1.2.1 Why are coatings used in tribological applications 18

1.2.2 Thermal spray processes 18

1.2.2.1 Flame spray process 20

1.2.2.2 High velocity processes such as HVOF and detonation gun process 20

1.2.2.3 Electric / wire arc process 20

1.2.2.4 Cold spray process 20

1.2.2.5 Plasma spray process 21

1.2.3 Materials for thermal spray coatings 22

1.2.3.1 Metals, Intermetallics and alloys 22

1.2.3.2 Ceramics 22

1.2.3.3 Polymers 23

1.2.4 Coating properties 23

1.3 Review of tribological behaviour of thermal spray coatings 26

1.3.1 Hardness 26

1.3.2 Roughness, material chemistry and porosity 26

1.3.3 Surface modification by solid lubricant thin films 27

1.3.4 Tribologically induced surface modifications 28
1.3.5 Interaction of thermal spray coatings with additives 29
1.4 Summary 29
1.5 References 31

Chapter 2 Materials and Methods 39
2.1 Materials 40
2.1.1 Lubricants and additives 40
2.1.2 Tribopair materials 40
2.1.2.1 APS coatings 40
2.1.2.2 Reference steel 41
2.2 Experimental methods 42
2.2.1 Techniques for studying tribological behaviour of materials 42
2.2.1.1 Linear reciprocating tribometer 42
2.2.1.2 MTM (Mini-Traction Machine) 43
2.2.1.3 SRV TE 77 reciprocating tribometer 45
2.2.2 Characterisation techniques 48
2.2.2.1 Wear measurement 48
2.2.2.1.1 Optical microscopy 48
2.2.2.1.2 Interferometry 48
2.2.2.2 Mechanical property measurement 48
2.2.2.2.1 Micro-Indenter 48
2.2.2.3 Physico-chemical and morphological measurements 49
2.2.2.3.1 Scanning Electron Microscopy (SEM) 49
2.2.2.3.2 Raman Spectroscopy 49
2.2.2.3.3 X-ray Photoelectron Spectroscopy (XPS) 50
2.2.2.3.4 Transmission Electron Microscopy (TEM) 50
2.3 Coating properties obtained after characterisation 52
2.3.1 Surface roughness parameters 52
2.3.2 Physico-chemical and mechanical properties of the coatings 53
2.3.2.1 Steel APS 53
2.3.2.2 Steel Mo APS 55
2.3.2.3 TiO_2 APS 57

2.4 Summary 61
2.5 References 62

Chapter 3 Tribological behaviour of reference steel and APS coatings under boundary lubrication conditions using various test configurations **63**
3.1 Ball-on-flat tribotests 64
3.1.1 Experimental 64
3.1.2 Results and Discussion 66
3.2 MTM tribotests 70
3.2.1 Experimental 70
3.2.2 Results and Discussion 71
3.3 Ring-on-liner tribotests 74
3.3.1 Experimental 74
3.3.2 Results and Discussion 76
3.4 Conclusions 78
3.5 References 79

Chapter 4 Tribological behaviour of TiO_2 APS coatings in presence of oil containing MoDTC 81
4.1 Experimental 82
4.1.1 MTM tribotest conditions 82
4.1.2 Surface analysis of the tribofilms 82
4.2 Results 83
4.2.1 Friction and wear results 83
4.2.2 Surface analysis of the tribofilms 85
4.2.2.1 SEM analysis 85
4.2.2.2 XPS analysis on the TiO_2 APS disc 86
4.2.2.3 Raman spectroscopy on the TiO_2 APS disc 88
4.2.2.4 FIB-TEM analysis on the tribofilm 90
4.3 Discussion 92
4.3.1 Low friction in case of TiO_2 APS coating 92
4.3.2 Low wear in case of TiO_2 APS coating 94
4.4 Conclusions 95

4.5 References 96

Chapter 5 Effect of various parameters on the tribological behaviour of steel / TiO_2 APS coating 99

5.1 Experimental 100

5.2 Results 102

5.2.1 Effect of roughness parameters 102

5.2.1.1 Tribological behaviour of steel / TiO_2 APS contact for samples with different average surface roughness 102

5.2.1.2 Effect of maintaining similar lambda ratio by changing the speed 105

5.2.1.3 Surface characterisation of the tribofilms using XPS 106

5.2.2 Effect of concentration of MoDTC 108

5.2.2.1 Tribological behaviour of steel / TiO_2 APS and steel / reference steel 108

5.2.2.2 Surface analysis of the tribofilms using XPS 110

5.2.3 Effect of temperature 112

5.2.3.1 Tribological behaviour of steel / TiO_2 APS and steel / reference steel 112

5.2.3.2 Surface analysis of the tribofilms using XPS 113

5.2.4 Effect of contact pressure 116

5.2.4.1 Tribological behaviour of steel / TiO_2 APS and steel / reference steel 116

5.2.4.2 Surface analysis of the tribofilms using XPS 117

5.2.5 Effect of change of counterpart material 120

5.2.5.1 Friction results for TiO_2 APS flats 120

5.2.5.2 Surface analysis of the tribofilms 122

5.3 Conclusions 124

5.4 References 125

Chapter 6 Effect of addition of TiO_2 particles with MoDTC in base oil on the tribological behaviour of steel / reference steel contact 127

6.1 Literature review 128

6.2 Materials and methods 132

6.2.1 Materials 132

6.2.2 Methods 133

6.2.2.1 Characterisation of the nanoparticles 133

6.2.2.2 Tribotests 133
6.3 Results 134
6.3.1 Characterisation of the nanoparticles 134
6.3.2 Tribological behaviour of steel / steel lubricated with different sizes and phases of TiO_2 particles 135
6.3.2.1 Friction and wear results 135
6.3.2.2 Surface analysis of the tribofilms 137
6.4 Discussion 141
6.4.1 Low friction in case of steel / reference steel contact lubricated with base oil + 0.5 wt % TiO_2 anatase 25 nm particles + 0.5 wt % MoDTC 141
6.4.2 Effect of change of concentrations of TiO_2 anatase 25 nm particles and MoDTC on the tribological behaviour of steel / reference steel contact 142
6.4.3 Effect of roughness on the tribological behaviour 143
6.5 Conclusion 145
6.6 References 146

Chapter 7 Discussion 151
7.1 Summary of the previous results 152
7.1.1. TiO_2 APS coating lubricated with base oil + MoDTC 152
7.1.2 Steel / reference steel contat lubricated with a blend of TiO_2 anatase nanoparticles and MoDTC 152
7.2 Mechanisms for the decomposition of MoDTC 153
7.2.1 Photocatalysis 155
7.2.1.1 TiO_2 APS coating 155
7.2.1.2 TiO_2 anatase nanoparticles 156
7.2.2 Tribocatalysis 161
7.2.2.1 Evidence of reduced species in the tribofilms formed on TiO_2 APS 162
7.2.2.2 Sources of negatively charged particles 163
7.2.3 Proposed mechanism for complete decomposition of MoDTC in presence of TiO_2 coating 164
7.3 Conclusions 166
7.4 References 167

170

General Conclusions

Perspectives **172**

Annex 1 **175**

Annex 2 **179**

Annex 3 **183**

Abstract

Nowadays to reduce friction and wear as well as gas emission and oil consumption of the passenger car engines, Atmospheric Plasma Spray (APS) coatings are used on cylinder liner. MoDTC (Molybdenum Di-Thiocarbamate), organometallic friction modifier has been previously used to reduce friction by formation of layered molybdenum disulphide flakes. This study focuses on tribochemical interaction of MoDTC with TiO_2 APS coating under mixed / boundary lubrication conditions. Fused and crushed micron sized powders were used to obtain a 70 µm thick TiO_2 coating. Various tribometers were used to carry out tribotests in presence of lubricant containing MoDTC. Steel / TiO_2 APS contact showed significant friction reduction than steel / reference steel contact. It was shown that the tribofilm is composed of MoS_2 and MoO_3 on TiO_2 APS flats while it is composed of Mo-oxysulphide, MoS_2 and MoO_3 on reference steel flats. It was shown that wear resistant Magneli phases are formed on the surface of TiO_2 APS disc, decreasing wear when the contact was lubricated only with base oil. Impact of various parameters like roughness, test temperature, contact pressure, concentration of MoDTC and change of counterpart materials from steel balls to ceramic balls, on the tribological behavior of TiO_2 APS was also studied. Results obtained were compared with contacts involving reference steel and it was confirmed that friction coefficient was always lower in case of contacts involving TiO_2 APS coating. Similar tribological results and chemistry were obtained for TiO_2 nanoparticles blended with MoDTC in case of steel / reference steel contact. Both the cases, TiO_2 APS and TiO_2 nanoparticles showed complete decomposition of MoDTC to form MoS_2. Tribocatalysis was suggested as the mechanism responsible for complete decomposition of MoDTC in case of TiO_2 based materials like TiO_2 APS coating and TiO_2 nanoparticles.

Keywords: APS coatings, TiO_2, MoDTC, MoS_2, TiO_2 nanoparticles, tribochemistry, Magneli phases, tribocatalysis

General Introduction

The increasing number of vehicles in the world is a cause of concern as they are responsible for majority of the air and noise pollution. Most of these vehicles use IC (Internal Combustion) engines which give out pollutant gases like NO_x and SO_x. Nowadays, engine design trends demand low weights, low fuel consumption, emission reduction for low environmental impacts, increased lifetime as well as higher engine efficiencies. After analysing the physical phenomena resulting in energy consumption of cars, Holmberg et al [1] concluded that

(a) In passenger cars, one third of the fuel energy is used to overcome the friction in the engine. Therefore, direct frictional losses are 28 % of the fuel energy.
(b) Reduction in frictional losses will lead to a threefold improvement in fuel economy as it will reduce exhaust and cooling losses at the same ratio.
(c) New technological development for friction reduction in passenger cars could reduce friction by 18 % in short term and by 61 % in the long term [1].

These developments in automotive sector concerning fuel consumption have lead to use of light metal aluminium and its alloys for engine components instead of steels and cast iron. However, it is difficult to protect the aluminium surfaces because of the friction, corrosion and wear behaviour in tribological contacts like piston ring-cylinder liner contact. As all the components of the IC engine act as a single system, the individual components must sustain certain temperature and pressure involved in combustion and also the friction and wear effects of contacts in lubrication conditions. Protection systems used are bushings, aluminium infiltrated porous ceramic or fiber inlay structures or galvanic coatings. However, there is an urgent need for engine systems with higher fuel economy and reduced emissions. To increase the efficiency and the longevity of the engine components, a flexible, low-cost and low-complexity thermal spray coating process is used on light metal alloys as well as steels, cast irons. The commercially used thermal spray coating processes for engine components are Atmospheric Plasma Spraying (APS), high velocity oxy fuel (HVOF) process and wire arc process. A wide range of materials can be coated predominantly by plasma, flame and electric arc spray for a wide range of applications. Generally for the piston ring – cylinder liner contact, atmospheric plasma spray process is widely used. Recent advances in surface engineering processes offer better chances to reduce wear and friction under boundary lubrication conditions and also in lower viscosity oils. The scope of this work allows us to study the tribological behaviour of various atmospheric plasma sprayed thermal spray coatings for cylinder liners under boundary lubricated conditions. Several properties of the coatings like

porosity, roughness, microstructure, hardness and elastic modulus do play an important role in tribological behaviour of thermal spray coatings in lubricated conditions. Therefore, these parameters are taken into consideration and discussed. Also the mechanisms responsible for controlling friction and wear under different lubrication conditions are hypothesized and discussed.

The main focus of this work is to study the tribological behaviour of APS coatings in presence of friction modifier additive Molybdenum Dialkyl – dithio Carbamate (MoDTC). Also, the effect of various parameters like roughness, concentration of MoDTC, temperature, contact pressure, change of additive combinations and change of counterpart materials on the tribological behaviour of APS coatings will be discussed.

Description of various chapters of the thesis is as follows:

Chapter 1 introduces the basics of tribology, various lubrication regimes and lubricant additives. A brief review of the industrial context of the piston ring-cylinder liner contact is carried out relating to its geometry, type of lubrication regimes involved and additives required as well as the materials used. This is followed by an introduction to thermal spray processes and their various types. Also, various type of materials used for thermal spray processes are reviewed. A review of tribological behaviour of thermal spray coatings under lubricated conditions is carried out according to how the various coating properties like porosity or roughness affect the tribological behaviour.

Chapter 2 deals with the materials and methods involved in this work. It gives a detailed account of all the materials used for tribopairs (ball, disc, flat) and their properties. This is followed by brief introduction of various tribometers used for tribotests as well as various characterisation techniques for investigating the tribofilms.

Chapter 3 compares the tribological behaviour of three different APS coatings with bulk reference steel under mixed and boundary lubrication conditions in presence of well-known additives MoDTC and ZDDP. To compare the tribological behaviour of the APS coatings with different configurations and to find the APS coating with the best tribological behaviour, three different configurations are used for tribotests including ball-on-flat reciprocating tribotests on a linear tribometer, ball-on-disc tribotests on MTM tribometer to understand the sliding / rolling behaviour and ring-on-liner tribotests on a reciprocating tribometer with conditions close to real applications.

Chapter 4 reports the tribological results obtained from the tribotests for the most interesting APS coating TiO_2. To understand the action mechanism of MoDTC with this coating, detailed surface characterization of the tribofilms on a nanoscale using various analysis techniques like XPS, SEM, TEM and Raman spectroscopy is carried out.

Chapter 5 deals with the effect of different parameters on the tribological behaviour of TiO_2 APS coating compared to reference steel. A study involving the effect of roughness parameters, concentration of MoDTC, temperature, Hertzian contact pressure and change of counterpart material is carried out.

Chapter 6 focuses on the tribological behaviour of TiO_2 micro and nanoparticles blended with MoDTC on steel / reference steel contact. Various sizes and phases of TiO_2 particles are used alone and in combination with MoDTC in base oil. Effect of concentration of nanoparticles and MoDTC as well as the effect of roughness by changing the flat material from reference steel to rough steel is investigated and discussed.

Chapter 7 discusses the different mechanisms involved in complete decomposition of MoDTC in steel / TiO_2 APS contact as well as steel / reference steel contact lubricated with a blend of TiO_2 nanoparticles and MoDTC. Different mechanisms are hypothesized in this chapter and conclusions are deduced regarding the best possible mechanism responsible for decomposition of MoDTC.

Conclusion summarises the various studies carried out and gives some insights on the perspectives of this work in case of APS coating materials.

Chapter 1

Literature review

The first part of this chapter talks about basics of lubrication, lubrication regimes, lubricant additives and their functions. The various engine contacts are discussed with a focus on piston ring – cylinder liner contact. Previously used materials for piston rings and cylinder liners are presented followed by the new materials. The need for lubrication in this contact is discussed considering the new materials introduced. Necessity of optimisation of lubricant additives for the new materials is justified.

The second part reviews the different thermal spray coating processes used for manufacturing various engine components. Tribological behaviour of thermal spray coatings under lubricated conditions is then discussed considering the literature on the properties like roughness, hardness, elastic modulus and porosity which influence the tribological behaviour of these thermal spray coatings.

1.1 Lubrication

Tribology is the study of friction, wear and lubrication. Friction is the resistance that a surface encounters when it moves over another surface. Wear is the material removal occurring due to movement of one solid over another or any plastic deformation of the solid occurring over a period of time. Lubrication is a method of applying a solid, liquid or gaseous substance over the material surface to reduce the friction and the wear [2].

Due to differences in the severity of contacts in various applications, lubrication can be divided into four different regimes. This is done on the basis of Stribeck curve [3-4] that describes the variation of friction coefficient as a function of product of sliding speed and lubricant viscosity divided by the applied pressure. Sometimes, lambda ratio, which is the ratio of minimum lubricant film thickness to the root mean square of sum of the average roughness of both the counterparts is used to differentiate the various lubrication regimes and is plotted on the X-axis of the Stribeck curve [5].

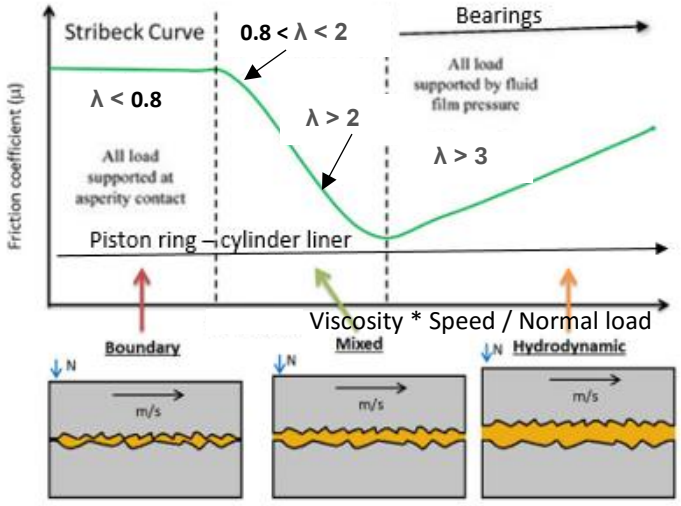

Fig 1.1 Stribeck curve showing different lubrication regimes in different engine components with related lambda ratio [3].

(1) Boundary lubrication regime :

When the lubricant film thickness, h_{min} is lower than the effective RMS roughness of the counterparts, the lambda ratio is lower than 0.8. Surface asperities are in contact during the motion between the two solids. The load is supported by the asperities in contact and the bulk viscosity of the oil has little or no effect on the tribological behaviour as the contact is under oil starvation. These kind of boundary lubrication conditions could result in high friction and wear. Therefore, a lubricant containing friction modifiers and antiwear additives is used to

reduce the friction and wear by forming chemical tribofilms on the surface of the counterpart materials.

(2) Mixed Lubrication regime :

In the mixed lubrication regime, surfaces are separated by a thin lubricating film but still some of the surface asperities are in contact. Therefore, the load is carried partially by the lubricating film and some surface asperities. Since there is some contact between the asperities in mixed lubrication, the lambda ratio is in between 0.8 and 2 (in between boundary lubrication and elasto-hydrodynamic lubrication regime).

(3) Elasto-hydrodynamic lubrication regime :

In elasto-hydrodynamic lubrication regime, the lubricant film thickness, h_{min} is high enough to completely separate the surfaces so as to reduce the friction and wear between the contact. Also, the lubricant film pressure is high enough to significantly influence the shape of film thickness profile. As the lubricant film thickness is much higher than the average surface roughness values of the counterparts, the lambda ratio is above 2.

(4) Hydrodynamic lubrication regime:

When the lubricant film thickness, h_{min} is extremely high compared to the average surface roughness and the gap between the solids is filled with a fluid which is wedge shaped, the gap becomes narrower in the direction of motion. Hydrodynamic lubrication occurs when the fluid is entrained in to the constriction between the surfaces and a hydrodynamic pressure forms to maintain the continuity of the fluid. Since the lubricant film thickness in hydrodynamic lubrication is much higher than the effective RMS roughness of the counterparts, the contact between the solids does not exist and the lambda ratio is higher than 3.

There are various ways to reduce friction in different contacts according to the regime. Lubricants are used accordingly with different additives acting differently in all the lubrication regimes.

1.1.1 Lubricants – Composition and functions

The fundamental reason to use a lubricant is to achieve desired friction and wear behaviour and maintain this despite the continuous degradation of the lubricant. Lubricants serve various other functions limiting the temperature by carrying away heat from fluid friction and fuel combustion, reducing corrosion by coating the metal parts and flushing debris between the moving parts, the lubrication film provides the ability to carry loads, to absorb shocks and vibrations, act as a coolant etc. To perform all these functions, different additives are necessary. Hence, lubricants used in various industries are composed of base oil – 80 % and additive package (various additives) – 20 %. Base oils used are typically mineral oils obtained from the distillation of crude oil or synthetic oils manufactured by using artificial chemical synthesis [6-7].

1.1.1.1 Lubricant additives

MoDTC and ZDDP are most commonly used additives for friction modifying and antiwear applications. List of different additives used in the engine and their functions are mentioned in the table 1.1.

Table 1.1 Different lubricant additives and their functions

Lubricant additive	**Function**	**Examples**
Antiwear	Reduces wear by formation of a protective chemical tribofilm	ZDDP
Antioxidant	Prolongs the oxidation of base oil even at high temperatures	Aromatic amines
Antifoam	Destabilises foam in oil formed due to addition of dispersants and detergents	Si-based molecules
Corrosion inhibitor	Forms a protective film and prevent chemical attack on metallic surfaces	Amine succinates
Detergent	Keeps the surface clean by preventing the build-up of carbon based varnishes	Sulfonates and salicylates Calcium carbonates
Dispersant	Non-metallic cleansing agents that solubilise and disperse contaminants	Succinimides
Extreme pressure	Prevents seizure of the contact materials in extreme pressure conditions	Polymer esters, polysulphides

Lubricant additive	Function	Examples
Friction modifier	Lowers friction in boundary lubrication regime between the contact surface by forming a layered low shear tribofilm on the contact surfaces	MoDTC, amines
Pour point depressant	Prevents the crystallisation of paraffin in oil by improving the flow properties	Polymeric compounds
Viscosity modifier	Improves the Viscosity Index (VI) by steric effect at high temperature	Poly-alkyl-methacrylate

In the next subsection, principle decomposition mechanisms of organometallic friction modifier MoDTC and the antiwear additive ZDDP are reviewed and discussed.

1.1.1.2 **Decomposition behaviour of additives**

1.1.1.2.1 MoDTC (Moylbdenum Dithiocarbamate):

MoDTC is the most widely used friction modifier additive in boundary lubrication conditions. Lot of research has been carried out to study this additive and various mechanisms have been proposed for its decomposition [8–11]. The molecule decomposes to form layered MoS_2 flakes on the surface of the material which reduces the friction between the tribopairs [12]. The decomposition of MoDTC has been shown to depend on various factors like lubricant temperature, maximum contact pressure, humidity, sliding speed, concentration of MoDTC, tribopair materials [8,13]. Effect of all these parameters has been studied predominantly in case of steel / steel contacts. It has been shown that an optimum set of parameters are required to ensure complete decomposition of MoDTC to MoS_2. Failing to reach these parameters results in higher friction as there is no or less formation of MoS_2 in the contact.

Lot of studies on the decomposition of MoDTC have been carried out. Grossiord *et al* [11] proposed a two-step decomposition mechanism. They suggested that electron transfer is necessary in the initial step to form an intermediate Mo-oxysulphide complex. This is illustrated in the schematic in the fig 1.2. Thiocarbamate group dissociates from the MoDTC molecule. In the second step, the two thiocarbamate groups combine to form thiuram disulphide and the Mo oxysulphide decomposes to form MoS_2 and MoO_2 which in turn oxidises to form MoO_3 in the contact. The tribofilm formed in this approach when characterised by XPS

revealed the formation of Mo-oxysulphide, MoS_2 and MoO_3. They showed that small flakes of MoS_2 are formed in an amorphous matrix of Fe, Mo, S, C and O as shown in fig 1.2 (b).

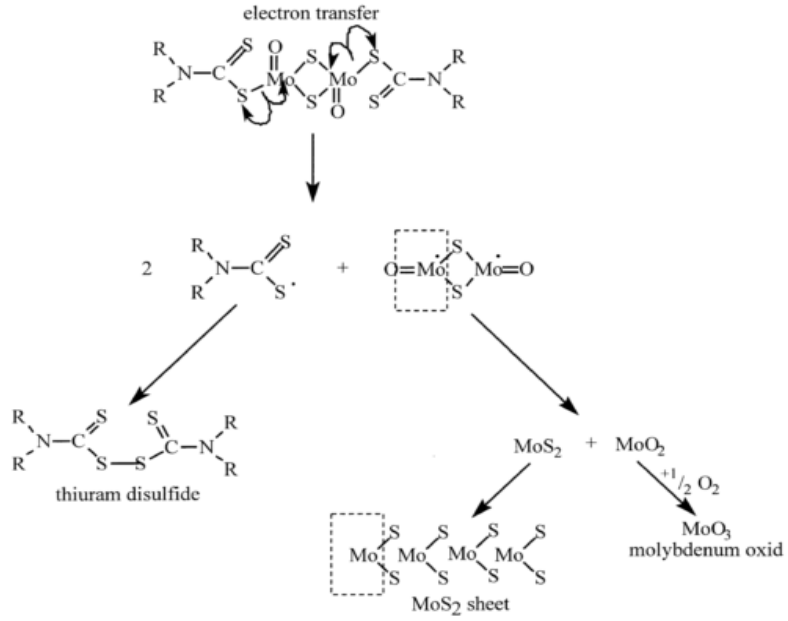

(a)

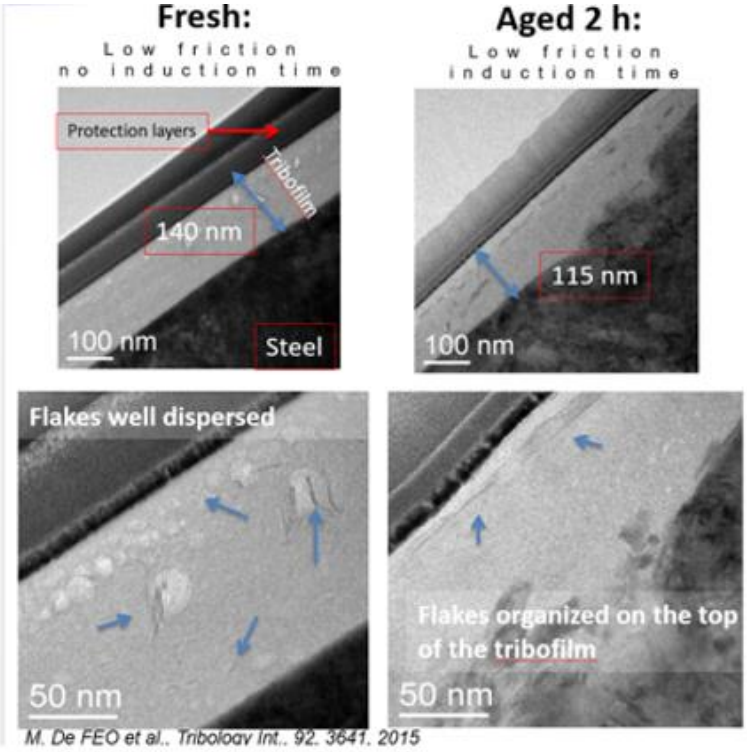

(b)

Fig 1.2 (a) Chemical reaction involved during decomposition of MoDTC to MoS_2 proposed by [11] **(b)** MoS_2 flakes formed in an amorphous matrix [12].

Khaemba et al [8] suggested an alternative reaction pathway for the decomposition of MoDTC and concluded that the Mo+6 contribution in XPS which was attributed to the formation of MoO_3 is due to $FeMoO_4$ which was confirmed by Raman spectroscopy. This mechanism involved two steps, rupture of the C – S bond in the MoDTC molecule under the influence of stress to form MoS_x followed by conversion of MoS_x to MoS_2. The schematic of two step decomposition mechanism is shown in fig 1.3. The MoS_x formed at an intermediate stage reacts with iron oxides to form $FeMoO_4$. If optimum set of parameters (temperature, pressure and concentration of MoDTC) are not used, decomposition of MoDTC is not complete

and leads to the formation of $FeMoO_4$ along with MoS_x and some amount of MoS_2 in the form of short flakes.

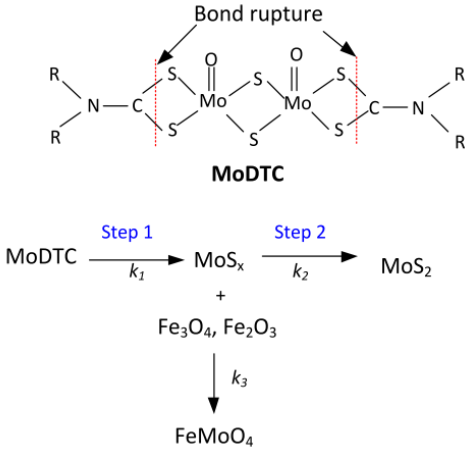

Fig 1.3 Two-step decomposition pathway of MoDTC to MoS_2 proposed by [8].

1.1.1.2.2 ZDDP (Zinc Dialkyl Dithio Phosphate):

ZDDP is the most widely used antiwear additive in the lubricants for various applications [14]. Despite the fact that it is the most used antiwear additive, initially it was used as a corrosion inhibitor [14] and antioxidant. It is also used for extreme pressure properties [15]. Interaction of ZDDP with MoDTC is well known and synergistic effects between them are reported [16], [17].

When ZDDP is used in base oil in tribological conditions on steel surfaces, it interacts with the steel surface and a tribochemical reaction takes place to form an antiwear film on the surface. This film formed is consumed and regenerated continuously protecting the steel surface. Chemical analyses on the tribofilms have confirmed that the film is composed of glassy iron – zinc polyphosphate chains with variable chain lengths and inclusions of iron and zinc sulphides [14]. This polyphosphate glasses have the ability to interact with Fe-oxides to

form iron polyphosphates [18-19]. ZDDP also acts as an antioxidant as it can decompose peroxy radicals as well as hydroperoxides [20]. Schematic of the ZDDP film formation is shown in the fig 1.4.

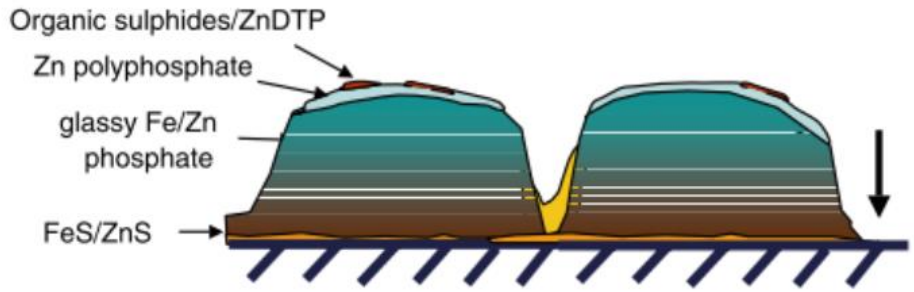

Fig 1.4 Schematic of the ZDDP antiwear tribofilm formed on a steel surface [14].

There are various mechanisms reported for the formation of antiwear film from ZDDP.

The most accepted one states that ZDDP is decomposed to form phosphates which react with the iron oxide and then a mixture of phosphates is formed [21-22]. In the end, a tribofilm is formed consisting of Fe, Zn glassy polyphosphates on the surface of the metal which helps in preventing the metal to metal contact and thereby avoids wear [14].

Lot of previous works report the interactions of ZDDP with various other additives like MoDTC, nanoparticles and it is observed that ZDDP has synergistic effects with most of them [9], [23–25]. In fact, ZDDP also acts as a reducing agent and provides sulphur in the contact to enhance the formation of low friction MoS_2 tribofilms on the surface. Morina *et al* [26] studied the effect of concentrations of MoDTC and ZDDP and came up with optimised set of concentrations that maximise the synergistic effects of friction and wear reduction.

1.1.2 Lubrication in engine contacts :

In an IC engine, all the lubrication regimes are observed. The piston ring – cylinder liner contact consists of a small portion of boundary lubrication regime at the TDC (Top Dead Centre) and BDC (Bottom Dead Centre). The major cause responsible for decreasing the engine efficiencies is the losses occurring due to friction and wear of various engine components at the boundary lubrication regime in piston ring-liner contact [1]. Internal moving parts in an IC engine are shown in fig 1.5.

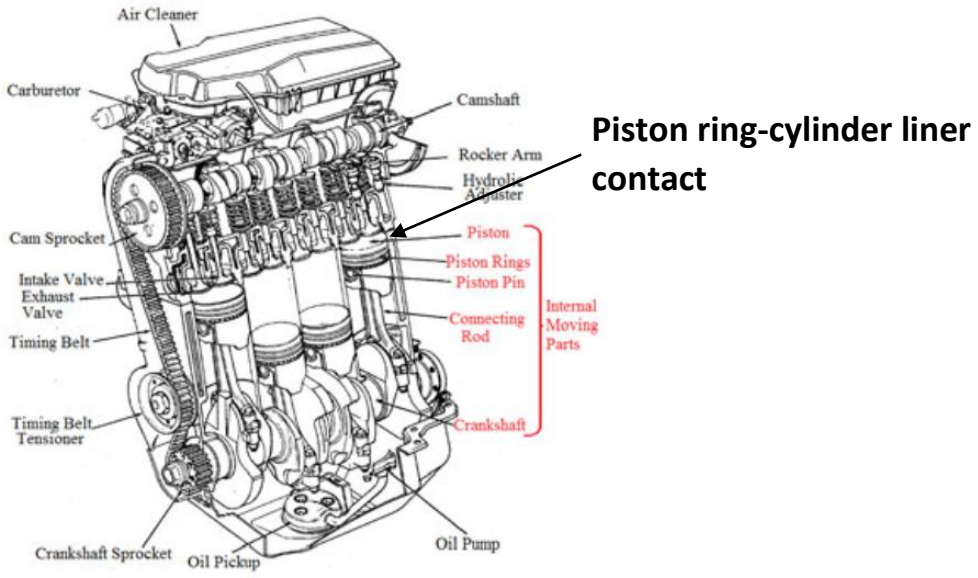

Fig. 1.5 Schematic of an Internal Combustion engine showing the internal moving parts [27].

These parts require various amounts of lubricants to avoid failure by scuffing and wear. As discussed before, lubricants are the molecules used in different types of engine contacts for various moving parts to avoid these friction losses. An oil supply system with a classical circuit is used to lubricate bearings, crankshafts, camshafts, valves and the piston pin. Piston skirt and the cylinder wall is lubricated by the oil flung off the connecting rod using centrifugal force or sometimes jets are used [27]. In this work, we will focus on the piston ring – cylinder liner contact.

1.1.2.1 *Piston ring – cylinder liner contact:*

The piston ring-cylinder liner contact is a complex system consisting of a pack of rings placed on top of the piston in the three grooves sliding against the cylinder liner in a reciprocating motion. Several phenomena occur in the contact related to the geometry of the materials and the operating conditions which have an impact on the engine performance [6], [27-28]. Cylinder liner consists of a special geometry on the surface such as the cross-hatching generated as a result of surface honing process. This cross-hatched grooves generate differences in the pressure and thereby increase the load carrying capacity [29-30]. Important parameters to be considered in this kind of contact are the ring-liner geometry, operating conditions and oil supply. Oil supply is extremely scarce and only a small amount of oil reaches the top compression ring. Also, it is not distributed uniformly and so the top and the bottom dead centre are in oil starvation. The top dead centre (TDC) and the bottom dead centre (BDC) are in boundary lubrication regime while the central part is in hydrodynamic lubrication

regimes as lot of oil flows when the piston moves up and down during compression stroke of the engine [27]. The various lubrication regimes involved in the piston ring - cylinder liner contact are shown in the fig 1.6.

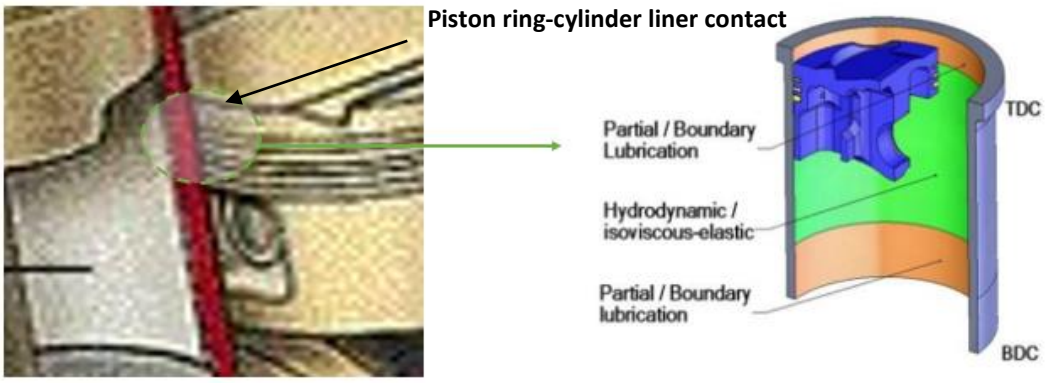

Fig 1.6 Cross section of a piston ring – cylinder contact showing the different lubrication regimes involved.

1.1.2.1.1 Piston rings:

A piston ring is a circular shaped elastic ring that fits in the groove provided in the piston head. A pack of piston rings consists of 2-5 different rings namely top compression ring (sealing and faces high temperature and pressure during combustion stroke), scraper ring (scraps some oil) and oil control ring (sealing and distribution of oil on the liner surface) is designed. All the rings are in pretension increasing from the top ring to the bottom from 5 to 60 N [31]. Traditional materials used for piston rings are nodular cast iron, steel and bronze due to their high hardness and toughness [32]. New materials like a-C:H DLC (Diamond Like Carbon) coatings, Cr and Mo based coatings as well Fe, Zn phosphate based antiwear coatings are being used on a commercial scale for piston ring applications as they can provide ultra-low friction and high wear resistance [33].

1.1.2.2 Cylinder liners:

It is a cylindrical component fitted in the engine block and serves as the inner wall of a cylinder. It forms a sliding surface for piston rings and retains the lubricant within its surface due to its special texture obtained by surface honing. Surface honing is used for mass production of cylinder liners used in internal combustion engines to obtain various surface textures [34]. Texture obtained on the surface of the liner features a special geometry, cross-hatched and plateaux grooves, so two preferential directions are obtained. Depending on the sliding direction used, differences are observed in the steady state friction coefficients with the

roughness grooves parallel to the sliding direction resulting in lower steady state friction coefficient. Dobrica *et al* [35] showed the importance of the roughness grooves by studying the effect of depth, density and number of roughness grooves / scratches. They concluded that deeper, denser and numerous grooves leads to poor bearing performance. On the contrary, Organisciak *et al* [36] suggested use of narrower and dense cross-hatched grooves for friction reduction and better redistribution of the lubricant.

To withstand the severe conditions of piston ring – liner contact, cast iron is the most widely used material for cylinder liners as it provides high wear resistance [37]. Following the recent trend of lightweight engines, some of the cast iron based materials used for liners were replaced by aluminium alloys. However, aluminium alloy cylinder liners fail to deal with high loads as they deform plastically during operation. Also, the hardness is lower than cast iron based materials leading to poor wear resistance. Thus, they are being replaced with APS coatings with ceramic, steel based powders used for spraying [38]. These coatings are interesting concerning the wear resistance and friction reducing properties. Also, they help in increasing engine efficiency and in reduction of oil consumption and emission [39].

1.1.3 Need for optimisation of additives for new materials used for piston ring- cylinder liner contact:

Recent trends to replace the previously existing piston ring – cylinder liner contact materials by a variety of thermal spray coatings could lead to change in the use of additives for these kind of contacts. Most of the additives like ZDDP, MoDTC have been studied and optimised for classical steel – steel and cast iron contacts. Lot of previous research works have shown that an iron containing surface is necessary to initiate the decomposition of MoDTC and ZDDP to form low friction MoS_2 flakes and the antiwear glassy phosphates respectively [40]. However, the interaction of such additives with commercial non Fe-based coating materials is still not known extensively. Therefore, there is a need to study the surface tribochemical interaction of additives with these kind of coatings for various commercial coatings to be used for cylinder liner applications. Optimisation of the additive actions in certain concentrations for materials will surely enhance the use of these new materials.

1.2 Thermal spray coatings in tribological applications

1.2.1 Why are coatings used in tribological applications?

The energy losses due to friction in various engine contacts are estimated to be between 5-7 % of the gross domestic product (GDP) [41]. Hundreds of engine components fail due to excessive wear. Excess oil consumption occurs as well as there is huge amount of emission. In passenger car engines, friction and wear reduction of the various components could reduce global fuel consumption significantly and thereby decrease the CO_2 emissions. Therefore, to reduce the fuel consumption and gaseous emissions as well as to increase the engine efficiencies, different coatings, lubricants and special structural designs could be used [42]. Thermal spray coatings are type of materials which are effective and flexible solutions for these problems [43]. Depending on the material chemistry, these coatings could change the tribological systems by reducing the friction coefficient and increasing the wear resistance. Optimisation of roughness parameters and the texture helps in increasing the load bearing capacity [36]. Also, processes like Atmospheric Plasma Spray (APS) are easy to carry out as the torch used for spraying is portable and can get access to intricate parts of any engineering component. A detailed description of the various thermal spray coating processes and their effect on coating properties is given in the next section.

1.2.2 Thermal spray processes

Thermal spray is a general term for a group of coating processes that apply thermal energy in various forms to melt, soften or accelerate metallic, ceramic, composite, polymer material particles or powders via an electric or chemical route. The heated / melted particles are accelerated towards a prepared surface using atomisation jets and process gases to form splats on the substrate as shown in the fig 1.7 [44]. The bond is formed with the surface as subsequent particles build up to form a lamellar structure. Thin splats formed undergo high cooling rates of around 10^6 K/s. They are generally spherical and then get spread on the surface. Rapid solidification takes place during the thermal spray process due to the large thermal gradient [45].

A major advantage of thermal spray processes is the range of materials that can be used for spraying. Any material that can be melted without decomposition can be sprayed using thermal spray process so materials with high melting points like tungsten, alumina, silica can be applied on any fully heat treated or machined substrate without any thermal distortion. Also, spraying

process can be carried out with extremely low heat input. Also, worn off part like cylinder liner can be removed and recoated by any of the thermal spray process [44-45].

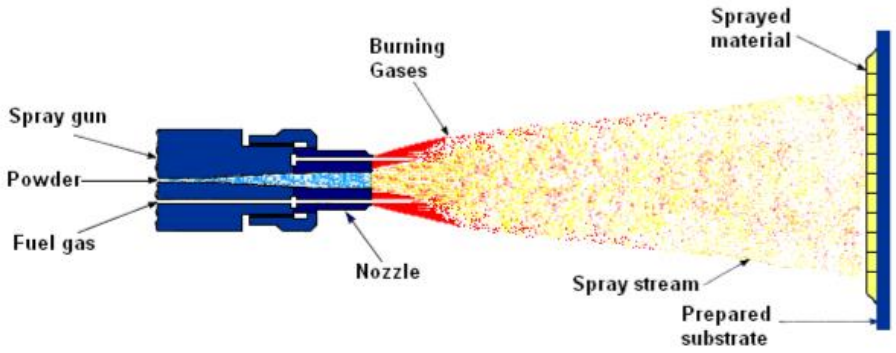

Fig 1.7 Schematic of a thermal spray process [44].

Microstructures of the coatings obtained after thermal spray powder process generally includes oxide inclusions, unmelted or resolidified particles and voids or pores. The size of the inclusions, voids or pores and the unmelted or resolidified particles depends on the powder particles size used for spraying as well as the jet speeds and cooling rates. Deposition rate of the melted powder can be controlled in order to obtain specific size of the pores, roughness parameters. High particle speeds and process temperature result in droplet deformation on impact producing thin layers called as splats [44-45]. These splats could lead to the formation of heterogeneous coatings. Solidified droplets go on depositing and form layers. Each droplet cools at high rates to form uniform, fine grained coatings. Fine grained coatings are found to be dense. The schematic of the deposit microstructure and the generic thermal spray powder consolidation process is shown in fig 1.8.

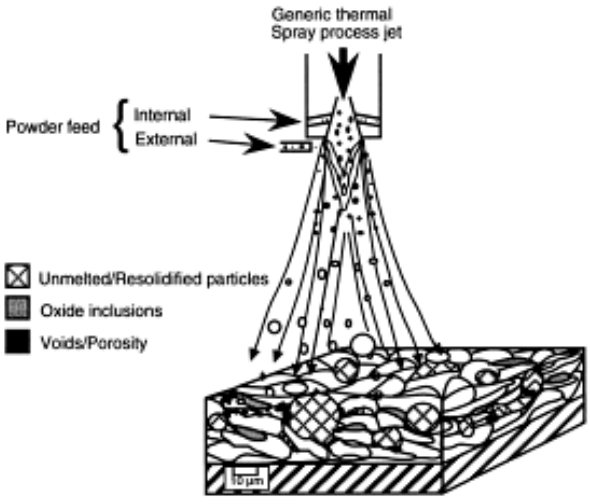

Fig 1.8. Schematic of a typical thermal spray powder process [45].

Types of thermal spray processes:

Thermal spray processes are classified on the sources used to heat the coating material in powder, wire or rod form and in molten or semi-molten state.

1.2.2.1 Flame spray process:

(1) Powder flame process:

Powdered feedstock is melted by the oxyfuel flame and then carried by the flame and high velocity air jets to be coated on the workpiece.

(2) Wire flame process

Flame melts the feedstock material and then the stream of air atomises the molten material and propels it towards the workpiece.

1.2.2.2 High velocity processes such as HVOF and detonation gun process

In HVOF (High-Velocity-Oxy-fuel) process, a fuel gas and oxygen are used to create a combustion jet at temperatures of 2500-3000 °C. Combustion takes place internally to generate a supersonic gas jet with high speeds resulting in extremely dense, well bonded coatings.

In detonation gun process, pre-encapsulated shots of feedstock powder are fed in to a 1 m long barrel along with oxygen and acetylene. A spark ignites the mixture and triggers a controlled explosion. The high temperatures and pressures generated inside the barrel blasts the particles towards the substrate. [44 - 45].

1.2.2.3 Electric/wire arc process

This process consists of two consumable wire electrodes connected to DC power source. They are fed in to the gun and meet to establish an arc between them which melts the tip of the wires. The molten metal is then atomised and accelerated towards the surface of the substrate [45].

1.2.2.4 Cold spray process

This process includes application of coatings by accelerating feedstocks of materials to speeds of 300-1200 m/s using nitrogen or helium as process gas. The expanded gas and the particle stream that comes out of the nozzle generates low temperatures. Any kind of material including polymers like UHWPE can be cold sprayed with good bonding to the substrate [46].

1.2.2.5 Plasma spray process

This includes vacuum and conventional plasma processes.

Vacuum plasma spraying includes low pressure (0.1 – 0.5 atm) plasma spray torches where the plasma becomes larger in length and diameter. The process takes place in vacuum and so the absence of oxygen produces dense, adherent and oxide free coatings. A summary of all thermal spray coating processes is listed in the table 1.2.

Conventional plasma or the Atmospheric Plasma Spray (APS) is the most commonly used commercial process for coating engine parts. In this process, the plasma is generated by superheating inert gas or a mixture of gases like argon and hydrogen by a DC (Direct Current) arc. This plasma generated is used to melt the feedstock powders when it is injected outside of nozzle system followed by acceleration of the workpiece by plasma jet. Commercial plasma guns operate in the range of 20-200 kW. To maintain low substrate temperature, cooling provision has to be done [30].

Table 1.2 Various thermal spray processes with their advantages and disadvantages [44, 48].

Criteria / Process	**Wire arc**	**HVOF**	**APS**
Choice of material	Metallic alloys Restricted choice of materials	Metallic alloys, carbides and composites Refractory materials	Metallic alloys, carbides and plastics High versatility
Heat transfer in the engine block	medium	High	Low
Reliability of the melting process	medium	High (powder) medium (wire)	High
Coating thickness	500 µm	200 µm	200 µm

APS is a low cost, flexible process and can coat materials to which wire based materials do not have access, like pure ceramics and metal matrix composites. Plasma generated can melt any existing material and therefore any material can be plasma sprayed. Most of the cylinder liners are coated by portable plasma torches like Rotaplasma torch [47]. The coatings used in this work are APS coatings.

1.2.3 **Materials for thermal spray coatings:**

The materials used in thermal spray processes range from soft metals to hard metal alloys and refractory ceramics as well as cermets, such as WC/Co, Cr_3C_2/NiCr, Cr_2O_3 and Al_2O_3. Detailed description of various materials used for thermal spray coating processes are mentioned in the three different sections below.

1.2.3.1 Metals, Intermetallics and alloys:

Most of the metals like tungsten, nickel, iron and aluminium and their alloys steel, bronze, brass, NiCr alloys can be thermally sprayed. These metals and alloys are advantageous as coatings since most of the properties like coefficient of thermal expansion, thermal conductivity etc. match with the substrate materials and they also increase the oxidation, corrosion and wear resistance. These kind of coatings are used in automotive components like cylinder liner, piston ring or valve stems, turbine engine blades etc. Different metal based alloys are used for thermal spray coatings as they provide excellent wear protection like in case of Ni and Co-based metal alloys (Ni-Cr-B-Si-C self-fluxing alloys, Inconel) and are considered for replacement of traditional Cr coatings [49].

1.2.3.2 Ceramics:

Since the temperatures in most of the thermal spray processes are high, most of the ceramics can be partially or completely melted and then be thermally sprayed. Metallic oxides such as titania, alumina, silica and carbides such as WC, Cr_3C_2, TiC, Mo_2C as well as nitrides such as TiN, CrN, AlN are thermally sprayed for coatings in engine applications. Since most of the ceramics are hard inert materials, sprayed ceramic coatings are used to provide wear resistance [50], thermal protection and corrosion resistance. Plasma spraying is the most convenient process for ceramics [30, 45].

1.2.3.3 Polymers:

Availability in particulate form is a mandatory requirement for thermal spraying of polymers. Polymers like thermoplastics, thermosets, copolymers including urethane, polyethylene, PTFE, PMMA are thermally sprayed mostly using HVOF and flame spray processes. Also, recently cold spraying of PMMA has been researched and various ways of cold spraying of polymers have been investigated [46, 51].

1.2.4 Coating properties:

For given coating materials and deposition processes, various coating properties are obtained for different deposition process parameters. This could further affect the tribological performance of the coatings. Generally, the change of coating properties and tribological performance is attributed to the change of process parameters which affects the coating microstructure.

Properties of the APS coatings:

Following are some of the properties of the thermal spray coatings that play a vital role in their tribological behaviour:

(a) Roughness:

Since the deposition rate of the powder particles during the thermal spray process is controlled, the size of the solidified particles obtained inside the particles should normally be the expected one. However, island like structures are formed on the surface of the coating. To make the surface of the coating more homogenous, various surface finishing processes like grinding, polishing, lapping and flat or surface honing (detailed explanation in annex 1) are used to obtain required surface roughness parameters for desired applications. Roughness is a vital property that influences the tribological behaviour of the materials. Average surface roughness is not the only parameter to be considered in case of cylinder liners. Surfaces with sharp spikes, deep pits or general isotropic structure may yield the same average roughness value since it does neither consider the differences in peaks and valleys nor does it provide information about the spatial distribution. Therefore, it is necessary to consider all the other 3D / 2D surface roughness parameters.

Ra and Rz parameters:

Ra, average surface roughness is the average deviation of the roughness from the main plateau surface for a defined length. Rz, is the average of the height of 5 highest peaks plus the depth of five deepest valleys over the defined length. R_a and R_z are dependent parameters; so R_z / R_a ratio should be considered to control the shape of the surface.

R_k parameters:

A recent attempt to standardize the bearing area parameters appears in the standard DIN 4776, with the introduction of Rk, Rpk and Rvk parameters. The bearing ratio curve used to calculate these parameters is shown in fig 1.9. Since these parameters are well suited for process control, it is necessary to understand the implications of the bearing area curve and how these parameters are derived from the bearing area curve. Bearing curve describes the surface texture of any object. It is the cumulative probability density function of the surface's profile height.

Use of bearing area curve involves the implementation of normal probability scale. It is known that if a normal curve is plotted on a probability scale, it forms a straight line; slope of the line is proportional to the exponent but with a Gaussian function and with a certain standard deviation. Similarly, when the bearing area curve of a plateau honed surface is plotted on a normal probability scale, it forms two straight lines, one for each of the distributions and so the roughness of both the areas can be deduced independently by measuring the slope of the lines. In this way, bearing area curve can be used as an accurate and intuitive description of a surface.

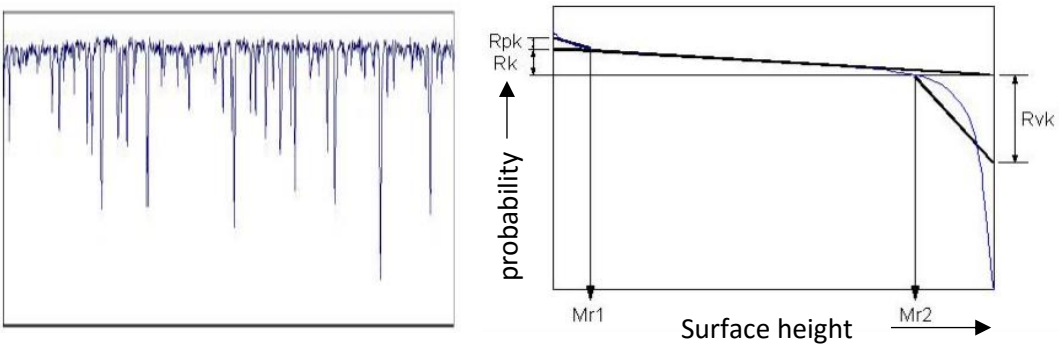

Fig 1.9 Typical profile obtained from plateau honing on the left and bearing ratio curve with its important roughness parameters is shown on the right [52, 53]**.**

R_k = surface bearing index from the bearing ratio curve

R_{pk} = average of the small peaks above the main plateau of the surface. These peaks will typically be worn off (or down) during the running-in period for a part.

R_{vk} = average of the depth of valleys which will retain lubricant in a functioning part.

R_{pk} parameter should be as low as possible to avoid wear as the smallest of this peaks are removed during the running-in period and R_{vk} parameter should be as high to an extent as it acts a lubricant reservoir. Considering the optimum wear resistance obtained with R_{pk} parameters and lubricant retention obtained with R_{vk} parameters, desired range of the roughness parameters for cylinder liners are shown in table 1.3. Special methods like plateau honing, diamond honing are used to generate this kind of parameters for the cylinder liners. This methods generate a rough surface and remove the peaked areas in a controlled manner.

Table 1.3 Desired roughness parameter values for the cylinder-liners:

R_a µm	**R_Z µm**	**R_k µm**	**R_{pk} µm**	**R_{vk} µm**
0.15 – 0.35	< 5	< 0.3	0.07 – 0.2	0.5 – 2.0

(b) Hardness and Elastic modulus:

Due to the presence of large number of voids or pores in the microstructure of the deposited coating, elastic modulus and the hardness of the coating is significantly reduced compared to its bulk counterpart. These properties are known to directly affect the wear resistance of the coating. Hardness and hardness / elastic modulus ratio can be directly related to wear resistance [54]. Higher hardness materials are desired to avoid wear. However, high hardness differences between the counterparts is not desired as it can lead to catastrophic wear.

(c) Porosity:

The structure of the coatings generally show some porosity 0-10 %, unmelted particles and fully melted and deformed splats. Voids are formed as sometimes the melted particles are not deposited uniformly in certain regions of the substrate. Use of wire and rod feedstock materials produces particle size distribution due to non-uniform heating and drag forces. Due to large pores or voids, the mechanical properties of the coating are affected. However, the presence of voids or pores could be advantageous as it can act as a reservoir for lubricants.

(d) Tensile strength and residual stress:

Tensile strength of the as-sprayed deposits ranges from 10-60% of the original material used. Also, residual stress is an important factor limiting adhesion and cohesion from rapid solidification of splats. Effects of the residual stresses have been investigated on the coating properties like bonding, hardness, friction and wear [55] and significant reduction of various properties can be observed due to the generation of residual stresses.

1.3 Review of tribological behaviour of thermal spray coatings:

Presence of coatings with a specific surface topography plays a vital role in the tribological performance of sliding components. Depending on the coatings used, it is possible to reduce friction and wear in dry as well as lubricated conditions. In this section, the review focuses on the tribological behaviour of thermal spray coatings only under lubricated conditions.

Tribological behaviour of various thermal spray coatings is different depending on the base oil, additives present in the lubricant, chemistry and the type of coating, coating properties like hardness, elastic modulus, roughness, porosity. Surfaces of different coatings due to the differences in their chemistries, interact in a different way with the additives present in the lubricant. To understand the various lubrication mechanisms governing the tribological behaviour of these kind of coatings under lubricated conditions, review of the various tribological studies is carried out on the basis of factors affecting the tribological behaviour of these thermal spray coatings [30, 47, 56].

1.3.1 Hardness:

As discussed earlier, hardness of the coatings deposited on a substrate directly affects the wear resistance and so it is an extremely important property in tribological contacts. It has been shown in various studies that ceramic materials exhibit better wear resistance due to their high hardness. Sliding of self-mated, plasma sprayed, partially stabilised 8% Y_2O_3-ZrO_2, exhibited better wear performance than the metallic substrate [57]. In a similar study, plasma sprayed Mo/Chromium carbide and Cr_2O_3 showed improved wear resistance as a piston ring coating compared to electroplated Cr [48]. Further increase in hardness by use of cermets like 8% Y_2O_3-ZrO_2, 20% Y_2O_3-ZrO_2 and Al_2O_3-ZrO_2 coatings were found to have superior wear resistance compared to cast iron used for liners [57-58]. Carbon steel coated with plasma sprayed Al_2O_3-40 wt % TiO_2 exhibited significant anti-wear improvement with an increase in TiO_2 from 13 wt% to 40 wt% [59].

1.3.2 Roughness, material chemistry and porosity:

Since the thermal spray coatings are generally sprayed with micron sized particles, the control of roughness becomes a serious issue. Various processes like lapping, surface honing, grinding polishing are used to obtain the required roughness parameters (mentioned in detail in annex 2). Tung *et al* [60] showed that rough thermally sprayed coatings show better interaction with MoDTC and leads to lower friction and wear. They studied the comparison of friction and wear

of stainless steel and coatings of nitride stainless steel as well as rough thermally sprayed CrN coating against cast iron cylinder bores lubricated in an ethanol fuel and engine oil blend [61]. In case of rough thermal spray coating CrN, they suggested that interaction of MoDTC and ZDDP occurred and led to formation of protective tribofilm, which acts to reduce wear as well as friction between piston ring and cast iron cylinder [62].

Similar work carried out by Nicholls *et al* [40] investigated the effect of fully formulated lubricant containing 1.2 wt % ZDDP on the tribological behaviour of AISI 52100 steel and A319 aluminum alloy cylinder coated with rough Fe using high velocity oxy fuel (HVOF) thermal spray process. The wear observed on both the materials was slight scuffing. HVOF coated Fe on aluminium alloy showed less wear than AISI 52100 steel inspite of similar chemical and mechanical properties of the tribofilm. This difference in wear performance was because of high initial surface roughness due to micropores in the surface of the HVOF samples [63]. These pores acted as a storage space to collect wear debris and in presence of abrasive zones during rubbing resulting in an increased wear rate.

Similar results related to porosity were obtained by Bach *et al* [64] where they performed wear tests on plasma sprayed SiC coatings against steel and showed that low wear resistance was obtained. Low wear resistance was attributed to large porosity in the coating and brittle Si phase in the matrix of SiC. However, a recent investigation by F. Mubarok *et al* [65] showed that even the size of the pores could equally affect the tribological performance. In their work, thermally sprayed SiC coatings showed better friction performance compared to bulk SiC obtained by liquid phase sintering against AISI 440C balls under PAO oil lubricated conditions. A film was formed at the contact and it comprised of SiO_2. This was due to the tiny pores produced during thermal spraying which were exposed and acted as lubricant reservoirs to promote the retention of a higher amount of SiO_2 fluid film at the contact zone. [65].

1.3.3 Surface modification by solid lubricant thin films:

It is known that formation of MoS_2 on the steel surface leads to friction reduction in tribological contacts. On this basis, certain soft metals such as In, Ag, Sn, Mo which possess low shear strength were applied as thin solid films (less than 1µm) on thermally sprayed coatings [66]. When such coatings were subjected to reciprocating tests in the presence of a synthetic oil at high temperature, extremely low friction coefficients and wear rates were achieved [67].

Also, bulk solid lubricant films of soft metals like Mo were observed to increase the lubricity of the surface by being sheared easily to act as a backup lubricant under boundary lubrication

conditions [68]. Thus, when the fully formulated lubricant failed, these solid lubricant films prevented direct contact. This phenomena was showed with coated Mo films on thermally sprayed ceramic coatings of Cr_2O_3, WC in oil lubricated conditions. Cr_2O_3 coatings modified by Mo films show reduced friction coefficient when tested with base oil than Cr_2O_3.

1.3.4 Tribologically induced surface modification:

Oxides of Cr, Mo, Ti, V are known to form hard substoichiometric oxide phases on the surface called Magneli phases [69]–[71]. These phases are generally formed at high temperatures and are wear resistant due to their higher hardness than conventional oxides. Evidences of formation of such wear-resistant hard Magneli phases were observed in numerous studies in case of Ti- based compounds. For example, Ozimina *et al* [72] investigated the tribological behaviour of HVOF sprayed composite coatings containing hard phases of Al_2O_3, SiC and TiN in the nickel matrix deposited on C45 steel. TiN was the most effective in wear reduction which was due to the tribologically induced formation of sub-stoichiometric wear resistant Magneli phases of TiO_2. ZDDP increased the wear resistance of the tribological systems with Ni-SiC and Ni-Al_2O_3 coatings but did not in case of TiO_2 [72]. Similar results were obtained in another study where tribological behaviour of triboreactive plasma sprayed titanium chromium oxide, (Ti,Mo) (C,N) +23 NiMO coated piston rings was investigated against cast iron cylinder liner, using bio-oils as reference. Plasma sprayed titanium oxide and (Ti,Mo)(C,N) +23 NiMO coatings exhibited good anti-wear and anti-scuffing properties [32].

Skopp *et al* also showed the tribologically induced formation of wear resistant Magneli phases Ti_nO_{2n-1} (n = 4 to 6) from thermally sprayed titanium sub-oxide coatings compared to Grey Cast. TiO_x coatings coated on GCI liners by APS and VPS process and triboactive Ti_nO_{2n-1} coated on piston rings by APS process were used for tribotests using several engine oils under mixed/boundary sliding conditions. Results indicated that TiO_x based liner coatings exhibited high wear resistance due to the formation of Ti_4O_7 which was showed using Raman spectra comparing them with the reference powders of Magneli phases. Also, Ti_nO_{2n-1} liner coatings exhibit a higher wear resistance than $TiO_{1.95-x}$. It was thus proved that the Magneli phases of TiO_2, Ti_nO_{2n-1} are more effective in reducing wear than just non-stoichiometric $TiO_{1.95-x}$ [73]. Thermally sprayed APS TiO_x piston ring coatings serve additionally as a promising alternative to commercial piston ring coatings made of strategic Mo based materials [74-75]. Titanium oxide coatings could potentially be the best candidate materials for cylinder liners in terms of wear resistance.

1.3.5 *Interaction of thermal spray coatings with additives*:

Tribological behaviour of thermal spray coatings has been investigated in presence of certain additives. One instance of additives acting in a better way with thermal spray coatings was studied by Yang *et al* [76]. They investigated the tribological behaviour of plasma sprayed Al_2O_3-40% ZrO_2 coating sliding against a Cr_2O_3 ceramic coating at 320°C in lubricated conditions. They showed that the coatings exhibit excellent anti-wear and friction properties depending on the additives present in the lubricants [77]. Plasma sprayed coating sliding against Cr_2O_3 produced *in situ* graphite films and so combined lubrication of liquid and solid films caused a significant decrease in coefficient of friction to 0.04. ZDDP present in the lubricants acted as an anti-wear additive and is effective in reducing the wear rate. [77]. Another similar work carried out by Jiang *et al* showed that plasma sprayed TiO_2 coating exhibits better friction and wear reduction properties. They studied the tribological behaviour of plasma sprayed TiO_2 coating with conventional metallic bearing materials. Base oil, friction modifier triphenyl thiophosphate and antiwear additive tricresyl thiophosphate were used as lubricants. TiO_2 coating coupled with copper lead alloy showed the best friction and wear reduction in presence of base oil.

1.4 Summary:

The first part of this chapter reviewed the basics of lubrication, lubricant formulation and the additive compositions. The second part reviewed the thermal spray processes used for various types of coatings, different kinds of materials used for thermal spray coatings on engine components and the tribological behaviour of these thermal spray coatings under lubricated conditions. It is clear that the general trend of the materials nowadays is towards improving the durability, engine efficiency and reducing oil consumption as well as emission. This has in turn changed the oil manufacturers towards bio-lubricants with low additive content, less ash as well as low phosphorus and sulphur content like the low SAPS lubricant.

From the review on tribological behaviour of thermal spray coatings, it can be summarised that various thermal spray coatings can reduce the friction and wear considerably in oil lubricated conditions in the engine contacts or when additives such as ZDDP or MoDTC are used. However, the coating properties like hardness and elastic modulus, thickness, surface roughness, porosity, coating adhesion to the substrate need to be taken into account. Poor adhesion is often experienced due to either lack of good bonding or coefficient of thermal expansion mismatch between the coating and the substrate which eventually leads to cracking

and spalling. The residual stresses in the coatings affects the bonding, hardness, friction properties and wear resistance considerably as observed in one of the studies. Also, for most of the thermal spray coatings, high initial surface roughness resulted in high wear due to micropores in the surface of the samples which collect wear debris and act as abrasive zones. In some cases, pores in the coatings are beneficial for wear reduction as seen in the case of thermally sprayed SiC coatings, where tiny pores act as lubricant reservoirs which promote retention of fluid film at the contact zone, thereby reducing wear. It can be concluded that the coating properties like the surface roughness, porosity and hardness play an important role and affect the tribological behaviour of thermal spray coatings.

Certain ceramic oxides like TiO_2, MoO_3 show the tribologically induced formation of non-stoichiometric oxides called Magneli phases which are wear resistant due to their high crystal strength. This can be advantageous when coatings are subjected to severe tribological conditions as the formation of these phases is favoured at high temperature and pressure.

Studies on tribological behaviour of thermal spray coatings in lubricated conditions show that use of small amount of additives like MoDTC, ZDDP, organic friction modifiers etc in fully formulated lubricants increase the performance of the contacts involving thermal spray coatings. These additives continue to lubricate the contacts by forming a tribofilm when the liquid lubricant is depleted and thereby avoid early wear. However, after the tribofilm is broken down, wear starts occurring and various wear mechanisms like abrasion, intersplat delamination, adhesion, erosion etc have been observed for thermal spray coatings. But there are certain type of wear resistant coatings like Ti or Mo oxide coatings which form sub-stoichiometric lubricious oxides in tribological conditions. These ceramic oxide coatings are promising for wear applications.

From the studies conducted on the interaction of various additives like ZDDP and MoDTC on thermal spray coatings, the exact tribochemistry involved on the tribopair surfaces is still unclear as most of the studies talk only about the better friction and wear behaviour but not the tribochemistry involved in the contacts. Therefore, there is a need to study the tribochemistry involved on the different plasma spray coatings lubricated with additives like MoDTC and ZDDP. Therefore, this study is focused on investigating the interaction of MoDTC additive on various APS coatings and also the performance of these APS coatings in boundary lubrication conditions.

1.5 References:

[1] K. Holmberg, P. Andersson, and A. Erdemir, "Global energy consumption due to friction in passenger cars," *Tribol. Int.*, vol. 47, pp. 221–234, 2012.

[2] T. Materials, "ASM MHb, Vol 18 Friction, Lubrication and Wear Technology," *Technology*, vol. 2, p. 3470, 2001.

[3] M. Woydt and R. Wäsche, "The history of the Stribeck curve and ball bearing steels: The role of Adolf Martens," *Wear*, vol. 268, no. 11–12, pp. 1542–1546, 2010.

[4] A. Erdemir, "Review of engineered tribological interfaces for improved boundary lubrication," *Tribol. Int.*, vol. 38, no. 3, pp. 249–256, 2005.

[5] B. J. Hamrock and D. Dowson, "Isothermal elastohydrodynamic lubrication of point contacts - Part 1 - Theoretical Formulation," *J. Lubr. Technol.*, vol., no. August, pp. 223–228, 1976.

[6] V. W. Wong and S. C. Tung, "Overview of automotive engine friction and reduction trends: Effects of surface, material, and lubricant-additive technologies," *Friction*, vol. 4, no. 1, pp. 1–28, 2016.

[7] G. W. Stachowiak, A. W. Batchelor, and T. A. Stolarski, "Engineering tribology," *Tribol. Int.*, vol. 27, no. 5, pp. 371–372, 1994.

[8] D. N. Khaemba, A. Neville, and A. Morina, "New insights on the decomposition mechanism of Molybdenum DialkyldiThioCarbamate (MoDTC): a Raman spectroscopic study," *RSC Adv.*, vol. 6, no. 45, pp. 38637–38646, 2016.

[9] M. I. De Barros'Bouchet, J. M. Martin, T. Le-Mogne, and B. Vacher, "Boundary lubrication mechanisms of carbon coatings by MoDTC and ZDDP additives," *Tribol. Int.*, vol. 38, no. 3, pp. 257–264, 2005.

[10] M. I. De Barros Bouchet, J. M. Martin, T. Le Mogne, P. Bilas, B. Vacher, and Y. Yamada, "Mechanisms of MoS_2 formation by MoDTC in presence of ZnDTP: Effect of oxidative degradation," *Wear*, vol. 258, no. 11–12, pp. 1643–1650, 2005.

[11] C. Grossiord, K. Varlot, J. M. Martin, T. Le Mogne, C. Esnouf, and K. Inoue, "MoS_2 single sheet lubrication by molybdenum dithiocarbamate," *Tribol. Int.*, vol. 31, no. 12, pp. 737–743, 1998.

[12] M. De Feo, C. Minfray, M.I. De Barros Bouchet, B. Thiebaut, Th. Le Mogne, B. Vacher, J.M. Martin "Ageing impact on tribological properties of MoDTC-containing base oil," *Tribol. Int.*, vol. 92, pp. 126–135, 2015.

[13] D. N. Khaemba, F. Jarnias, B. Thiebaut, A. Neville, and A. Morina, "The role of surface roughness and slide-roll ratio on the decomposition of MoDTC in tribological contacts," *J. Phys. D. Appl. Phys.*, vol. 50, no. 8, p. 85302, 2017.

[14] H. Spikes, "The history and mechanisms of ZDDP," *Tribol. Lett.*, vol. 17, no. 3, pp. 469–489, 2004.

[15] M. A. Nicholls, T. Do, P. R. Norton, M. Kasrai, and G. M. Bancroft, "Review of the lubrication of metallic surfaces by zinc dialkyl-dithiophosphates," *Tribol. Int.*, vol. 38, no. 1, pp. 15–39, 2005.

[16] A. Morina, A. Neville, M. Priest, and J. H. Green, "ZDDP and MoDTC interactions in boundary lubrication — The effect of temperature and ZDDP / MoDTC ratio," vol. 39, pp. 1545–1557, 2006.

[17] A. Morina, A. Neville, M. Priest, and J. H. Green, "ZDDP and MoDTC interactions and their effect on tribological performance - Tribofilm characteristics and its evolution," *Tribol. Lett.*, vol. 24, no. 3, pp. 243–256, 2006.

[18] J. M. Martin, "Antiwear mechanisms of zinc dithiophosphate: a chemical hardness approach," *Tribol. Lett.*, vol. 6, no. 1, pp. 1–8, 1999.

[19] T. Onodera., "A theoretical investigation on the abrasive wear prevention mechanism of ZDDP and ZP tribofilms," *Appl. Surf. Sci.*, vol. 254, no. 23, pp. 7976–7979, 2008.

[20] T. Colclough and J. I. Cunneen, "923. Oxidation of organic sulphides. Part XV. The antioxidant action of phenothiazine, zinc isopropylxanthate, zinc di-isopropyldithiophosphate, and zinc dibutyldithiocarbamate, in squalene," *J. Chem. Soc.*, no. 0, pp. 4790–4793, 1964.

[21] M. Crobu, A. Rossi, F. Mangolini, and N. D. Spencer, "Tribochemistry of Bulk Zinc Metaphosphate Glasses," *Tribol. Lett.*, vol. 39, no. 2, pp. 121–134, 2010.

[22] J. M. Martin, "Antiwear mechanisms of zinc dithiophosphate: a chemical hardness approach," *Tribol. Lett.*, vol. 6, no. 1, pp. 1–8, 1999.

[23] A. Tomala, B. Vengudusamy, M. Rodríguez Ripoll, A. Naveira Suarez, M. Remškar, and R. Rosentsveig, “Interaction Between Selected MoS2 Nanoparticles and ZDDP Tribofilms,” *Tribol. Lett.*, vol. 59, no. 1, p. 26, 2015.

[24] P. U. Aldana, B. Vacher, T. Le Mogne, M. Belin, B. Thiebaut, and F. Dassenoy, “Action mechanism of WS2 nanoparticles with ZDDP additive in boundary lubrication regime,” *Tribol. Lett.*, vol. 56, no. 2, pp. 249–258, 2014.

[25] M. Kano and J. Ye, “The Effect of ZDDP and MoDTC Additives in Engine Oil on the Friction Properties of DLC-Coated and Steel Cam Followers.”

[26] A. Morina and A. Neville, “Understanding the composition and low friction tribofilm formation/removal in boundary lubrication,” *Tribol. Int.*, 2007.

[27] J. B. Heywood, *Internal Combustion Engine Fundementals*, vol. 21. 1988.

[28] “International Council on Combustion Engines" The Efficient BASicity (EBAS): a method to assess the performance durability of marine cylinder lubricants,” *©CIMAC Congress*, 2013.

[29] P. Ernst and G. Barbezat, “Thermal spray applications in powertrain contribute to the saving of energy and material resources,” *Surf. Coatings Technol.*, vol. 202, no. 18, pp. 4428–4431, 2008.

[30] P. Ernst, “SUMEBore - The Coating Solution to Protect Cylinder Liner Surfaces,” *SAE Int. J. Engines*, vol. 5, no. 4, pp. 2012-01–1992, 2012.

[31] P. Andersson, J. Tamminen, and C. E. Sandström, “Piston ring tribology: A literature survey,” *VTT Tied. - Valt. Tek. Tutkimusk.*, no. 2178, pp. 3–105, 2002.

[32] A. Igartua.., “Biolubricants and triboreactive materials for automotive applications,” *Tribol. Int.*, 2009.

[33] S. Yazawa, I. Minami, and B. Prakash, “Reducing Friction and Wear of Tribological Systems through Hybrid Tribofilm Consisting of Coating and Lubricants,” *Lubricants*, vol. 2, pp. 90–112, 2014.

[34] P. Ernst and B. Distler, “Optimizing the Cylinder Running Surface / Piston System of Internal Combustion Engines Towards Lower Emissions,” *SAE Tech. Pap.*, vol. 4, no. Ic, 2012.

[35] M. B. Dobrica, M. Fillon, M. D. Pascovici, and T. Cicone, “Optimizing surface texture for hydrodynamic lubricated contacts using a mass-conserving numerical approach,” *Proc. Inst. Mech. Eng. Part J J. Eng. Tribol.*, vol. 224, no. 8, pp. 737–750, Jun. 2010.

[36] M. Organisciak, G. Cavallaro, and A. A. Lubrecht, “Starved Hydrodynamic Lubrication of the Piston Ring Cylinder Liner Contact: Preliminary Study of the Influence of Surface Texturing,” in *Life Cycle Tribology*, vol. Volume 48, M. P. D. Dowson G. Dalmaz and A.A. Lubrecht BT - Tribology and Interface Engineering Series, Ed. Elsevier, 2005, pp. 573–583.

[37] F. H. Stott, J. E. Breakell, and R. C. Newman, “The corrosive wear of cast iron under potentiostatically-controlled conditions in sulphuric acid solutions,” *Corros. Sci.*, 1990.

[38] T. Zorn, G. Nentwich, A. Pichler, B. Gmbh, and C. Kg, “Plasma Coating to Replace Cast Iron Cylinder Liners in Production,” 2012.

[39] P. Ernst and B. Distler, “Optimizing the Cylinder Running Surface / Piston System of Internal Combustion Engines Towards Lower Emissions,” *SAE Tech. Pap.*, vol. 4, no. Ic, pp. 1–16, 2012.

[40] M. A. Nicholls *et al.*, “Chemical and mechanical properties of ZDDP antiwear films on steel and thermal spray coatings studied by XANES spectroscopy and nanoindentation techniques,” *Tribol. Lett.*, 2003.

[41] B. Bhushan, *Tribology and mechanics of magnetic storage devices*. Springer Science & Business Media, 2012.

[42] P. Ernst, “SUMEBore Cylinder Liner Surface Coating Reduction of Lubricant Oil Consumption on a Tier-0 EMD 16-710 Diesel Engine Presentation Overview Introduction Engine Test with EMD 16-710 Setup SUMEBore – The Coating Solution Process Overview APS Coating Process.”

[43] E. Expo, P. Ernst, S. M. Ag, and C. Jenckes, “The successful use of Plasma Spray Cylinder Coatings in a NASCAR Sprint Cup Series : Background,” 2010.

[44] F. Reidenbach, “ASM Handbook Surface Engineering,” *ASM Int. USA*, vol. 5, p. 157, 1994.

[45] R. Knight and R. W. Smith, “Thermal spray forming of materials,” *Powder Met.*

Technol. Appl., vol. 7, pp. 408–419, 1998.

[46] K. Ravi, Y. Ichikawa, T. Deplancke, K. Ogawa, O. Lame, and J.-Y. Cavaille, "Development of Ultra-High Molecular Weight Polyethylene (UHMWPE) Coating by Cold Spray Technique," *J. Therm. Spray Technol.*, vol. 24, no. 6, pp. 1015–1025, 2015.

[47] P. Ernst and K. Fletcher, "SUMEBore – thermally sprayed protective coatings for cylinder liner surfaces," pp. 1–12, 2011.

[48] Š. Houdková, F. Zahálka, M. Kašparová, and L. M. Berger, "Comparative study of thermally sprayed coatings under different types of wear conditions for hard chromium replacement," *Tribol. Lett.*, vol. 43, no. 2, pp. 139–154, 2011.

[49] G. Bolelli *et al.*, "Micromechanical properties and sliding wear behaviour of HVOF-sprayed Fe-based alloy coatings," *Wear*, vol. 276–277, pp. 29–47, 2012.

[50] G. Bolelli, V. Cannillo, L. Lusvarghi, and T. Manfredini, "Wear behaviour of thermally sprayed ceramic oxide coatings," *Wear*, vol. 261, no. 11–12, pp. 1298–1315, 2006.

[51] K. Ravi, Y. Ichikawa, K. Ogawa, T. Deplancke, O. Lame, and J.-Y. Cavaille, "Mechanistic Study and Characterization of Cold-Sprayed Ultra-High Molecular Weight Polyethylene-Nano-ceramic Composite Coating," *J. Therm. Spray Technol.*, vol. 25, no. 1–2, pp. 160–169, 2016.

[52] "Roughness measuring systems from Jenoptik – Surface texture parameters in practice Surface texture measurement with Jenoptik Division of a surface."

[53] "Development of a basis for 3D surface roughness standards." .

[54] A. Leyland and A. Matthews, "On the significance of the H/E ratio in wear control: A nanocomposite coating approach to optimised tribological behaviour," *Wear*, vol. 246, no. 1–2, pp. 1–11, 2000.

[55] M. Buchmann, R. Gadow, and A. Killinger, "Thermally Sprayed Coatings For Engine Applications," pp. 1–8.

[56] C. Donnet and A. Erdemir, "Historical developments and new trends in tribological and solid lubricant coatings," *Surf. Coatings Technol.*, vol. 180–181, pp. 76–84, 2004.

[57] H. S. Ahn and O. K. Kwon, “Wear behaviour of plasma-sprayed partially stabilized zirconia on a steel substrate,” *Wear*, vol. 162, pp. 636–644, 1993.

[58] H.-S. Ahn, J.-Y. Kim, and D.-S. Lim, “Tribological behaviour of plasma-sprayed zirconia coatings,” *Wear*, vol. 203, pp. 77–87, 1997.

[59] M. A. Zavareh, A. A. D. M. Sarhan, B. B. A. Razak, and W. J. Basirun, “Plasma thermal spray of ceramic oxide coating on carbon steel with enhanced wear and corrosion resistance for oil and gas applications,” *Ceram. Int.*, vol. 40, no. 9 PART A, pp. 14267–14277, 2014.

[60] S. C. Tung and H. Gao, “Tribological characteristics and surface interaction between piston ring coatings and a blend of energy-conserving oils and ethanol fuels,” *Wear*, vol. 255, no. 7–12, pp. 1276–1285, 2003.

[61] S. C. Tung and H. Gao, “Tribological investigation of piston ring coatings operating in an alternative fuel and engine oil blend,” *Tribol. Trans.*, vol. 45, no. 3, pp. 381–389, 2002.

[62] C. Grossiord, J. Martin, K. Varlot, B. Vacher, T. Le Mogne, and Y. Yamada, “Tribochemical interactions between Zndtp, Modtc and calcium borate,” *Tribol. Lett.*, vol. 8, no. 4, pp. 203–212, 2000.

[63] A. Edrisy, T. Perry, Y. . Cheng, and A. . Alpas, “Wear of thermal spray deposited low carbon steel coatings on aluminum alloys,” *Wear*, vol. 251, no. 1–12, pp. 1023–1033, 2001.

[64] F. W. Bach, K. Möhwald, and B. Drößler, “Development of a Technique for Hard Coating of Component Parts by Synthesis of Silicon Carbide in Thermal Spray Processes,” *Therm. Spray 2005 Therm. Spray Connect. Explor. its Surf. potential*, pp. 1099–1104, 2005.

[65] F. Mubarok and N. Espallargas, “Tribological behaviour of thermally sprayed silicon carbide coatings,” *Tribol. Int.*, vol. 85, pp. 56–65, 2015.

[66] A. Erdemir, O. O. Ajayi, G. R. Fenske, R. A. Erck, and J. H. Hsieh, “The synergistic effects of solid and liquid lubrication on the tribological behavior of transformation-toughened ZrO_2 ceramics,” *Tribol. Trans.*, vol. 35, no. 2, pp. 287–297, 1992.

[67] A. Erdemir, R. A. Erck, G. R. Fenske, and H. Hong, “Solid/liquid lubrication of

ceramics at elevated temperatures," *Wear*, vol. 203, pp. 588–595, 1997.

[68] J. Wei, X. Zhang, and Q. Xue, "The tribological properties of ceramic coatings modified by molybdenum films under oil-lubricated conditions," *Thin Solid Films*, vol. 266, no. 1, pp. 48–51, 1995.

[69] L. Liborio and N. Harrison, "Thermodynamics of oxygen defective Magnéli phases in rutile: A first-principles study," *Phys. Rev. B - Condens. Matter Mater. Phys.*, vol. 77, no. 10, pp. 1–10, 2008.

[70] M. Woydt, "Oil Free Machinery and 'Zero Wear'- Dream or Reality?," *Tribol. Online*, vol. 6, no. 1, pp. 101–112, 2011.

[71] M. N. Gardos, "Magn´ eli phases of anion-deficient rutile as lubricious oxides. Part I. Tribological behavior of single-crystal and polycrystalline rutile (Ti_nO_{2n-1})," *Tribol. Lett.*, vol. 8, pp. 65–78, 2000.

[72] D. Ozimina, M. Madej, and T. Kałdoński, "The wear resistance of HVOF sprayed composite coatings," *Tribol. Lett.*, vol. 41, no. 1, pp. 103–111, 2011.

[73] A. Skopp, N. Kelling, M. Woydt, and L. M. Berger, "Thermally sprayed titanium suboxide coatings for piston ring/cylinder liners under mixed lubrication and dry-running conditions," *Wear*, vol. 262, no. 9–10, pp. 1061–1070, 2007.

[74] J. Landa, I. Illarramendi, N. Kelling, M. Woydt, A. Skopp, and M. Hartelt, "Potential of thermal sprayed Ti_nO_{2n-1}-coatings for substituting molybdenum-based ring coatings," *Ind. Lubr. Tribol.*, vol. 59, no. 5, pp. 217–229, 2007.

[75] B. Criqui, T. Linneman, G. Desplanches, and M. Woydt, "Tribological performances of new triboactive (Ti, Mo)(C, N) and $Ti_{n-2}Cr_2O_{2n-1}$ as piston ring and cylinder liner coatings interacting with bio-no-tox lubricants," 2006.

[76] Y. Wang, Y. Jin, and S. Wen, "The analysis of the friction and wear mechanisms of plasma-sprayed ceramic coatings at 450 ° C," *Wear*, vol. 128, no. 3, pp. 265–276, 1988.

[77] Y. Y. Yang, Y. S. Jin, and T. Yan, "Effect of a surface film on the friction and wear properties of plasma-sprayed Al_2O_3 - 40 % ZrO_2 coatings," *Wear*, vol. 210, no. 1–2, pp. 136–144, 1997.

Chapter 2

Materials and Methods

In this chapter, materials used for tribotests including the tribopairs and the lubricants are listed. This is followed by experimental methods used to study the piston ring – cylinder liner contact on a laboratory scale. These include tribological testing equipments for friction and wear study like the ball-on-flat tribometer, TE 77 reciprocating tribometer in specific configurations and MTM tribometer. Purpose of using different characterisation techniques like optical microscopy, SEM, TEM, XPS and Raman spectroscopy are explained. These characterisation techniques are used to investigate the structure and morphology of the coating and the tribofilm. Interferometry is used for surface roughness and wear measurements. Micro-indentation technique is used for measuring mechanical properties of the materials like the hardness and elastic modulus. Properties obtained for the various APS coatings used in this study are mentioned at the end of the chapter.

2.1 Materials

In this section, lubricants and additives, materials used for flats, balls and discs are described.

2.1.1 Lubricants and additives:

Lubricants used in this study are provided by TOTAL S.A. Base oil used is a standard group III mineral oil. It has a viscosity of 0.026 Pa.s at 40°C and 0.008 Pa.s at 100°C with a sulphur content less than 0.05 wt %. Commonly known friction modifier additive MoDTC (Molybdenum dithiocarbamate) and anti-wear additive ZDDP (Zinc dialkyl-dithiophosphate) are used in different concentrations in base oil for various tribotests. Chemical structure of MoDTC and ZDDP is shown below in fig 2.1 and fig 2.2. MoDTC consists of Mo, S, R alkyl groups. X in the figure could be S or O atoms and R groups are mix of C3 and C6 alkyl chains. Similarly, in case of ZDDP, R represents an alkyl group. MoDTC is blended in base oil in different weight percentages ranging from 0.01 - 0.5.

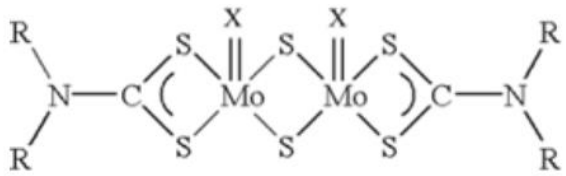

Fig 2.1 Chemical structure of Molybdenum Di-Thiocarbamate (MoDTC).

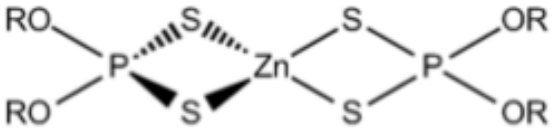

Fig 2.2 Chemical structure of Zinc Dialkyl-Dithio-Phosphate (ZDDP**).**

2.1.2 Tribopair materials :

Materials used for tribotests like the balls, discs and flats are mentioned in this section.

2.1.2.1 APS coatings

The most important material used for tribotesting in this study are the commercial APS coatings obtained from Oerlikon. The APS coatings are atmospheric plasma sprayed on steel substrates. Parts were obtained in various shapes and sizes according to the requirements for the tribotests. Different surface modification processes are used to obtain desired surface roughness parameters like surface grinding, flat honing (mentioned in annex 1) in case of flats and discs, surface honing in case of liner parts. Thickness, porosity, composition of the different APS

coated flats and discs as obtained from the manufacturer as well as the bulk reference steel used in this study are mentioned in table 2.1.

Table 2.1 Composition, thickness and porosity of APS coatings and reference steel.

Flat materials	**Composition (atomic %)**	**Thickness as deposited (µm)**	**Final thickness (µm)**	**Porosity (%)**
AISI 52100 Steel (reference)	Fe – (1%) C – (0.15 – 0.35 %) Si – (0.25 – 0.45 %) Mn – (1.4 %) Cr – (0.1 %) Mo	-	-	-
Steel APS	Fe – (1.2 %) C – (1.4 %) Cr – (1.2 %) Mn	330	60	3.6
Steel + 30 % Mo APS	Fe – (1.2 %) C – (1.4 %) Cr – (1.2 %) Mn + 30 % Mo	300	180	2.8
TiO_2 APS	TiO_2 in rutile phase	80	70	1

2.1.2.2 Reference steel

To compare the results obtained from tribological tests of APS coatings with a reference material (AISI52100), reference steel flats are used. Also, the counterpart material used for all the tests is a standard steel ball for the specific configuration. As obtained values of hardness of the steel is 7 GPa and elastic modulus is 210 GPa. Poisson's ratio is 0.30. All the parts received are mirror polished and the roughness parameters measured using Stylus analysis in Interferometry are mentioned in tables 2.2 and 2.3:

Table 2.2 Roughness parameters for reference steel ball and steel flat:

Material	R_a (µm)	R_Z (µm)	R_k (µm)	R_{pk} (µm)	R_{vk} (µm)
Steel flat	0.01 ± 0.05	0.06 ± 0.04	0.03 ± 0.01	0.03 ± 0.01	0.03 ± 0.02

For MTM ball-on-disc tribotests, balls are purchased from PCS instruments, UK which are mirror polished (R_a = 40 nm). Two types of discs are used, smooth and rough.

Table 2.3 Roughness parameters for smooth and rough steel discs and MTM steel ball.

Material	R_a (µm)	R_Z (µm)	R_k (µm)	R_{pk} (µm)	R_{vk} (µm)
Steel disc (smooth)	0.05 ± 0.03	0.05 ± 0.01	0.03 ± 0.02	0.03 ± 0.01	0.03 ± 0.01
Steel disc (rough)	0.15 ± 0.05	0.90 ± 0.20	0.40 ± 0.07	0.15 ± 0.05	0.33 ± 0.07
Steel ball	0.04 ± 0.01	0.04 ± 0.01	0.02 ± 0.01	0.02 ± 0.01	0.02 ± 0.01

2.2 Experimental Methods

Various experimental methods used for studying the tribological behaviour of the materials as well as the surface characterisation techniques used for evaluation of the tribofilm are explained in detail in this section.

2.2.1 Techniques for studying tribological behaviour of materials

2.2.1.1 Linear reciprocating tribometer:

Linear reciprocating tribometer is used in ball-on-flat configuration to evaluate the tribological properties of tribopairs involving APS coatings and reference steel materials.

Various reasons to use the linear reciprocating tribometer are

(a) contact uses pure reciprocating sliding conditions with high severity which are similar to the real piston ring- cylinder liner contact compared to other configurations,

(b) easy measurement of wear on the ball as well as flat and the average friction coefficient compared to other configurations

(c) ease of operation and

(d) excellent repeatability.

Inputs and outputs:

Ball is fixed on the sample holder on top and the flat is fixed on the sample holder which is fixed on the platform at the bottom. Motor is attached to the ball assembly which induces a linear reciprocating motion of the ball on the flat for a fixed stroke length at a set frequency. Load is applied from the bottom where weights are attached. A load cell is used as a sensor to measure the load. Heating coils are placed inside the platform to heat the assembly to the

required temperature and a thermocouple is fixed on the sample holder to measure the exact oil temperature.

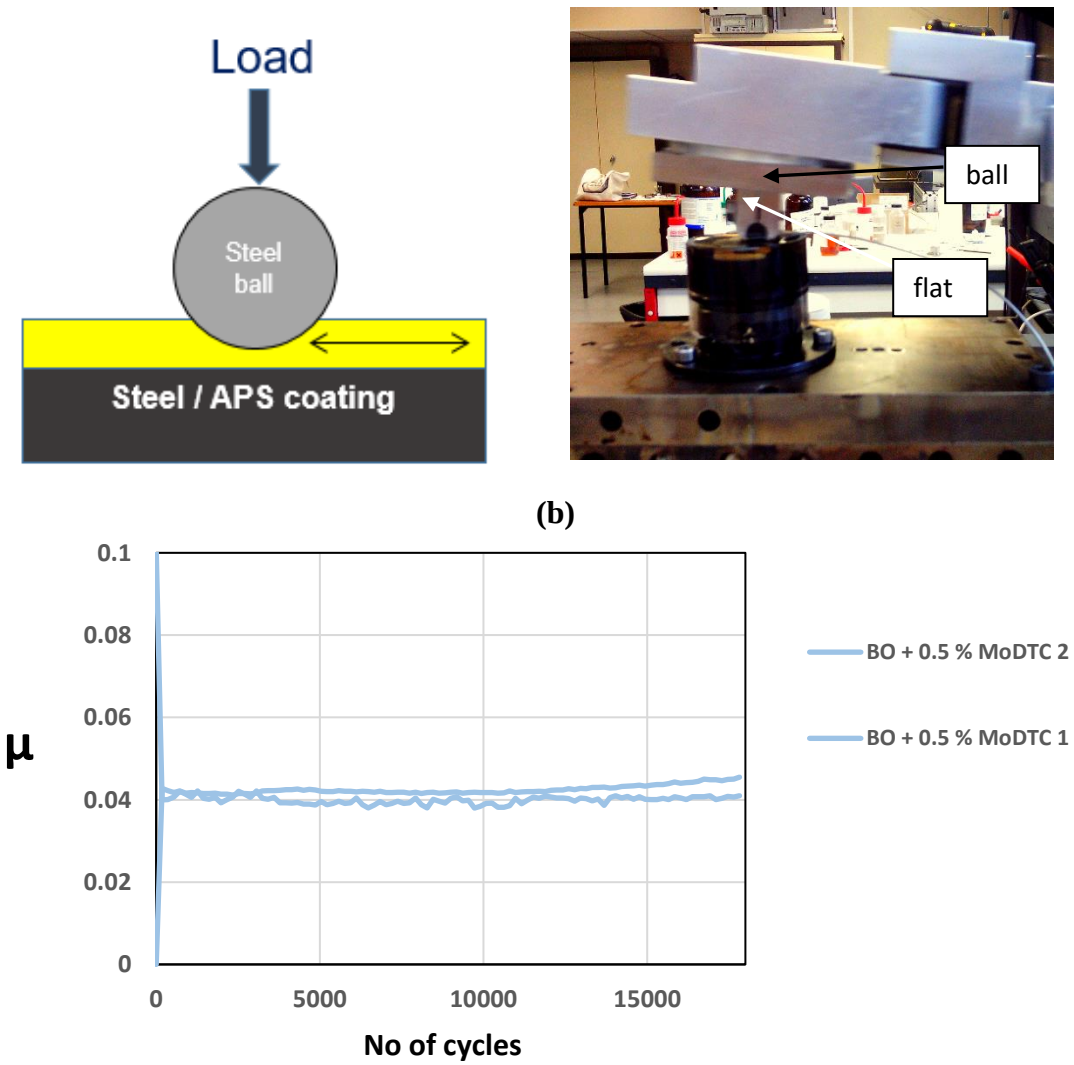

Fig. 2.3 (a) Schematic of ball-on-flat configuration **(b)** Repeatibility of the tribotests carried out.

Both the ball and flat are cleaned in an ultrasound bath before the test for at least 15 minutes using *n*-heptane as a solvent. In this type of configuration, a motor induces the motion of the ball while the flat remains stationary on the fixed holder as shown in fig 2.3 (a). The amplitude and frequency of sliding can be varied as required. Since the configuration involves reciprocating sliding, ball stops at the end point when it reaches the fixed amplitude and slides back to the other end point where it stops again. Each test was repeated at least twice and the results obtained were almost similar as shown in one of the examples in the fig 2.3 (b). Therefore, the reproducibility of the results obtained was found to be good with the ball-on-flat tribometer.

Average dynamic friction coefficient is calculated by taking the ratio of obtained tangential force to the applied normal force. This software involves consideration of a single cycle of the test. Filters are applied to the tangential and normal forces to avoid noise during the test. Average friction coefficient is calculated by taking the ratio of filtered tangential force to filtered normal force for cycles ranging from constant values of friction observed from the curves. While calculating the average dynamic friction coefficient, the static part observed at the end is avoided.

2.2.1.2 MTM (Mini-Traction Machine) tribometer:

To study the tribological behaviour in sliding / rolling conditions and to control the different lubrication regimes, Mini- Traction machine (MTM) from PCS Instruments is used. It uses ball-on-disc configuration. Ratio of amount of sliding to the amount of rolling is given by slide to roll ratio (SRR). SRR is the ratio of amount of sliding to amount of rolling the contact undergoes. This can be varied by changing the amount of rotation of the ball against the disc. If the disc is rotated and the ball is stationary, then the SRR is 200 % and the contact is in pure sliding conditions. A schematic of the MTM equipment is shown in fig 2.4.

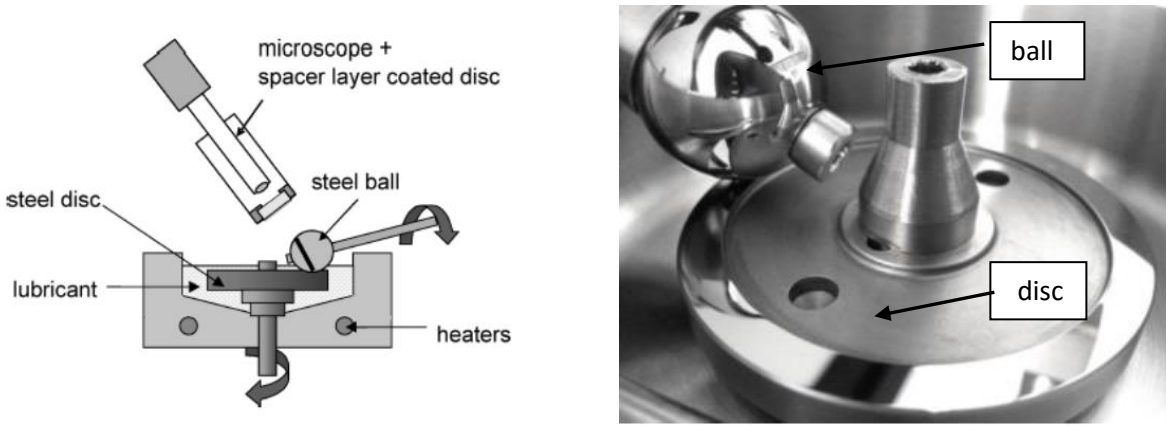

Fig 2.4 Schematic of MTM equipment **[1].**

MTM tribometer was used because:

(a) Measures the tribofilm formation and growth by SLIM imaging technique by capturing images at certain steps during the test
(b) investigate the effect of SRR on tribofilm formation
(c) Ease of alignment and easy to use due to automatic operation

This configuration consists of a ball which is fitted on the shaft free to rotate and the disc fixed at the bottom of an oil bath. Lubricant is added after fixing the ball and disc in the oil bath. To

attain a given test temperature, lubricant in the oil bath is heated using heaters and the temperature is measured by the thermocouples present in the oil bath. Ball and discs are rotated at different speeds during the tests to obtain the desired Slide-to Roll Ratio (SRR). Stribeck curves are obtained by changing rolling velocity or load for a given SRR value.

Tests are run using customised profiles with information on temperature, speed, load, steps and the rate of data acquisition. Various parameters like load, temperature, speed, SRR, Stribeck curve steps can be altered according to the requirements.

An optical microscope is fixed to the MTM equipment and is used to capture real time images of the wear scar as well as thickness of the tribofilm formed on the ball during the tribotest. This is done by spacer layer interferometry technique. The schematic and the working principle of this technique is shown in fig 2.5. This technique involves a glass disc coated with a semi-reflective chromium layer and placed inside the glass window. When the light is passed through this disc, part of the light is reflected at the Cr layer and the remaining passes through and is reflected by the steel ball. So when the two beams combine, an interferometric image is formed which can measure the thickness of the tribofilm formed on the steel ball.

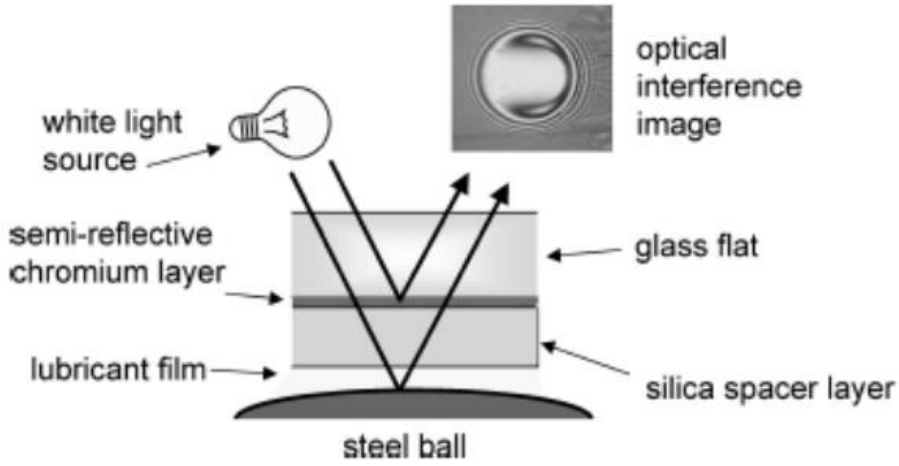

Fig 2.5 Schematic of spacer layer interferometry technique **[1].**

To obtain the images, ball is unloaded from the disc and then loaded against the glass window where an image is obtained using a camera attached to the microscope given that the alignment is perfect.

2.2.1.3 SRV TE 77 reciprocating tribometer:

Cameron PLINT SRV TE 77 reciprocating tribometer in ring-on-liner configuration is used to investigate the friction and wear performance of different materials and lubricants.

The main reasons to use this kind of tribometer are as follows:

(a) Use of real parts with the same dimensional and surface properties – original piston ring and parts cut from the cylinder liner
(b) Use of exactly similar conditions to the real engine contact like low pressures of around 50 – 200 MPa and temperatures of 150 – 200°C.
(c) Control of oil flow in the contact

Load, temperature, stroke length and reciprocation speed is set according to the requirements in the profile. Table 2.4 shows the specifications of this equipment.

Table 2.4 PLINT TE 77 test specifications:

Load	**5 - 1000 N**
Temperature	Ambient – 600 ° C
Frequency	2 - 50 Hz
Stroke length	0 – 25 mm
Friction force	50 – 500 N
Test duration	Operator choice
Contact geometry	Ball-on-flat, cylinder-on-flat, ring-on-liner

Ring-on-liner configuration:

This type of configuration considers use of real parts with similar geometry used in the piston ring-cylinder liner contact. The PLINT TE 77 equipment in ring-on- liner configuration is shown in fig 2.6 (a). Schematic for the ring-on-liner tribometer used is shown in the fig 2.6 (b). It can be observed that a complete commercial top compression ring is used along with a small part cut from the cylinder liner placed at the bottom. Ring is fixed inside a sample holder and load is applied on the ring and then it slides on the liner in a reciprocating motion.

A thermocouple is placed in the oil bath which measures the temperature of the lubricant. The movement in this contact is horizontal and the oil flow is controlled with a sensor attached to the oil bath. An assembly is placed above the ring to apply the desired load in the contact. It is

extremely important to check the alignment in the contact as the contact pressure at all points has to be the same to obtain the accurate value of friction coefficient. To verify the alignment, some amount of oil is applied at the contact surface of the ring and it is slid on the cylinder liner for 3-4 cycles at extremely low load. If the oil is observed at all points in the wear scar, the alignment can be assumed to be correct. Also, the wear track is observed at the end of the test and the alignment of the contact can be confirmed to be good / bad after observing the wear scar. Load and temperature is gradually increased from the beginning of the test in the running-in period. This period is followed by a constant load, temperature and speed regime known as steady state friction regime. Average friction coefficient is calculated by taking the ratio of the applied normal load to the obtained tangential force.

(a)

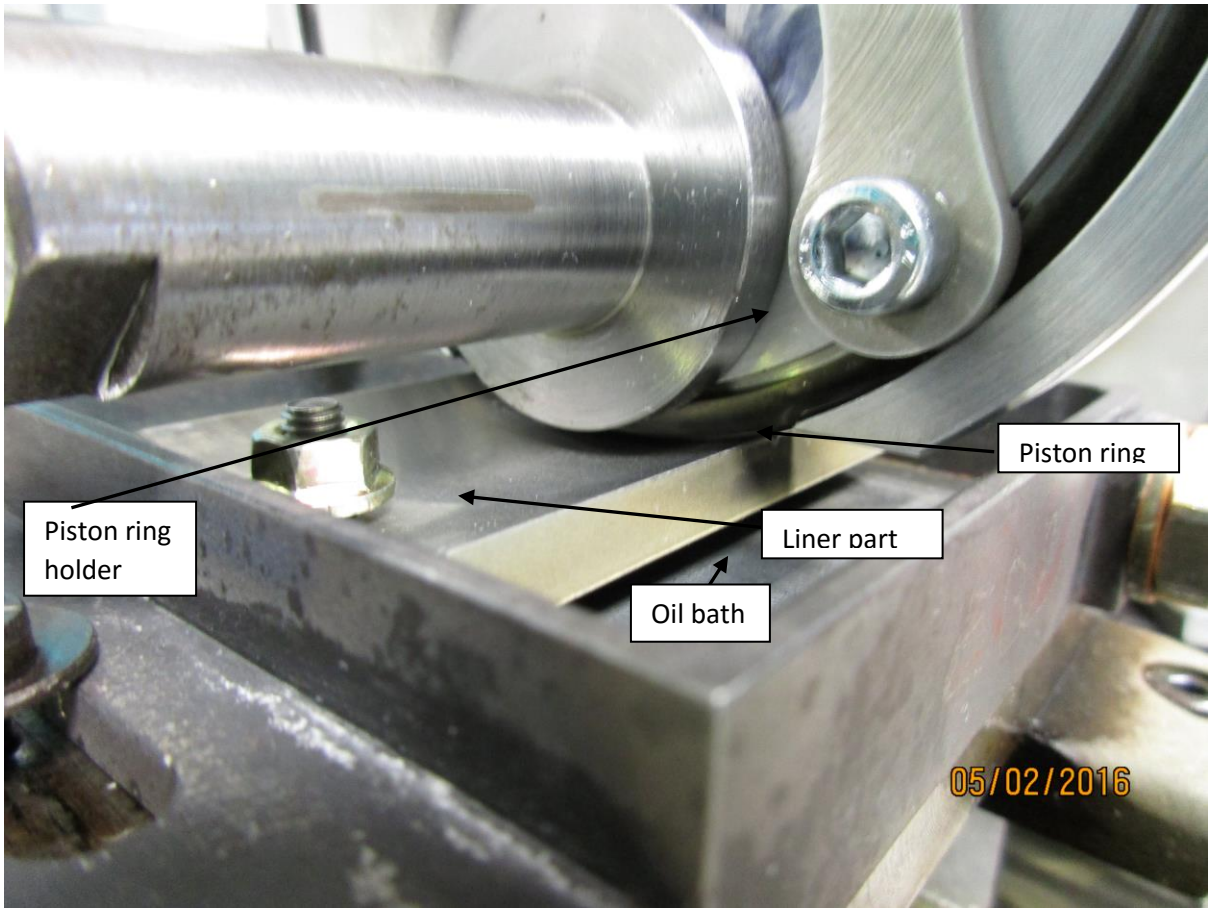

(b)

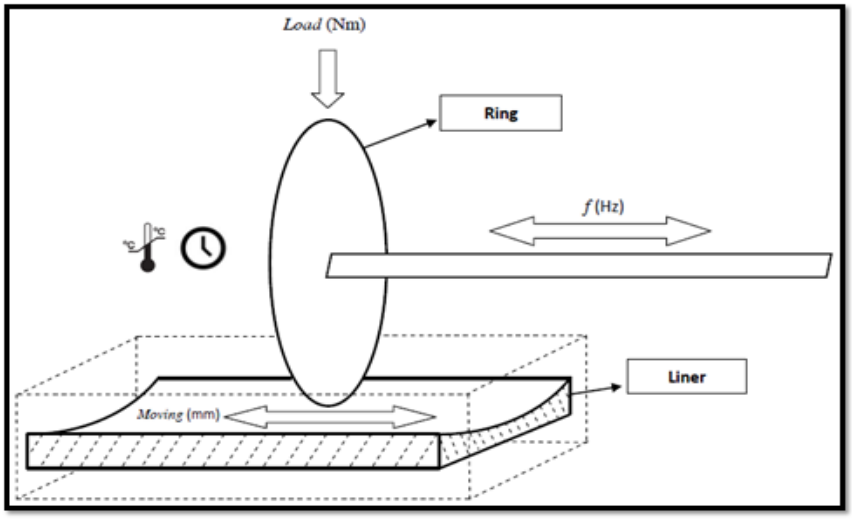

Fig 2.6 (a) PLINT TE 77 ring-on-liner configuration with mounted cylinder liner part in the sample holder (b) Schematic of the ring-on-liner configuration.

2.2.2 Characterisation techniques:

2.2.2.1 Wear measurement

2.2.2.1.1 Optical Microscopy:

Optical microscope is used to measure the wear scar diameter as well as observe the tribofilms on the tribopairs. It is done using OLYMPUS BX51M. Estimated values of the wear scar diameter are obtained using the measuring tools available in the software. This optical microscope is used in different magnifications ranging from 2.5 X to 100 X according to the images required to estimate the wear scar diameters on the balls and the wear scar width on the flats and discs.

2.2.2.1.2 Interferometry:

Roughness parameter measurements as well as 3D images of wear tracks are obtained after tribotests with white light interferometry. The principle of Interferometry is described in annex 2.

Conditions, apparatus and its uses:

Bruker Interferometer GT K1 equipped with two light sources (green and white) and two lenses (5X and 50X) is used. Optical images are obtained at one of these two magnifications. Measurements are carried out on the wear scar to evaluate different parameters like surface roughness, peak heights, kurtosis, skewness, valley depths, wear volume, surface area.

2.2.2.2 Mechanical property measurement

2.2.2.2.1 Micro-Indenter:

Since the thickness of the coatings to be used is in micron range, microindentation results are used in this case to calculate hardness and elastic modulus. Micro-Indenter is used to measure the hardness and elastic modulus for different materials like micron sized coatings. Measuring the mechanical properties of thick films of a few microns is not possible with the conventional hardness testers used for bulk materials. The mechanical properties of coatings vary in different regions because of the porosity, peaks and valleys generated during the coatings process. Microindentation is a method used for measuring the mechanical properties down to the microscale making it useful for thick plasma spray coatings. The principle is detailed in Annex 2.

(a) *Conditions, apparatus and applications:*

Hardness and elastic modulus of all the coatings as well as reference steel materials are measured using Zwick micro-indenter. This kind of micro hardness tester covers Vickers and Knoop hardness testers within the load range from HV 0.01 to HV 2. Load used varies from 0.1 N to 2 N. The hardness tester is equipped with an automatic 6-position turret for up to 2 indenters and up to 4 lenses. This allows the equipment to carry out Vickers and Knoop hardness measurements easily. A wide practical application range is ensured with objective lenses covering total magnifications from 25 X to 1000 X. The front panel display and integrated microscope allow easy operation and timesaving hardness testing. The test cycle is fully automatic and dwell time can be set as required. Load change is automatic and set in the menu. The intensity of the illumination can be stored for each objective lens individually. The advantage of this software is that it creates an overview image of the specimen in high resolution to define indentation positions. This allows single or multiple traverses to be configured and carried out accurately on the specimen surface. The system is operated and controlled entirely by the software and is particularly used for automated multiple traverse testing.

2.2.2.3 Physico-chemical and morphological measurements:

2.2.2.3.1 Scanning Electron Microscopy (SEM):

SEM is carried out before as well as after the tribotests. Sample is prepared by cleaning it with acetone / heptane before placing it on a sample holder which is inserted inside and then vacuum is generated inside the chamber. Topography of the surface as well as tribofilms is observed

and a general idea of tribofilm composition is obtained using SEM-EDS. Equipment used is a VEGA-TESCAN SEM with EDX (Energy Dispersive X-ray analysis) for semi-quantitative compositional analysis. The principle of SEM is explained in Annex 2.

2.2.2.3.2 Raman Spectroscopy:

Raman spectroscopy is a spectroscopic technique based on Raman effect used to study the presence of different compounds in a material and in this case is used to study the composition of the tribofilm formed. The principle of Raman spectrscopy is explained in Annex 2.

Raman spectrometer used in this study is a Renishaw Invia spectrometer with a 488 nm laser. Optical microscope attached to the Raman spectrometer was used with an objective of 50 X to identify the positions for the analysis on the wear scar. Spectra were obtained at 1 mW laser power and 1 s exposure time with several accumulations to improve the signal to noise ratio. Attenuation laser power percentage used was 10%. All the parameters were chosen in such a way to avoid laser damage on the sample. Peaks were fitted using the WiRE program and Gaussian / Lorentzian curves to determine the peak frequencies. Raman spectroscopy is used to identify the compounds present on the surface as well as inside the wear scar. In this case, tribofilms formed from MoDTC can be easily distinguished.

2.2.2.3.3 X-ray Photoelectron Spectroscopy (XPS):

The equipment used in this study is an ULVAC – PHI Versaprobe Spectrometer equipped with a monochromatized AlKα X – ray source (1486.6 eV). Spot size used is 100 µm. Calibration of binding energy was done using Au $4f_{7/2}$ and Au$4f_{5/2}$ with known binding energies at 87.7 eV and 84 eV respectively following the calibration procedure from the manufacturer. Charge compensation system is used to compensate the charging effect. Additional charge correction was done by fixing the C1s peak (C-C bond) at 284.8 eV. The tribofilm is initially searched using scanning X-ray induced secondary electron image (SXI). This image depicts chemical contrast and thus if the tribofilm is present inside the wear scar, it can be easily spotted. Initially, a survey spectrum was recorded on a point inside the tribofilm with a pass energy of 187.85 eV in the range 0 – 1100 eV to identify all the elements present in the tribofilm. Then, high resolution spectra were obtained with a range of 20 eV for all the elements and a pass energy of 23.5 eV. The chemical species corresponding to different binding energy values are attributed using XPS handbook and various references. The peaks are fitted with a Shirley background and the quantification is done with various sensitivity factors [4]. All other parameters like peak area ratio, the difference between the binding energy of the doublets and

the FWHM were fixed for respective contributions to get accurate composition of the tribofilm. All the peaks were fitted and analysed using PHI Multipak software.

This instrument is generally used to identify the different elements present in different oxidation states quantitatively present on the subsurface in the order of few nanometres like in case of thin tribofilms.

2.2.2.3.4 Transmission Electron Microscopy (TEM):

Morphological characterisation of the tribofilms is carried out using TEM. Also, the elements present in different structures of the tribofilm can be observed as well as quantified from the EDS analyser attached to the TEM.

Microscope used to observe the FIB lamellas of the tribofilms as well as the nanoparticles is a JEOL 2010F operating with an accelerating voltage of 200 kV equipped with EDS. Also, another microscope was used which is an FEI Titan Environmental Transmission Electron Microscope (ETEM), operated at 300 kV accelerating voltage. This ETEM is a Cs corrected instrument. The EDS data was recorded with an EDS detector manufactured by Oxford Instruments. Carbon contaminations were minimized by operating the ETEM in a high vacuum with an active cold-trap. Before each observation, a beam-shower was performed (magnification was reduced and the beam was used to illuminate the sample).

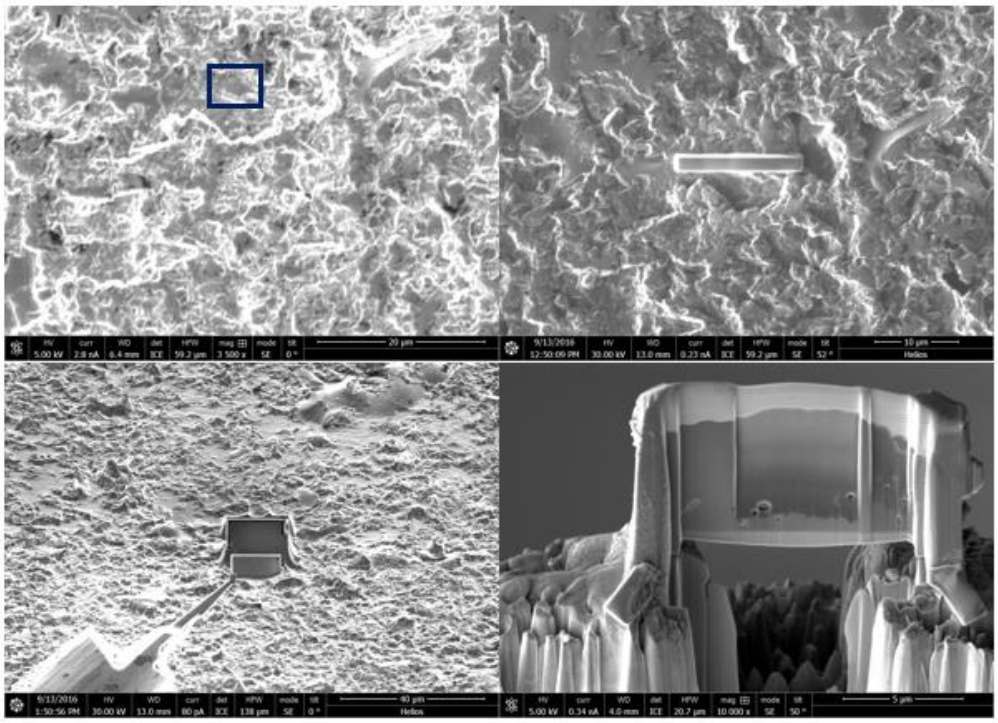

Fig 2.12 Stepwise preparation of the FIB lamella obtained from the tribofilm on the TiO_2 APS disc to be observed in the TEM

For the Focused Ion Beam (FIB) cut, SEM was carried out before to decide upon an area with higher intensity of tribofilm elements in the wear scar. A cross-sectional cut was done using a FIB. To prepare the FIB lamella, a Pt layer was deposited as a protective layer for the tribofilm and then Ga^+ ions were used for nanomachining. Subsequent thinning was carried out to ensure that the lamella is transparent to observe in the TEM. Images of all these steps are shown in the fig 2.12 (starting from the top left to bottom right).

2.3 Coating properties obtained after characterisation:

Generally, the type of thermal spray process as well as the coating deposition parameters influence the microstructure and the properties of the coatings produced. Since in this work, deposition parameters and the process used are fixed, as the APS coatings are manufactured by SUMEBore technology from Oerlikon Metco and Sorevi, their influence on the coating properties is not discussed in detail. Rotaplasma gun is used to coat the different powders on high speed steel / cast iron substrates. Coatings obtained are commercial steel based and ceramic based coatings used for passenger car engines. For this work, three different powders are used to coat the substrates. All the properties obtained after the deposition process like the roughness, porosity, hardness, elastic modulus are discussed in detail. Fused and crushed micron sized powders were used for spraying. Details are listed in table 2.5.

Table 2.5 Powder sizes used for APS process.

Powder	**Spray Powder size (µm)**
Steel	- 45 / + 10
Steel + 30 wt % Mo	- 45 / + 10
TiO_2, fused and crushed	- 25 / + 10

2.3.1 Surface roughness parameters

Roughness parameters for the APS coatings are measured with two different techniques – Stylus analysis (2D) and surface parameters by height (3D), both using the Bruker Interferometer. In this case, only the 2D R parameters are obtained from Stylus analysis in X-direction option. R parameters obtained by Stylus-2D analysis are listed in table 2.6.

Table 2.7 Measured values **for APS coated flats** by Interferometry: (Stylus X analysis – 2D)

APS coating	R_a (µm)	R_Z (µm)	R_k (µm)	R_{pk} (µm)	R_{vk} (µm)
Steel APS	0.14 ± 0.07	0.90 ± 0.10	0.25 ± 0.05	0.26 ± 0.12	0.38 ± 0.45
Steel Mo APS	0.18 ± 0.05	0.80 ± 0.15	0.30 ± 0.05	0.27 ± 0.15	0.32 ± 0.14
TiO_2 APS	0.10 ± 0.02	0.35 ± 0.10	0.17 ± 0.05	0.09 ± 0.06	0.17 ± 0.05

Since different flat materials like flat coupons and discs were used for tribotests and the processes used for surface finishing them was different, roughness parameters are also measured using the above mentioned ways for APS coated discs and they are listed in table 2.7.

Table 2.7 Measured values for **APS discs** by Interferometry: (Stylus X analysis)

APS coating	R_a (µm)	R_Z (µm)	R_k (µm)	R_{pk} (µm)	R_{vk} (µm)
Steel APS	0.17 ± 0.05	0.77 ± 0.5	0.23 ± 0.04	0.25 ± 0.07	0.47 ± 0.1
Steel Mo APS	0.19 ± 0.04	0.80 ± 10	0.26 ± 0.05	0.31 ± 0.06	0.59 ± 0.07
TiO_2 APS	0.11 ± 0.05	0.50 ± 0.20	0.27 ± 0.10	0.09 ± 0.04	0.14 ± 0.05

2.3.2 Physico-chemical and mechanical properties of the coatings:

All the APS coatings are characterised for mechanical properties like hardness and elastic modulus. Also, to know the exact composition and topography of the surface before tribotests, SEM and XPS is carried out. Optical microscopy is used to observe the surface.

2.3.2.1 Steel APS:

Steel APS coating was obtained from micron sized steel powder melted and coated on a high speed steel substrate. Final structure consists of pores, oxide inclusions etc. These pores mostly

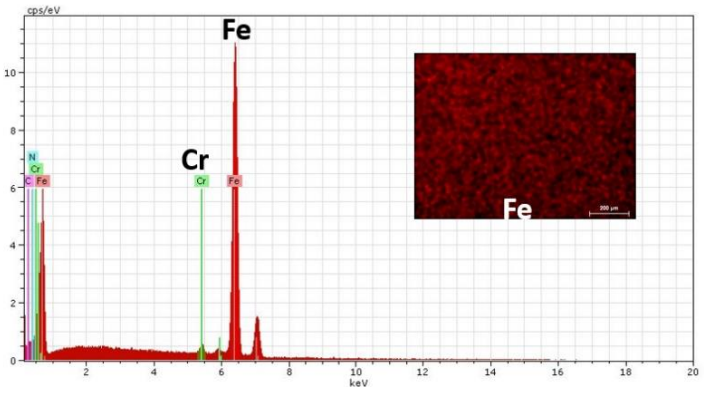

Fig 2.13 SEM-EDS spectra for Steel APS sample with Fe map.

consists of carbon. Homogenous Fe matrix is observed in SEM-EDS as can be observed in the fig 2.13 with some amount of Cr. General XPS spectra of the steel APS coating is shown in fig 2.14. This clearly shows the presence of C, Fe, O on the surface.

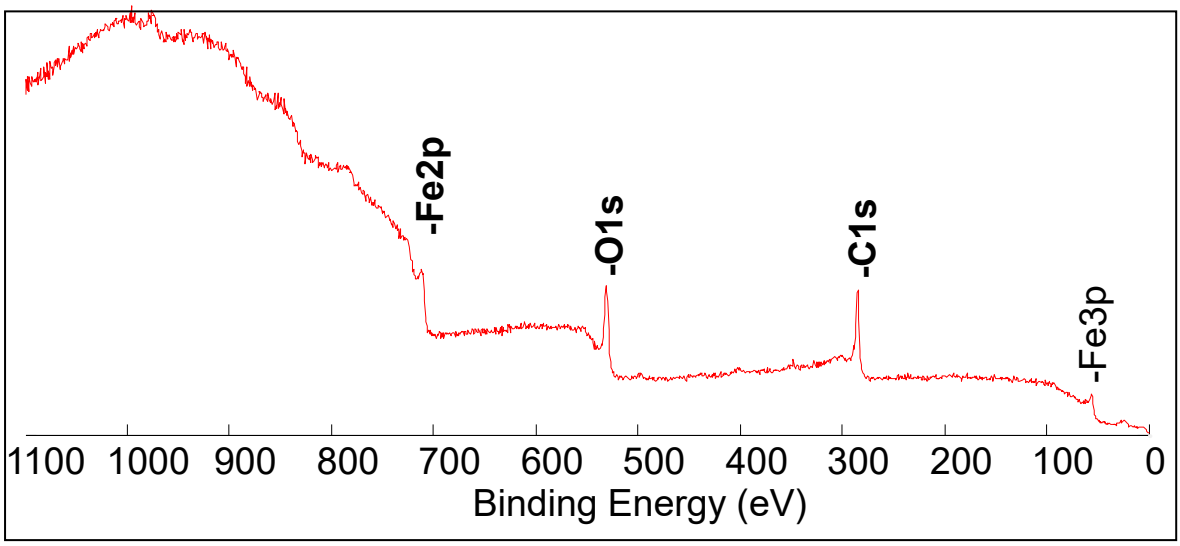

Fig 2.14 General XPS spectra for the Steel APS coating.

Hardness and elastic modulus:

Microindentation is carried out on at least 20 points for both rough and polished samples to minimise the error in measuring hardness and elastic modulus. Loads of 0.5 N and 1 N are used to ensure that there is no effect of substrate on hardness measurements as the thickness of APS coating is hundreds of microns. Optical images on 4 of the 20 points are shown in the fig 2.15. Indentation is clearly observed and the hardness values are found to be in a similar range for all the four points.

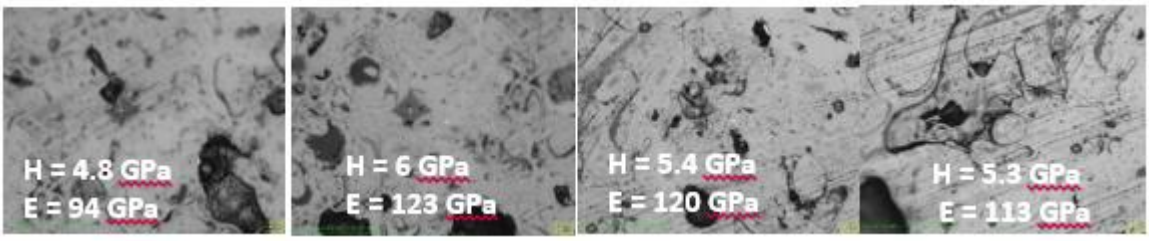

Fig 2.15 Polished Steel APS sample with 0.5 N indents on 4 different points.

Average hardness and elastic modulus values obtained for 0.5 N and 1 N for both rough and polished steel APS coating are summarized in the table 2.8.

Table 2.8. Hardness and elastic modulus at different loads for Steel APS coating.

Type of Steel APS	Load	Hardness GPa	Elastic Modulus GPa
Polished	0.5 N	4.8 ± 1.5	120 ± 30
	1 N	4.5 ± 1.5	110 ± 30
Rough	0.5 N	3.5 ± 1.5	100 ± 20
	1 N	4.5 ± 2	110 ± 20

2.3.2.2 Steel Mo APS coating::

Steel Mo APS coating was obtained from micron (45 µm) sized steel powder mixed with 30 % Molybdenum (45 µm power) and then melted and coated on a high speed steel substrate. Final structure consists of pores, oxide inclusions and patches of Molybdenum. Fe matrix is observed in SEM-EDS with micron sized patches of Molybdenum. These are observed in the fig 2.16. Fe and Mo are present at different locations in the structure which is evident from the SEM-EDS map images. General XPS survey carried out on an area of 100 μm^2 is shown in fig 2.17 and it confirms the presence of Fe as well as Mo throughout the matrix but huge amount of carbon is observed on the surface which could be due to the contamination occurring during the APS process.

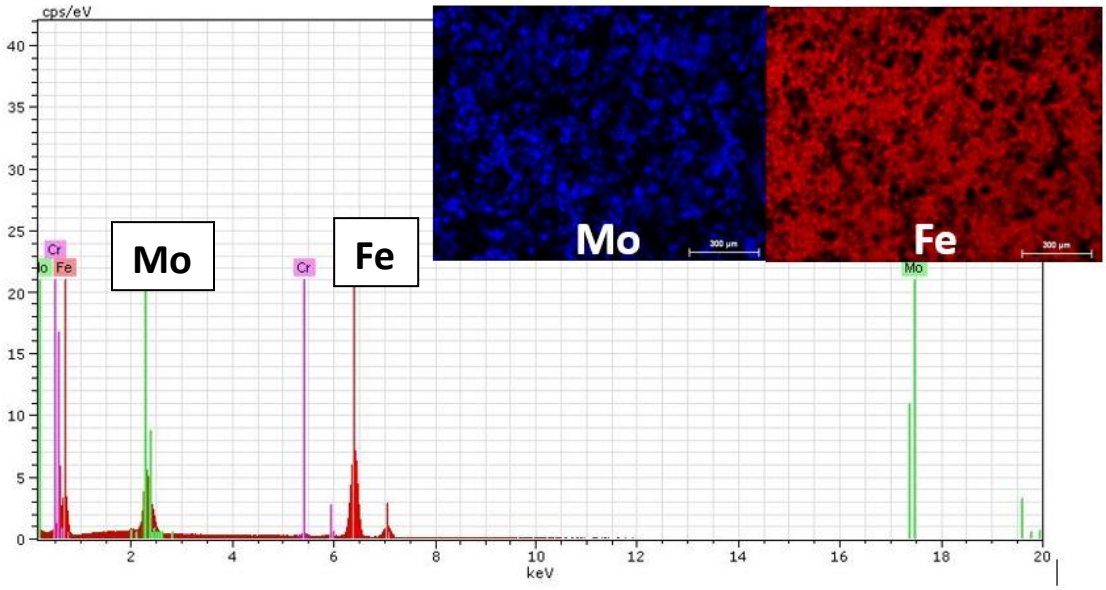

Fig 2.16 SEM-EDS spectra for Steel Mo APS coating with individual maps for Fe and Mo.

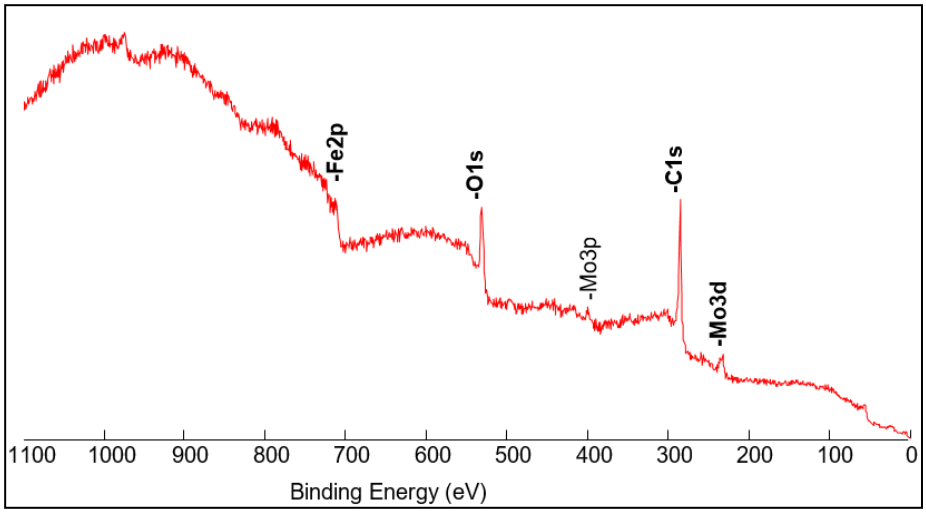

Fig 2.17 General XPS survey spectra for Steel Mo APS coating.

Hardness and elastic modulus:

Microindentation is carried out on at least 20 points for both rough and polished samples to minimise the error in measuring hardness and elastic modulus. Loads of 0.5 N and 1 N are used to ensure that there is no effect of substrate on hardness measurements as the thickness of APS coating is few microns. Patches of Mo showed lower hardness values (1st from the left) than the Fe matrix which can be observed in the fig 2.18. Elastic modulus values in the patches do not show any difference compared to Fe matrix. Since the APS coating is not a bulk material like the reference steel obtained as well as it is mixed with Mo, the elastic modulus obtained is considerably reduced due to the APS process as well as the porosity in the coating. Also, since

the porosity of the coating is not accurately known, the values of the modulii show drastic variations.

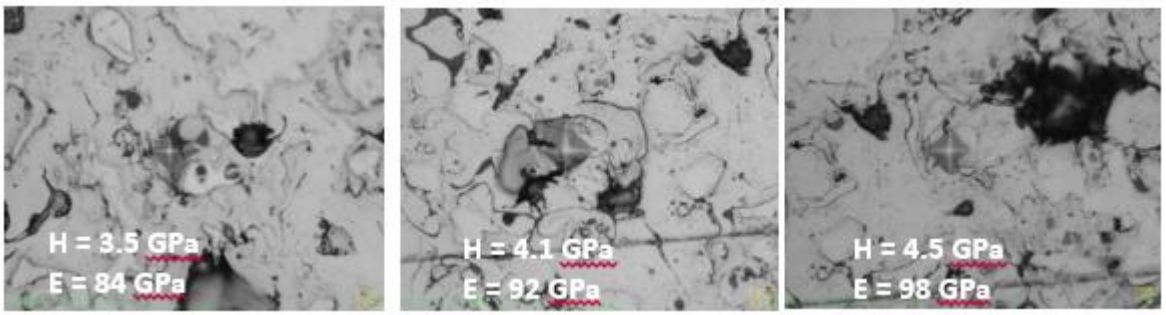

Fig 2.18 Polished Steel APS sample with 0.5 N indents in 3 different positions.

Average hardness and elastic modulus values obtained for 0.5 N and 1 N for both rough and polished Steel APS coating are summarized in the table 2.9.

Table 2.9. Hardness and elastic modulus at different loads for Steel Mo APS coating

Type of Steel Mo APS	Load	Hardness GPa	Elastic Modulus GPa
Polished	0.5 N	4.5 ± 1.5	100 ± 20
	1 N	4 ± 1	90 ± 15
Rough	0.5 N	4.7 ± 1.5	90 ± 15
	1 N	4.5 ± 2	100± 20

2.3.2.3 TiO_2 APS coating:

Micron sized, fused and crushed titanium dioxide powder used for deposition of TiO_2 APS coating was characterised using SEM and Raman spectroscopy. Raman spectra for micron sized powder and for the respective APS coating are compared in Fig 2.19 (a). It can be observed that the powder consists of broad peaks shifted to lower values compared to crystalline TiO_2 rutile. This suggests that the powder is an oxygen deficient powder with a stoichiometry of TiO_x. (x = 1.95 - 1.98). This can be confirmed from the black colour of the powder which is also due to its non-stoichiometry. However, Raman spectrum of the TiO_2 APS coating shows distinct and sharper peaks at the rutile positions confirming the crystallinity of the coating[6].

XRD of TiO_2 APS coating is shown in fig 2.19 (b). It can be clearly observed that the diffraction pattern consists of peaks assigned to planes in rutile phase of TiO_2 compared to JCPDS 88-

1175 card for rutile. Sharp peaks are observed at 27°, 36° and 55° indicating the presence of TiO_2 in rutile phase. Since the APS process is carried out in atmosphere, it could be that the non-stoichiometric TiO_x powder gets oxidised with x reaching close to 2.

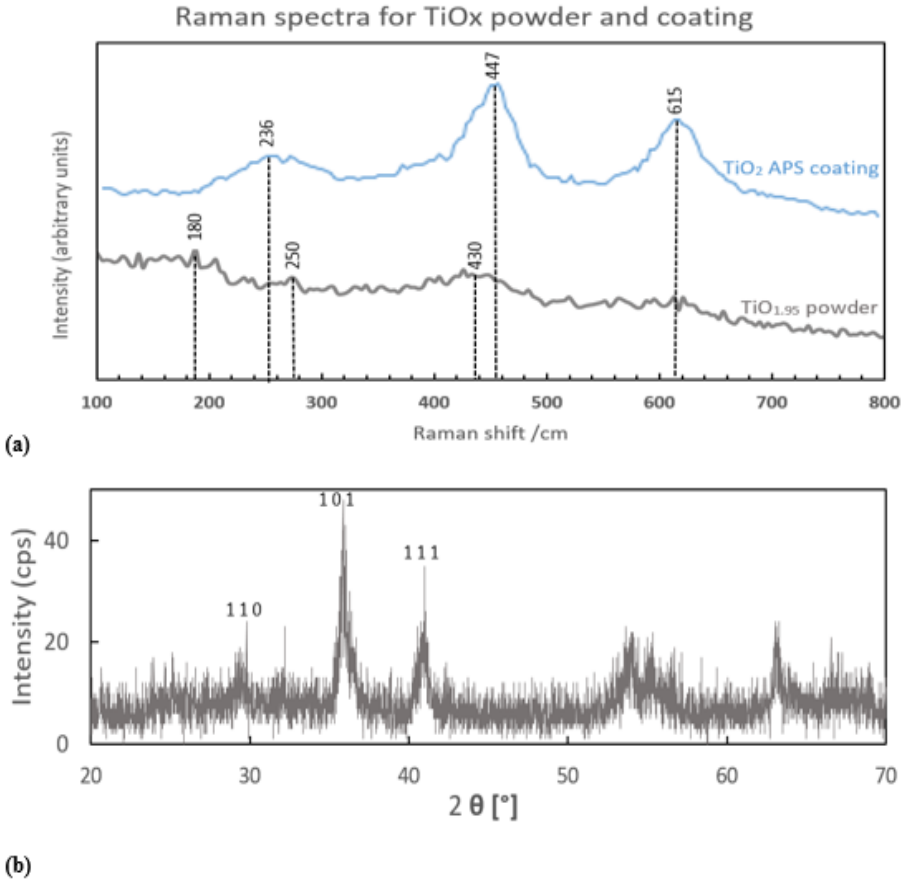

Fig 2.19 (a) Raman spectra of the commercial fused and crushed micron sized TiO_x powder (black) used for the APS process and the corresponding TiO_2 coating (blue). (b) X-ray diffraction pattern of the commercial TiO_2 APS coating.

SEM micrographs for the fused and crushed powder of titanium dioxide are shown in fig 2.20 (a) and (b). It can be clearly observed that the particles are irregular in shape and the size of the particles is around 25 µm. SEM images were also obtained for the TiO_2 APS coating and are shown in fig 2.20 (c) and (d). SEM images show the formation of splats used for oil retention, coarse and fine pores on the as-deposited APS coating. The presence of TiO_2 can be confirmed from amount of titanium and oxygen present in SEM EDS which are in the ratio 1:2. SEM micrograph along with the EDX spectra showing the presence of Ti and O is shown in fig 2.20 (e). Final structure is quite dense as the particle size is lower than steel based APS coatings.

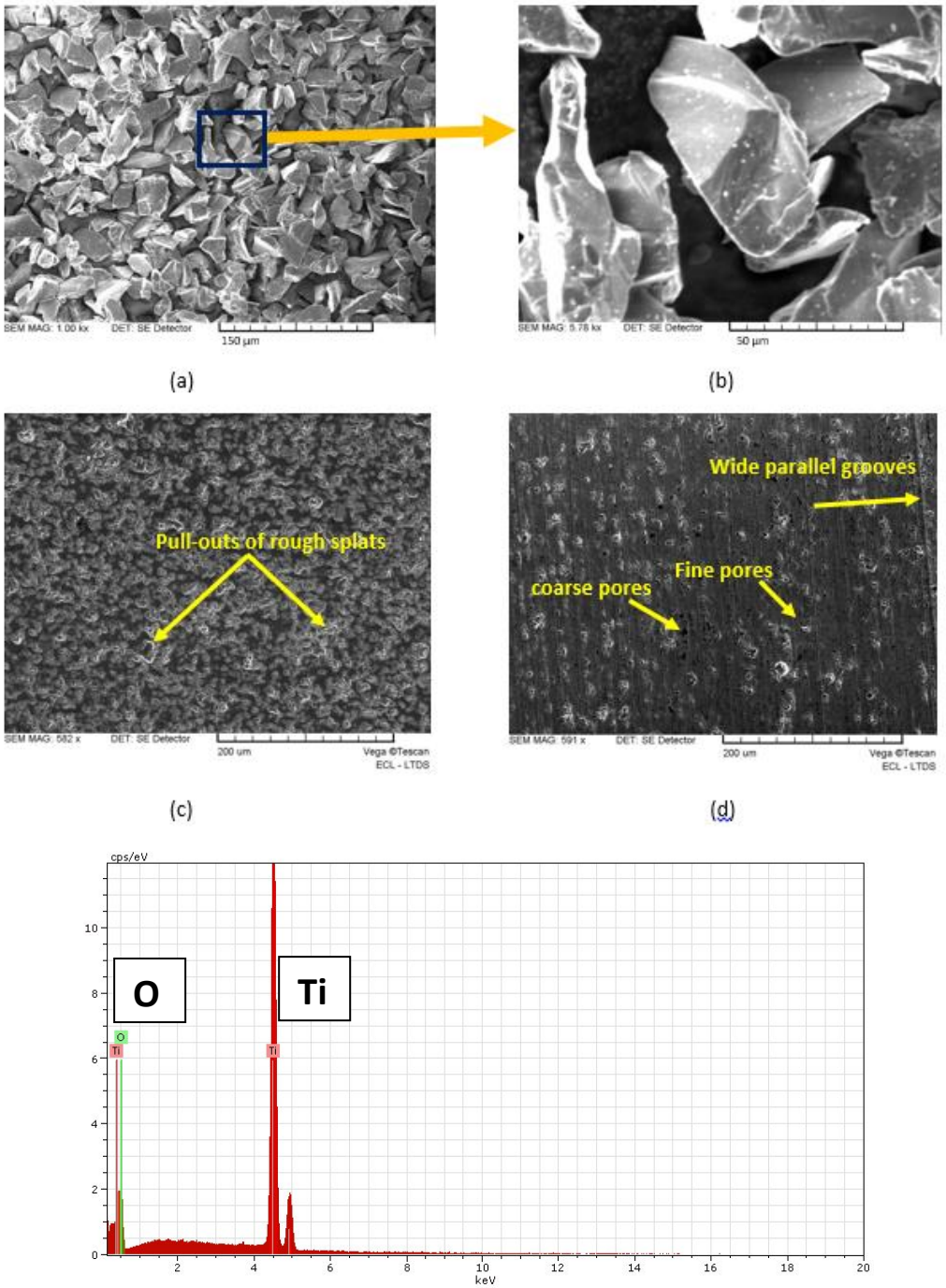

Fig 2.20. (a) Morphology of as-received $TiO_{1.95\text{-}1.98}$ fused and crushed powder used for the APS coating (b) enlarged view of the irregular shape powder particles (c) SEM micrograph of TiO_2 disc produced by the APS process showing the pull-outs used for oil retention (d) SEM micrograph of TiO_2 flats with a certain direction of wide parallel grooves. (e) SEM-EDS spectra for TiO_2 APS coating.

General XPS survey carried out on 100 μm^2 area confirms the presence of Ti and O throughout the matrix. Also, high resolution scan of Ti shows that titanium is only present in oxide form

as the titanium 2p peak is fitted using a binding energy value of 458.5 eV assigned to oxide contribution of TiO_2. This is shown in fig 2.21 and 2.22 respectively.

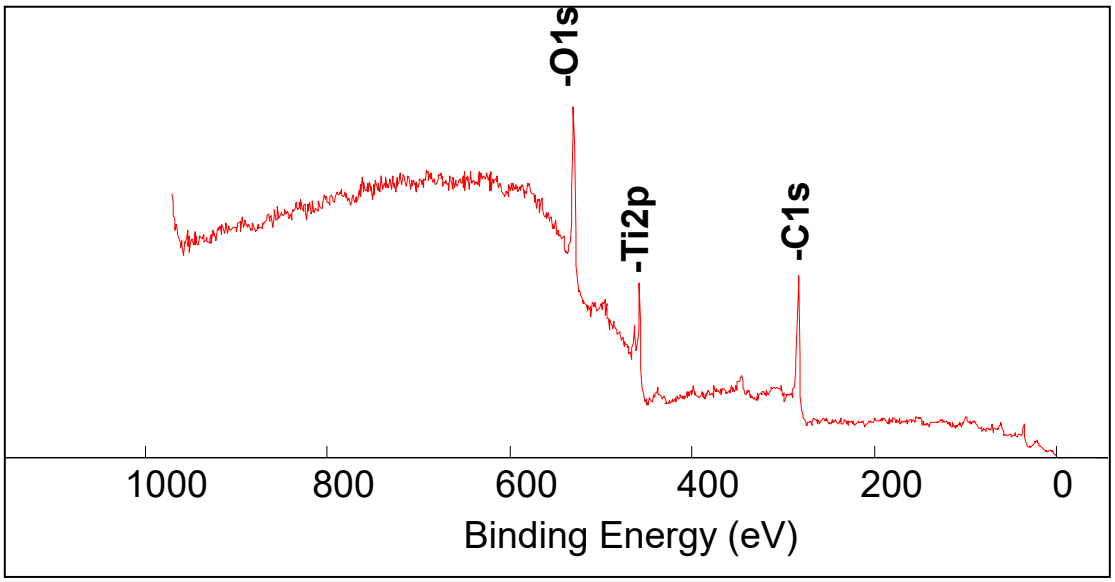

Fig 2.21 XPS survey spectra for TiO_2 APS coating.

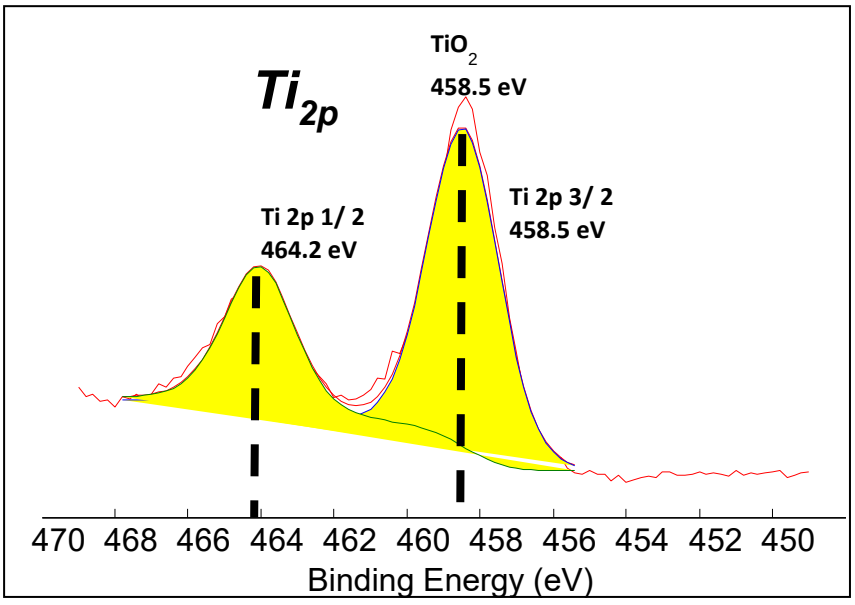

Fig 2.22 XPS spectra for Ti2p contribution shows titanium is present in oxide form.

Hardness and Elastic modulus:

Average hardness and elastic modulus values obtained for 0.5 N and 1 N for both rough and polished TiO_2 APS coating are summarized in the table 2.10. TiO_2 APS coating showed higher hardness as well as elastic modulus compared to steel based coatings steel APS and Steel Mo APS. This was expected as the bulk TiO_2 rutile is harder than steel. However, around 30-35 %

reduction was observed in case of the elastic modulus of the TiO_2 APS coating which could be attributed to the pores present.

Table 2.10. Hardness and elastic modulus at different loads for TiO_2 APS coating

Type of TiO_2 APS	Load	Hardness GPa	Elastic Modulus GPa
Polished	0.5 N	7.5 ± 1.5	155 ± 10
	1 N	7.3 ± 1.5	152 ± 15
Rough	0.5 N	7 ± 1.5	160 ± 20
	1 N	7 ± 1	155 ± 20

2.4 Summary:

In this chapter, materials used for various tribotests were discussed. This was followed by detailed explanation of all the experimental methods used to study tribological behaviour of piston ring-cylinder liner contact on a laboratory scale with the inputs and outputs and the purpose of using a specific configuration. Test profiles are developed on these equipments to use conditions as close to the real engine conditions as possible.

Second part detailed about the various characterisation techniques used before and after the tribotests to analyse the surface topography, composition, mechanical properties as well as investigate the tribochemistry by analysing the tribofilm structure and composition.

The surface, mechanical and physico-chemical properties of the materials used in this study were measured by various characterisation techniques. These properties are listed along with detailed description for the characterisation of each of the APS coating. Hardness, elastic modulus, roughness parameters and surface composition using SEM and XPS before tribotesting for all the APS coatings are mentioned and discussed.

2.5 References:

[1] Fujita H, Glovnea R. P, Spikes H, Part 1 Experimental 'Tribology Transations' Vol 48, 558-566, 2005.

[2] Wiora D. G, Weber M. & Chanbai S. in Encyclopedia of Tribology (eds. Wang, Q. J. & Chung, Y.W.) 2483–2488

[3] Oliver W.C. and Pharr G.M., J. Mater. Res. 7, 1564 (1992).

[4] Wagner C.D, Davis L.E, Zeller M.V, Taylor J.A, Raymond R.H, Gale L.H, Empirical atomic sensitivity factors for quantitative analysis by electron spectroscopy for chemical analysis, Surface and Interface analysis, Vol.3(5), 211-225, 1981.

[5] Spikes H 'The History and Mechanisms of ZDDP'. Tribology Letters 17, 469-489 (2004).

[6] Wang J, Zhang Q, Yin S, Sato T, Saito F. Raman spectroscopic analysis of sulphur doped TiO_2 by co-grinding with TiS2. Journal of Phys Chem Solids 2007;68: 189–92.

Chapter 3

Tribological behaviour of reference steel and APS coatings under boundary lubrication conditions using various test configurations

This chapter shows the tribological results obtained for steel sliding against reference steel and APS coatings with various test configurations like ball-on-flat, ball-on-disc (MTM) and ring-on-liner which resemble the piston ring- cylinder liner engine contact on a laboratory scale. The main aim of this chapter is to find out the APS coating with the best tribological properties. Contacts were lubricated with base oil alone and then with MoDTC and ZDDP as well as the combination of both the additives. Results obtained with different configurations were compared and the conclusion was made regarding the use of various configurations.

3.1 Ball-on-flat tribotests

3.1.1 Experimental

Reference steel, TiO_2 APS, steel APS, steel Mo APS coatings were used as flat materials. Reference steel flats and balls were made of AISI 52100 steel. The average surface roughness (R_a) of the reference steel flat is less than 20 nm and of the reference steel ball is less than 40 nm. Standard group III mineral oil is used as a base oil with MoDTC and ZDDP additives. The additives were used alone and then in combination with each other in base oil in specific concentrations as shown in the table 3.1. The concentration of the additives were decided by taking into account the concentrations used in the commercial TOTAL lubricants that contain MoDTC and ZDDP.

Table 3.1 List of lubricants used for tribotests.

Lubricant	Designation
Base oil	BO
Base oil + 1 % ZDDP	BO + ZDDP
Base oil + 0.5 % MoDTC	BO + MoDTC
Base oil + 1 % ZDDP + 0.5 % MoDTC	Base oil + MoDTC + ZDDP

The roughness parameters for steel APS, steel Mo APS and TiO_2 APS coated flats used for this type of tribotest are recalled in table 3.2. Also, the hardness and elastic modulus are recalled. Thickness of steel APS, steel Mo APS and TiO_2 APS coatings were 60 µm, 180 µm and 70 µm respectively. All the properties are listed in table 3.2.

Table 3.2 Surface roughness parameters and the mechanical properties for the APS coated flats.

APS coating	R_a (µm)	R_k (µm)	R_{pk} (µm)	R_{vk} (µm)	Hardness (GPa)	Elastic modulus (GPa)
Steel APS	0.19 ± 0.05	0.30 ± 0.05	0.26 ± 0.12	0.49 ± 0.10	5 ± 2	130 ± 30
Steel Mo APS	0.18 ± 0.07	0.29 ± 0.05	0.24 ± 0.10	0.52 ± 0.05	4 ± 2	110 ± 30
TiO_2 APS	0.12 ± 0.02	0.17 ± 0.05	0.09 ± 0.06	0.17 ± 0.05	7 ± 1	160 ± 20

Reciprocating sliding tests were carried out with reference steel (AISI 52100) balls against reference steel flats, steel APS flats, steel Mo APS flats and TiO_2 APS flats. Temperature of 100°C with a sliding speed of 0.05 m/s and a maximum Hertzian contact pressure of 0.7 GPa for 1 hr is used. All the tests were repeated for at least two times to confirm the reproducibility of the results. From the Hertzian theory of contact mechanics, normal loads were adjusted taking into account the elastic moduli estimated from the micro-hardness tests. Also, to ensure that the tests are carried out in boundary or mixed lubrication conditions, lambda ratio was calculated. Conditions used for the ball-on-flat tribotests are mentioned in the table 3.3 below. Wear scar diameters on the balls and the wear scar width on the flats were measured using an optical microscope. Wear scar diameter on the ball and the wear scar width on the flats / discs were compared with the respective Hertzian diameters.

Table 3.3 Ball-on-flat tribotest conditions

Normal Load	6 N – Reference steel, 9 N – Steel APS, 11 N – Steel Mo APS, 7 N – TiO_2 APS
Lambda ratio	Steel = 2 mixed lubrication; Steel APS = 0.9; boundary lubrication Steel Mo APS = 0.95; boundary lubrication TiO_2 APS = 0.95; boundary lubrication
Temperature	100 ° C
Frequency and stroke length	5 Hz and 5 mm
Max Pressure	0.7 GPa
Test duration	1 hr, 18000 cycles
Ball material **Flat material**	AISI 52100 Steel AISI 52100 Steel, Steel APS Steel Mo APS, TiO_2 APS

3.1.2 Results and discussion

Fig 3.1 (a), (b), (c) and (d) shows the friction behaviour of steel / reference steel, steel / TiO_2 APS, steel / steel APS and steel / steel Mo APS respectively under lubricated conditions (mentioned in table 3.3). The test results shown are for one of the two repetitions carried out for each lubricant.

In case of reference steel, steady state friction coefficient obtained is 0.12 when lubricated with base oil. In case of all other contacts lubricated with base oil, the friction coefficient obtained is higher (0.13 - 0.14). Addition of ZDDP in the base oil reduces the friction coefficient by a certain extent in all the contacts. Addition of MoDTC in the base oil reduces the friction coefficient to 0.05 – 0.06 in case of steel / reference steel, steel / steel APS and steel / steel Mo APS. It should be noted that the roughness parameters in case of reference steel and steel based APS samples are considerably different. Average friction coefficient is calculated for a steady state regime after 5000 cycles. It is slightly lower in case of rough steel based APS and steel Mo APS than that compared to reference steel. However, in case of TiO_2 APS sample, lowest friction coefficient of 0.04 is obtained from the beginning of the test with almost no induction time. Also, smoother friction curves are obtained in case of steel / reference steel and steel / TiO_2 APS compared to the steel based APS contacts. This could be attributed to the high roughness of steel based APS flats that causes high wear on the ball continuously during the test. Addition of both the additives in the base oil shows higher steady state friction coefficient in all the contacts than when the contacts were lubricated with only MoDTC.

Another striking difference between the friction behaviour of the contacts is that the steel based APS contacts requires higher time compared to TiO_2 APS to reach lower friction when lubricated with base oil + MoDTC as well as base oil + MoDTC + ZDDP.

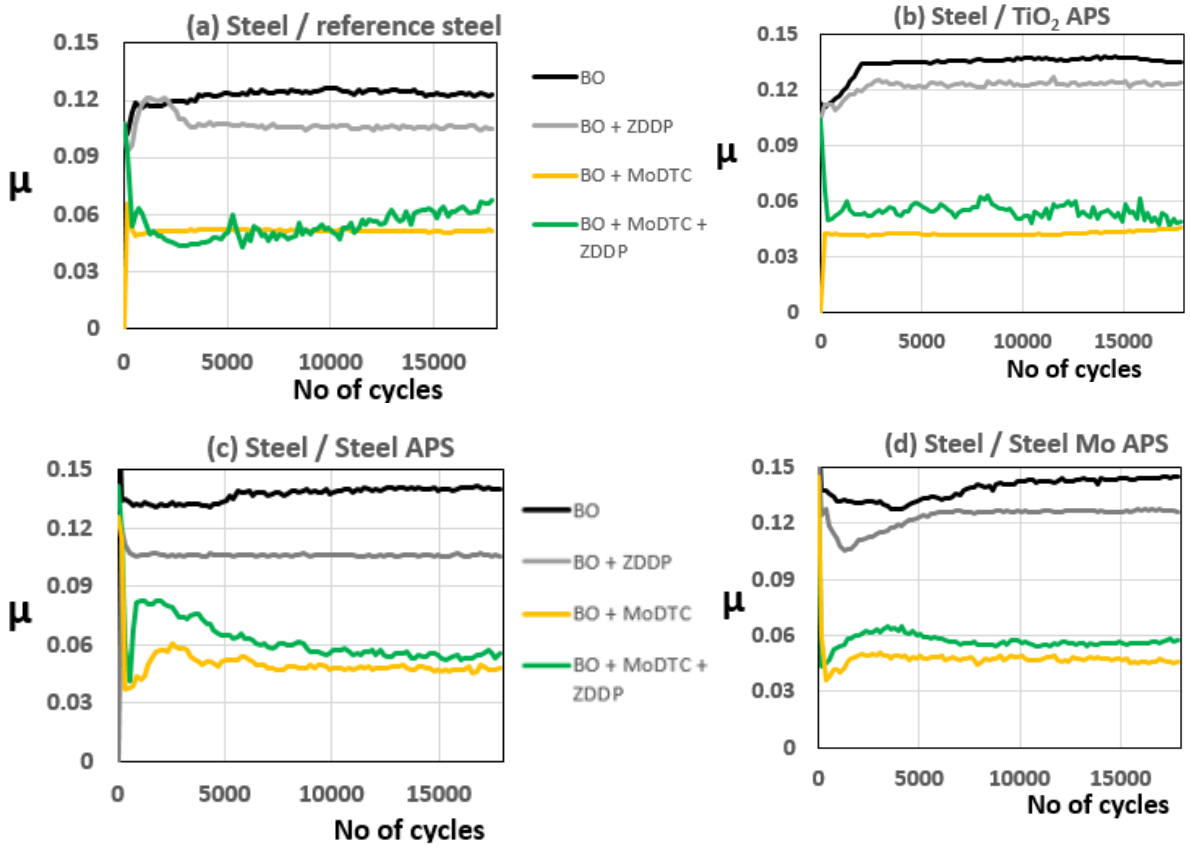

Fig.3.1 Friction curves in presence of base oil and base oil + 0.5 % MoDTC for (a) Steel / Reference steel (b) Steel / Steel APS (c) Steel / TiO_2 APS tested on ball-on-flat tribometer

Steady state friction trends obtained for all the contacts lubricated with base oil, base oil + MoDTC, base oil + ZDDP and base oil + ZDDP + MoDTC are shown in the fig 3.2. It can be observed that steel / TiO_2 APS contact (encircled with red) shows the best friction behaviour when lubricated with base oil + MoDTC.

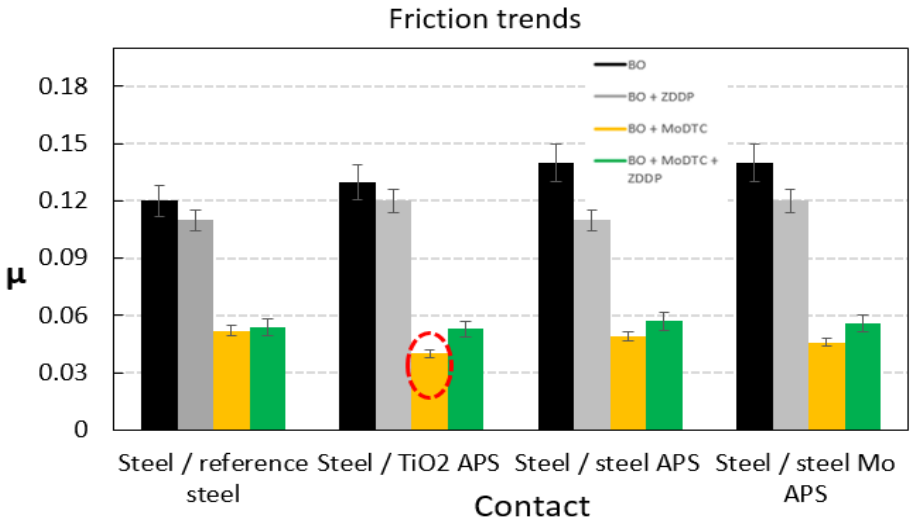

Fig. 3.2 Friction trends for steel / reference steel, steel / TiO_2 APS, steel / steel APS and steel / steel Mo APS contacts lubricated with base oil, base oil + ZDDP, base oil + MoDTC and base oil + ZDDP + MoDTC.

From the Hertzian theory of contact mechanics, Hertzian diameters calculated for steel / reference steel, steel / TiO_2 APS steel / steel APS and steel / steel Mo APS are 126 µm, 145 µm, 160 µm and 178 µm respectively. As the Hertzian diameter is not the same for the different tribopairs, percentage of wear above the Hertzian diameter is shown to make the comparison easier. Comparison of the wear on the steel balls for all the contacts lubricated with base oil, base oil + ZDDP, base oil + MoDTC and base oil + ZDDP + MoDTC is shown in fig 3.3. It can be observed that high wear is observed in case of steel / reference steel and steel / steel APS contacts when lubricated with base oil. As the anti-wear additive ZDDP is added in the base oil, the wear is drastically reduced in all the steel based contacts (steel / reference steel, steel / steel APS and steel / Mo APS). Also, when the steel based contacts are lubricated with the combination of MoDTC and ZDDP, the friction is reduced due to MoDTC and the wear is also reduced due to ZDDP [1–4]. However, in case of steel / TiO_2 APS, the percentage wear above the Hertzian diameter is similar for all the lubricants. Therefore, it can be concluded that there is no reduction in wear observed when ZDDP is used alone or in combination with MoDTC in case of steel / TiO_2 APS.

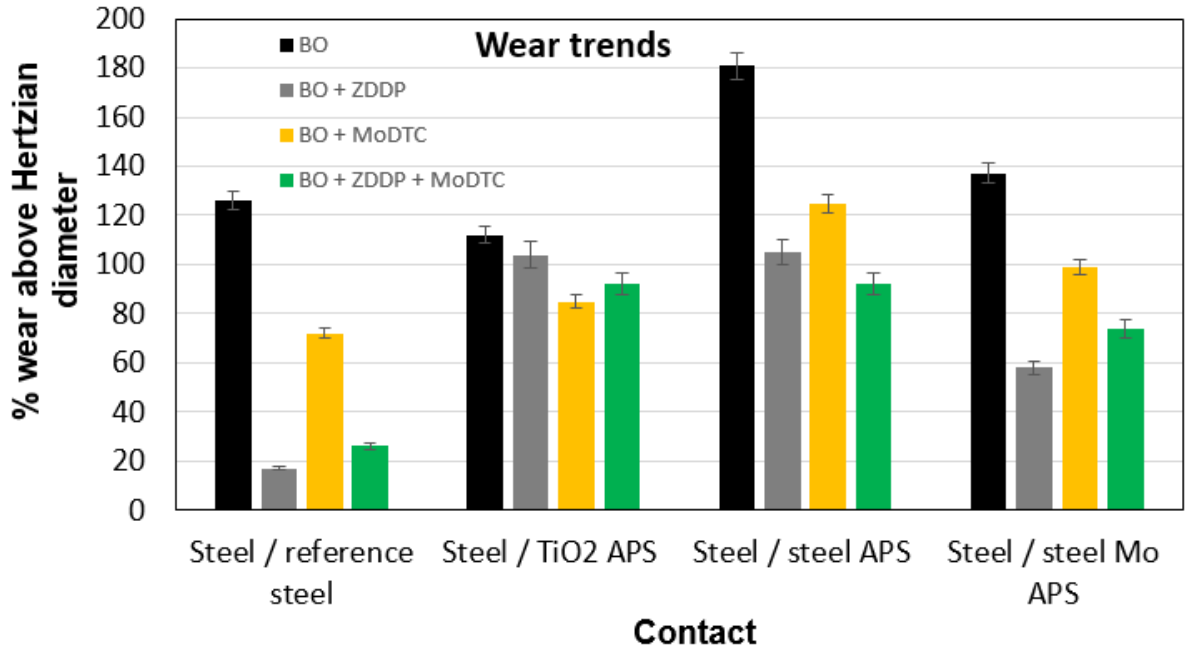

Fig 3.3 Comparison of percentage wear on the steel balls above Hertzian diameter for steel / reference steel, steel / TiO_2 APS, steel / steel APS and steel / steel Mo APS contacts lubricated with base oil, base oil + ZDDP, base oil + MoDTC and base oil + ZDDP + MoDTC.

From the friction and wear results obtained, it is clear that steel / TiO_2 APS contact shows the lowest average friction coefficient when it is lubricated with base oil + MoDTC. All the other contacts involving steel show higher friction coefficient. This difference in behaviour could be due to use of different counterpart material in TiO_2 APS as compared to steel based materials. This change in chemistry of the material could affect the tribochemistry.

Synergy is observed in case of steel / steel in terms of friction and wear behaviour when ZDDP and MoDTC are mixed together in base oil. This is not the case with other contacts like steel / steel APS, steel / steel Mo APS and steel / TiO_2 APS where it is observed that the friction is a bit higher when MoDTC and ZDDP are mixed together compared to only MoDTC. Also, for steel / TiO_2 APS contact, expected wear reduction is not observed for MoDTC + ZDDP and in fact the wear is a bit higher than with only MoDTC or ZDDP. Another striking feature observed in steel / TiO_2 APS contact is that the % wear above Hertzian diameter is in the same range whatever the lubricant used compared to other contacts where the additives like ZDDP when added in the base oil reduce the wear considerably. Lubrication even with only base oil shows wear reduction compared to steel / reference steel contact. This implies that the coating shows some wear reducing properties by itself. This different tribological behaviour in case of

steel Mo APS and TiO_2 APS coatings suggests that the chemistry of the coatings is playing an important role in controlling the friction and wear obtained at the end of the test.

3.2 MTM (Mini – Traction Machine ball-on-disc) tribotests:

To study the kinetics of tribofilm formation and growth and also the effect of SRR on the tribological behaviour of the contacts, MTM tribotests were carried out.

3.2.1 Experimental

The previous reciprocating tests with the ball-on-flat configuration used base oil, MoDTC, ZDDP and a combination of both as lubricants. It was found that steel / TiO_2 APS contact lubricated with base oil + MoDTC showed the best friction and wear behaviour compared to other APS coatings. To investigate more on the kinetics and growth of tribofilm formation when the contacts are lubricated with base oil + 0.5 % MoDTC, ball-on-disc tribotests were carried out using a commercial Mini – Traction Machine (MTM). Disc materials used were rough reference steel, steel APS, steel Mo APS and TiO_2 APS coatings. The roughness parameters for the discs were presented in chapter 2. Test conditions used are mentioned in table 3.5.

Table 3.4. MTM test conditions

Temperature	110°C
Speed	0.4 m/s
Pressure	750 MPa
Normal load	15 N (steel / reference steel) 20 N (steel / TiO_2 APS) 26 N (steel / steel APS) 32 N (steel / steel Mo APS)
Disc material	Reference steel (Ra = 150 nm)
	TiO_2 APS disc (Ra = 120 nm)
Ball material	Reference Steel (Ra = 20 nm) Diameter = 19.5 mm
SRR %	100 %
Lubricant	Base oil + 0.5 % MoDTC

The test profile included a traction curve in the first step where the SRR (Slide to Roll Ratio) was increased from 5 % to 100 %. Alternate ball-on-disc friction and SLIM (3D Space Layer Imaging) steps are included in the test profile to study the kinetics and evolution of the tribofilm on the steel ball. Ball-on-disc friction steps are carried out with a rolling speed of 0.4 m/s and a SRR of 100 %. For the SLIM imaging steps, the ball is unloaded and using interferometry, images are recorded to measure the thickness of the film [5]. Also, SRR used is 100 % which means it is a 50 % sliding - 50 % rolling contact. Lubricant used was base oil + 0.5 % MoDTC at a maximum Hertzian contact pressure of 0.75 GPa for all the tribotests and the results were compared for all the contacts.

3.2.2 Results and discussion

Fig 3.5 (a), (b), (c) and (d) show the friction behaviour of steel / reference steel, steel / TiO_2 APS, steel / steel APS and steel / steel Mo APS respectively lubricated with base oil + 0.5 % MoDTC. In case of steel / reference steel, steady state friction coefficient obtained is 0.05. For all the steel based contacts (steel APS and steel Mo APS), steady state friction coefficient values obtained are in the range of 0.055 – 0.065. A certain amount of time is required to reach steady state friction coefficient in case of steel and steel Mo APS which could be due to the rough discs where the asperity peaks get removed at the beginning of the test. Steel / TiO_2 APS contact shows the lowest steady state friction coefficient of 0.04 from the beginning of the test.

SLIM images are taken alternately along with ball-on-disc friction steps. Images of four different steps are selected and shown for all the contacts in the fig 3.4. It is observed that the kinetics of tribofilm formation and growth is faster in case of steel / TiO_2 APS than the other steel based contacts which is evident from the friction curves as the friction coefficient is lower from the beginning. Also, steel / reference steel contact requires certain amount of time during the test to reach a steady state friction coefficient which is not the case with TiO_2 APS. This is in agreement with the SLIM images on the steel ball sliding against reference steel disc as they show no tribofilm formation in the beginning of the test. MoDTC additive requires some induction time to get activated and form the low friction tribofilm in case of reference steel. While, in case of steel / TiO_2 APS, the tribofilm is formed from the beginning of the test which suggests that MoDTC is activated and forms low friction tribofilm ($\mu = 0.04$). Steel / steel APS shows similar behaviour as observed in case of reference steel. However, steel / steel Mo APS contacts showed thick tribofilm formation and so the friction coefficient observed is a bit lower compared to steel APS. However, the average friction coefficient is higher in both the steel

based APS contacts compared to TiO_2 APS. All the friction curves show some spikes which are due to alternate unloading of the ball for the SLIM imaging steps.

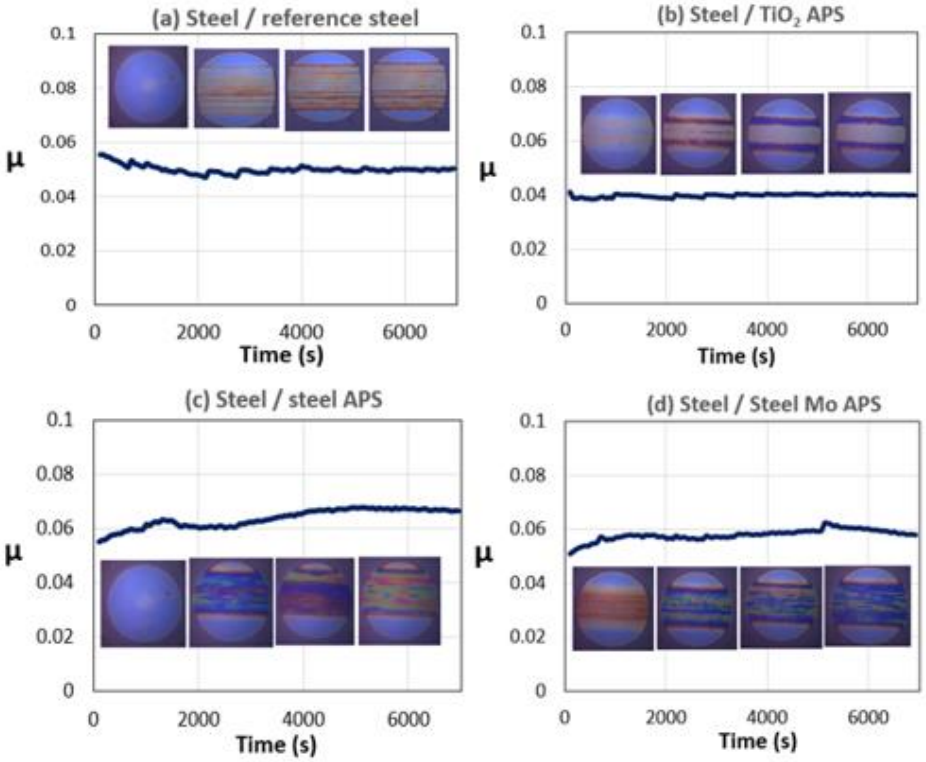

Fig 3.4 Friction curves in presence of base oil and base oil + 0.5 % MoDTC for (a) Steel / Reference steel (b) Steel / Steel APS (c) Steel / TiO_2 APS tested on ball-on-disc MTM tribometer.

Steady state friction trends for all the contacts lubricated with base oil + 0.5 % MoDTC are shown in the fig 3.5. It can be observed that steel / TiO_2 APS contact shows the best friction behaviour ($\mu = 0.04$). The steady state friction coefficients observed for all the other steel based contacts are much higher ($\mu = 0.05 – 0.063$) compared to steel / TiO_2 APS contact ($\mu = 0.04$). As discussed earlier, it also shows faster kinetics of tribofilm formation and growth compared to other steel based contacts.

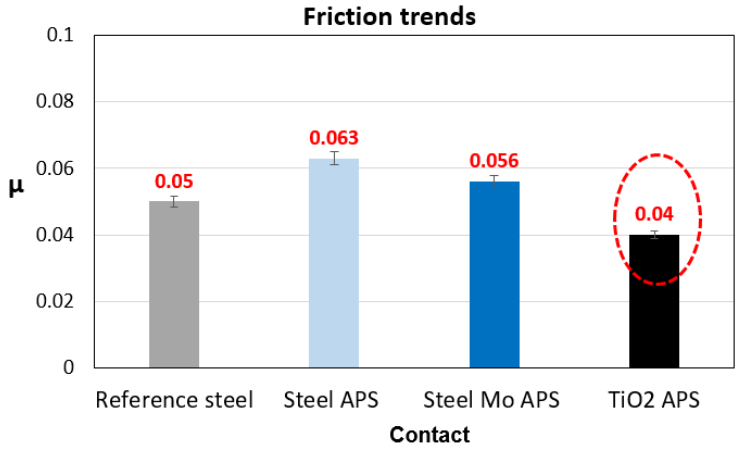

Fig 3.5 Friction trends for steel / reference steel, steel / steel APS, steel / steel Mo APS and steel / TiO_2 APS contacts lubricated with base oil + 0.5 % MoDTC.

Fig 3.6 shows the wear trends on the steel ball and the respective discs sliding against them when the contacts are lubricated with base oil + 0.5 % MoDTC. Steel / TiO_2 APS contact shows the lowest wear on both the disc and the ball (< 20 % above the Hertzian diameter). It can be observed that high wear is obtained in case of steel balls tested against steel and steel Mo APS which could be due to the high roughness of the discs that generate lot of deep scratches on the balls. In case of steel / reference steel contact, the wear is minimal on both the counterparts but still higher than in case of steel / TiO_2 APS contact.

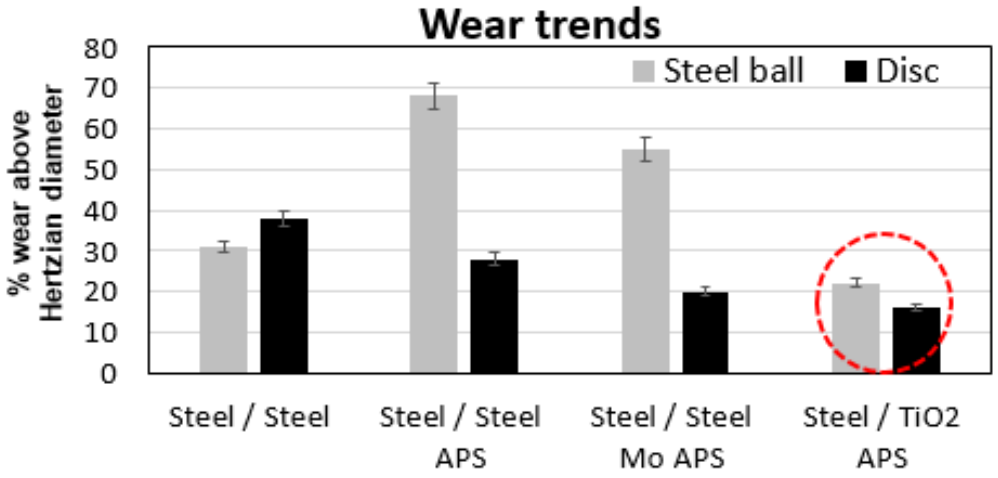

Fig 3.6 % wear above Hertzian diameter for steel ball / reference steel disc, steel / steel APS, steel / steel Mo APS and steel / TiO_2 APS contacts lubricated with base oil + 0.5 % MoDTC.

It can be concluded that average friction coefficient as well as the % wear above Hertzian diameter on the ball and disc is the lowest in case of steel / TiO_2 APS when the contact is lubricated with base oil + 0.5 % MoDTC. Faster kinetics of tribofilm formation and growth is

observed in steel / TiO_2 APS and steel / steel Mo APS compared to steel / steel and steel / steel APS evident from the SLIM images shown on top of the corresponding friction curves. Extremely thick tribofilms are formed on the steel ball in case of steel APS and steel Mo APS which could be due to the rough counterpart material leading to higher asperity asperity contact and faster tribofilm formation. However, the rough counterpart material causes higher wear on the ball as well as the friction coefficient is higher in these coatings. In case of steel / TiO_2 APS the tribofilm is formed from the beginning of the test as well but the wear is lower whatever the lubricant used. As discussed earlier, this could be due to the chemistry of the TiO_2 APS coating that helps in reducing the wear.

3.3 Ring-on-liner tribotests

3.3.1 Experiments:

Considering the previous results obtained with TiO_2 APS coatings and also to investigate the tribological behaviour of TiO_2 APS coatings in conditions as well as geometry of the parts close to real applications, ring-on-liner reciprocating tribotests were carried out with the commercial iron phosphate coated piston ring against TiO_2 APS liners on modified PLINT TE 77 tribometer. Liner parts were obtained by cutting TiO_2 APS liners. The roughness parameters for the liners are mentioned in the table 3.6. The roughness parameters are different in this case as the process used for obtaining the desired surface is surface honing and not grinding used for flats and discs in the previous tests. Ring-on-liner reciprocating tests are carried out to investigate the behaviour of TiO_2 APS coating in real engine conditions which are obtained from the literature [6-7]. Conditions used for the PLINT tribometer are mentioned in the table 3.7.

Table 3.6 Roughness parameters for the liners used

Liner	R_a (µm)	R_k (µm)	R_{pk} (µm)	R_{vk} (µm)
TiO_2 APS	0.14 ± 0.04	0.14 ± 0.09	0.16 ± 0.07	0.25 ± 0.05

Table 3.7 Ring-on-liner tribotest conditions

Temperature	150°C
Amplitude	3 mm
Time / Frequency	1.5 hrs / 5 – 40 Hz
Pressure	50 MPa
Normal Load	250 N for TiO_2 APS liner
Liner material	TiO_2 APS liner
Lubricants	Base oil + 0.5 % MoDTC

Detailed description of the PLINT tribometer used for ring-on-liner reciprocating tribotests is given in the Chapter 2.

Procedure used for the ring-on-liner reciprocating test is shown in the fig 3.7. Similar conditions are used such as to mimic the real engine contact. It consists of initial running-in period where the temperature, load and frequency are gradually increased to the final desired values of 150°C, 220 N and 40 Hz respectively. The test profile includes four cycles. Each cycle consists of the ring sliding on the liner for 2 minutes at five different frequencies of 40 Hz, 20 Hz, 10 Hz, 5 Hz and 2.5 Hz. This is done to evaluate the friction behaviour of the tribopairs at different speeds and therefore different lubrication regimes which exist in a real ring-liner contact in an engine. Ring-on-liner reciprocating sliding steps at various frequencies are carried out and the friction behaviour is obtained for the duration of the test. Lubricant used was base oil + 0.5 % MoDTC. Tests were carried out at a maximum Hertzian contact pressure of 50 MPa. Wear scars on the rings and the liners were analysed using an optical microscope.

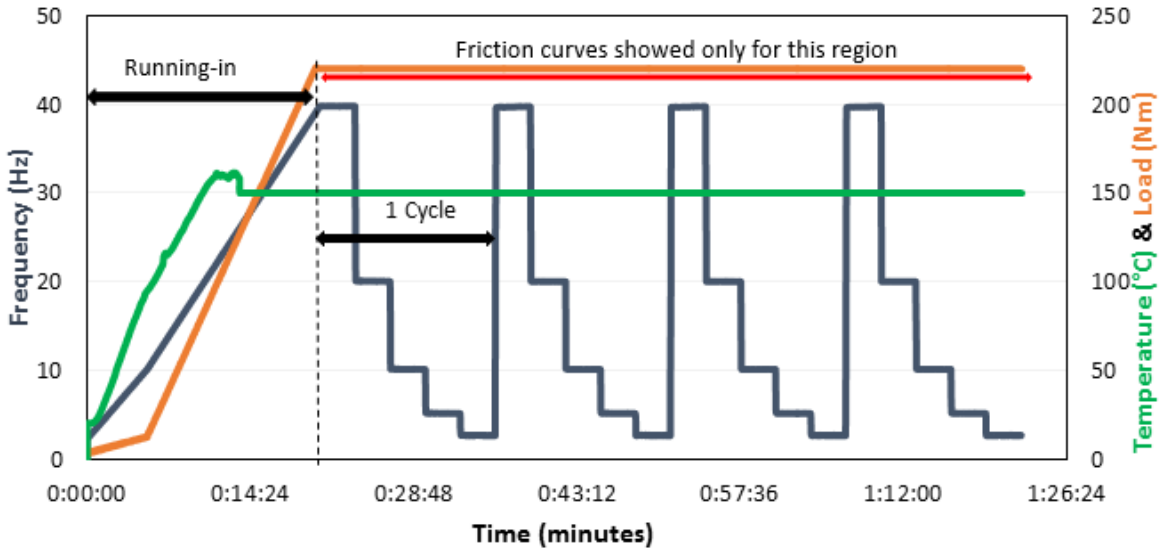

Fig 3.7 Procedure used for the ring-on-liner reciprocating tribotests.

3.3.2 Results and discussion

Average friction behaviour obtained for the contact Fe-phosphate ring / TiO_2 APS liner lubricated with base oil + 0.5 % MoDTC is shown in fig 3.8. TiO_2 APS liner shows average friction coefficient of 0.06 at frequencies of 5 and 2.5 Hz. This suggests that at lower speeds the contact is under boundary lubrication regime and therefore MoDTC additive is activated to form MoS_2 which could lead to stable friction coefficients. On the contrary, at higher speeds friction coefficients are not stable when the contact is in hydrodynamic lubrication regime. There is not enough contact between asperities and the friction modifier MoDTC is not activated completely in this regime. The friction behaviour for all cycles is found to be repeatable. Similar behaviour is observed in all the four cycles of the tribotest which suggests that a stable tribofilm is formed on the coating even after numerous speed changes.

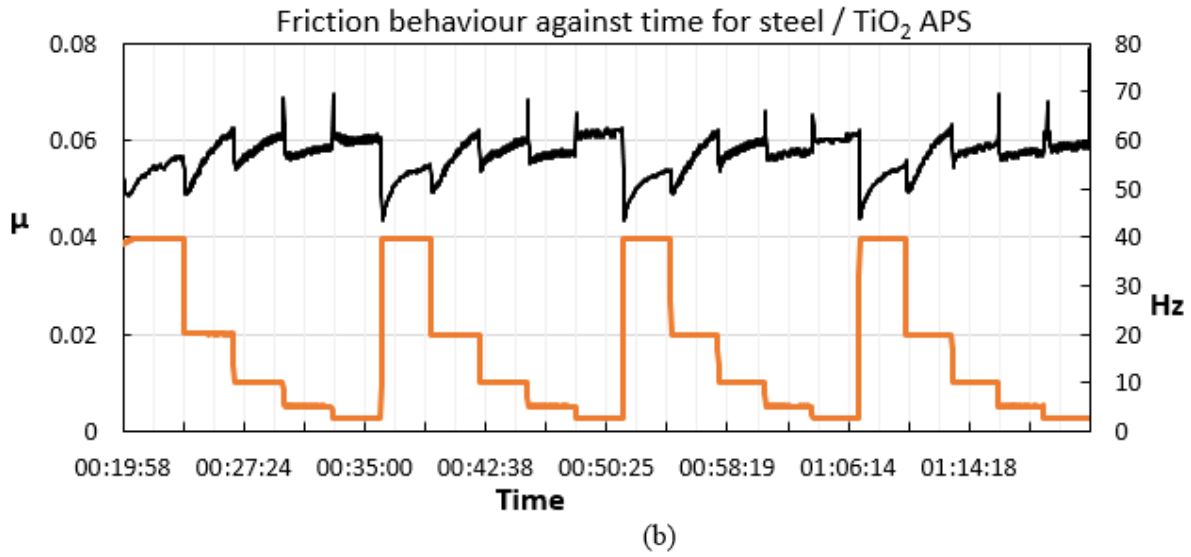

Fig 3.8 Real time behaviour of the contact Fe-phosphate ring / TiO_2 APS liner at different speeds.

Fig 3.9 shows the wear scars obtained on the TiO_2 APS liner as well as the commercial Fe-phosphate ring sliding on both the liners lubricated with base oil + 0.5 % MoDTC. Hertzian diameter for the Fe-phosphate ring / TiO_2 APS contact is 280 µm and the obtained wear scar width is around 320 µm on the ring and 350 µm on the liner. Percentage wear obtained above Hertzian diameter is extremely low as can be observed from the optical images of the wear scars. This could be either due to formation of low friction tribofilm which is relevant where low friction coefficient is observed at low speeds (boundary lubrication regime).

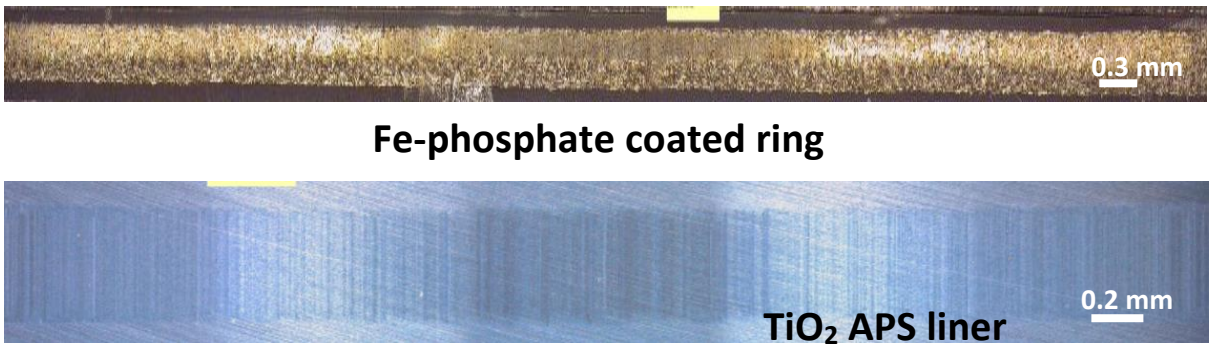

Fig 3.9 Optical images of the wear scars obtained on the piston ring and the TiO_2 liner.

From the tribological results obtained in case of ball-on-flat, MTM and ring-on-liner tribotests, it is clear that TiO_2 APS coating shows the best friction and wear behaviour amongst all the APS coatings used when it is lubricated with base oil + 0.5 % MoDTC. This could be due to several reasons like the difference in chemistry of the coating, tribochemistry involved in the contact in case of TiO_2 APS. It also shows faster kinetics of tribofilm formation and growth. Also, in real engine conditions, TiO_2 APS liner shows lower friction coefficient. Also, Raman spectroscopy carried out on the TiO_2 APS liner showed the formation of MoS_2. Therefore, in

the subsequent chapters, study on the tribological interaction of MoDTC on TiO_2 APS flats / discs will be carried out in detail.

3.4 Conclusions

From the results and discussions for steel / reference steel, steel / steel APS, steel / steel Mo APS and steel / TiO_2 APS contacts lubricated with base oil, MoDTC, ZDDP and the combination of both with different test configurations, following are the conclusions deduced:

(1) Steel / TiO_2 APS contact showed the best tribological behaviour when lubricated with base oil + MoDTC. Also, synergy of friction and wear behaviour between ZDDP and MoDTC was observed in case of all the steel / steel and steel / steel APS but not in case of steel / steel Mo APS and steel / TiO_2 APS. This was suggested to be due to differences in chemistry of the coatings. The wear observed was similar for whatever oil used in case of steel / TiO_2 APS.

(2) Tribotests carried out on a ball-on-disc MTM tribometer lubricated with base oil + MoDTC showed that steel / TiO_2 APS contact showed better kinetics of tribofilm formation, evolution and growth compared to reference steel, steel APS and steel Mo APS. Also, wear obtained was the lowest in case of steel / TiO_2 APS contact.

(3) Ring-on-liner tribotest results revealed that TiO_2 APS liner showed similar tribological behaviour (friction and wear) compared to the previous tests carried out with other configurations when it was slid against a commercial Fe phosphate based piston ring in conditions closer to the real engine.

3.5 References

[1] A. Morina, A. Neville, M. Priest, and J. H. Green, “ZDDP and MoDTC interactions in boundary lubrication — The effect of temperature and ZDDP / MoDTC ratio,” vol. 39, pp. 1545–1557, 2006.

[2] M. I. De Barros’Bouchet, J. M. Martin, T. Le-Mogne, and B. Vacher, “Boundary lubrication mechanisms of carbon coatings by MoDTC and ZDDP additives,” *Tribol. Int.*, vol. 38, no. 3, pp. 257–264, 2005.

[3] M. A. Nicholls, T. Do, P. R. Norton, G. M. Bancroft, M. Kasrai, T. M. Capehart, Y. Cheng, T. Perry “Chemical and mechanical properties of ZDDP antiwear films on steel and thermal spray coatings studied by XANES spectroscopy and nanoindentation techniques,” *Tribol. Lett.*, 2003.

[4] C. G. a and T. P. J.M. Martin a, Th. Le Mogne a, “Tribochemistry of ZDDP and MoDTC chmisorbed films,” *Tribol. Lett.*, vol. 2, pp. 313–326, 1996.

[5] P. M. Society of Tribologists and Lubrication Engineers., H. A. Spikes, J. Hutchinson “The development of a spacer layer imaging method (SLIM) for mapping elastohydrodynamic contacts,” *Tribol. Trans.*, vol. 39, no. 4, pp. 915–921, 1988.

[6] R. Cordtz, J. Schramm, A. Andreasen, S. S. Eskildsen, and S. Mayer, “Modeling the distribution of sulfur compounds in a large two stroke diesel engine,” *Energy and Fuels*, 2013.

[7] O. Akalin and G. M. Newaz, “Piston Ring-Cylinder Bore Friction Modeling in Mixed Lubrication Regime: Part II—Correlation With Bench Test Data,” *J. Tribol.*, vol. 123, no. 1, p. 219, 2001.

Chapter 4

Tribological behaviour of TiO_2 Atmospheric Plasma Spray (APS) coating in presence of oil containing MoDTC

From the results obtained in chapter 3, it was concluded that steel / TiO_2 APS contact shows the best tribological behaviour whatever the configuration used. Therefore, this chapter focuses on the study of tribological behaviour of ceramic based TiO_2 APS coating compared with conventional uncoated steel material under mixed / boundary lubrication in presence of base oil containing MoDTC. MTM tribotests are carried out to investigate the kinetics of the tribofilm evolution and growth. This is followed by tribotests to study the effect of addition of ZDDP to MoDTC and their effect on the wear behaviour. Tribofilm morphology and chemistry are compared on the surface of the tribofilms formed on both the tribopairs using SEM, XPS, Raman spectroscopy and TEM.

Introduction

This chapter focuses on the study of interaction of MoDTC additive on TiO_2 APS coating and its comparison with reference steel. The detailed surface characterisation of the tribofilms formed on the ceramic oxide and steel surfaces is carried out. Also, the better friction and wear behaviour obtained with TiO_2 APS contact is discussed. Effect of addition of the anti-wear additive ZDDP to MoDTC containing base oil is also investigated and compared with steel / steel contact.

4.1 Experimental

4.1.1 MTM tribotest conditions

MTM tests were carried out to study the change in lubrication regimes and the kinetics of tribofilm formation and growth during the tribotest. Anti-wear additive ZDDP was also added to the oil containing MoDTC to study the effect of anti-wear additive on the tribological properties of TiO_2 APS coating.

The conditions used for the MTM tribotests as well as the materials used were similar to that used in the MTM section of Chapter 3.2.1. The roughness parameters for the discs and the MTM conditions are mentioned in the table 3.4 and 3.5 respectively of Chapter 3. Similar profile mentioned in chapter 3 was used but with a slight modification. Two Stribeck curve steps were added to observe the change of friction coefficient and lubrication regimes with the rolling speed. The lubricant used for the tests is base oil + 0.5 wt % MoDTC. For the subsequent tests to study the effect of ZDDP, 1 wt % ZDDP is added to base oil + 0.5 wt % MoDTC.

4.1.2 Surface analysis of the tribofilms

All the samples were cleaned once with *n*-heptane before surface characterisation. Wear scars on the balls and the discs were analysed using an optical microscope and were then compared with the respective Hertzian diameters. The morphology and the composition of the wear scar and the nature of the tribofilm formed on the disc was observed using VEGA – TESCAN Scanning Electron Microscope (SEM) equipped with EDX for semi-quantitative compositional analysis.

Tribofilm composition was characterised using X – ray Photoelectron Spectroscopy (XPS). Raman Spectroscopy was also carried out on the wear scars of the tribopairs to analyse the exact composition of the tribofilm.

Transmission Electron Microscope (TEM) was used to observe the FIB lamella of the tribofilm on the ball and the APS disc.

4.2 Results

4.2.1 Friction and wear results

Fig 4.2 shows the friction curves along with the SLIM images for steel / reference steel and steel / TiO_2 APS contacts. From the SLIM images taken on the steel ball at four different steps, it is observed that the kinetics of tribofilm formation and growth is faster in case of steel / TiO_2 APS. This is also evident from the friction curves as there is no induction time observed in case of steel / TiO_2 APS whereas some induction time is required to form the tribofilm and reach the steady state regime in case of steel / reference steel. Below the respective friction curves, Stribeck curves obtained at steps A (after 2100 s) and B (after 7000 s) are shown. These results obtained are similar to the ones obtained in chapter 3 where Stribeck curve was not added to the profile. The only difference is the value of friction coefficient which was found to be slightly higher in the previous case. This could be due to higher activation of the surface due to repetitive rubbing and change of speed when Stribeck curve steps are added.

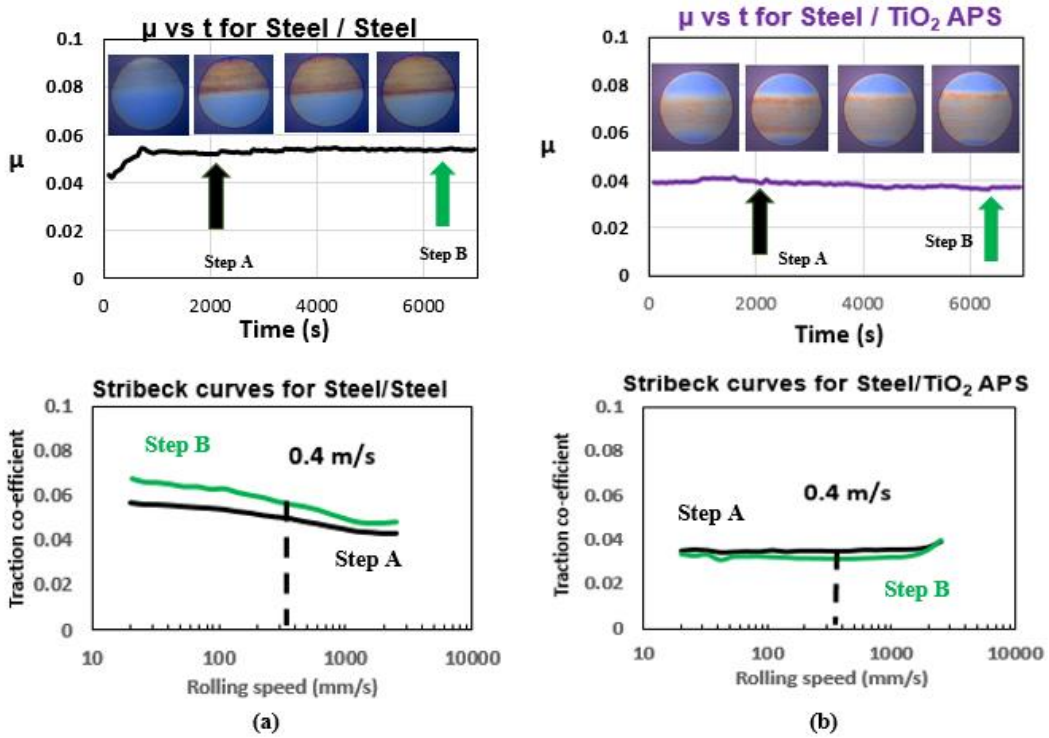

Fig 4.2 MTM friction coefficient vs time curves along with the SLIM images at 4 different steps and Stribeck curves at 2 different steps during the tribotest for (a) Steel / reference steel (b) Steel / TiO_2 APS when lubricated with base oil + 0.5 % MoDTC.

Fig 4.3 (a) shows the comparison of friction trends obtained for different lubricants (base oil, base oil + 0.5 % MoDTC and base oil + 0.5 % MoDTC + 1 % ZDDP) after MTM tribotests. Addition of MoDTC in base oil reduces the friction coefficient from 0.11 – 0.12 to 0.04 – 0.05 which was also observed in case of ball-on-flat results shown in chapter 3. Steel / TiO_2 APS shows the lowest friction coefficient in all the cases when it is lubricated with base oil + 0.5 % MoDTC.

There is no effect of addition of ZDDP to MoDTC on the friction coefficient as it remains constant ($\mu = 0.05$). SLIM images on the ball are recorded at various steps to investigate the evolution of the tribofilm formation. Images at four different steps are shown for both the tests. In case of steel / steel, a small amount of induction time is observed to reach the steady state friction coefficient; where the tribofilm formation is not so evident in the first image; whereas in case of steel / TiO_2, no induction time is observed and the SLIM images show the tribofilm formation from the beginning of the test. Kinetics of tribofilm formation is faster which is evident from the uniform tribofilm formed. Friction coefficient remains constant in the range of 0.037 – 0.039. Results obtained are coherent with chapter 3. Stribeck curves for both the cases are shown in fig.6. Black and green arrows in the friction curves indicate the steps where Stribeck curve steps are carried out.

Fig 4.3 (b) shows the comparison of the wear obtained on the balls and the discs. In case of steel / steel, addition of 1 % ZDDP in base oil with 0.5 % MoDTC clearly shows the wear reduction as observed by Morina *et al* [1]. Synergy exists between MoDTC and ZDDP in that case as the friction is reduced because of MoDTC and then the wear is reduced due to anti-wear properties of ZDDP. However, on the contrary, there is no antiwear effect observed after the addition of ZDDP to MoDTC in case of steel / TiO_2 APS contact as the wear observed is similar in the case of all the lubricants. Therefore, synergy between MoDTC and ZDDP is not observed in the last case. Since low wear is observed even in case of base oil, it could be due to intrinsic wear resistant properties of the TiO_2 APS coating under tribological conditions.

(a)

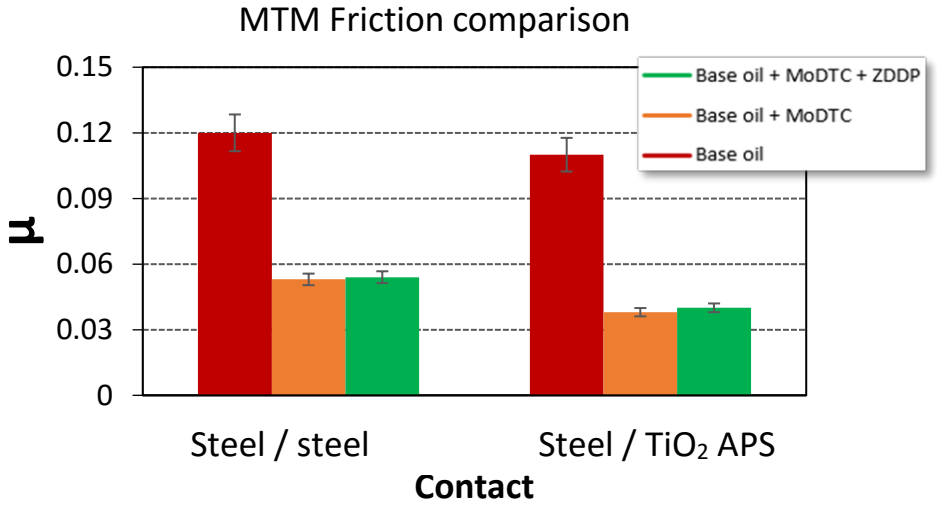

(b)

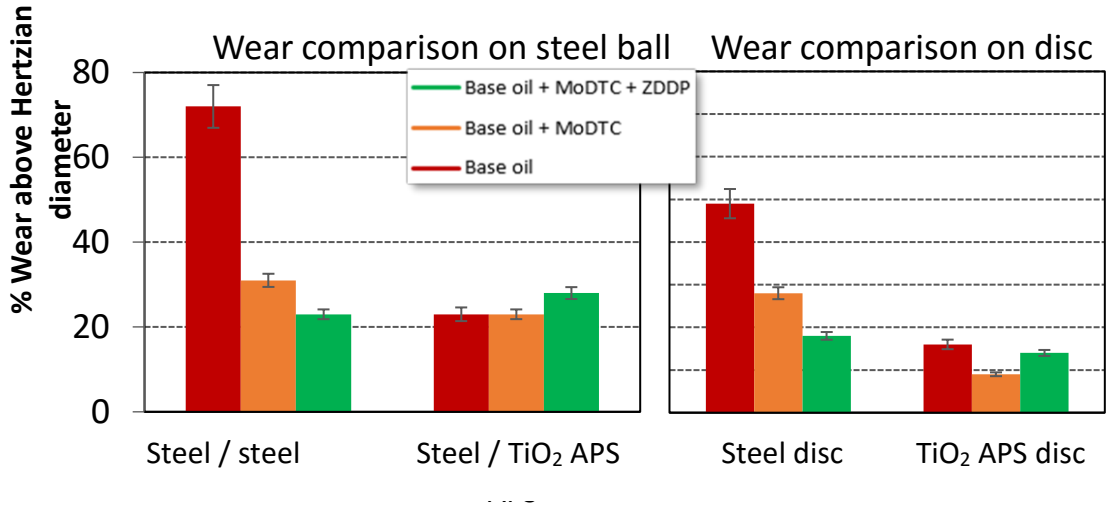

Fig 4.3 (a) Friction trends (b) Wear trends on the ball and the disc for steel / rough reference steel & steel / TiO_2 APS when lubricated with base oil, base oil + MoDTC and base oil + MoDTC + ZDDP.

4.2.2 Surface analysis of the tribofilms

4.2.2.1 SEM analysis

Fig 4.4 (a) shows the SEM micrographs of the wear scar obtained on the TiO_2 APS disc after MTM tribotest in presence of base oil + MoDTC. The subsequent images (b), (c), (d), (e) and (f) show the individual maps for various elements present in the wear scar. Since the coating is rough, the tribofilm formed on the TiO_2 APS disc is patchy. Mo and S are observed in patches in exactly the same position suggesting the formation of MoS_2 in the wear scar along with the substrate contributions of Ti and O.

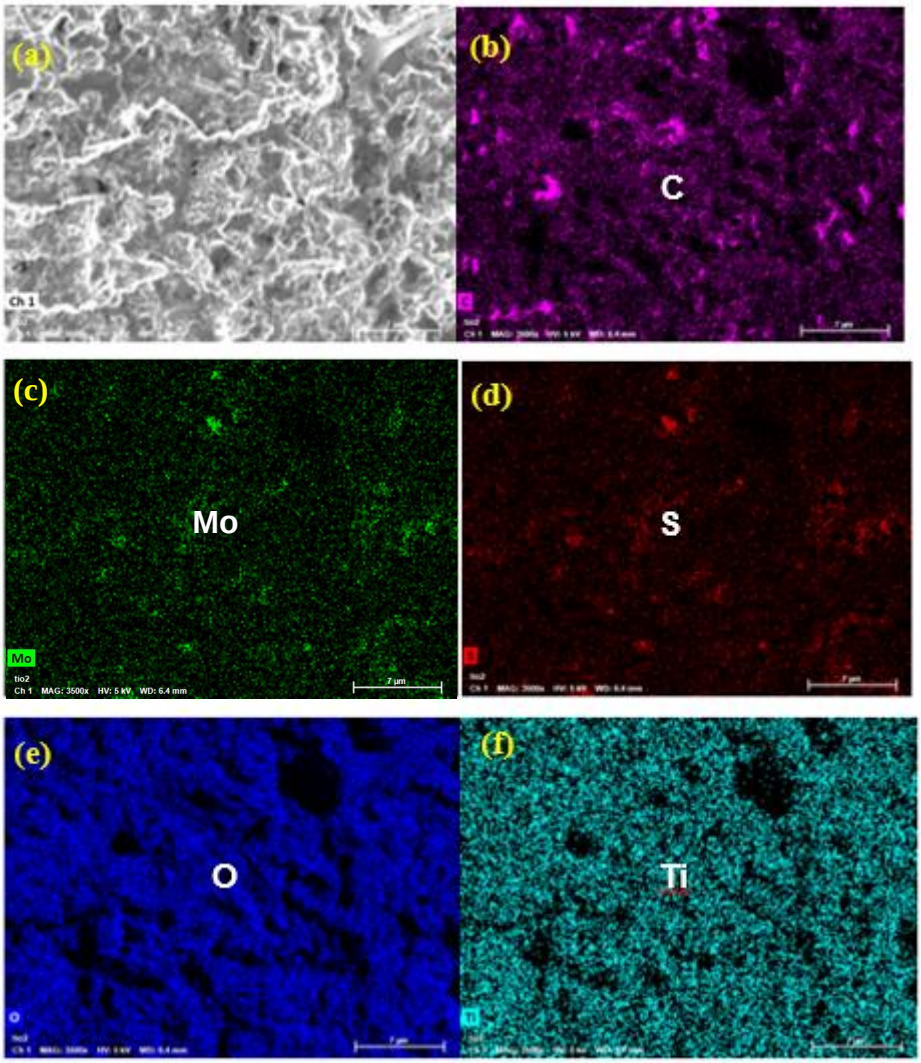

Fig 4.4 (a) SEM image with individual EDX maps for (b) Carbon (c) Molybdenum (d) Sulphur (e) Oxygen (f) Titanium present in the tribofilm of the wear track on TiO_2 APS disc obtained after MTM tribotest in presence of base oil + MoDTC .

4.2.2.2 XPS analysis on the TiO_2 APS disc

Following the tribotests, the tribopairs were analysed by XPS to investigate the reasons for friction reduction. Initially, the wear scar is observed using SXI imaging. Then a survey is carried out inside and outside the wear scar to confirm the presence of various elements in the tribofilm. High resolution spectra are obtained for selected elements present in the tribofilm. Analyses are carried out on both the tribopairs (balls and flats). Results obtained are similar in both cases as both the flat and ball show the formation of pure MoS_2 and MoO_3 but no Mo-oxysulphide in case of TiO_2 APS flat and the steel ball sliding against it. Therefore, the results obtained from the flats are used for comparison. Fig 4.5 shows the high resolution XPS spectra obtained on an area of 100 μm^2 inside the tribofilm in case of steel flat (fig 4.5 (a)) and TiO_2

APS flat (fig 4.5 (b)). Mo3d peak is divided in to 3 different contributions – MoS_2 (B.E = 229.0 ± 0.2 eV), MoS_xO_y (B.E = 229.7 ± 0.2 eV) and MoO_3 (B.E = 232 ± 0.2 eV). Mo3d peak is fitted with various possibilities [2] and the one with the lowest chi square value is used for analysis. Error for the binding energies is 0.5 eV. Fitting is done using the binding energy values assigned to the different contributions in the literature for sulphide, oxysulphide and oxide of Mo [2]. Reference binding energy values used for oxysulphides are for sputtered Mo-oxysulphide thin films [3]. Also, the FWHM (Full-width Half Max) values for all the contributions are close to each other and same for the doublet peaks of different Molybdenum contributions. S2s part in the Mo3d peak is also fitted taking in to account the binding energy fitted for the sulphide contribution in S2p peak. Similarly, for the sulphate contribution, S2s peak was fitted but the contribution is negligible compared to the other Mo contributions in Mo3d peak. Therefore, it is not shown in the XPS spectra below.

As presented in fig 4.5, it is clear that higher amount of MoS_2 is observed in case of TiO_2 APS flat compared to the reference steel flat with no oxysulphides. Mo peaks showing oxysulphide compounds are found only in case of steel / reference steel contacts. This can be confirmed from the XPS binding energy positions of oxysulphides obtained in the literature [4-5].

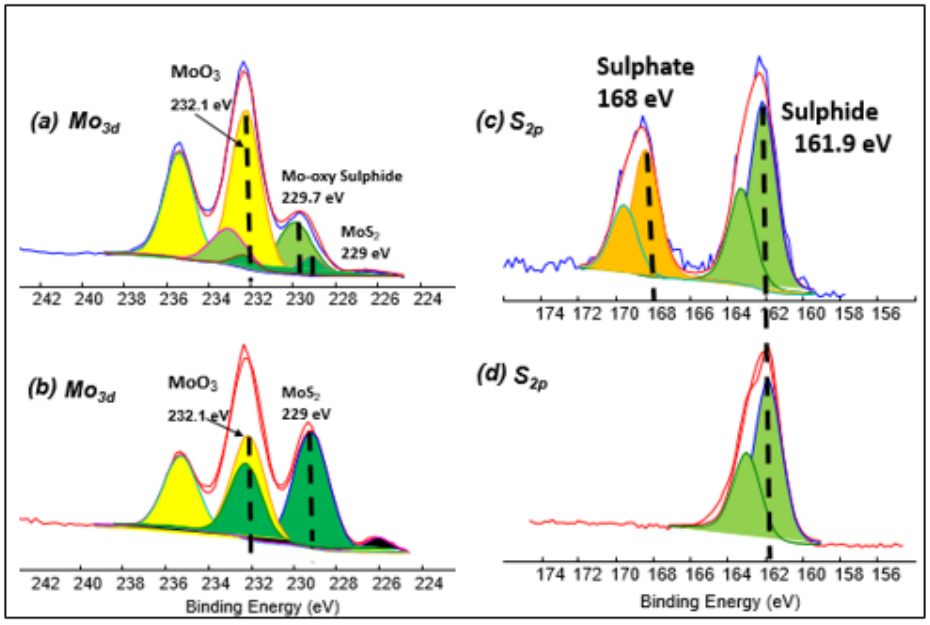

Fig 4.5 XPS spectra for reference steel and TiO_2 APS flats, tested in base oil + 0.5 % MoDTC against steel balls: (a) Mo3d peak on the steel flat (b) Mo3d peak on TiO_2 APS flat (c) S2p peak on the steel flat (d) S2p peak on the TiO_2 APS flat.

In case of the reference steel flat, S2p peak shows the presence of both sulphide (161.9 eV) and sulphate (168 eV) contributions; whereas in case of TiO_2 flat, the sulphate contribution is

absent. This indicates no Mo-oxysulphides are formed on TiO_2 APS which is in agreement with the low friction coefficient as MoS_2 formed remains in the pure state without being oxidised.

4.2.2.3 Raman Spectroscopy on the wear scar (TiO_2 APS disc):

Since the wear scars obtained on the discs were heterogeneous as seen from the SEM images, Raman spectroscopy was carried out on several points on the wear scar to find out the different compounds present. Fig 4.6 shows the Raman spectra on two different points inside the tribofilm. Bands observed at 290 cm^{-1}, 386 cm^{-1}, 405 cm^{-1} are assigned to crystalline MoS_2 [27, 36]. Bands observed at 246 cm^{-1}, 450 cm^{-1} and 605 cm^{-1} are assigned to rutile phase of TiO_2 [8, 9]. There are some bands which are at a lower Raman shift of 427 cm^{-1} and 547 cm^{-1} and these are assigned to oxygen deficient phases of TiO_2 called Magneli phases (Ti_nO_{2n-1}), n possibly between 4 and 6 as shown in the fig 4.6 (a) [10]. Magneli phase peaks are observed when lubricated with base oil as well as base oil + MoDTC. All these results suggest that the tribofilm formed is made up of different chemical compounds like TiO_2 in rutile phase, Magneli phases and MoS_2. It can be concluded that the tribofilm is patchy in nature.

(a)

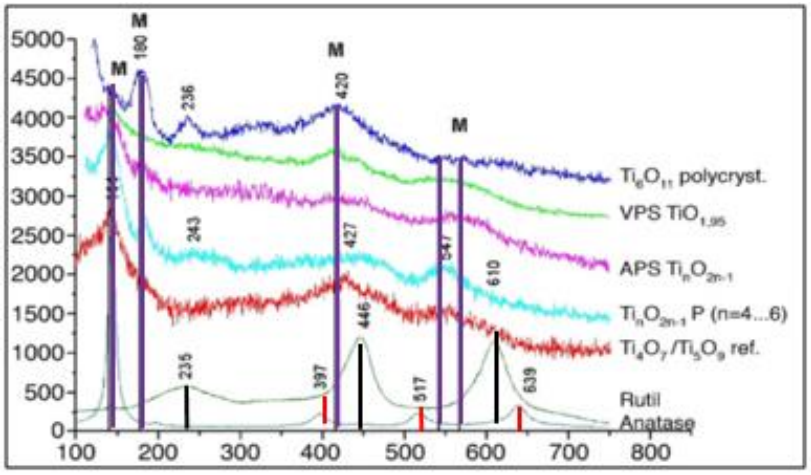

(b)

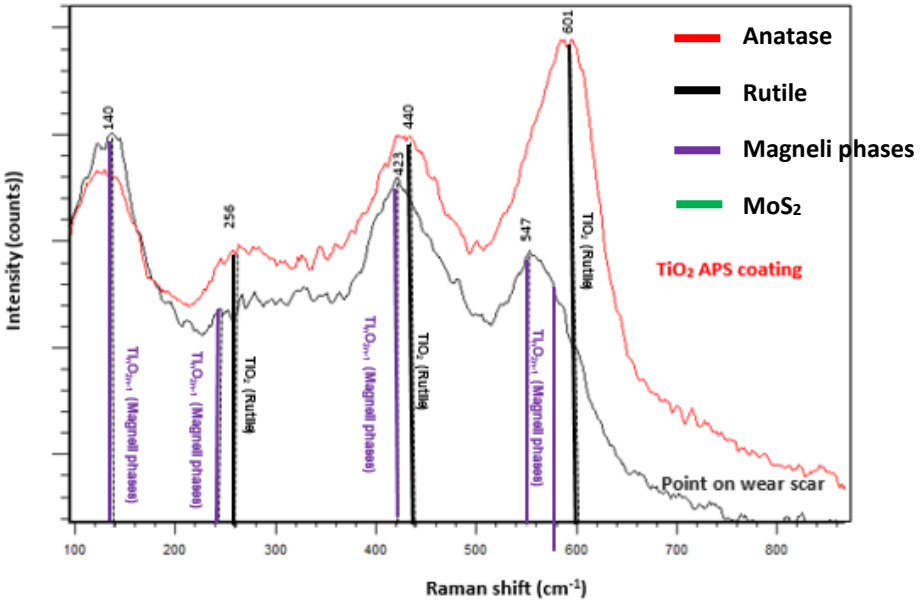

(c)

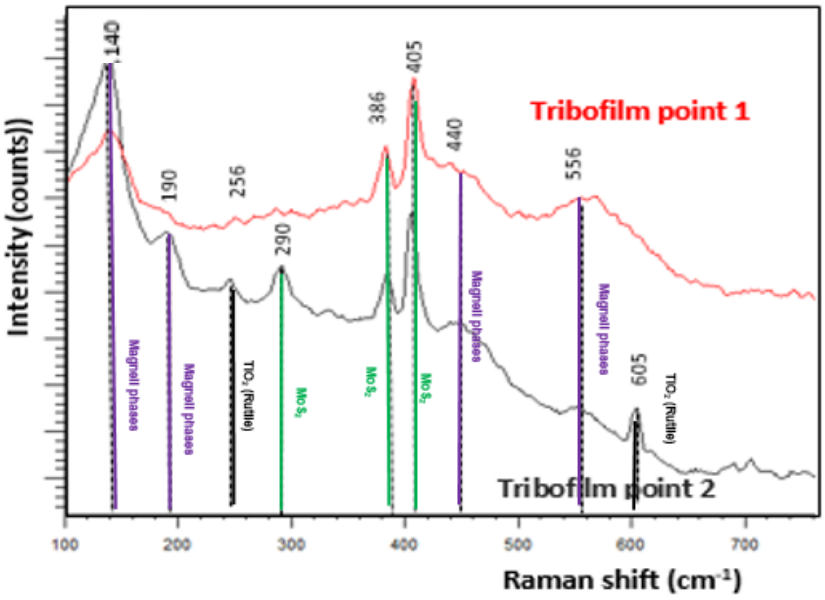

Fig 4.6. (a) Reference Raman spectra for Magneli phases [10] (b) Raman spectra inside and outside the wear scar when lubricated with base oil. (c) Raman spectra on two different points inside the tribofilm when lubricated with base oil + MoDTC

4.2.2.4 FIB-TEM analysis on the tribofilm (TiO_2 APS disc)

To confirm the presence and investigate the morphology of MoS_2 in case of steel / TiO_2 APS, FIB-TEM is carried out on a small region of the tribofilm on TiO_2 APS disc when it is lubricated with base oil + MoDTC. From the TEM images shown in fig 4.7 (a), it is clear that long and crystalline MoS_2 flakes are formed on the surface of TiO_2 coating. The tribofilm (about 5 nm thick) is found to be made of two to five layers of MoS_2 flakes. These sheets are confirmed to be MoS_2 as the basal plane distance of hexagonal MoS_2 is known to be 6 Å and matches with the ones in the images. Magnified images in the fig 4.7 (a) show MoS_2 flakes which are clearly distinguishable. This is in agreement with the XPS and Raman results which showed the formation of MoS_2 in the tribofilm. TEM-EDX analysis is carried out on the flakes and on the substrate. The atomic % of the elements on both the points is shown in the table below the TEM micrographs in the fig 4.7 (a). The composition of point 1 clearly shows the presence of TiO_2 substrate and that of point 2 shows the presence of Mo and S clearly indicating that the flakes are made of MoS_2.

TEM-EDX analysis is carried out at different points in the image to investigate the composition of the tribofilm. Fig. 4.7 (b) shows the different points at which EDX is carried out. Points 1 shows the TiO_2 APS coating ; point 2 shows a matrix of titanium, oxygen, carbon, iron, molybdenum and sulphur; point 3 shows the crystalline region with Mo and S tribofilm and point 4 shows the protective Pt layer. The elemental composition at different points is shown in the table below the images. It is clear that point 4 is a short MoS_2 flake as the stoichiometry matches with the atomic % of Mo and S. The presence of MoS_2 flakes is also previously confirmed by XPS and Raman spectroscopy.

Comparing the TEM micrographs obtained for the tribofilm on TiO_2 APS with those obtained on steel flat under similar conditions by De Feo *et al* as shown in the fig 4.7 (c) [2], it is clear that short MoS_2 flakes are present in an amorphous matrix in case of steel flat and long, crystalline MoS_2 flakes are present on top of the TiO_2 substrate without any matrix.

(a)

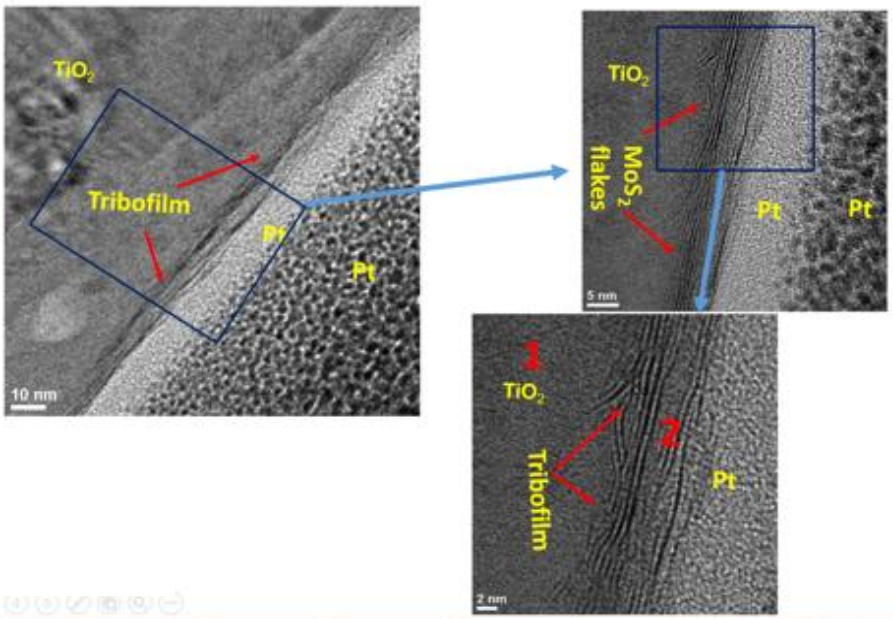

Element	C	O	S	Ti	Fe	Mo	Total
Point 1	3.0	57.2	0.0	38.8	0.0	0.0	100.00
Point 2	7.5	23.9	40.5	1.9	0.0	26.2	100.00

(b)

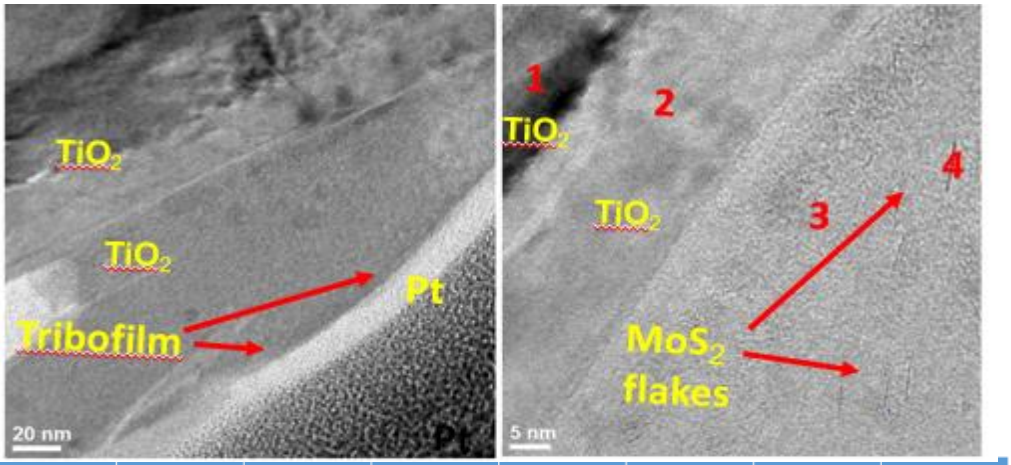

Element	C	O	S	Ti	Fe	Mo	Total
Point 1	1	61.7	0.1	37.0	0.1	0.0	100.00
Point 2	2.7	60.1	0.2	36.8	0.1	0.0	100.00
Point 3	13.4	52.8	10.6	10.5	6.0	6.7	100.00
Point 4	8.3	50.0	21.3	2.9	8.0	9.4	100.00

(c)

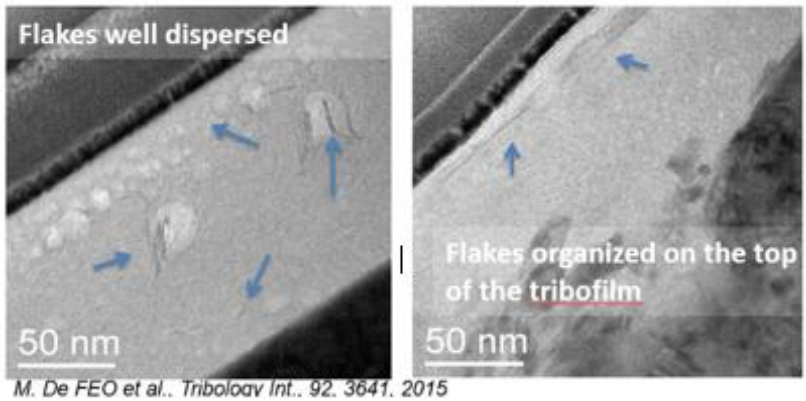

M. De FEO et al., Tribology Int., 92, 3641, 2015

Fig 4.7 (a) TEM micrographs of the FIB lamella cut from the tribofilm on TiO_2 APS disc along with the EDS analysis on 2 different points **(b)** TEM images along with the EDS analysis on 4 different points in the tribofilm. **(c)** TEM micrographs of the FIB lamella cut from the tribofilm on steel flat in the previous work by De Feo *et al* [2].

Fig 4.8 below shows the TEM EDS individual elemental maps captured with ETEM microscope. Rectangular area inside the image is used for capturing the maps. This area includes the substrate (TiO_2), tribofilm (MoS_2 flakes) and the Magneli phases. From the individual elemental maps, it can be clearly observed that Ti (orange), O (green) are seen in the top area which suggests that this part is the substrate and Mo (red), S (blue) are seen in the bottom area just below the substrate. These elemental maps show that the tribofilm composed of Mo and S seems to be directly attached to the substrate made of Ti and O which could be Magneli phases or TiO_2 (rutile).

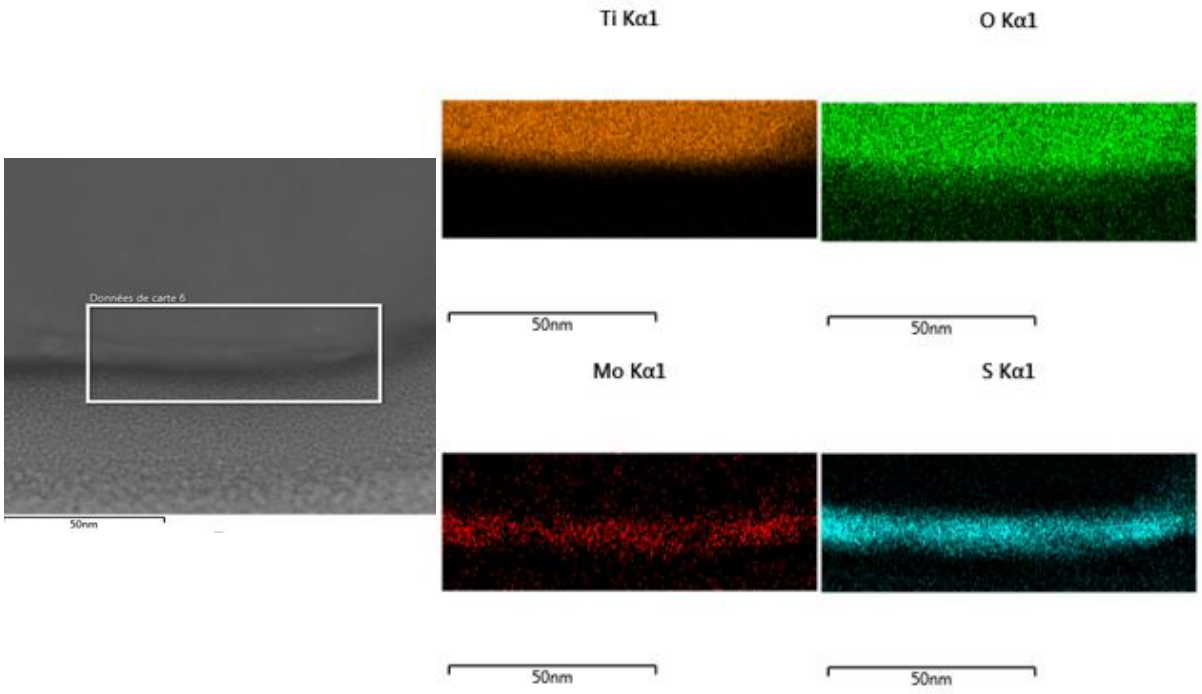

Fig 4.8 TEM EDS individual elemental maps for Ti, O, Mo and S.

4.3 Discussion

4.3.1 Low friction in case of TiO_2 APS coating

The most important results obtained in this chapter is that the TiO_2 APS coating shows lower friction coefficient and lower wear than the conventional reference steel as well as the steel APS coating. Reasons for low friction in TiO_2 APS coating are discussed as follows.

(1) Tribochemistry:

Surface characterisation of the tribofilm by XPS depicts the formation of pure MoS_2 with no oxysulphides and MoO_3 in case of steel / TiO_2 APS, whereas a lot of Mo-oxysulphide and small amount of MoS_2 and MoO_3 are formed in case of reference steel and steel APS. The presence of oxysulphides was confirmed from the XPS of pure Mo-oxysulphide thin films. It was shown by De Feo *et al* [2] that presence of Mo-oxysulphides in the tribofilm leads to higher friction coefficient. This is because oxygen atoms disturb the layered structure of MoS_2. The results obtained in this study are in agreement with this as presence of Mo-oxysulphide on the tribofilm formed on steel flat shows increase in friction coefficient. Also, the increase in friction coefficient is not extremely high as the content of sulphur present in the MoO_xS_y is still higher than that of oxygen. Friction coefficient goes on increasing as the oxygen content increases in the MoO_xS_y molecule [2]. Various compounds observed in the different tribofilms are summarised in table 4.1.

Table 4.1 List of different compounds formed in the tribofilms

Tribopair	**Tribofilm composition**
Steel / reference steel	MoS_2 + MoO_xS_y + MoO_3, Sulphate
Steel / TiO_2 APS	MoS_2 + MoO_3, No sulphate

Raman analysis confirms the formation of MoS_2 in the tribofilm as pure MoS_2 crystalline peaks are observed and no amorphous peaks for MoS_x are seen [30]. This suggests that there is only one type of Mo – S compound forming in the tribofilm and that is MoS_2.

(2) Morphology:

TEM analysis on the FIB lamella shows the formation of long, crystalline MoS_2 flakes throughout the tribofilm (which are responsible for friction reduction) compared to short flakes in case of reference steel inside a matrix composed of molybdenum, sulphur, carbon, oxygen and iron as observed by De Feo *et al* [2] and De Barros *et al* [12] as shown in the fig 4.7 (c). In case of steel / steel contact, short flakes are distributed in an amorphous matrix. However, in case of TiO_2 APS coating, there is a slight change in the substrate due to formation of Magneli phases and few layers of MoS_2 flakes are found to be on the surface of the coating.

MoO_3 (amorphous) detected in the XPS could be present in the space between the MoS_2 flakes on the top surface. Elemental TEM EDS maps confirm that the flakes are composed of Mo and S and are directly attached to the substrate made of Ti and O. Therefore, the morphology as well as the composition of the tribofilm could affect the friction coefficient.

4.3.2 Low wear in case of TiO_2 APS coating

From the MTM test results, high wear is observed in case of steel / reference steel when lubricated with base oil. Wear is reduced a bit after addition of MoDTC and then reduces a lot after addition of ZDDP to the oil containing MoDTC. Results obtained here are in agreement with the previous works [13] where it was observed that steel / steel contacts show the synergistic friction and wear behaviour between MoDTC and ZDDP.

On the other hand, TiO_2 APS coating shows the best wear behaviour amongst all the tribopairs tested. The interesting result to be noted is that the wear reduction is observed even when the tribopairs are lubricated with only base oil. There is no further wear reduction observed if the friction modifier MoDTC and the antiwear additive ZDDP is added to the base oil. In this case, synergy is not observed between MoDTC and ZDDP. To understand this interesting wear behaviour of the APS coating, Raman spectroscopy was carried out on various points in the tribofilm. It was observed that the crystalline rutile peaks are shifted to a lower value when lubricated with base oil. This lower energy peaks are attributed to wear resistant Magneli phases [10]. These phases are known to be wear resistant in tribological conditions [14]–[16]. It has been shown that Magneli phases are formed at high temperatures in tribological conditions when Ti –Mo (C,N) coatings are tested in dry conditions [15]. Magneli phases are known to form on bulk TiO_2 coating or any other Ti containing molecule like nitrides, carbonitrides which gets reduced to sub-stoichiometric oxides like Ti_4O_7 with crystallographic shear planes [15]. Reduction in the amount of oxygen from $TiO_{1.98}$ to $TiO_{1.66 - 1.75}$ leads to short interatomic Ti- Ti distances and this phenomena increases the crystal strength of the material and thereby increases the wear resistance [17]. Also, when MoDTC is added to the base oil, these peaks are observed again on different points in the tribofilm. Since the wear is reduced to a maximum, there is no further reduction observed even after addition of ZDDP. Wear reduction observed cannot be attributed to the mechanical properties of the coating as the hardness of the TiO_2 APS coating is similar to that of reference steel. Also, lower wear is observed on the steel ball confirming that the hardness of TiO_2 is not high enough to cause high wear on the steel ball.

4.4 Conclusions:

This chapter investigated the interaction of MoDTC with TiO_2 APS coating with a detailed characterisation study of the tribofilms formed on the TiO_2 APS coating. This coating showed better wear behaviour than reference steel even when it was lubricated with base oil.

Following are conclusions drawn from this chapter:

(1) 15-20 % friction reduction is observed when steel ball is slid against TiO_2 APS flat in presence of MoDTC compared to steel / reference steel.

(2) This friction reduction is due to two factors:

(a) tribochemistry – MoS_2 and MoO_3 formed compared to small amount of MoS_2, MoO_3 and MoO_xS_y in case of reference steel and steel APS

(b) morphology of the tribofilm – long crystalline flakes directly attached to the TiO_2 surface are observed whereas short flakes were observed from the literature embedded in a Fe, Mo, S, C, O matrix in case of steel / steel contact.

(3) Low wear was obtained in case of steel / TiO_2 APS even when lubricated with base oil; and is attributed to the tribologically induced transformation of rutile to substoichiometric oxide, (Ti_nO_{2n-1}), n possibly between 4 and 6 to form wear-resistant Magneli phases. So the addition of ZDDP in the lubricant has no further effect on wear reduction.

4.5 References:

[1] A. Morina, A. Neville, M. Priest, and J. H. Green, "ZDDP and MoDTC interactions in boundary lubrication — The effect of temperature and ZDDP / MoDTC ratio," vol. 39, pp. 1545–1557, 2006.

[2] M. De Feo , C. Minfray, M. I. De Barros Bouchet, B. Thiebaut, Th. Le Mogne, B. Vacher, J. M. Martin, "Ageing impact on tribological properties of MoDTC-containing base oil," *Tribol. Int.*, vol. 92, pp. 126–135, 2015.

[3] L. Benoist and D. Gonbeaua, "X-ray photoelectron spectroscopy characterization of amorphous molybdenum oxysulfide thin films," vol. 258, 1995.

[4] E. Schmidt, C. Sourisseau, G. Meunier, and A. Levasseur, "Amorphous molybdenum oxysulfide thin films and their physical characterization," *Thin Solid Films*, 1995.

[5] E. Schmidt, F. Weill, G. Meunier, and A. Levasseur, "New amorphous molybdenum oxysulfides obtained in the form of thin films and their characterization by TEM," *Thin Solid Films*, vol. 245, no. 1–2, pp. 34–39, 1994.

[6] D. N. Khaemba, A. Neville, and A. Morina, "A methodology for Raman characterisation of MoDTC tribofilms and its application in investigating the influence of surface chemistry on friction performance of MoDTC lubricants," *Tribol. Lett.*, 2015.

[7] D. N. Khaemba, A. Neville, and A. Morina, "New insights on the decomposition mechanism of Molybdenum DialkyldiThioCarbamate (MoDTC): a Raman spectroscopic study," *RSC Adv.*, vol. 6, no. 45, pp. 38637–38646, 2016.

[8] U. Balachandran and N. G. Eror, "Raman spectra of titanium dioxide," *J. Solid State Chem.*, vol. 42, no. 3, pp. 276–282, 1982.

[9] P. Narayanan, "Raman spectrum of rutile (TiO_2)," *Proc. Indian Acad. Sci. …*, pp. 279–283, 1950.

[10] A. Skopp, N. Kelling, M. Woydt, and L. M. Berger, "Thermally sprayed titanium suboxide coatings for piston ring/cylinder liners under mixed lubrication and dry-running conditions," *Wear*, vol. 262, no. 9–10, pp. 1061–1070, 2007.

[11] D. N. Khaemba, F. Jarnias, B. Thiebaut, A. Neville, and A. Morina, "The role of

surface roughness and slide-roll ratio on the decomposition of MoDTC in tribological contacts," *J. Phys. D. Appl. Phys.*, vol. 50, no. 8, p. 85302, 2017.

[12] M. I. De Barros'Bouchet, J. M. Martin, T. Le-Mogne, and B. Vacher, "Boundary lubrication mechanisms of carbon coatings by MoDTC and ZDDP additives," *Tribol. Int.*, vol. 38, no. 3, pp. 257–264, 2005.

[13] A. Morina, A. Neville, M. Priest, and J. H. Green, "ZDDP and MoDTC interactions and their effect on tribological performance - Tribofilm characteristics and its evolution," *Tribol. Lett.*, vol. 24, no. 3, pp. 243–256, 2006.

[14] M. Woydt, "Oil Free Machinery and 'Zero Wear'- Dream or Reality?," *Tribol. Online*, vol. 6, no. 1, pp. 101–112, 2011.

[15] M. Woydt, "Tribological characteristics of polycrystalline Magnéli-type titanium dioxides," *Tribol. Lett.*, vol. 8, no. 2–3, pp. 117–130, 2000.

[16] J. Landa, I. Illarramendi, N. Kelling, M. Woydt, A. Skopp, and M. Hartelt, "Potential of thermal sprayed Ti n O2 n-1-coatings for substituting molybdenum-based ring coatings," *Ind. Lubr. Tribol.*, vol. 59, no. 5, pp. 217–229, 2007.

[17] M. N. Gardos, "The effect of anion vacancies of the tribological properties of rutile ({$TiO_{\{2-x\}}$})," *Tribol. Trans.*, vol. 31, no. 4, pp. 427–436, 1988.

Chapter 5

Effect of various parameters on the tribological behaviour of steel / TiO_2 APS coating

In the previous chapter, tribological behaviour of steel / TiO_2 APS contact followed by the detailed characterization of tribofilms was presented. This chapter focuses on the impact of various parameters like roughness, test temperature, contact pressure, concentration of MoDTC and change of counterpart materials from steel balls to ceramic balls, on the tribological behavior of steel / TiO_2 APS contact. Ball-on-flat tribotests were carried out on a linear tribometer lubricated with base oil containing MoDTC. Results obtained are discussed along with the investigation of the tribofilm composition obtained on the surface of the flats. Comparison of steel / TiO_2 APS contact is made with steel / reference steel contact on the basis of friction, wear and tribofilm characterisation.

5.1 Experimental:

TiO_2 APS coated flats and AISI 52100 steel flats as well as the counterpart materials (standard steel balls) were used with similar specifications as mentioned in chapter 3. Lubricant used is grade III base oil with MoDTC in base oil. Tribotests were carried out in ball-on-flat configuration on a linear reciprocating tribometer in boundary lubrication conditions as in the table 5.1 below.

Table 5.1. Ball-on-flat tribotest conditions

Temperature	20°C / 60°C /100 ° C
Frequency	5 Hz
Stroke length	5 mm
Average Sliding Speed	0.05 m / s
Normal load	7 N – Steel / TiO_2 APS; 6 N – Steel / Steel
Max Pressure	0.4 GPa / 0.7 GPa / 1 GPa
Test duration	1 hr, 18000 cycles
Ball material **Flat material**	AISI 52100 Steel, Al_2O_3, ZrO_2 AISI 52100 Steel, TiO_2 APS
Lubricant	Base oil + 0.01 / 0.03 / 0.05 / 0.1 / 0.3 / 0.5 wt % MoDTC

Following is the list of parameters studied:

(1) Effect of roughness:

To study the effect of roughness on the tribological behavior of TiO_2 APS, samples were obtained with different roughness parameters by a variety of surface finishing processes described in Annex 1. Tests were carried out at 100 °C with a maximum Hertzian contact pressure of 0.7 GPa.

(2) Effect of concentration of MoDTC :

To study the effect of concentration of MoDTC on the tribological behavior of steel / reference steel and steel / TiO_2 APS contacts, tests were performed with varying concentrations of MoDTC starting from 0.01 wt %, 0.03 wt %, 0.05 wt %, 0.1 wt %, 0.3 wt % to 0.5 wt % in base oil at 100 °C with a maximum Hertizan contact pressure of 0.7 GPa and a sliding speed of 0.05 m / s.

(3) Effect of test temperature:

To study the effect of temperature on the tribological behavior of steel / steel and steel / TiO_2 APS contacts, tribotests were performed at three different temperatures of 20°C, 60°C and

100°C with a maximum Hertzian contact pressure of 0.7 GPa , a sliding speed of 0.05 m / s lubricated with base oil + 0.3 % MoDTC.

(4) Effect of contact pressure:

To study the effect of pressure on the tribological behavior of steel / steel and steel / TiO_2 APS contacts, tribotests were performed at three different maximum Hertzian contact pressures of 0.4 GPa, 0.7 GPa and 1 GPa at 100 °C with a sliding speed of 0.05 m / s and lubricated with base oil + 0.3 % MoDTC.

(5) Effect of change of counterpart material:

To study the effect of change of counterpart material on the tribological behaviour of reference steel and TiO_2 APS flats, counterpart material was changed from steel balls to alumina and zirconia balls. Also, the effect of absence of Fe on the formation of MoS_2 was studied in ceramic/ceramic contacts. Tests were carried out at 100 ° C with a maximum Hertzian contact pressure of 0.7 GPa, a sliding speed of 0.05 m /s and lubricated with base oil + 0.3 % MoDTC. Wear scar analysis is carried out using optical microscopy on both the counterparts. Surface analysis of the tribofilms is carried out using XPS. Comparison of tribological behaviour is made for various parameters for steel / reference steel and steel / TiO_2 APS contacts.

5.2 Results and discussion:

5.2.1 Effect of roughness parameters

5.2.1.1 Tribological behavior of Steel / TiO_2 APS contact for samples with different average surface roughness:

Roughness plays an important role in tribology as the lubrication regimes changes in the contact when the roughness is varied. Average surface roughness (R_a) was obtained in the range of 0.12 to 0.33 µm for TiO_2 APS coatings by variety of surface finishing processes detailed in annex.

The samples obtained by different surface finishing process are grinding – denoted by A, lapping 1 (15 min 15 micron 15 min 6 micron) denoted by B (detail procedure is mentioned in annex 1), lapping 2 (20 min 6 micron) denoted by C, polishing denoted by D and flat honing denoted by E. All the roughness parameters as well as the corresponding lambda ratios for the samples are listed in table 5.2.

Table 5.2 Roughness parameters for TiO_2 APS flats

Surface finishing process	R_a (µm)	R_k (µm)	R_{pk} (µm)	R_{vk} (µm)	Lambda ratio
Grinding (A)	0.12 ± 0.02	0.50 ± 0.15	0.09 ± 0.03	0.17 ± 0.10	0.94
Lapping 1 (B)	0.26 ± 0.02	0.30 ± 0.10	0.11 ± 0.02	0.49 ± 0.46	0.51
Lapping 2 (C)	0.15 ± 0.02	0.40 ± 0.15	0.06 ± 0.03	0.60 ± 0.15	0.8
Polishing (D)	0.04 ± 0.01	0.10 ± 0.03	0.07 ± 0.04	0.09 ± 0.03	1.8
Flat honing (E)	0.33 ± 0.02	1.1 ± 0.10	0.39 ± 0.04	2.5 ± 0.03	0.42

It can be found that the samples A and C show similar average surface roughness in the range of 0.12 – 0.15 µm. Also, the other parameters like R_k and R_{pk} are similar. Due to the change in surface finishing process from grinding to lapping, the R_{vk} parameter is increased in case of sample C. R_{pk} parameters are found to be in the same range for the samples A – D. Lambda ratios are calculated using the equation mentioned in annex 2. From the values of lambda ratio, the lubrication regime of the contact could be found out. In this case, the lambda ratio changes from 0.4 (boundary lubrication) to 1.8 (mixed lubrication) for steel / TiO_2 APS contact with the different R_a of TiO_2 samples. Also, the other parameters like R_k and R_{vk} keep on changing randomly due to different surface finishing processes and so it is difficult to study the effect of

change of all the roughness parameters on the tribological behavior. Therefore, only the effect of change of R_a is investigated in this section.

(a) Friction behaviour:

Friction curves obtained for steel / TiO_2 APS (different roughness parameters) lubricated with base oil + 0.5 % MoDTC at 0.7 GPa of maximum Hertzian contact pressure are shown in fig 5.1. Comparison shows that the friction coefficient obtained is different at different roughness values and is in the range of 0.04 - 0.07.

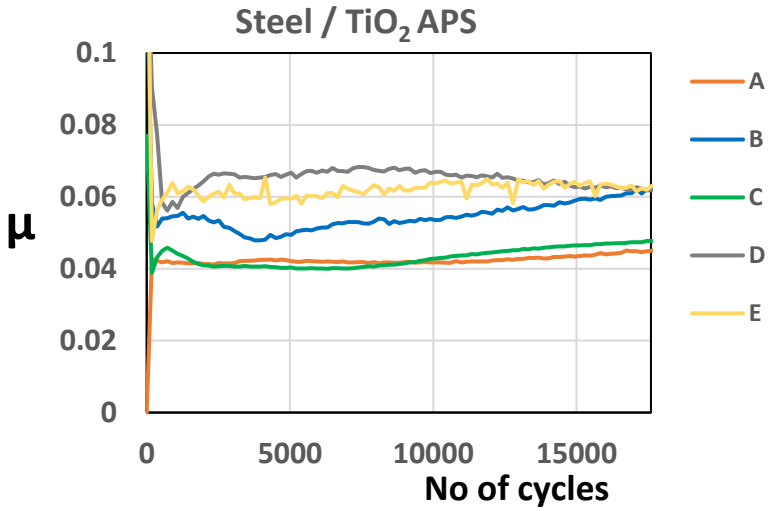

Fig 5.1 Comparison of friction curves for steel / TiO_2 APS obtained with different surface finishing process and with different roughness parameters lubricated with base oil + 0.5 % MoDTC at a maximum Hertzian contact pressure of 0.7 GPa.

It is observed that the friction behaviour of steel / TiO_2 APS contact obtained with samples A and C is similar along with their steady state friction coefficient (0.04). As discussed before, this could be due to the similarities in the value of average surface roughness. Since the R_a is similar, the lambda ratio for the steel / TiO_2 APS contact with sample A and C are close to each other (0.94 and 0.8 respectively) which suggests that both the contacts are in mixed lubrication regime.

Sample D shows higher friction coefficient in the range of 0.065 – 0.07 compared to A and C. Decrease in the severity from the lambda ratio of 0.8 to 1.8 could reduce the activation of friction modifier MoDTC and lead to higher friction compared to A and C.

Friction behavior as well as the steady state friction coefficient is found to be similar for the tests with samples D and E (0.065 – 0.07). As discussed before, the contact is in mixed lubrication regime in case of sample D and boundary lubrication regime in case of sample E. However, the friction behavior is still found to be similar. For sample D, this could be due to less contact between asperities for the polished surface leading to less activation of MoDTC.

For sample E, high friction could be due to high number of deep roughness grooves on the surface of sample E. It has been previously shown that the friction coefficient is higher if there is a presence of deep, irregularly shaped roughness grooves and if the test is carried out perpendicular to the direction of sliding which is the case here [1-2].

Tribochemistry involved is found to be similar in all the contacts where MoS_2 and MoO_3 formation is observed with no oxysulphides in all the cases but may be in different amounts. Failure in complete or partial activation of MoDTC additive plays an important role in determining the steady state friction coefficient in case of samples with different roughness parameters. Also, the surface coverage of the MoS_2 tribofilm could be a factor that varies as the friction coefficient changes considerably in different cases.

(b) Wear behaviour:

Wear scar diameters on the steel balls slid against TiO_2 APS coating with different roughness parameters are shown in the fig 5.2. The maximum Hertzian diameter for the steel / TiO_2 APS contact is 145 µm. It can be observed that the wear scar diameter is similar in case of tests with sample A (fig 5.2 (a)) and C (fig 5.2 (b)). As discussed before, the friction behavior, lambda ratio and the lubrication regime in case of these two contacts was similar. This suggests that since the contacts possess similar lambda ratio and so the tribological behaviour is found to be similar.

Sample C shows the highest wear scar diameter on the steel ball in all the cases. In case of sample E, steel ball shows a lot of abrasive wear due high R_a and R_{pk} which is evident from the deep scratches present in the optical image shown in the fig 5.2 (e). However, the wear occurs at the beginning and then the friction coefficient remains stable during the test unlike in case of sample C where the friction coefficient goes on increasing.

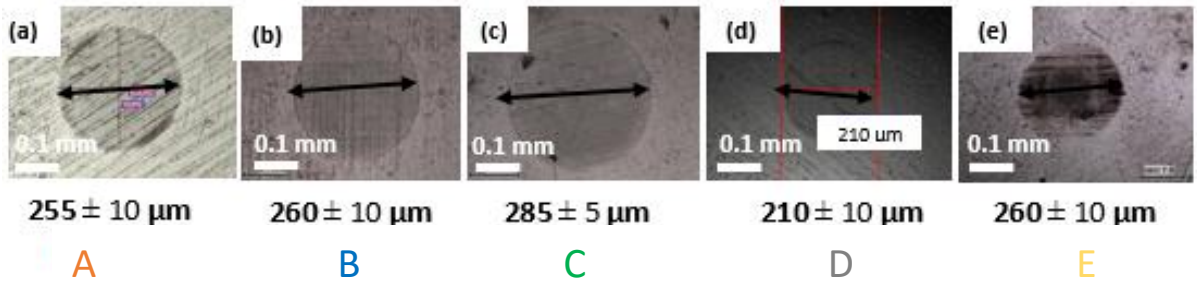

Fig 5.2 Optical images of wear scar diameters on the steel ball slid against TiO_2 APS with different surface finishing processes (a) Grinding (b) Lapping 2 (c) Lapping 1 (d) Polishing (e) Flat honing.

On the contrary, the sample D shows the lowest wear scar diameter on the steel ball. This is because of less contact between asperities leading to less severity which is not enough to activate the friction modifier MoDTC completely to form MoS_2 and reach low friction. This is

in agreement with the previous work by Khaemba *et al* [3], where it was showed that higher roughness helps in faster and complete decomposition of MoDTC in steel / steel contact.

From the above results, it is clear that the most important roughness parameter affecting the tribological behaviour of steel / TiO_2 APS contact is the **average surface roughness R_a and therefore the lambda ratio**. Therefore, when the contact is in mixed or boundary lubrication regime i.e. with **similar lambda ratio**, it **shows similar friction behaviour**.

5.2.1.2 Effect of maintaining similar lambda ratio by changing the speed :

To find out if any other roughness parameter is affecting the tribological behaviour as well as to confirm the discussion regarding the similarity in lambda ratio and lubrication leads to similar friction behaviour in steel / TiO_2 APS contacts, further tribotests are carried out by maintaining similar lambda ratio of sample C (λ = 0.8) for samples B (lapping 2) and D (polishing). Therefore, to maintain the λ close to 0.8 for sample B (λ = 0.51) and sample D (λ = 1.8), sliding speed was changed accordingly. For the sample D (λ = 1.8), the amplitude was reduced from 5 mm to 2.5 mm and thereby changing the sliding speed from 0.05 m / s to 0.025 m / s. For the sample B (λ = 0.51), the amplitude was increased from 5 mm to 10 mm and thereby changing the sliding speed from 0.05 m / s to 0.1 m /s.

Fig 5.3 shows the comparison of friction curves obtained for steel / TiO_2 APS contact after the samples B and D are modified to lambda ratio close to that of sample C (λ = 0.8) and sample A (λ = 0.95). The new curves with the change of speed to maintain similar lambda ratios are shown with the legend **B' (faint grey)** which is the lapped 2 sample with increased speed and **D'(dark grey)** which is the polished sample with reduced speed.

It can be observed that the steady state friction coefficient of the samples B' and D' obtained with similar lambda ratios to the samples A and C is reduced to 0.04. The friction trends are found to be exactly similar to that obtained for the samples A and C as discussed in the previous section. This could be explained on the basis of our initial hypothesis regarding contact between asperities and the lubrication regimes. As the speed is adjusted by maintaining the similar lambda ratio of around 0.8, the contact is in similar lubrication regime as the samples A and C, so there is enough contact between asperities which leads to activate the friction modifier MoDTC and thereby reduce friction coefficient.

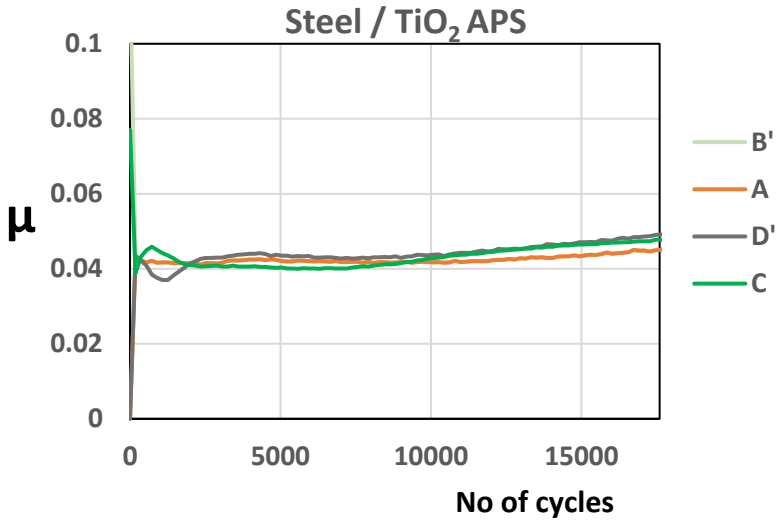

Fig 5.3 Comparison of friction curves for steel / TiO_2 APS obtained with similar lambda ratios by changing the sliding speed lubricated with base oil + 0.5 % MoDTC.

Comparison of the wear scar diameters on the steel balls slid against TiO_2 APS coating for samples B' (change of lambda ratio from sample B) and D'(change of lambda ratio from sample D) is shown in the fig 5.4. It can be observed that the wear scar diameter is increased in case of the sample D' compared to sample D (from fig 5.2) when the sliding speed is reduced to achieve the lambda ratio close to 0.8. This suggests that the contact has become more severe and more contact between asperities leads to higher wear scar diameter. Wear scar diameter is slightly increased from 285 µm in sample B to 300 µm in sample B'.

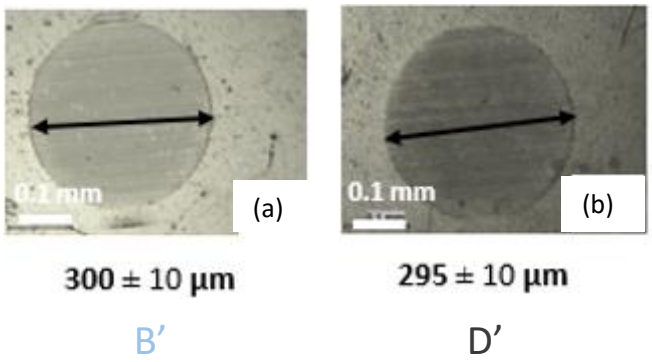

Fig 5.4 Optical images of wear scars on the steel ball slid against TiO_2 APS for samples B' and D' which are the samples with change of lambda ratio for B and D.

5.2.1.3 Surface characterization of the tribofilms using XPS:

To confirm if similar tribochemistry is obtained when the lambda ratio is in the same range for steel / TiO_2 APS contact, XPS was carried out. The high resolution Mo3d XPS spectra inside the tribofilm on TiO_2 APS flats obtained with different roughness samples but with similar lambda ratios are shown in the fig 5.5. Similar fitting procedure, binding energies for various

contributions and analysis area are used as mentioned in Chapter 4 Section 4.2.2.2. Therefore, it is clear that MoS_2 is observed in all cases whenever the lambda ratio is less than 1 and in the similar range. Tribochemistry (presence of MoS_2 and MoO_3) observed is similar in case of the samples which results in similar friction coefficients as well friction behavior. Therefore, it can be concluded that the samples with similar lambda ratios show similar tribofilm composition and similar friction coefficient in case of TiO_2 APS.

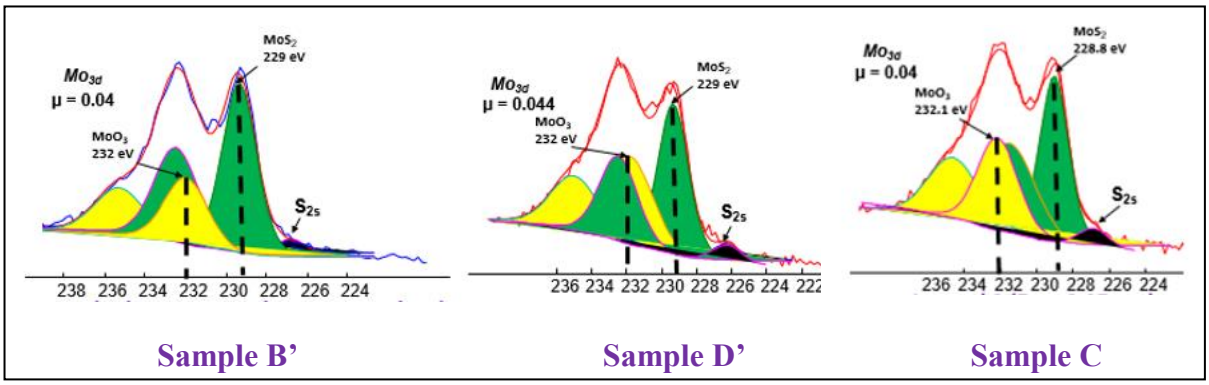

Fig 5.5 Comparison of high resolution Mo3d XPS spectra inside the tribofilm on TiO_2 APS flats obtained with different surface finishing processes and different roughness parameters but with similar lambda ratio when lubricated with base oil + 0.5 % MoDTC at Hertzian contact pressure of 0.7 GPa and a temperature of 100°C.

From the friction and wear results obtained for steel / TiO_2 APS contact for various average surface roughness values of TiO_2 APS, it can be concluded that the trends observed show non-Stribeck behaviour. Friction coefficient is found to be high for extremely polished sample (R_a = 40 nm) as well as extremely rough sample (R_a = 330 nm) whereas the other samples more or less show similar friction coefficients which are lower than the extremely polished and extremely rough sample. This suggests that the lowest friction coefficient obtained is for a certain range of lambda ratio (in this case from 0.8 to 1). However, wear is observed on the steel ball for the polished sample (even when the contact is in hydrodynamic regime), since there is contact between the counterparts at the beginning of the tribotest but the friction modifier additive MoDTC is not activated enough to reach low friction coefficients.

5.2.2 Effect of concentration of MoDTC :

5.2.2.1 Tribological behavior of steel / TiO_2 APS and steel / reference steel

Comparison of friction results for steel / reference steel and steel / TiO_2 APS contacts is shown in fig 5.6 when the concentration of MoDTC in base oil is lowered from 0.5 wt % to 0.01 wt % MoDTC in base oil. The major difference between steel / TiO_2 APS and steel / reference steel is the value of steady state friction coefficient obtained.

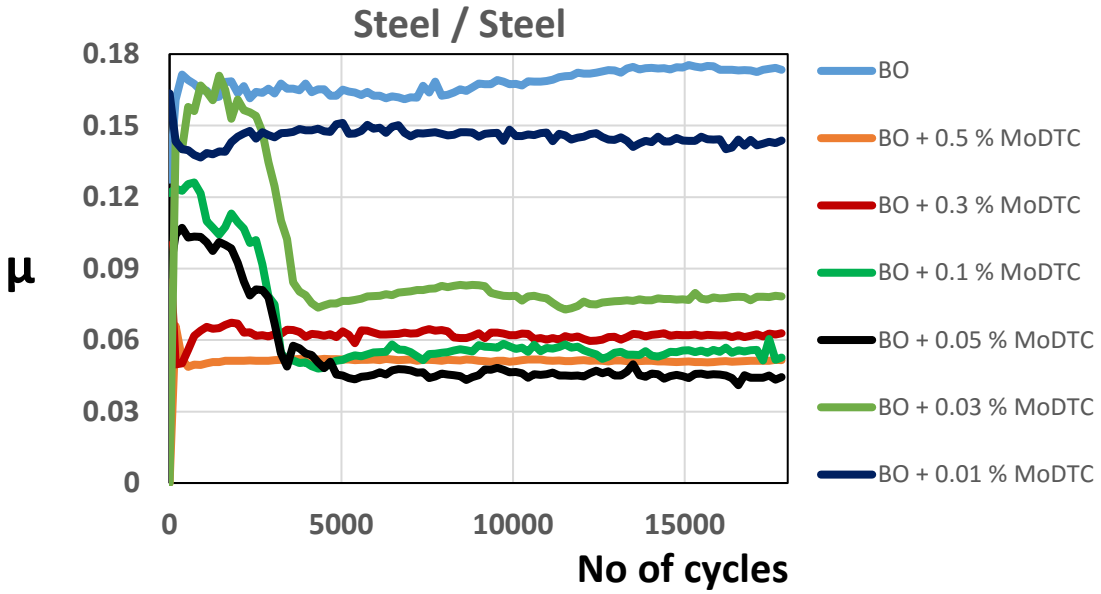

(a)

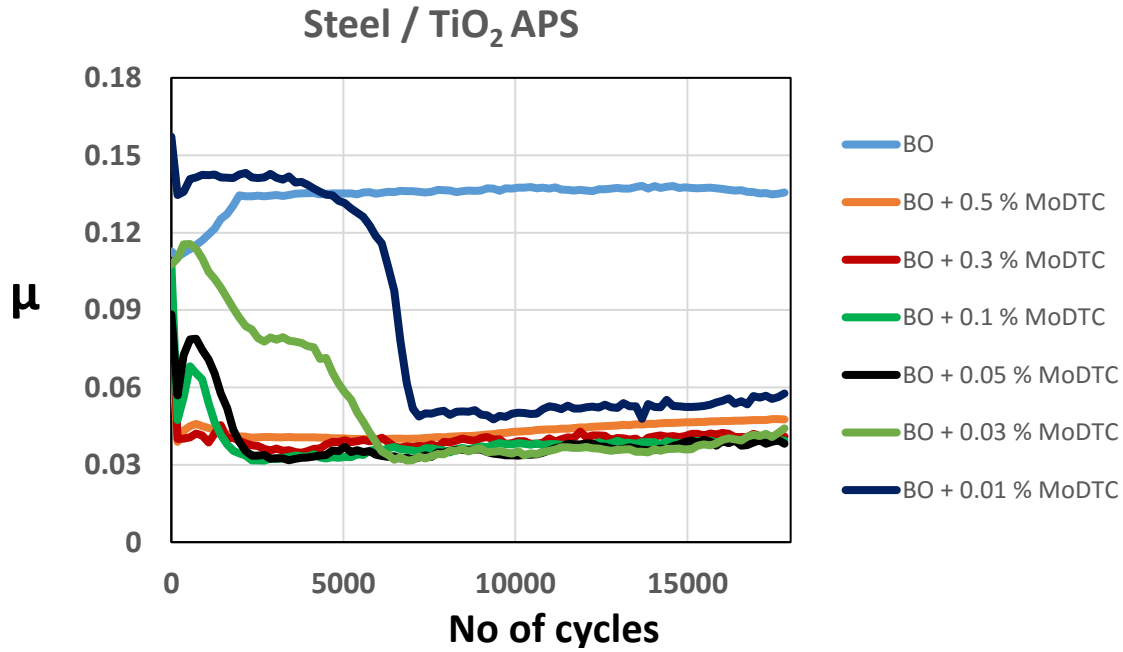

(b)

Fig 5.6 Friction curves at various concentrations of MoDTC in base oil for (a) Steel / reference steel (b) Steel / TiO_2 APS at 100°C with maximum contact pressure of 700 MPa.

In case of steel / TiO_2 APS contact, steady state friction coefficient is similar at all concentrations whereas in case of steel / reference steel contact, steady state friction coefficient increases as the concentration of MoDTC is reduced in base oil from 0.5 wt % MoDTC ($\mu \approx 0.045$) to 0.01 wt % MoDTC ($\mu \approx 0.12$). Friction curves show that even 0.01 wt % of MoDTC in base oil is enough to achieve low friction in case of steel / TiO_2 APS with some induction time required; whereas in case of steel / reference steel, friction behavior at 0.01 wt % is similar to that of the base oil. Induction time is observed in steel / reference steel when it is lubricated with base oil + 0.03, 0.05, 0.1 wt % MoDTC as shown in fig 5.6 (a). However, in case of steel / TiO_2 APS, induction time appears only below concentration of 0.1 % MoDTC as shown in fig 5.6 (b).

The percentage of wear above Hertzian diameter for steel / reference steel and steel / TiO_2 APS is compared in the histogram shown in fig 5.7. For base oil + 0.01 wt % MoDTC, it is observed that percentage of wear above the respective Hertzian diameters on the steel ball is lower in case of TiO_2 APS compared to reference steel. All the other concentrations show similar wear behavior probably due to formation of friction reducing tribofilm by decomposition of MoDTC on the contact surface.

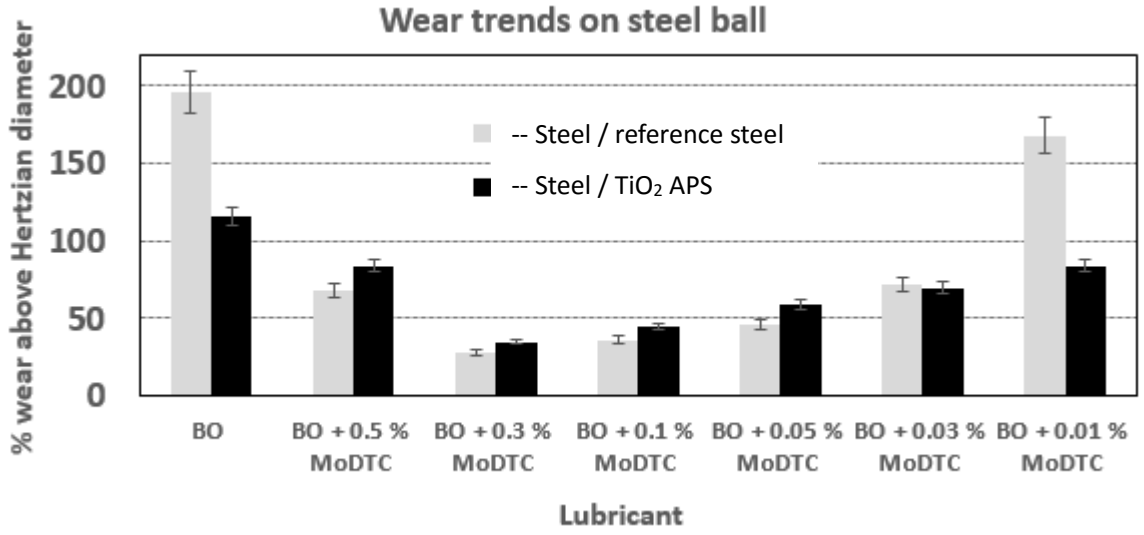

Fig 5.7 Comparison of wear trends on the steel ball tested against reference steel and TiO_2 APS flats lubricated with various concentrations of MoDTC in base oil.

Low friction behavior at 0.01 wt % MoDTC in case of TiO_2 APS suggests that a tribofilm is formed whereas it is not formed in case of reference steel flat as it shows higher wear and friction coefficient similar to that of base oil. The best combination of low wear and low friction coefficient without any induction time is observed in case of steel / TiO_2 APS contact when it is lubricated with base oil + 0.3 % MoDTC. Also, the wear and friction behavior for steel /

reference steel is better when it is lubricated with base oil + 0.3 % MoDTC compared to other concentrations. Therefore, base oil + 0.3 % MoDTC is used as a lubricant for further parametric studies.

5.2.2.2 Surface analysis of the tribofilms using XPS:

To investigate the reduction in friction coefficient even at low concentration of MoDTC in case of TiO_2 APS and the differences in friction coefficients between reference steel and TiO_2 APS, XPS was carried out. To analyze the reduction in friction coefficient, Mo3d spectra obtained for three different concentrations (0.01, 0.05 and 0.3 wt % MoDTC) are compared for reference steel and TiO_2 APS flats in fig 5.8. Similar fitting procedure, binding energies for various contributions and analysis area are used as mentioned in Chapter 4 Section 4.2.2.2.

From the results obtained for various concentrations, three concentrations are selected to compare the tribochemistry of reference steel and TiO_2 APS flats.

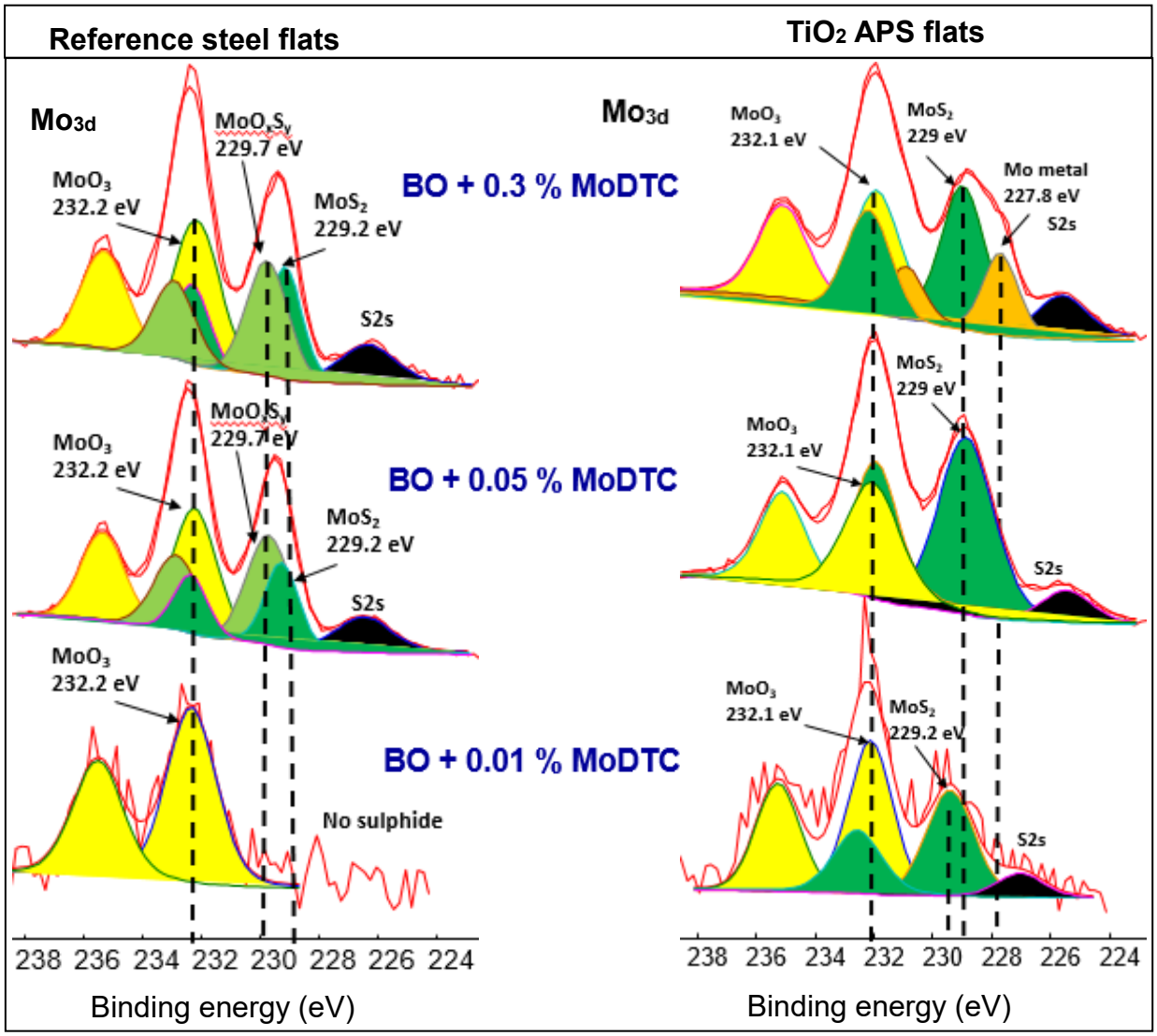

Fig 5.8 Comparison of high resolution Mo3d XPS spectra for reference steel (left) and TiO_2 APS flats (right) lubricated with (from the top) base oil + 0.3 %, base oil + 0.05 % and base oil + 0.01 % MoDTC.

The Mo3d peak is divided into Mo metal – 227.8 ± 0.2 eV (orange peaks), sulphide – 229 ± 0.2 eV (dark green peaks, Mo+4), oxide – 232 ± 0.2 eV (yellow peaks, Mo+6) and oxysulphide – 229.7 ± 0.2 eV (light green peaks) and all the respective contributions are fitted using the binding energy values of Mo3d obtained from literature [4-6].

XPS results comparison at various concentrations of MoDTC showed that in case of 0.3 wt % of MoDTC in base oil with TiO_2 APS flat, MoS_2 and MoO_3 is observed in the Mo3d spectra along with more reduced Mo compound at the binding energy of 227.8 eV assigned to molybdenum metal. At 0.01 wt % MoDTC in base oil, in case of reference steel, Mo3d spectra shows that only MoO_3 is formed inside the tribofilm with no Mo-sulphides. This is in agreement with the friction behavior ($\mu \approx 0.12$) which is similar to that of base oil. However, in case of the tribofilm on the TiO_2 APS flat, MoS_2 is formed even at the lowest concentration of 0.01 wt % MoDTC and low friction is achieved.

Comparison at various concentrations of MoDTC shows that **MoS_2 formation occurs at all concentrations in case of TiO_2 APS with no oxysulphides whereas in case of reference steel** flats **MoO_xS_y contribution is observed with some MoS_2.**

5.2.3 Effect of temperature:

5.2.3.1 Tribological behavior of steel / TiO_2 APS and steel / reference steel

Fig 5.9 shows the comparison of friction curves obtained for steel / reference steel and steel / TiO_2 APS. Three different temperatures of 20°C, 60°C and 100°C were used at a constant maximum Hertzian pressure of 0.7 GPa lubricated with base oil + 0.3 % MoDTC.

For the tests conducted at room temperature (20°C), it is observed that the steady state friction coefficient obtained for steel / TiO_2 APS ($\mu \approx 0.06$) is lower than for steel / reference steel ($\mu \approx 0.08$). Also, for the tests conducted at 60°C and 100°C, it is observed that the steady state friction coefficient obtained for steel / TiO_2 APS ($\mu \approx 0.055$ at 60°C and $\mu \approx 0.04$ at 100°C) is lower than for steel / reference steel ($\mu \approx 0.065$ at 60°C and $\mu \approx 0.052$ at 100°C). Higher temperature is required to achieve low friction in case of reference steel; whereas in case of TiO_2 APS, lower friction could be reached even at room temperature ($\mu \approx 0.065$).

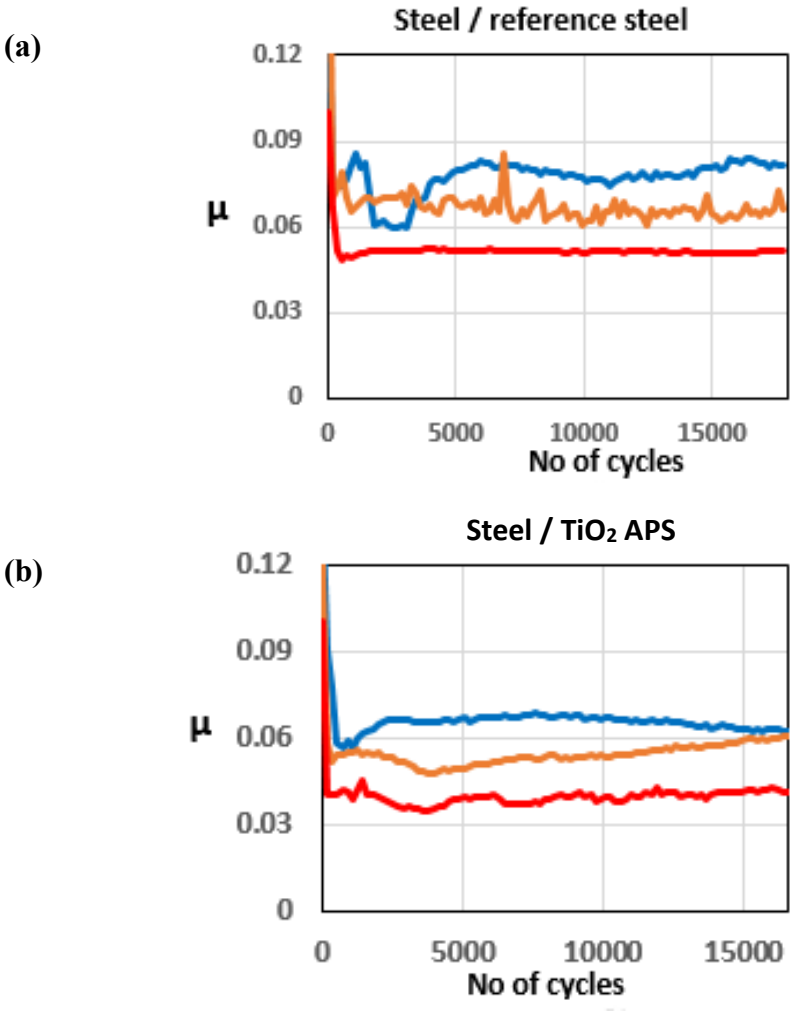

Fig 5.9 Comparison of friction behaviour for (a) Steel / steel (b) Steel / TiO_2 APS at different temperatures lubricated with base oil + 0.3 % MoDTC at 0.7 GPa.

Fig 5.10 shows the trends for the comparison of percentage wear above the Hertzian diameters on the steel ball for steel / reference steel and steel / TiO_2 APS contacts at different temperatures of 20 °C, 60 °C and 100 °C when lubricated with base oil + 0.3 % MoDTC. It can be observed that % wear above Hertzian diameter is higher in case of steel balls against reference steel flats at 20°C and 60°C as compared to steel balls against TiO_2 APS flats.

When the temperature is reduced to lower values, the viscosity of the oil is increased and the lubrication regime is changed. However, since wear is observed in both the contacts and it is higher at low temperatures, contact between asperities is still present due to significant Hertzian contact pressure. The lower wear obtained at higher temperatures could be due to the complete activation of MoDTC whereas it fails to activate completely at low temperatures leading to higher wear. This could be further confirmed by XPS analysis showing different amount of MoS_2. Similar trends of friction and wear behaviour in steel / reference steel were observed by Khaemba *et al* [7] when they studied the effect of temperature on the tribological behaviour.

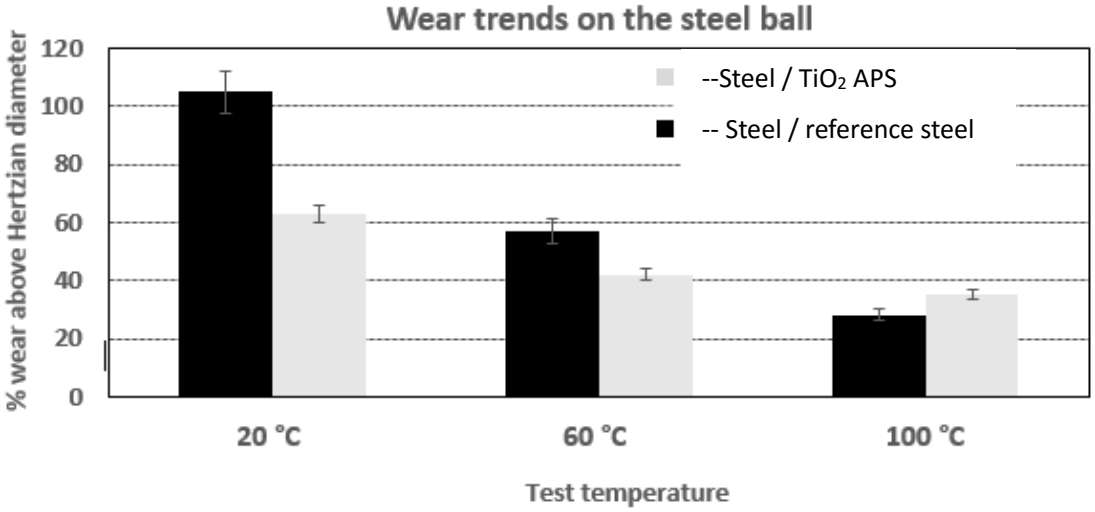

Fig 5.10 Comparison of wear trends on the steel ball tested against reference steel and TiO_2 APS flats lubricated with base oil + 0.3 % MoDTC at different temperatures (20 °C, 60 °C and 100 °C).

5.2.3.2 Surface analysis of the tribofilms using XPS:

To analyse the differences in friction behavior at different temperatures, Mo3d high resolution spectra were obtained for reference steel (left side) and TiO_2 APS flats (right side) and are shown in fig 5.11. Similar fitting parameters and procedure were used for fitting the Mo3d peak as mentioned in the concentration section.

Comparison of tribochemistry at various test temperatures for steel and TiO_2 APS flats shows that **MoS_2 is obtained in case of steel / TiO_2 APS contact at all temperatures**. However, in case of reference steel flats, MoO_xS_y contribution along with MoO_3 is observed at low

temperatures of 20°C and 60°C. However, MoS_2 is formed at higher temperatures with MoO_3 and MoO_xS_y which is in agreement with the lower friction coefficient of 0.055.

In case of TiO_2 APS, MoO_3 content is found to dominate compared to MoS_2 at lower temperatures of 20°C and 60°C. This does not affect the friction behaviour (μ remains the same) as the friction coefficient is affected only by presence of MoS_2 inside the tribofilm.

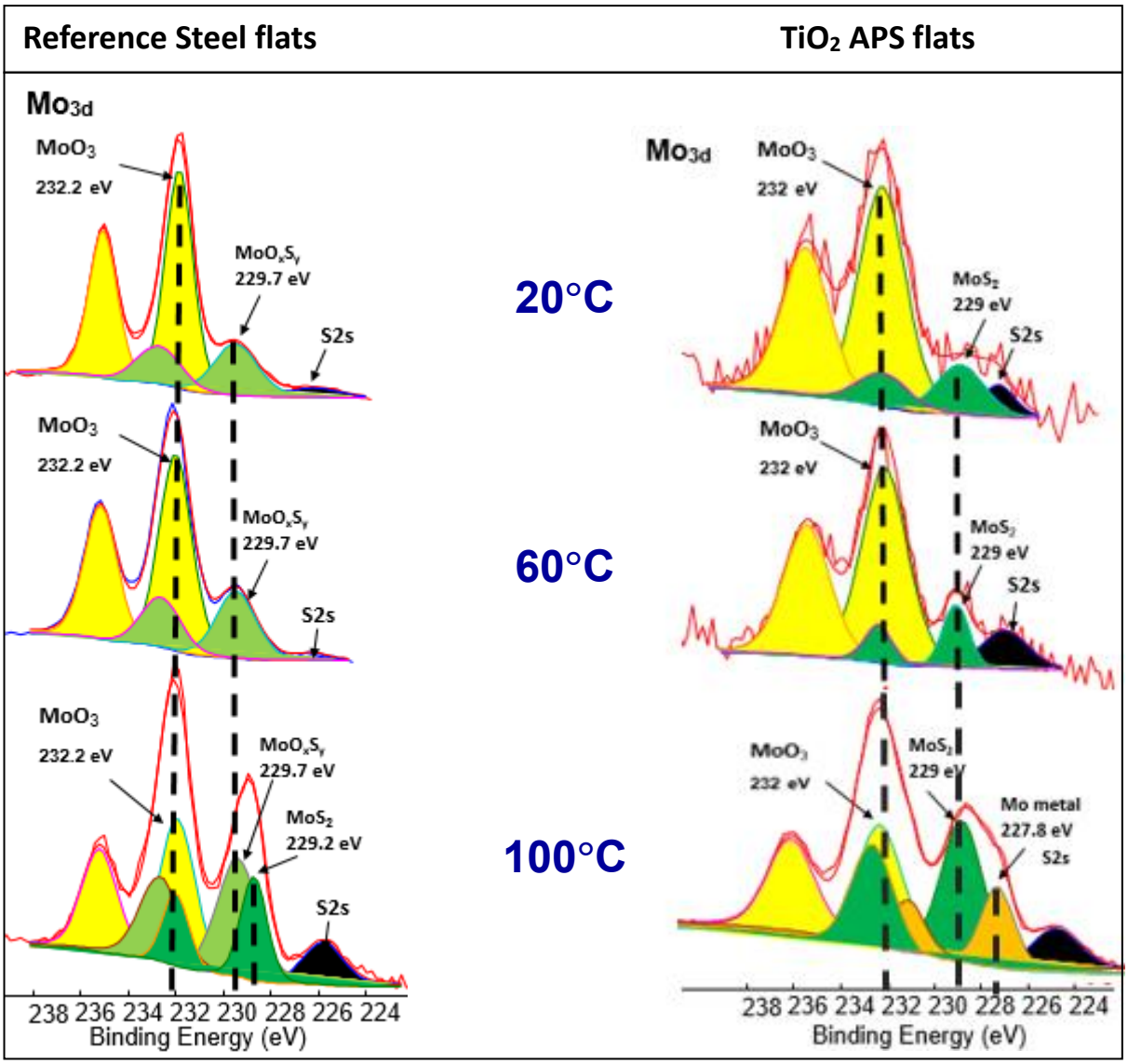

Fig 5.11 Comparison of high resolution XPS Mo3d spectra for reference steel (left) and TiO_2 APS flats (right) at different temperatures of 20°C, 60°C and 100°C lubricated with base oil + 0.3 % MoDTC at a maximum Hertzian contact pressure of 0.7 GPa.

Temperature provides energy for chemical reaction to occur. In this case, decomposition of MoDTC requires high temperatures to form MoS_2 [10] in case of steel / steel contacts. Therefore, Mo-oxysulphides are formed and pure MoS_2 is not formed at low temperatures in case of reference steel flat. Similar effect was observed by Khaemba *et al* [7] in case of steel /

reference steel contact, where they studied the effect of temperature on the decomposition of MoDTC and suggested that high temperatures are required to form pure MoS_2. They suggested that products like $FeMoO_4$ are formed where Mo is in similar oxidation state as in case of MoO_3 observed in this study. MoS_x is also formed as an intermediate where the oxidation state of Mo remains higher (+5 or +6) which is similar to the case of MoO_xS_y in this study. Thus, it can be concluded **that higher temperatures are required to decompose MoDTC to MoS_2 in case of reference steel but not in case of TiO_2 APS**.

In case of steel / TiO_2 APS contact, complete decomposition of MoDTC occurs even at lower temperatures but at a slower rate. The amount of MoS_2 covering the surface may be different. Thus, the friction coefficient obtained is higher at 20°C than at 100°C in case of TiO_2 APS flats. Thus, low test temperature slows the rate of decomposition of MoDTC, but does not prevent MoDTC to decompose and form MoS_2 which helps in reducing friction coefficient compared to steel / reference steel contact.

5.2.4 Effect of contact pressure:

5.2.4.1 Tribological behavior of steel / TiO_2 APS and steel / reference steel:

Comparison of friction results obtained for steel / reference steel and steel / TiO_2 APS contacts at different pressures of 0.4 GPa, 0.7 GPa and 1 GPa and at a constant temperature of 100°C lubricated with base oil + 0.3 % MoDTC is shown in fig 5.12. For all the pressures, it is observed that the steady state friction coefficient obtained for steel / TiO_2 APS ($\mu \approx 0.05$ at 0.4 GPa, $\mu \approx 0.042$ at 0.7 GPa and 1 GPa) is considerably lower than for steel / reference steel ($\mu \approx 0.085$ at 0.4 GPa, $\mu \approx 0.06$ at 0.7 GPa and $\mu \approx 0.052$ at 1 GPa).

For reference steel flats, friction coefficient is the lowest at 1 GPa and the highest at 0.4 GPa. This suggests that high pressure is required to obtain the lowest friction coefficient in case of reference steel; whereas in case of TiO_2 APS, even at low pressures, lower friction coefficient of 0.05 is obtained. Therefore, it can be concluded that **friction behaviour of the steel / TiO_2 APS contact is insensitive to pressure to a certain extent whereas steel / reference steel contact is sensitive to pressure.**

(a)

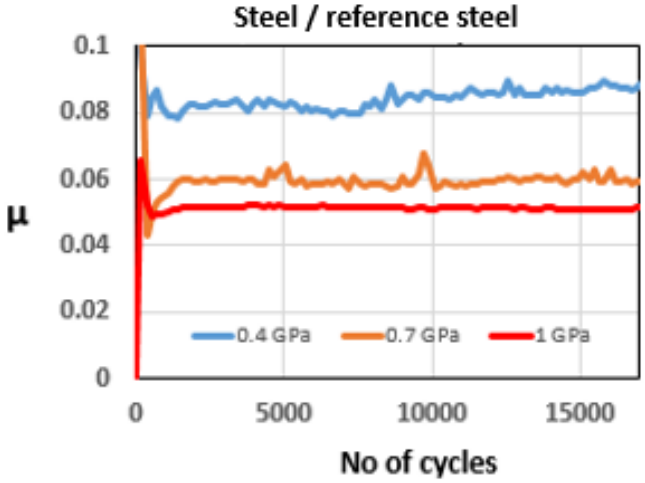

(b)

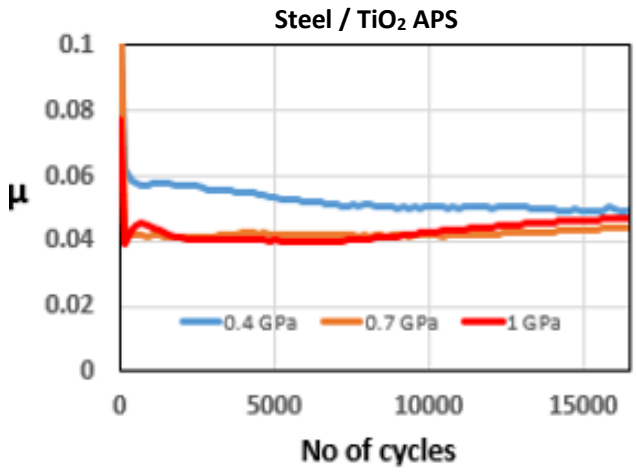

Fig 5.12 Comparison of friction behaviour at different pressures for (a) Steel / steel (b) Steel / TiO_2 APS lubricated with base oil + 0.5 % MoDTC at 100°C.

Fig 5.13 shows the trends for the comparison of % wear above the Hertzian diameters on the steel ball for steel / reference steel and steel / TiO_2 APS contacts at different pressures of 0.4 GPa, 0.7 GPa and 1 GPa when lubricated with base oil + 0.3 % MoDTC. In case of steel / reference steel contact, it can be observed that the wear is clearly higher at 0.4 GPa than at 0.7 GPa and 1 GPa. This higher wear is related to higher friction coefficient at lower pressures and is probably observed because MoDTC is not activated which is evident from the friction behaviour. It can be observed that the % wear above Hertzian diameter is considerably lower in case of steel / TiO_2 APS contact at 0.4 GPa and 1 GPa than steel / reference steel contact. At 0.7 GPa, the wear observed is almost similar in both the contacts. Also, comparing the % wear above Hertzian diameter for different pressures in case of steel / TiO_2 APS contact, they are found to be in a similar range (34 – 48 %) which suggests that the effect of the additive is similar at all pressures.

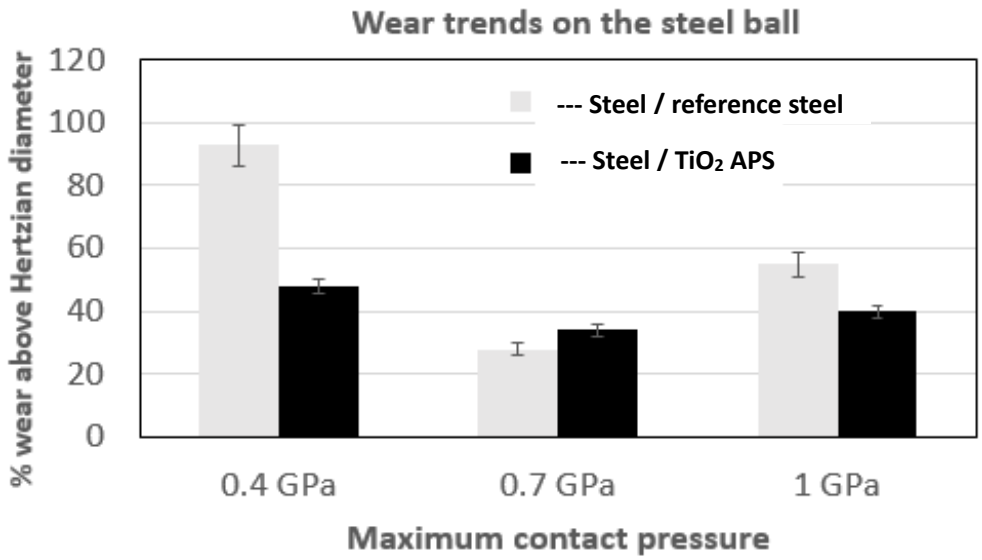

Fig 5.13 Comparison of wear trends on the steel ball tested against reference steel and TiO_2 APS flats lubricated with base oil + 0.3 % MoDTC at different contact pressures (0.4 GPa, 0.7 GPa and 1 GPa).

5.2.4.2 Surface analysis of the tribofilms using XPS:

To investigate the differences in friction behavior at different pressures, Mo3d high resolution spectra were obtained at different pressures for reference steel and TiO_2 APS flats. Comparison of the XPS spectra is shown in fig 5.14. Similar fitting procedure and parameters were used for fitting Mo3d peaks as mentioned in the concentration section.

Comparison at various test pressures for steel and TiO_2 APS flats shows that **MoS_2 is formed on the surface of TiO_2 APS at all pressures** which suggests complete decomposition of

MoDTC to MoS_2.

In case of steel / reference steel contact, **only MoO_xS_y** contribution is observed at **0.4 GPa** and as the pressure is increased to **0.7 GPa and 1 GPa, MoS_2 is observed along with MoO_xS_y.** The presence of MoS_2 at higher pressures explains the lower friction coefficient obtained ($\mu \approx 0.06$ at 0.7 GPa and $\mu \approx 0.052$ at 1 GPa). From the results, it can be suggested that higher pressures are required for complete decomposition of MoDTC to MoS_2 in case of reference steel like mentioned in the literature [7]. At 0.4 GPa, higher friction coefficient is observed because the amount of MoO_xS_y is higher in the tribofilm.

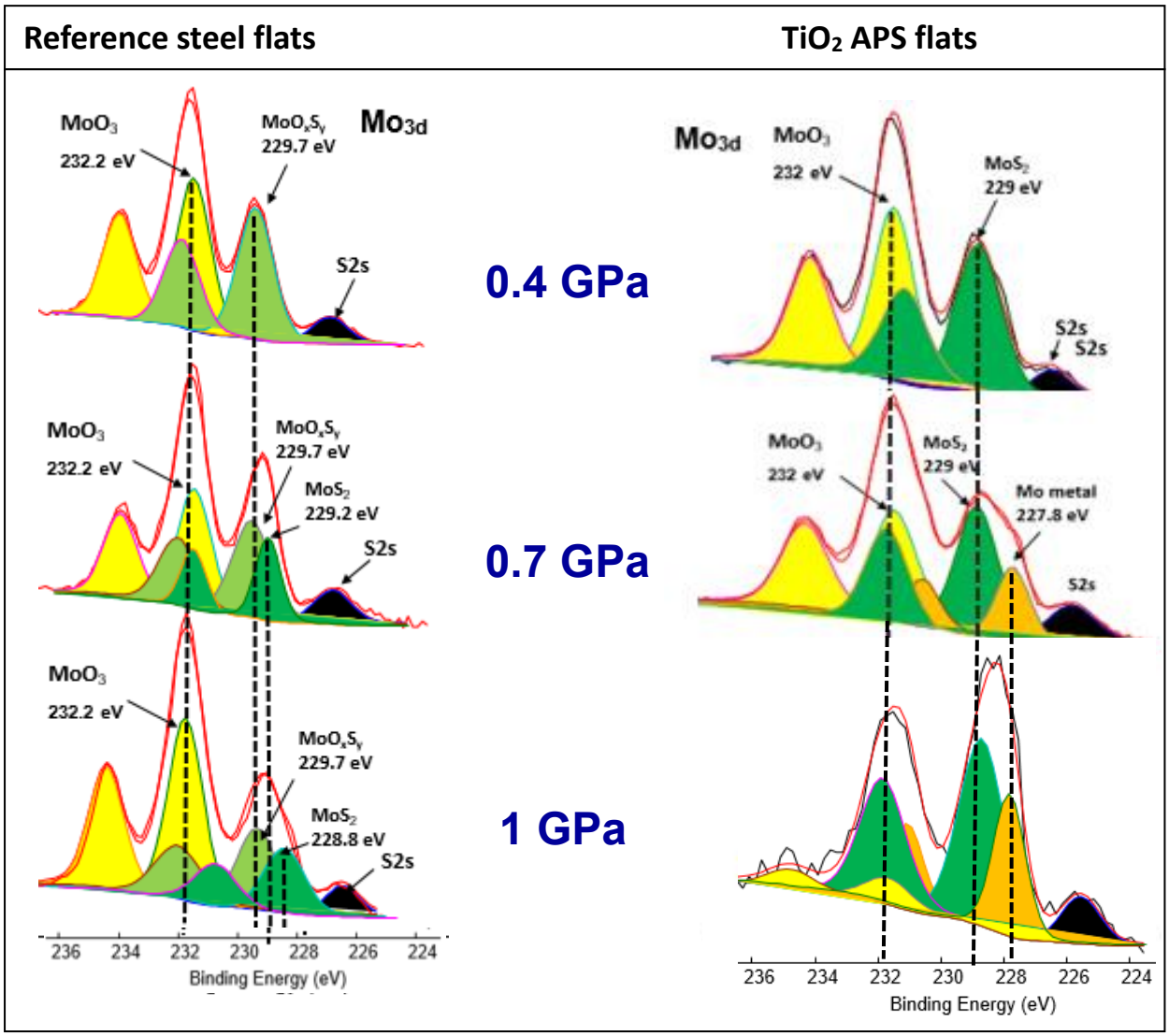

Fig 5.14 Comparison of high resolution XPS Mo3d spectra for reference steel (left) and TiO_2 APS flats (right) at different pressures of 0.4 GPa, 0.7 GPa and 1 GPa lubricated with base oil + 0.3 % MoDTC at a constant temperature of 100°C.

On the contrary, in case of steel / TiO_2 APS contact, MoS_2 is formed at all pressures which corresponds to the lower friction coefficients. The amount of MoS_2 and MoO_3 formation in the tribofilm may be different but this does not affect the friction coefficient considerably as the friction coefficient is more dependent on MoS_2 covering the surface than the presence of MoO_3. This suggests that decomposition of MoDTC additive proceeds even at the lowest pressure of 0.4 GPa. Also, at maximum Hertzian contact pressures of 0.7 GPa and 1 GPa, presence of more reduced Mo contribution attributed to Mo metal is observed. This could be due to further reduction of Mo compounds formed in the tribofilm. This behaviour is not observed in case of steel / reference steel.

5.2.5 Effect of change of counterpart material

Counterpart material sliding against TiO_2 APS coating was changed to Al_2O_3 and ZrO_2 balls to investigate the effect of absence of iron in the contact. Table 5.3 lists the properties for the changed counterpart materials (balls).

Table 5.3 Properties of the ball materials

Ball material	Ra	Hardness (GPa)	Elastic modulus (GPa)
ZrO_2	20 nm	13	200
Al_2O_3	20 nm	16	380

5.2.5.1 Friction results for TiO_2 APS flats

Comparison of friction results obtained for steel / TiO_2 APS, ZrO_2 / TiO_2 APS and Al_2O_3 / TiO_2 APS contacts lubricated with base oil + 0.3 % MoDTC are shown in fig 5.15. It can be observed that all the three contacts - steel / TiO_2 APS, ZrO_2 / TiO_2 APS and Al_2O_3 / TiO_2 APS show similar steady state friction coefficient (μ = 0.04). There is no effect of change of counterpart material on the friction behaviour.

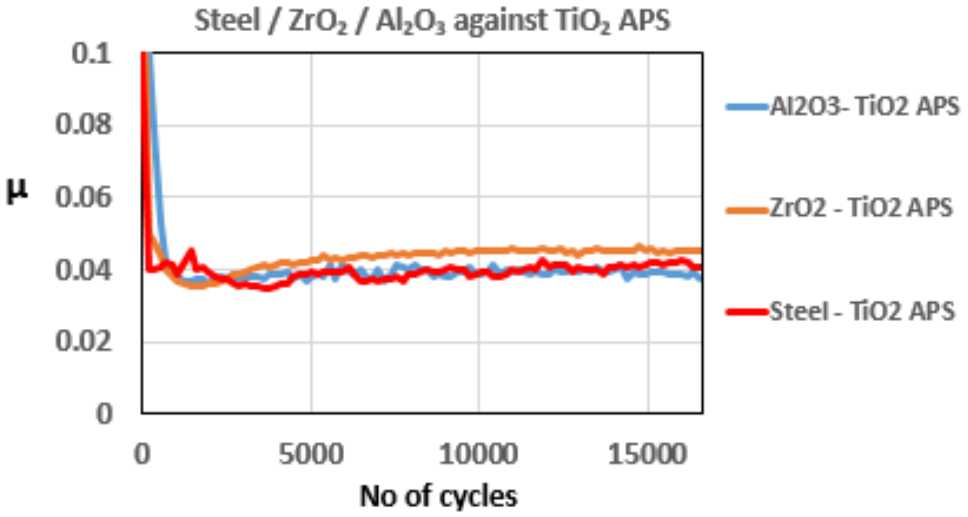

Fig 5.15 Comparison of friction behaviour for steel / TiO_2 APS, ZrO_2 / TiO_2 APS and Al_2O_3 / TiO_2 APS at a maximum Hertzian contact pressure of 0.7 GPa lubricated with base oil + 0.3 % MoDTC and a constant temperature of 100°C.

Optical images of wear scars on both the tribopairs in case of steel / TiO_2 APS, ZrO_2 / TiO_2 APS and Al_2O_3 / TiO_2 APS contacts are shown in fig 5.16. Hertzian diameters are mentioned on the top of optical images for each contact. It can be observed that the wear observed in case of all the three contacts is similar to each other and is in the range of 30-40 % above the Hertzian

diameter on both tribopair materials. Low wear is observed on the TiO_2 APS coating due to the wear resistant properties of TiO_2 APS coating [8].

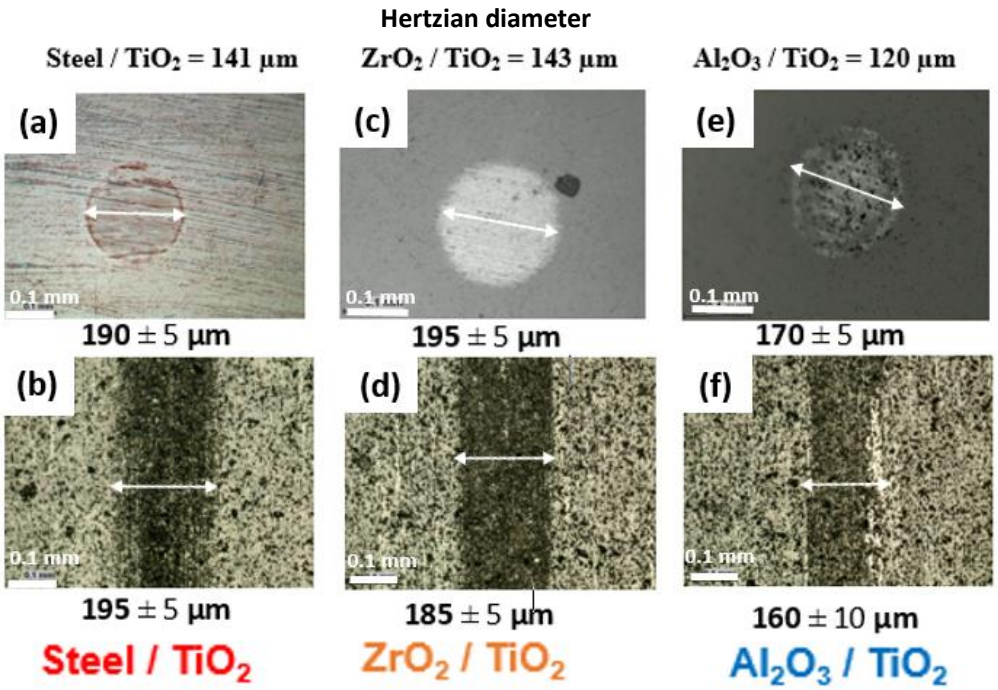

Fig 5.16. Optical images of the wear scars on (a) **steel ball** vs reference steel flat, (b) steel flat, (c) **steel ball** vs TiO_2 flat, (d) TiO_2 flat, (e) **steel ball** vs steel APS, (f) steel APS flat when lubricated with base oil + MoDTC.

Fig 5.17 shows the wear trends on the different balls and TiO_2 APS flats tested against them. It is clear from the percentage of wear above Hertzian diameter on both the ball and the flats that the wear occurring in all the contacts is limited.

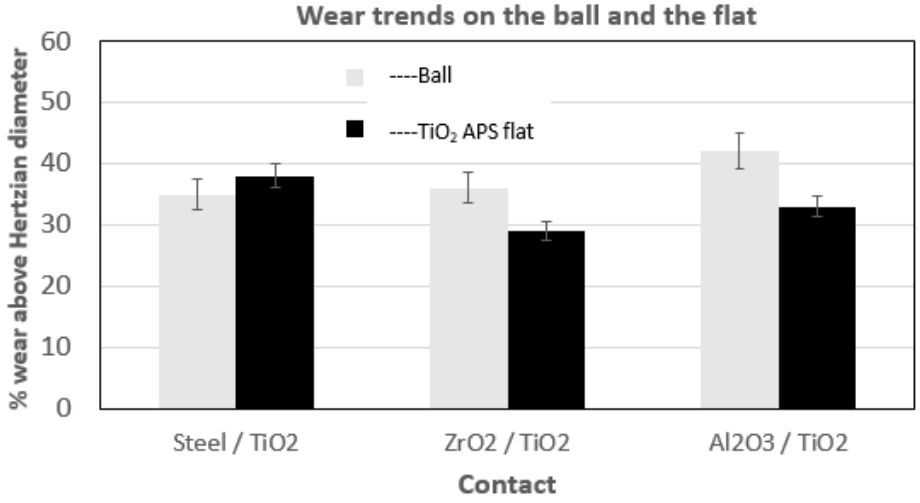

Fig 5.17 Comparison of wear trends on the various balls tested against TiO_2 APS flats lubricated with base oil + 0.3 % MoDTC at a pressure of 0.7 GPa and temperature of 100°C.

5.2.5.2 Surface analysis of the tribofilms :

To investigate the differences in the tribological behavior of steel, ZrO_2 and Al_2O_3 balls sliding against TiO_2 APS flats, Mo3d high resolution spectra were obtained on the wear scars of reference steel and TiO_2 APS flats. Comparison of the Mo3d and C1s high resolution XPS spectra for each contact is shown in fig 5.18. Similar fitting procedure and parameters were used for fitting the Mo3d peak as mentioned in the concentration section. The only difference in the fitting procedure used in this case is the addition of a new contribution in the Mo spectra at the binding energy of 227.9 ± 0.2 eV which was assigned to the carbide species (Mo_xC) [5].

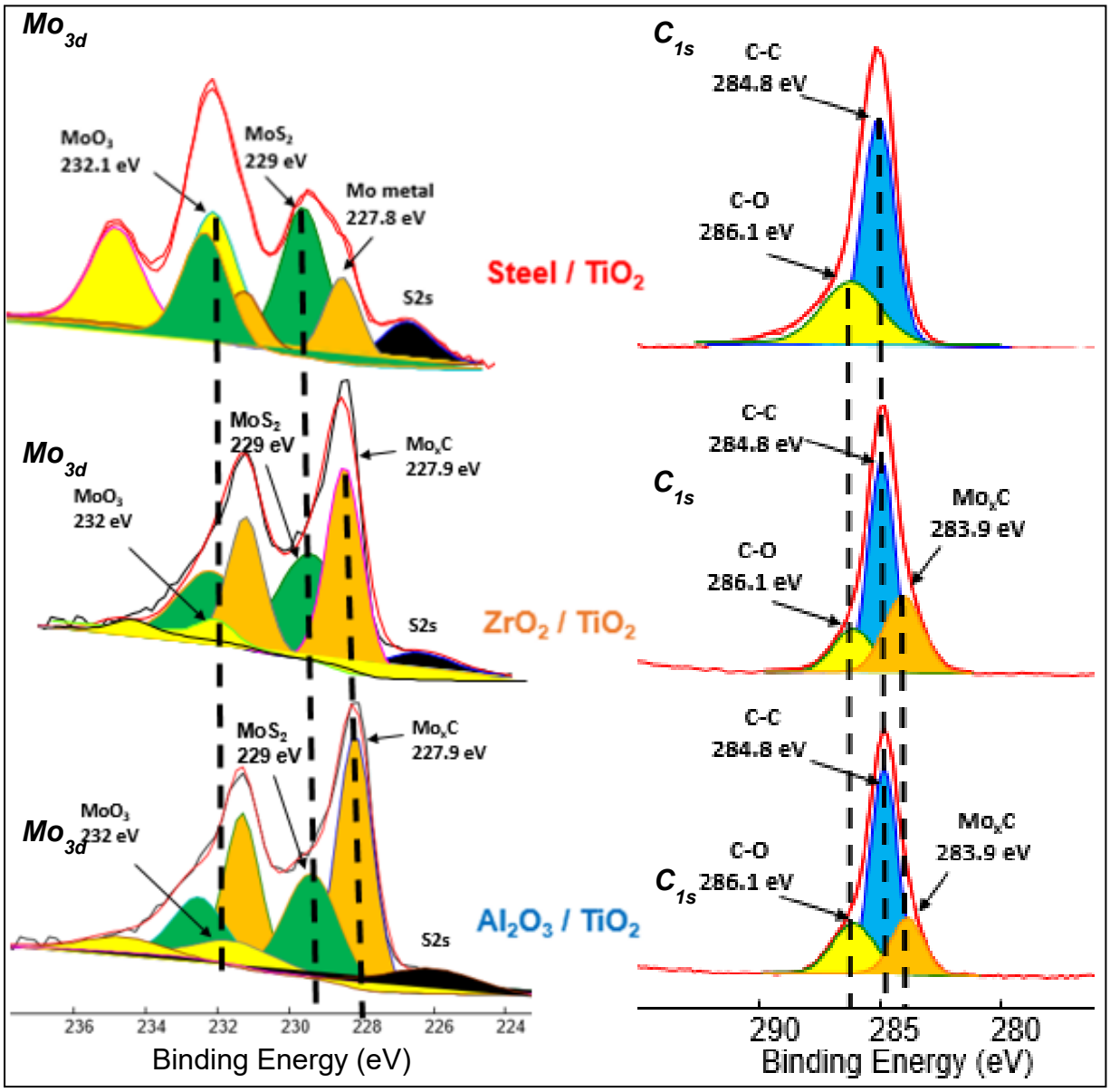

Fig 5.18 Comparison of high resolution XPS Mo3d and C1s spectra for TiO_2 APS flats (right) sliding against steel, ZrO_2 and Al_2O_3 balls respectively (from top to bottom) at maximum contact pressure of 0.7 GPa lubricated with base oil + 0.3 % MoDTC at a constant temperature of 100°C.

C1s spectra was fitted with two or three different contributions. Binding energy values used for various carbon species were C-C (284.8 ± 0.2 eV), C-O (286.1 ± 0.2 eV) and carbide (283.9 ± 0.2 eV). It is clear from the C1s spectra obtained in case of ZrO_2 / TiO_2 APS and Al_2O_3 / TiO_2 APS contacts that carbide species is present which was also observed in the Mo3d peaks. Therefore, from the above results it can be confirmed that Mo_xC species is formed in the contact involving ZrO_2 and Al_2O_3 balls. However, in case of steel / TiO_2 APS, C1s peak does not show any carbide contribution but the Mo3d spectra shows the presence of a contribution with binding energy close to that of carbide. This contribution is assigned to molybdenum metal as the binding energies of Mo-metal and Mo-carbide are close to each other.

Comparison of the tribochemistries for different balls sliding against TiO_2 APS flats shows that MoS_2 along with MoO_3 is obtained with some reduced Mo contributions which is in agreement with the friction coefficient (μ = 0.04). Similar friction coefficient is obtained due to the formation of MoS_2 in all the cases with no MoO_xS_y. However, in case of steel / TiO_2 APS, MoS_2 and MoO_3 is observed along with further reduced contribution of molybdenum assigned to molybdenum metal (227.8 ± 0.2 eV). Also, in case of ZrO_2 / TiO_2 APS and Al_2O_3 / TiO_2 APS contacts, MoS_2 is observed but along with a new contribution at much lower energies assigned to Mo_xC (227.9 ± 0.2 eV). This could be due to further reduction of molybdenum contribution to Mo+4 (MoC) or Mo+2 (Mo_2C).

From the XPS results, Mo-carbide (Mo+2 or +4) and Mo-sulphide (Mo+4) is formed in case of Al_2O_3 / TiO_2 APS and ZrO_2 / TiO_2 APS contacts with MoO_3 (Mo+6) whereas in case of steel / TiO_2 APS contact, MoO_3 (Mo+6) is formed along with MoS_2 (Mo+4) and Mo metal (Mo in oxidation state of 0). This clearly suggests that there is more reduction of MoDTC molecule in case of ceramic / ceramic contact than with steel / ceramic contact.

5.3 Conclusions:

This chapter investigated the role of various parameters like roughness, reduction in concentration of MoDTC, test temperature, contact pressure and change of counterpart materials on the tribological behavior of steel / TiO_2 APS. Comparisons were made with reference steel on the basis of tribological results and the tribochemistry involved for the temperature, pressure and concentration parameters.

Following are the conclusions obtained from this chapter:

(1) Studies on the **effect of roughness** in case of steel / TiO_2 APS contact showed that the tribological behaviour obtained with different surface finishing processes is found to be similar for samples with similar average surface roughness R_a and therefore lambda ratio. **Similar steady state friction coefficients are observed when all the samples have similar lambda ratio** as the contact remains in the same lubrication regime.

(2) **MoS_2 is formed and low friction is achieved in case of steel / TiO_2 APS contact when the concentration of MoDTC is as low as 0.01 wt % in base oil** compared to the steel / reference steel contacts where MoS_2 formation is not observed.

(3) **MoS_2** is formed and lower friction coefficient is achieved in case of steel / TiO_2 APS contact at all temperatures compared to steel / reference steel contact.

(4) **Studies on the effect of pressure showed that steel / TiO_2 APS** exhibited lower friction coefficient than steel / reference steel contact **due to MoS_2 formation at lowest pressure of 0.4 GPa**. It can be concluded that steel / TiO_2 APS contact is insensitive to pressure whereas in steel / reference steel contact, the friction behaviour changes a lot with change in pressure.

(5) **Effect of change of counterpart material in case of TiO_2 APS from steel balls to ceramic balls** showed increase in amount of conversion of MoDTC to reduced Mo species like MoS_2, Mo metal as well as MoC, Mo_xC (carbides) along with traces of molybdenum oxides. Also, change of counterpart material from steel ball to ceramic balls led to **absence of Fe in the contact** and the tribological results obtained lead to the conclusion that **presence of Fe is not required to decompose MoDTC to form MoS_2 on the surface of non-Fe counterparts.**

5.4 References

[1] P. L. Menezes and S. V. Kailas, “Role of surface texture and roughness parameters on friction and transfer film formation when UHMWPE sliding against steel,” *Biosurface and Biotribology*, vol. 2, no. 1, pp. 1–10, 2016.

[2] P. L. Menezes, Kishore, S. V. Kailas, and M. R. Lovell, “Role of surface texture, roughness, and hardness on friction during unidirectional sliding,” *Tribol. Lett.*, vol. 41, no. 1, pp. 1–15, 2011.

[3] D. N. Khaemba, F. Jarnias, B. Thiebaut, A. Neville, and A. Morina, “The role of surface roughness and slide-roll ratio on the decomposition of MoDTC in tribological contacts,” *J. Phys. D. Appl. Phys.*, vol. 50, no. 8, p. 85302, 2017.

[4] M. De Feo , C. Minfray, M. I. De Barros Bouchet, B. Thiebaut, Th. Le Mogne, B. Vacher, J. M. Martin, “Ageing impact on tribological properties of MoDTC-containing base oil,” *Tribol. Int.*, vol. 92, pp. 126–135, 2015.

[5] M. De Feo , C. Minfray, M. I. De Barros Bouchet, F. Meunier, L. Yang, B. Thiebaut, Th. Le Mogne, J. M. Martin, “MoDTC lubrication of DLC-involving contacts. Impact of MoDTC degradation,” *Wear*, vol. 348–349, pp. 116–125, 2016.

[6] E. Schmidt, F. Weill, G. Meunier, and A. Levasseur, “New amorphous molybdenum oxysulfides obtained in the form of thin films and their characterization by TEM,” *Thin Solid Films*, vol. 245, no. 1–2, pp. 34–39, 1994.

[7] D. N. Khaemba, A. Neville, and A. Morina, “New insights on the decomposition mechanism of Molybdenum DialkyldiThioCarbamate (MoDTC): a Raman spectroscopic study,” *RSC Adv.*, vol. 6, no. 45, pp. 38637–38646, 2016.

[8] A. Skopp, N. Kelling, M. Woydt, and L. M. Berger, “Thermally sprayed titanium suboxide coatings for piston ring/cylinder liners under mixed lubrication and dry-running conditions,” *Wear*, vol. 262, no. 9–10, pp. 1061–1070, 2007.

[9] M. N. Gardos, “Magneli phases of anion-deficient rutile as lubricious oxides. Part I. Tribological behavior of single-crystal and polycrystalline rutile (Ti_nO_{2n-1}),” *Tribol. Lett.*, vol. 8, pp. 65–78, 2000.

[10] B. Dacre and C. H. Bovington, “The adsorption and desorption of zinc di-isopropyldithiophosphate on steel,” *ASLE Trans.*, vol. 25, no. 4, pp. 546–554, 1982.

[11] B. J. Hamrock and D. Dowson, “Isothermal Elastohydrodynamic Lubrication of Point Contacts: Part IV—Starvation Results,” *J. Lubr. Technol.*, vol. 99, no. October, p. 15, 1976.

Chapter 6

Effect of addition of TiO_2 particles with MoDTC in base oil on the tribological behavior of steel / reference steel contact

From the previous chapters, it was observed that better results are obtained with steel / TiO_2 APS contact when lubricated with MoDTC compared to steel / reference steel contact. Considering these results and the literature review carried out on TiO_2 as well as MoS_2, TiO_2 nano as well as micro particles were blended with MoDTC in base oil to be used as a lubricant in steel / reference steel contact. The tribological behavior of the blend on steel / reference steel contact was investigated using linear ball-on-flat tribometer. Surface characterization of the tribofilms was carried out using XPS and FIB TEM on the reference steel flat. Blend with the best tribological properties was used for parametric studies which included tests with reduction in concentration of TiO_2 nanoparticles and MoDTC in base oil. Also, effect of roughness was investigated with rough steel APS coating.

6.1 Literature review:

Automotive industry involves the use of various additives like friction modifiers, antiwear additives to overcome the friction losses in an engine. However, these additives involve use of certain elements like P, S, Zn which are harmful for the environment. Nanoparticles are one of those additives which can replace these harmful additives as they can effectively improve friction behavior by formation of a protective tribofilm on the surface [1-4].

Nanoparticles are effective in boundary lubrication regime as the lubricant film thickness is lower than the diameter of the nanoparticles [3-4]. There are numerous advantages of using nanoparticles as additives. They are relatively insensitive to temperature and tribochemical reactions are limited or non-existent compared to traditional additives [5-6]. Generally, lamellar structured nanoparticles like MoS_2, WS_2 and graphite are used as solid lubricants in boundary lubrication regime as their layered structure involving Mo or W bonded to S with weak Van der waal's forces leads to low shear between the surfaces and so low friction [7-9] .

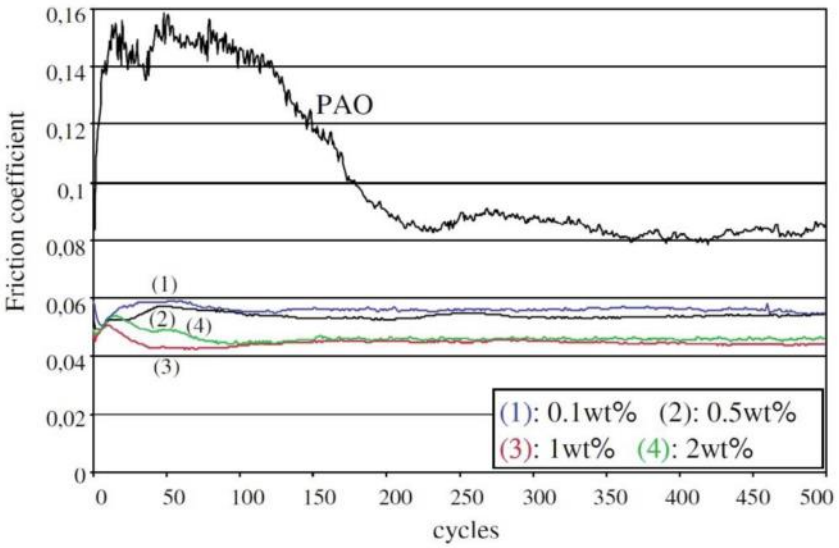

Fig 6.1 Friction reduction effect of (inorganic fullerene) IF-WS_2 nanoparticles in PAO [10] .

Joly Pottuz *et al* [10] showed that lower friction coefficient is obtained with a blend of IF-WS_2 nanoparticles in PAO than when PAO is used alone as shown in fig 6.1. They analysed the worn steel surfaces lubricated by IF-WS_2 nanoparticles in PAO under boundary lubrication conditions and room temperature which revealed the presence of WS_2 sheets. Considering the better friction results obtained by MS_2 nanoparticles, exfoliation mechanism was proposed by Lahouji *et al* [11–13], governed by morphological changes caused by the contact pressure which could be responsible for the formation of the lamellar sheets leading to low friction as shown in the schematic in fig 6.2. Also, Aldana *et a*l have shown that WS_2 nanoparticles are

effective in reducing friction and show synergistic effect when used in combination with ZDDP for gearbox applications [14]. Similar friction and wear behaviour was obtained for IF-MoS_2 nanoparticles by Tannous *et al* [11]. Similar friction reduction was also observed by Hu *et al* [15] for hollow MoS_2 nanoparticles in liquid paraffin where they found that the concentration of 1.5 wt % of nanoparticles is the most effective in friction reduction as well as wear reduction. Authors claimed that increase in the concentration of the nanoparticles leads to increase in agglomeration which increases collision between nanoparticles leading to a negative impact on tribological properties.

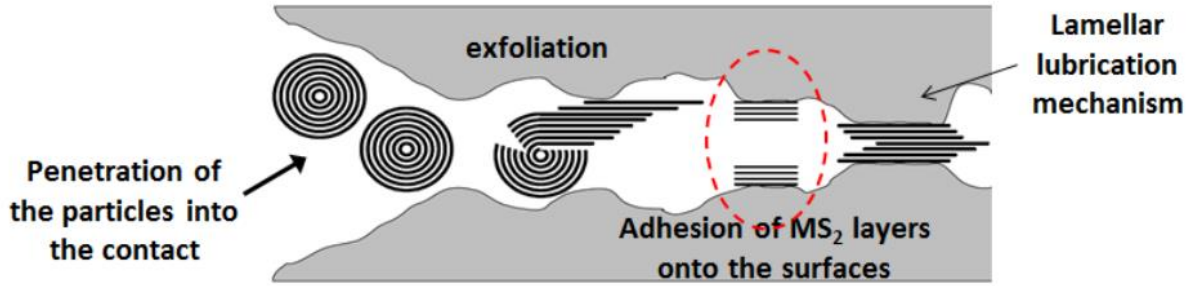

Fig 6.2 Schematic showing the exfoliation mechanism of MS_2 nanoparticles [11]–[13].

As discussed above, metal dichalcogenide nanoparticles have been generally used in reducing friction and wear. However, carbon based materials like nanotubes and nanoparticles, ceramic oxides like TiO_2, Al_2O_3, ZnO, CuO, nanoparticles have also been studied for their tribological properties and are found to be good in friction reduction, [5-6; 16-17].

TiO_2 nanoparticles are one of the nanomaterials used for photocatalytic applications due to their excellent thermal and chemical properties [18-19]. They exist in three different forms or phases namely anatase, rutile and brookite. Rutile is the most stable chemical form of TiO_2. Also, certain phases of TiO_2 exist in certain sizes. TiO_2 nanoparticles in anatase and rutile forms are known to exhibit photocatalysis in presence of UV light [20–22]. This photocatalytic effect leads to generation of free radicals in the form of electrons and holes on the surface of TiO_2 nanoparticles in UV or visible light [23-24]. The holes help in oxidation and the electrons help in reduction reactions as shown in the schematic for photocatalytic effect in the fig 6.3.

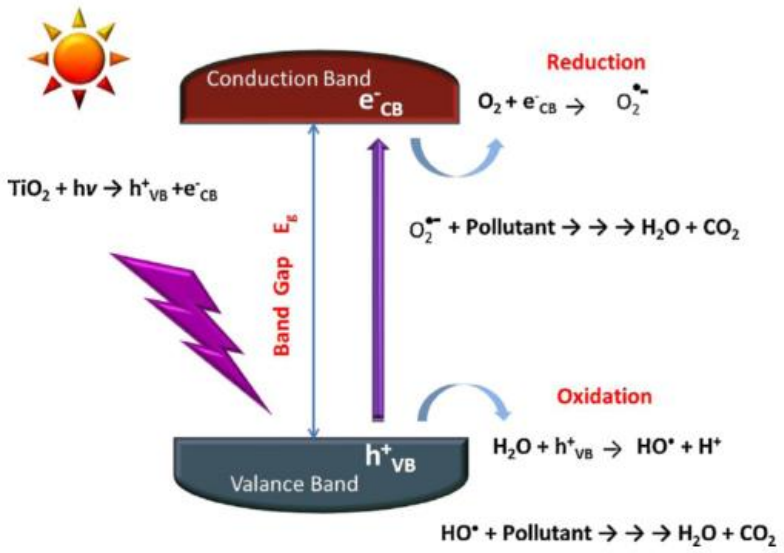

Fig 6.3 Schematic of photocatalysis in TiO_2 nanoparticles [23].

Taking into account the photocatalytic behaviour which helps in oxidation or reduction, TiO_2 nanoparticles are used for oxidative and hydrogen desulphurization of oils to remove heavy organic molecules from the oils [22;25–28]. The efficiency of photocatalysis in TiO_2 nanoparticles is limited due to strong electron-hole recombination and low activation ability of the surface [18; 29-30]. The electron-hole recombination depends on the band gap of the nanoparticles in different phases of TiO_2. If the bandgap is high, the electron hole recombination is reduced and so the electrons and holes remain stable on the surface. The photocatalytic effect is higher in case of anatase nanoparticles due to their higher bandgap compared to rutile [23].

To enhance the photocatalytic effect in presence of visible light as well as to avoid the electron hole recombinations, co-catalysts are used with the semiconductors which not only extract enough negative or positive charges out of the semiconductor surface but also serve as active sites for reduction or oxidation [31-32]. One of those co-catalysts used is MoS_2 nanoclusters [21]. MoS_2 is an ideal candidate as an electrocatalyst due to its high H_2 activation ability [33]. To overcome the limitations of both TiO_2 nanoparticles and MoS_2 nanoclusters in photocatalysis, nanocomposites are synthesized by *in-situ* growing of TiO_2 nanocrystals on MoS_2 nanosheets [34–36]. These tend to form a physical bond between MoS_2 and TiO_2 nanoparticles to form a nanocomposite which shows good photocatalytic behavior.

Addition of TiO_2 nanoparticles as an additive to the oil showed stable friction coefficient due to the formation of protective films on the counterpart surfaces in steel / steel contacts [37]. Also, it has been shown that TiO_2 nanoparticles exhibit a higher load bearing capacity

compared to the oil used without TiO_2 nanoparticles [38]. Ali *et al* [16] showed that use of TiO_2 nanoparticles in combination with Al_2O_3 with an optimum concentration of 0.25 wt % in base oil led to significant friction and wear reduction as well as reduction in friction losses when used in a piston ring-cylinder liner contact.

From the literature review and the previous results obtained from other chapters, it is clear that:

(a) Better friction and wear results were obtained with steel / TiO_2 APS contact in presence of oil containing MoDTC compared to steel / reference steel

(b) TiO_2 anatase nanoparticles show good photocatalytic behaviour (which could help in reduction of additives in the contact) as well as tribological behaviour (reduction in friction and wear)

(c) Interaction between TiO_2 nanoparticles with MoS_2 nanosheets is observed and the formation of a physical bond between them could help in forming a stable compound.

Considering the above arguments and also to investigate more the interaction between MoDTC and TiO_2, TiO_2 particles, with different sizes and phases are blended with MoDTC in base oil to study their tribological behavior in presence of steel / reference steel contact. Also, the effect of concentration of the nanoparticles with MoDTC in base oil is studied.

6.2 Materials and methods

6.2.1 Materials

AISI 52100 steel balls and flats were used as materials in ball-on-flat configuration. Rough steel APS coating was also used as a flat material for the study on effect of roughness. The properties of the tribopairs like average surface roughness (R_a = 50 nm), hardness and elastic modulus are similar to the materials used in the previous section mentioned in Chapter 3.

Lubricant used is a base oil (as mentioned in chapter 3) with the addition of MoDTC and with or without the addition of TiO_2 particles with different phases and sizes. Various sizes and phases of TiO_2 particles were purchased from Sigma Aldrich Inc. The various sizes and phases of TiO_2 particles used are mentioned in table 6.1 and the various formulations used are mentioned in the table 6.2. Blends were prepared for the various types of particles in base oil. The blends were stirred using magnetic stirrers at 60°C for 2 hours.

Table 6.1 Various sizes and phases of TiO_2 particles used

Size	Phase
< 25 nm	Anatase
< 100 nm	Rutile
< 5 µm	Rutile
< 45µm	Anatase

Table 6.2 Lubricant formulations used

Lubricant	Designation
Base oil	BO
Base oil + 0.5 wt % MoDTC	BO + MoDTC
Base oil + 0.5 wt % TiO_2 anatase particles + 0.5 wt % MoDTC	BO + TiO_2 anatase + MoDTC
Base oil + 0.5 wt % TiO_2 anatase particles	BO + TiO_2 anatase
Base oil + 0.5 wt % TiO_2 rutile particles	BO + TiO_2 rutile
Base oil + 0.5 wt % TiO_2 rutile particles + 0.5 wt % MoDTC	BO + TiO_2 rutile + MoDTC

The reference blends of base oil + 0.5 wt % TiO_2 anatase (25 nm) nanoparticles (white colored) and base oil + 0.5 wt % TiO_2 anatase + 0.5 % MoDTC (milky light green colored) are shown in fig 6.4. It can be observed that base oil + 0.5 wt % TiO_2 anatase clearly shows sedimentation of the nanoparticles at the bottom whereas the blend containing the mixture of TiO_2 anatase

nanoparticles and MoDTC shows well dispersed nanoparticles with no sedimentation when they are kept steady for 6 hrs after blending. Addition of TiO_2 anatase 25 nm particles in base oil containing MoDTC formed a stable suspension. Therefore, the solution did not require any dispersant for keeping the nanoparticles dispersed.

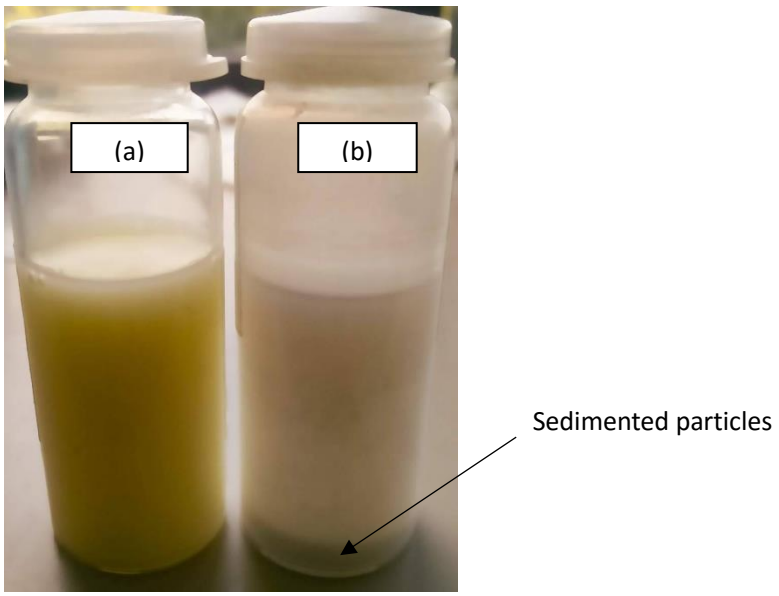

Fig 6.4 (a) 0.5 wt % TiO_2 anatase 25 nm particles blended with 0.5 wt % MoDTC in base oil (b) 0.5 wt % TiO_2 anatase 25 nm particles in base oil**.**

6.2.2 Methods

6.2.2.1 Characterisation of the TiO_2 nanoparticles

The TiO_2 anatase and rutile nanopowders were characterized to investigate their size and morphology by TEM (specifications mentioned in Chapter 2).

6.2.2.2 Tribotests

Linear reciprocating ball-on-flat tests were carried out with reference steel balls against reference steel flats. Tribotest conditions used are similar to that used in Chapter 3 table 3.3. The only difference in this case is the lubricant used and the way it is inserted in the contact. Since the nanoparticles get sedimented easily, a single drop of the lubricant blend is used in the contact so that it remains in the contact for the complete duration of the test.

As discussed in the literature review section of this chapter, TiO_2 anatase nanoparticles are unstable at the size of more than 50 nm and so it was not possible to have both the TiO_2 particle phases with same sizes. Therefore, to study the effect of size and phase of TiO_2 particles on the tribological behavior of steel / reference steel, tribotests were performed with two different sizes for rutile (100 nm and 5 µm) as well as anatase (25 nm and 45 µm) TiO_2 particles. Tests

were carried out at a maximum Hertzian pressure of 0.7 GPa and a sliding speed of 0.05 m/s. Wear scar analysis is carried out using optical microscopy on both the counterparts. Depending on the results obtained, the tribofilm on the sample with the best tribological behaviour was analysed by XPS. The tribofilm morphology and the composition was also investigated using TEM. FIB lamellas were prepared from a small micron sized part of the tribofilm on the steel ball as well as the reference steel flat.

6.3 Results:

6.3.1 Characterisation of the TiO_2 nanoparticles

TEM micrographs shown in the fig 6.5 illustrate the morphology of the **TiO_2 rutile** nanoparticles. Shape of the particles was found to be ellipsoidal. The particles are found to be nanocrystalline as clear atomic arrangement is observed. The size of the particles is in the range of 80 – 100 nm. No agglomeration is observed in case of rutile nanoparticles.

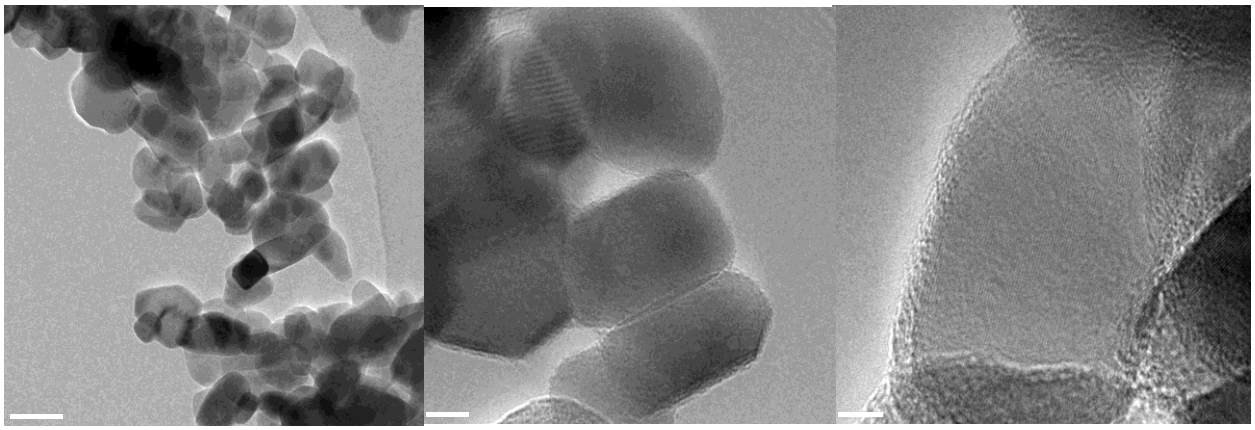

Fig 6.5 TEM micrographs for rutile TiO_2 nanoparticles

TEM micrographs shown in fig 6.6 illustrate the morphology of the **TiO_2 anatase** nanoparticles. Shape of the particles was found to be ellipsoidal with hexagonal patches on their surface. Also, the particles are found to be almost purely nanocrystalline as clear atomic arrangement is observed. The size of the TiO_2 anatase nanoparticles is found to be in the range of 25-50 nm. Some agglomeration is observed in case of anatase nanoparticles.

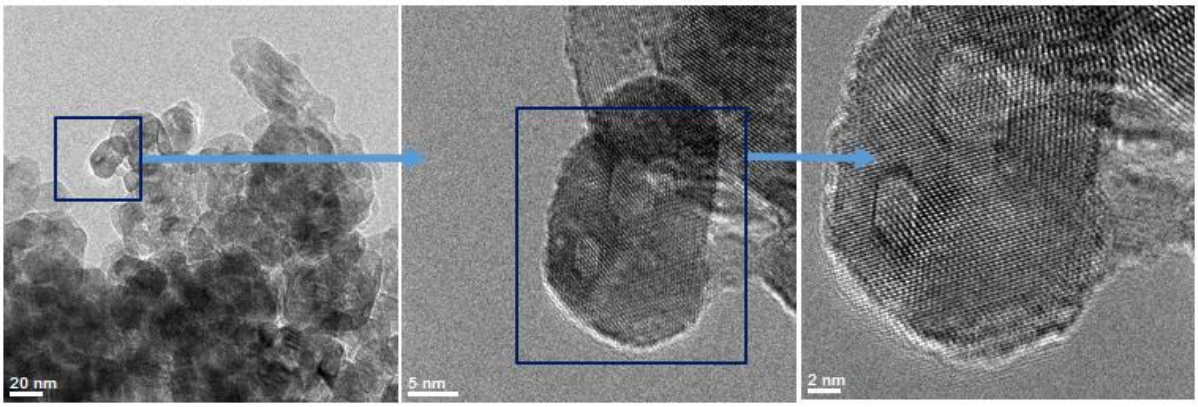

Fig 6.6 TEM micrographs for TiO_2 anatase nanoparticles.

6.3.2 Tribological behaviour of steel / steel lubricated with different sizes and phases of TiO_2 particles:

6.3.2.1 Friction and wear results:

Comparison of friction results for steel / reference steel contact when lubricated with base oil and addition of **TiO_2 rutile particles** in combination with or without MoDTC is shown in fig 6.7 (a). Similar friction comparison for steel / reference steel contact when lubricated with base oil and the addition of **TiO_2 anatase particles** in combination with or without MoDTC is shown in fig 6.7 (b).

From the comparison of friction results shown in fig 6.7 (a), it is found that the reference lubricant consisting of base oil + 0.5 wt % TiO_2 rutile (100 nm and 5 µm) particles show similar friction behaviour. As soon as 0.5 wt % MoDTC is added to this blend, friction coefficient is reduced. The lubricant blend base oil + 0.5 wt % TiO_2 rutile 100 nm particles shows the lowest steady state friction coefficient ($\mu \sim 0.042$). However, 5 µm TiO_2 rutile particles blended with MoDTC do not reduce the friction coefficient considerably. It can be observed that this friction coefficient is higher than the tests carried out with only base oil + 0.5 wt % MoDTC. This suggests that the micron sized TiO_2 rutile particles negatively affect the friction behaviour. This could be because of failure of the particles to remain in the contact due to large size of the roughness grooves less than the size of the particles. This suggests that there is no friction reduction effect observed when micron sized TiO_2 rutile particles are added in MoDTC.

From the comparison of friction results shown in fig 6.7 (b), it is found that the reference lubricant consisting of base oil + 0.5 wt % TiO_2 anatase particles (25 nm and 45 µm) show similar friction behaviour. As soon as MoDTC is added to this blend, friction coefficient is reduced. The lubricant blend base oil + 0.5 wt % TiO_2 anatase 25 nm particles shows the lowest steady state friction coefficient ($\mu \sim 0.038$). Friction coeffcieint observed in case of 0.5 wt %

TiO_2 anatase 45 µm particles blended with 0,5 wt % MoDTC in base oil is higher than the tests carried out with only base oil + 0.5 wt % MoDTC. This could again be due to failure of the particles to remain in the contact to act as a third body with high hardness and cause excessive abrasive wear in the contact.

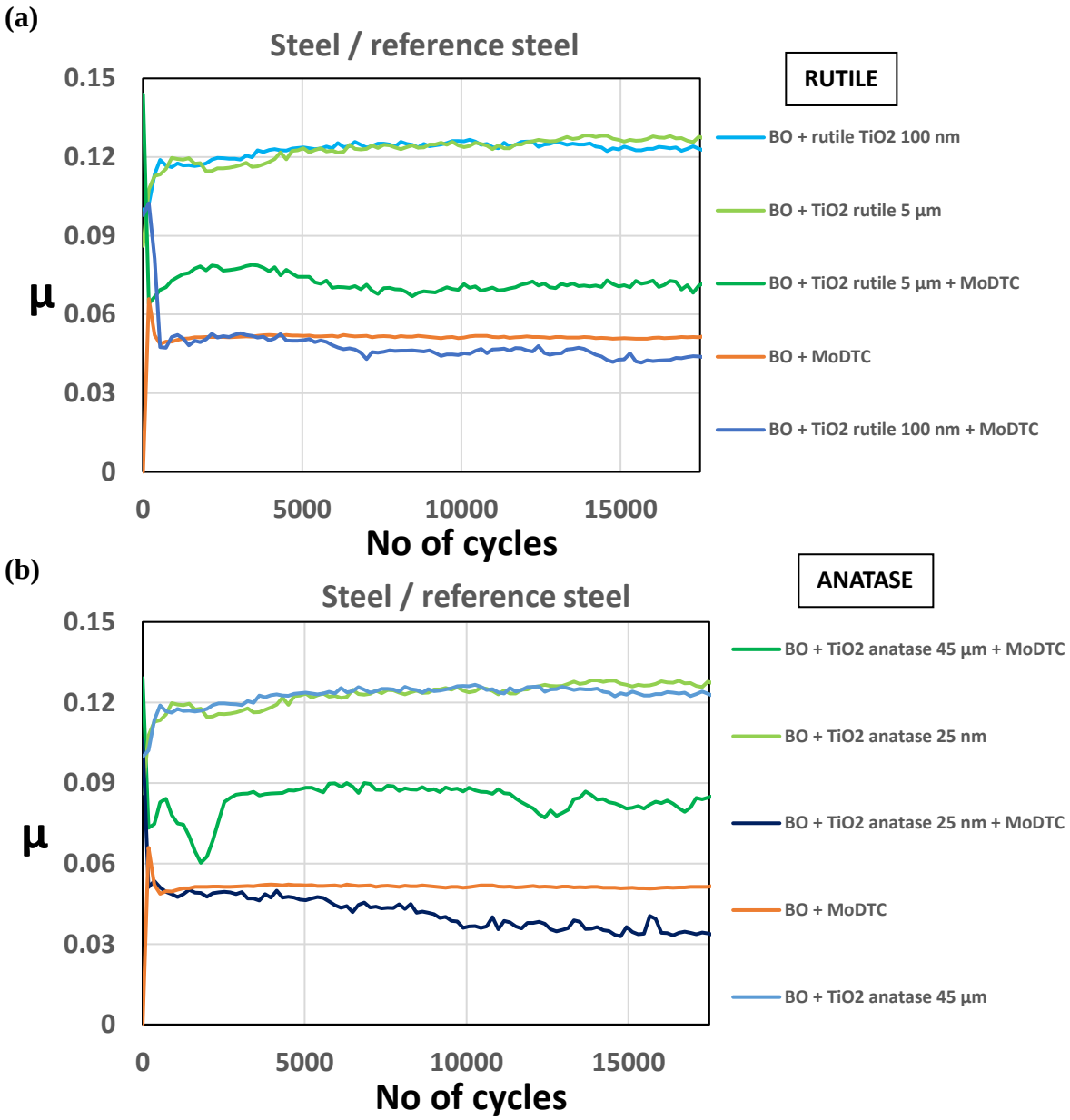

Fig 6.7 Friction comparison for steel / reference steel contact with different blends made of various sizes of (a) anatase TiO_2 particles (b) rutile TiO_2 particles with and without addition of MoDTC in base oil test.

Steel / reference steel contact lubricated with base oil + 0.5 wt % TiO_2 anatase 25 nm particles + 0.5 wt % MoDTC shows the lowest friction behaviour of all cases. Therefore, for further investigation concerning wear and surface characterization of tribofilms, only the results obtained with 0.5 wt % TiO_2 anatase 25 nm particles blended with 0,5 wt % MoDTC in base

oil are presented.

Wear comparison for steel / reference steel contact is shown in fig 6.8. % wear above Hertzian diameter of steel balls is compared for base oil, base oil + 0.5 wt % MoDTC, base oil + 0.5 wt % TiO_2 anatase 25 nm particles and base oil + 0.5 wt % TiO_2 anatase 25 nm particles + 0.5 wt % MoDTC. From the comparison, it is clear that addition of 0.5 wt % anatase TiO_2 25 nm nanoparticles to base oil + 0.5 wt % MoDTC reduces the wear considerably compared to only base oil + 0.5 wt % MoDTC or base oil + 0.5 wt % anatase nanoparticles blended in base oil. Significant wear reduction is observed as TiO_2 anatase 25 nm nanoparticles are added to base oil and the wear is reduced even more when the nanoparticles are used in combination with MoDTC.

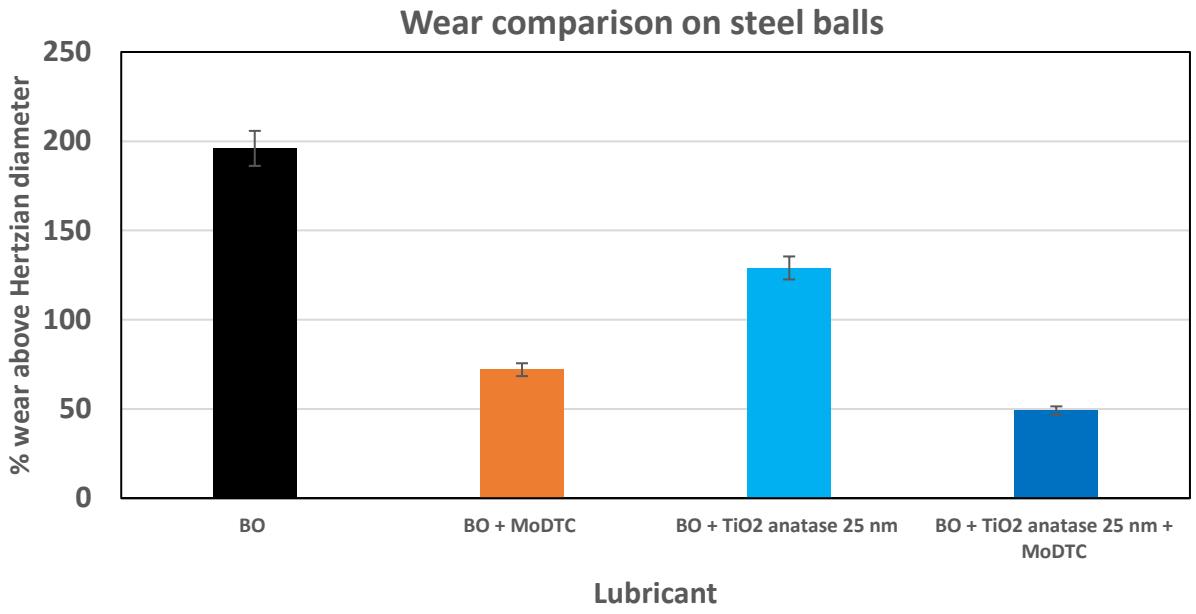

Fig 6.8 Wear comparison on the steel ball for steel / reference steel contact when lubricated with base oil, base oil + 0.5 wt % MoDTC, base oil + 0.5 wt % TiO_2 anatase, base oil + 0.5 wt % TiO_2 anatase + 0.5 wt % MoDTC.

6.3.2.2 Surface analysis of the tribofilms –

(1) XPS analysis on the reference steel flats:

To investigate the differences in tribological behavior observed in case of reference steel flats when they are lubricated with only 0.5 wt % MoDTC in base oil and then after addition of 0.5 wt % TiO_2 anatase 25 nm particles with MoDTC in base oil, XPS was carried out. The high resolution Mo3d and S2p XPS spectra inside the tribofilm on reference steel flats lubricated with base oil + 0.5 wt % MoDTC and base oil + 0.5 wt % TiO_2 anatase 25 nm particles + 0.5 wt % MoDTC are shown in the fig 6.9. Similar fitting procedure, binding energies for various contributions and analysis area are used for Mo3d and S2p peaks as mentioned in Chapter 4

Section 4.2.2.2. It was found that the tribochemistry observed is different for both the lubricants which is in agreement with the friction behaviour obtained. For the contact lubricated with base oil + 0.5 wt % MoDTC, presence of Mo-oxysulphide justifies the higher friction coefficient of 0.052 [39]. For the contact lubricated with base oil + 0.5 wt % TiO_2 anatase 25 nm nanoparticles + 0.5 wt % MoDTC, only MoS_2 and MoO_3 is formed inside the tribofilm with no oxysulphides which is in agreement with the better friction behaviour and the steady state friction coefficient which goes on decreasing until it reaches the value of 0.038. S2p peaks showed sulphide and sulphate contribution when the contact was lubricated with base oil + 0.5 wt % MoDTC. However, only sulphide contribution was observed when the contact is lubricated with base oil + 0.5 wt % TiO_2 anatase 25 nm particles + 0.5 wt % MoDTC. Sulphate contribution observed at 168 eV in S2p peak in case of base oil + 0.5 % MoDTC is extremely less in S2s compared to Mo3d contributions and so does not affect the overall fit of Mo3d peak. Exactly similar friction coefficient and tribochemistry was observed in case of steel / TiO_2 APS contact under similar conditions as discussed in Chapter 4.

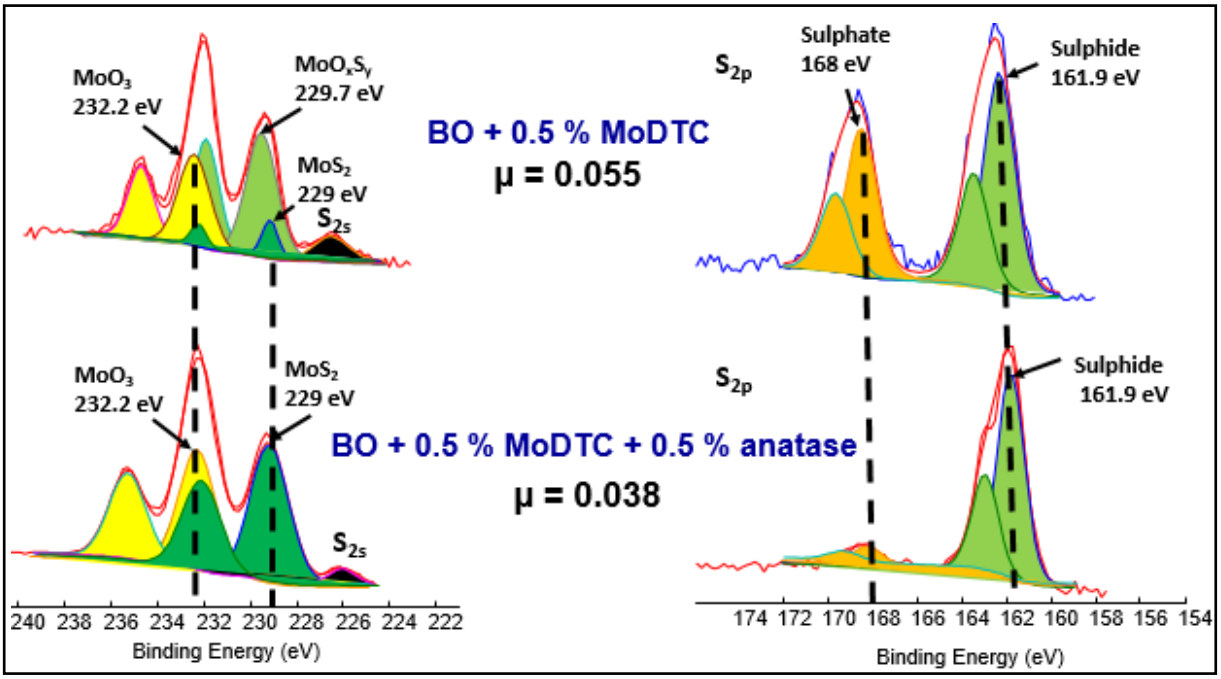

Fig 6.9 XPS spectra for reference steel flats, tested in base oil + 0.5 wt % MoDTC and base oil + 0.5 wt % MoDTC + 0.5 wt % TiO_2 anatase against steel balls: (a) Mo3d peak on the steel flat (b) Mo3d peak (c) S2p peak on the steel flat (d) S2p peak.

(2) FIB-TEM analysis on the steel ball and the reference steel flat

To confirm the presence and investigate the morphology of MoS_2 flakes and TiO_2 nanoparticles present in the tribofilm, FIB-TEM was carried out on a small region of the tribofilm on

reference steel flat and the steel ball when it was lubricated with base oil + 0.5 wt % MoDTC + 0.5 wt % TiO_2 anatase 25 nm particles. From the TEM images shown in fig 6.10 (a), it is clear that long and crystalline MoS_2 flakes are formed in layers and are attached to TiO_2 anatase nanoparticles. TiO_2 anatase nanoparticles can be clearly observed due to different atomic arrangement, morphology as well as shape (circular or ellipsoidal). The tribofilm (about 50 – 60 nm thick) is found to be made of two to five layers of MoS_2 flakes and TiO_2 anatase nanoparticles. These flakes / sheets are confirmed to be MoS_2 as the basal plane distance of hexagonal MoS_2 is 6 Å and matches with those in the previous works [40]. Magnified images in the fig 6.10 (a) show MoS_2 flakes and TiO_2 anatase nanoparticles which are clearly distinguishable. This is in agreement with the XPS results which showed the formation of MoS_2 and TiO_2 anatase nanoparticles in the tribofilm.

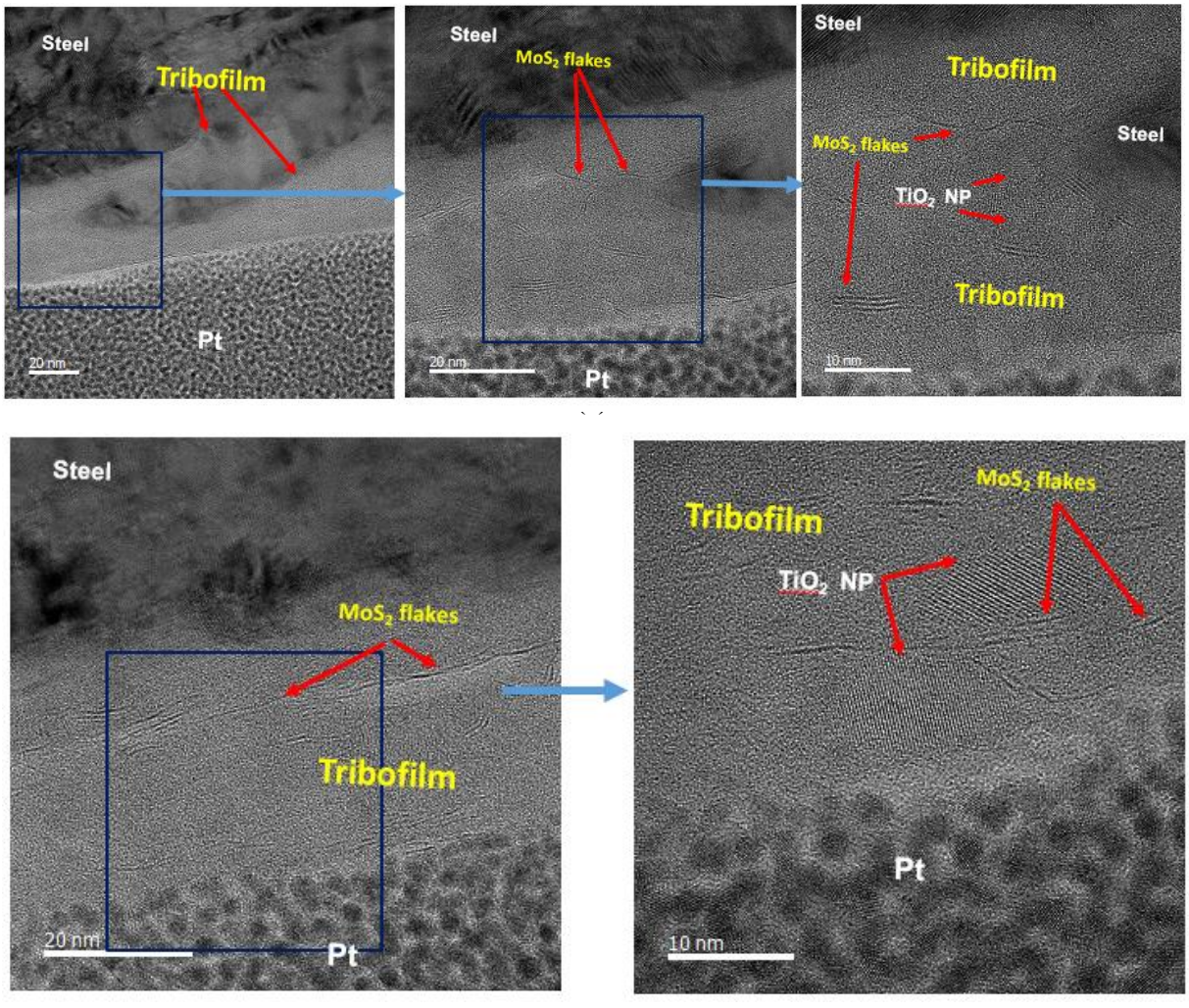

(b)

Fig 6.10 (a) TEM micrographs of the FIB lamella cut from the tribofilm on reference steel flat **(b)** Magnified TEM images showing MoS_2 flakes and TiO_2 anatase nanoparticles on steel ball.

To confirm the presence of MoS_2 and TiO_2 nanoparticles in the tribofilm, EDS mapping was

carried out on the steel ball and is shown in fig 6.11. Rectangular area inside the image was used to capture the maps. This area includes the substrate (steel), tribofilm (MoS_2 flakes and TiO_2 anatase nanoparticles).

(a)

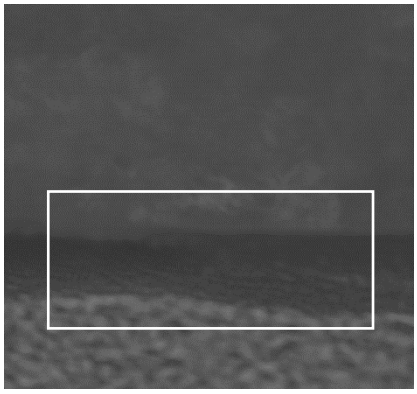

(b)

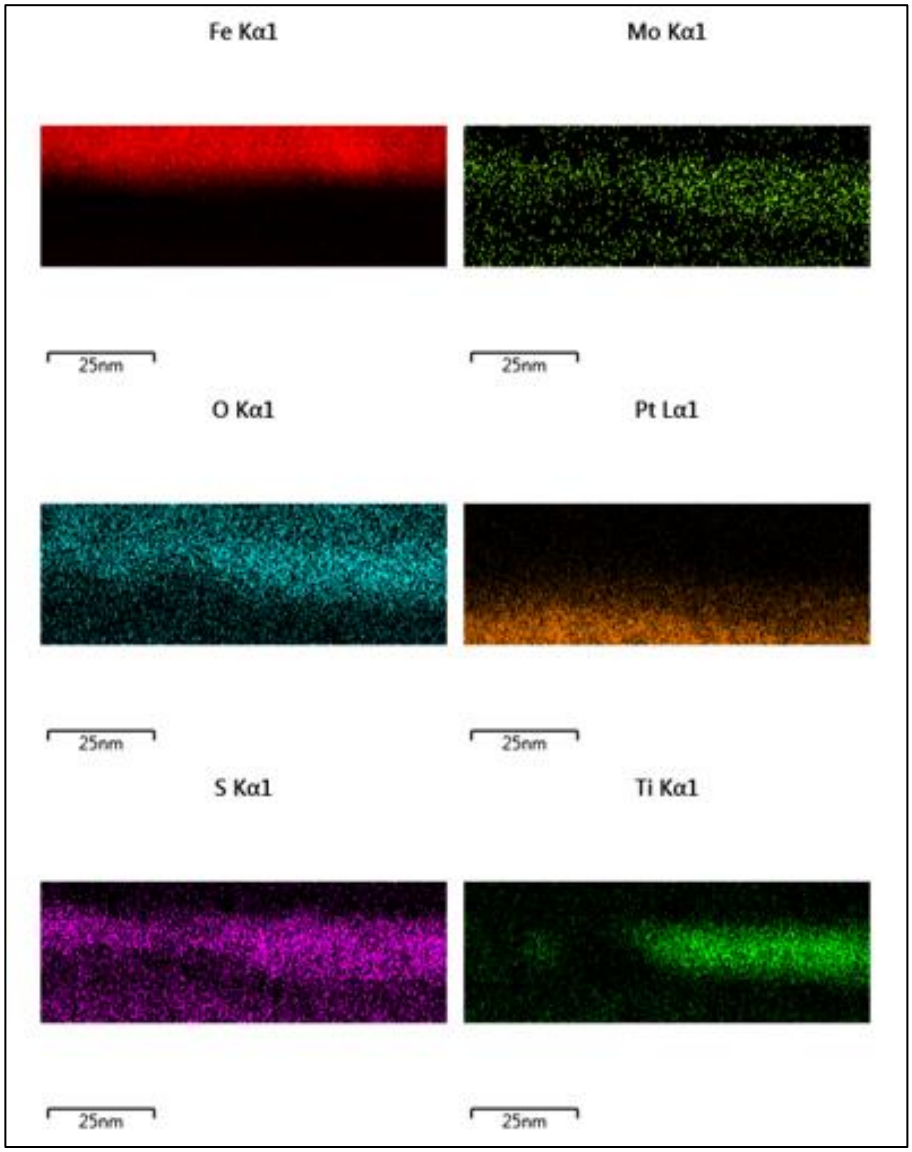

Fig 6.11 (a) TEM-EDS image for maps on steel ball (b) TEM EDS maps for the image shown in (a).

From the individual elemental maps for Ti, Pt, O, S, Fe and Mo, it can be clearly observed that

Ti (orange), O (green) are present in circular patches along with MoS_2 in the tribofilm zone which suggests the presence of MoS_2 flakes and TiO_2 nanoparticles in the tribofilm. Top part of the FIB cross section was the Pt protection layer which can be clearly observed in the fig 6.11 (b). Substrate consisting of Fe and O is also observed on the top of the elemental mapping image. These elemental maps confirm that a thick tribofilm composed of layers of MoS_2 and TiO_2 nanoparticles is formed on the steel ball.

6.4 Discussion

6.4.1 Low friction in case of steel / reference steel contact lubricated with base oil + 0.5 wt % TiO_2 anatase 25 nm particles + 0.5 wt % MoDTC:

The most important result obtained in this chapter is that the TiO_2 anatase and rutile nanoparticles when blended with MoDTC in base oil show significant reduction in steady state friction coefficient which is similar to the case of steel / TiO_2 APS contact. Reasons for low friction in steel / reference steel contact when lubricated with the blend of anatase TiO_2 nanoparticles and MoDTC in base oil are discussed as follows:

(1) Tribochemistry:

Surface characterisation of the tribofilm by XPS depicts the formation of pure MoS_2 and MoO_3 in case of steel / reference steel when it is lubricated with base oil + 0.5 wt % TiO_2 anatase 25 nm nanoparticles + 0.5 wt % MoDTC, whereas a lot of Mo-oxysulphide and MoS_2 and MoO_3 are formed in case of steel / reference steel when the contact is lubricated with base oil + MoDTC. Various compounds observed inside the tribofilms on reference steel flat for two different lubricants are summarised in table 6.3. From the results discussed above, tribochemistry observed is confirmed to be exactly similar to that observed in case of steel / TiO_2 APS contact lubricated with base oil + 0.5 wt % MoDTC.

Table 6.3 List of different compounds formed in the various tribofilms.

Lubricant	Tribofilm composition
Base oil + 0.5 wt % MoDTC	MoS_2 + MoO_xS_y + MoO_3, TiO_2 Sulphate
Base oil + 0.5 wt % TiO_2 anatase 25 nm particles + 0.5 wt % MoDTC	MoS_s + MoO_3, TiO_2 No sulphate

(2) Morphology:

TEM analysis on the FIB lamella showed the formation of long, crystalline MoS_2 flakes throughout the 50 – 60 nm tribofilm which are responsible for friction reduction. Tribofilm was made of layers of MoS_2 flakes and TiO_2 nanoparticles. Therefore, there could be the rolling effect of the particles or the mechanical mixing of TiO_2 nanoparticles and MoS_2 which helps in reducing the friction coefficient in case of steel / reference steel contact.

6.4.2 Effect of change of concentrations of TiO_2 anatase 25 nm particles and MoDTC on the tribological behaviour of steel / reference steel contact:

Considering the better friction results obtained with 0.5 wt % TiO_2 anatase 25 nm nanoparticles blended with 0.5 wt % MoDTC and also with reduction in concentration of MoDTC in case of steel / TiO_2 APS coating, concentration of TiO_2 anatase 25 nm particles and MoDTC was reduced from 0.5 wt % to 0.1 wt % in base oil. Similar conditions were used as that used for ball-on-flat reciprocating tribotests.

Comparison of friction results for steel / reference steel and steel / steel APS contacts is shown in fig 6.12. When the concentration of MoDTC as well as the anatase TiO_2 25 nm particles in base oil is lowered from 0.5 wt % to 0.1 wt % in base oil, induction time is observed as shown in the sky blue curve. However, this induction time is reduced compared to the case where the contact is lubricated with only base oil + 0.1 wt % MoDTC which suggests that the addition of nanoparticles leads to faster decomposition of MoDTC to MoS_2. Steady state friction coefficient is still low even if 0.1 wt % MoDTC and 0.1 wt % TiO_2 anatase 25 nm particles are used in the base oil. Therefore, reduction in concentration of MoDTC and TiO_2 anatase 25 nm particles helps in faster decomposition of MoDTC compared to only 0.5 wt % MoDTC.

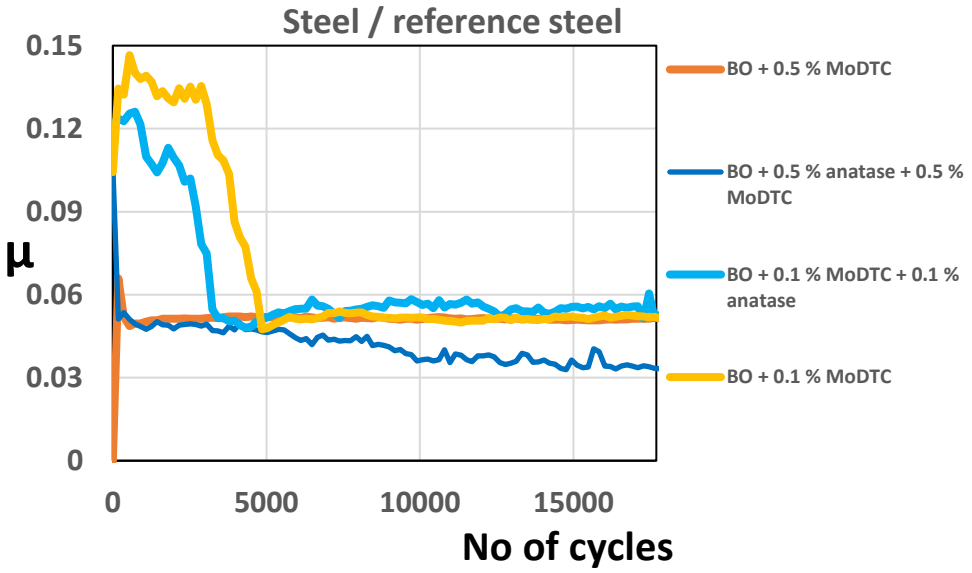

Fig 6.12 Friction behaviour for steel / reference steel when lubricated with base oil + 0.1 wt / 0.5 wt % MoDTC and base oil + 0.1 wt / 0.5 wt % anatase TiO_2 25 nm + 0.1 wt / 0.5 wt % MoDTC.

6.4.3 Effect of roughness on the tribological behaviour

As discussed in the literature review, rough materials often showed better tribological results when lubricated with nanoparticles [41]. Therefore, to study the effect of roughness using the blend of 0.5 wt % TiO_2 anatase 25 nm particles and 0.5 wt % MoDTC in base oil, rough steel APS coating was used instead of reference steel flat. The average roughness parameter (R_a = 0.2 µm) is much higher than reference steel flat (R_a = 0.04 µm). Therefore, the lambda ratio is lower than steel / reference steel contact and the contact becomes more severe (boundary lubrication conditions).

Friction curves with and without addition of various concentrations of MoDTC and TiO_2 anatase 25 nm particles are shown in fig 6.13. From the results discussed before, steady state friction coefficient obtained was 0.039 for steel / reference steel contact. However, steady state friction coefficient was found to be much lower (µ = 0.031) for steel / steel APS contact when lubricated with base oil + 0.5 wt % MoDTC + 0.5 wt % TiO_2 anatase 25 nm particles. Similarly, when the concentration of MoDTC as well as the TiO_2 anatase 25 nm particles was reduced, lower steady state friction coefficient was observed in steel / steel APS contact than steel / reference steel contact with no induction time.

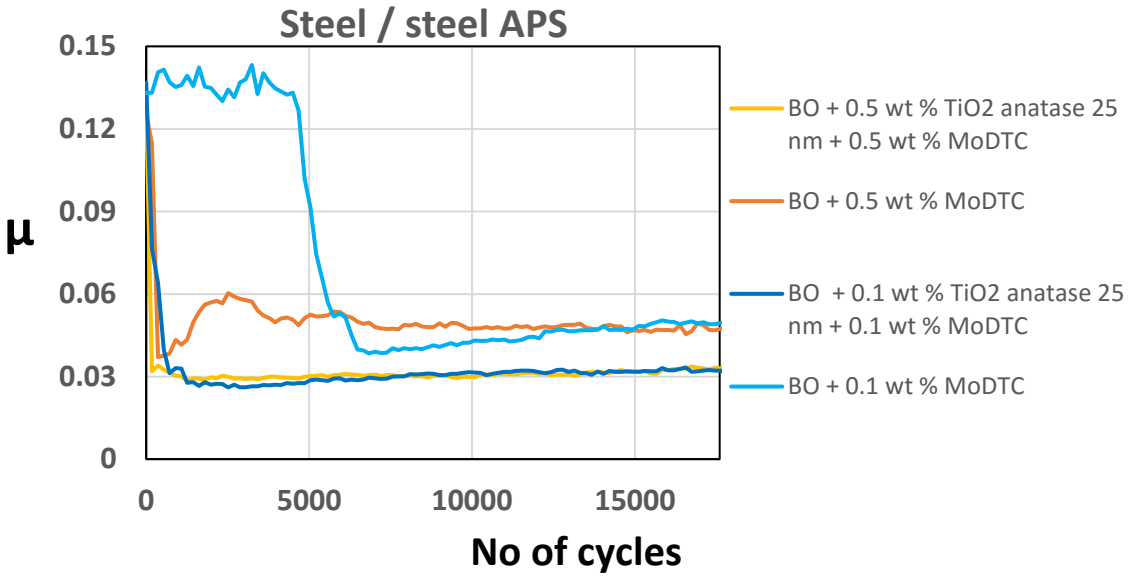

Fig. 6.13 Friction behaviour for steel / steel APS contact lubricated with base oil + 0.5 / 0.1 wt % MoDTC and base oil + 0.5 / 0.1 wt % MoDTC + 0.5 / 0.1 wt % TiO_2 anatase 25 nm particles.

Friction coefficient is found to be constant from the beginning of the test which suggests that the decomposition of MoDTC is faster which could be attributed to rough surfaces which lead to more contact between asperities. The other reason for lower friction could be the roughness parameters like R_a, R_{pk} and R_{vk} for steel APS which are higher (R_s = 0.2 µm, R_{pk} = 0.22 µm and R_{vk} = 0.25 µm) than reference steel; so the nanoparticles which are around 25-40 nm in diameter could easily penetrate the roughness grooves as well the pores present in the coating modify roughness and thereby reduce the friction coefficient. However, no direct proof of penetration of nanoparticles in the roughness grooves is observed in this study.

To investigate the differences in friction behaviour, XPS was carried out and it was found that the tribochemistry observed is similar to reference steel flat except sharp Mo-sulphide peak contribution as shown in fig 6.14. As discussed before, this could be due to faster decomposition of MoDTC to form crystalline MoS_2 and sharp peaks. Faster decomposition was evident from the absence of induction time in case of steel / steel APS contact.

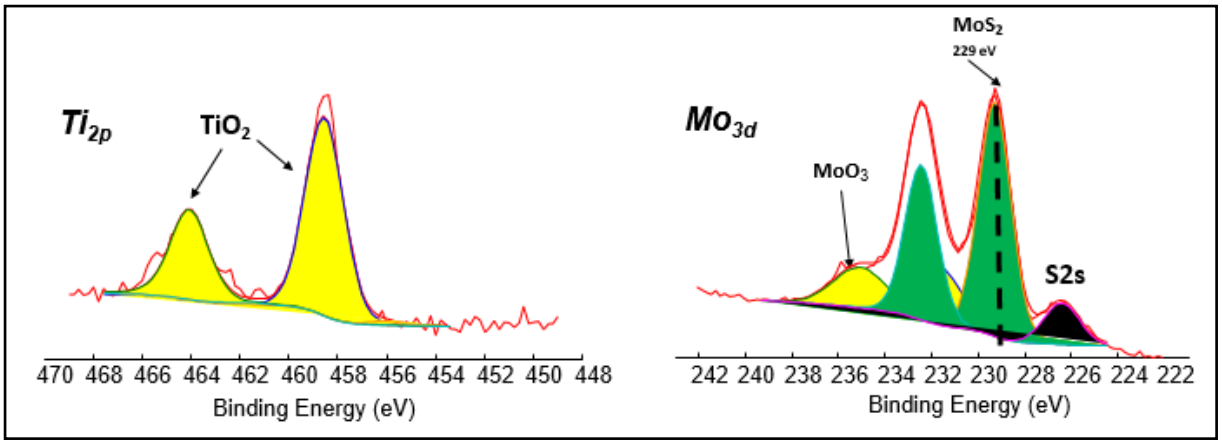

Fig 6.14 XPS high resolution spectra for Ti2p and Mo3d on steel APS flat tested in base oil + 0.5 wt % MoDTC + 0.5 wt % TiO_2 25 nm anatase particles against steel balls.

As shown in the previous chapter in steel / TiO_2 APS contact lubricated with base oil + 0.5 wt % MoDTC, TiO_2 APS coating helps in complete decomposition of MoDTC and leads to the formation of only MoS_2 and MoO_3 with no oxysulphides. Similar tribochemistry is observed in case of TiO_2 anatase nanoparticles present in the contact along with 0.5 wt % MoDTC additive. This suggests that presence of TiO_2 anatase nanoparticles helps in complete decomposition of MoDTC. This effect is enhanced when the counterparts are rough. This could be one of the reasons for low friction coefficient observed in case of steel APS flat.

6.5 Conclusion

(1) A stable dispersion is formed in case of TiO_2 anatase 25 nm particles and MoDTC and rutile TiO_2 100 nm particles and MoDTC in base oil which helps the lubricant remain in the contact easily.

(2) Tribological behaviour of the steel / reference steel contact lubricated with anatase and rutile phase TiO_2 nano and microparticles showed that only nanosized particles are effective in friction reduction when blended with MoDTC.

(3) Blend of 0.5 wt % TiO_2 anatase 25 nm particles and 0.5 wt % MoDTC in base oil showed the lowest friction coefficient compared to all other phases and sizes of TiO_2 particles used in combination with MoDTC as a lubricant in steel / reference steel contact.

(4) Lower friction coefficient obtained in steel / reference steel contact lubricated with addition of 0.5 wt % TiO_2 anatase 25 nm particles to 0.5 wt % MoDTC in base oil than only MoDTC in base oil is due to

(a) Tribochemistry:

Pure MoS_2 and MoO_3 is formed with no oxysulphides and sulphates observed for the

case of base oil + 0.5 wt % MoDTC + 0.5 wt % TiO_2 anatase 25 nm particles.

(b) Morphology:

TEM analysis showed the formation of thick tribofilm composed of layers of long crystalline MoS_2 flakes and anatase TiO_2 25 nm particles over one another.

(5) Reduction in concentration of both TiO_2 anatase 25 nm particles and MoDTC from 0.5 wt % to 0.1 wt % in steel / reference steel contact showed that they are still effective unlike the case of only 0.1 % MoDTC in base oil where lot of induction time was observed. This suggests that addition of small amount of TiO_2 anatase 25 nm particles to MoDTC in base oil leads to complete decomposition of MoDTC to form MoS_2 and leads to lower friction coefficient.

(6) Discussion on effect of roughness showed reduction in steady state friction coefficient when the rough steel APS coating was rubbed against steel ball lubricated with base oil + 0.5 wt % MoDTC + 0.5 wt % TiO_2 anatase 25 nm particles.

6.6 References

[1] P. U. Aldana, F. Dassenoy, B. Vacher, T. Le Mogne, B. Thiebaut, and A. Bouffet, "Antispalling Effect of WS_2 Nanoparticles on the Lubrication of Automotive Gearboxes," *Tribol. Trans.*, vol. 59, no. 1, pp. 178–188, 2016.

[2] W. Dai, B. Kheireddin, H. Gao, and H. Liang, "Roles of nanoparticles in oil lubrication," *Tribol. Int.*, vol. 102, pp. 88–98, 2016.

[3] J. Kogovek and M. Kalin, "Various MoS_2, WS_2 and C-based micro- and nanoparticles in boundary lubrication," *Tribol. Lett.*, vol. 53, no. 3, pp. 585–597, 2014.

[4] R. R. Sahoo and S. K. Biswas, "Effect of layered MoS_2 nanoparticles on the frictional behavior and microstructure of lubricating greases," *Tribol. Lett.*, vol. 53, no. 1, pp. 157–171, 2014.

[5] A. Hernández Battez, J. L. Viesca, R. González, D. Blanco, E. Asedegbega, and A. Osorio, "Friction reduction properties of a CuO nanolubricant used as lubricant for a NiCrBSi coating," *Wear*, 2010.

[6] A. Hernández Battez *et al.*, "CuO, ZrO_2 and ZnO nanoparticles as antiwear additive in oil lubricants," *Wear*, vol. 265, no. 3–4, pp. 422–428, 2008.

[7] C. Grossiord, K. Varlot, J. M. Martin, T. Le Mogne, C. Esnouf, and K. Inoue, "MoS_2 single sheet lubrication by molybdenum dithiocarbamate," *Tribol. Int.*, vol. 31, no. 12, pp. 737–743, 1998.

[8] D. Maharaj, B. Bhushan, F. A. Wear, and A. M. Nems, "Effect of MoS_2 and WS_2

Nanotubes on Nanofriction and Wear Reduction in Dry and Liquid Environments.pdf," pp. 323–339, 2013.

[9] L. Rapoport, N. Fleischer, and R. Tenne, "Applications of WS_2 (MoS_2) inorganic nanotubes and fullerene-like nanoparticles for solid lubrication and for structural nanocomposites," *J. Mater. Chem.*, vol. 15, no. 18, pp. 1782–1788, 2005.

[10] L. Joly-Pottuz, F. Dassenoy, M. Belin, B. Vacher, J. M. Martin, and N. Fleischer, "Ultralow-friction and wear properties of IF-WS2 under boundary lubrication," *Tribol. Lett.*, vol. 18, no. 4, pp. 477–485, 2005.

[11] J. Tannous *et al.*, "Understanding the Tribochemical Mechanisms of IF-MoS_2 Nanoparticles Under Boundary Lubrication," *Tribol. Lett.*, vol. 41, no. 1, pp. 55–64, 2011.

[12] I. Lahouij, B. Vacher, F. Dassenoy, and J.-M. Martin, "Real-Time TEM Imaging of Compression and Shear of Single Fullerene-Like MoS_2 and WS_2 Nanoparticles," *Tribol. Lubr. Technol.*, vol. 68, no. 12, p. 21, 2012.

[13] I. Lahouij, F. Dassenoy, L. de Knoop, J.-M. Martin, and B. Vacher, "In situ TEM observation of the behavior of an individual fullerene-like MoS_2 nanoparticle in a dynamic contact," *Tribol. Lett.*, vol. 42, no. 2, pp. 133–140, 2011.

[14] P. U. Aldana, B. Vacher, T. Le Mogne, M. Belin, B. Thiebaut, and F. Dassenoy, "Action mechanism of WS_2 nanoparticles with ZDDP additive in boundary lubrication regime," *Tribol. Lett.*, vol. 56, no. 2, pp. 249–258, 2014.

[15] X. Hu, "On the size effect of molybdenum disulfide particles on tribological performance," *Ind. Lubr. Tribol.*, vol. 57, no. 6, pp. 255–259, Dec. 2005.

[16] M. K. A. Ali, H. Xianjun, L. Mai, C. Qingping, R. F. Turkson, and C. Bicheng, "Improving the tribological characteristics of piston ring assembly in automotive engines using Al_2O_3 and TiO_2 nanomaterials as nano-lubricant additives," *Tribol. Int.*, vol. 103, pp. 540–554, 2016.

[17] Y. Y. Wu, W. C. Tsui, and T. C. Liu, "Experimental analysis of tribological properties of lubricating oils with nanoparticle additives," *Wear*, vol. 262, no. 7–8, pp. 819–825, 2007.

[18] S. M. Gupta and M. Tripathi, "A review of TiO_2 nanoparticles," *Chinese Sci. Bull.*, vol. 56, no. 16, pp. 1639–1657, 2011.

[19] Y. Ma, X. L. Wang, Y. S. Jia, X. B. Chen, H. X. Han, and C. Li, "Titanium Dioxide-Based Nanomaterials for Photocatalytic Fuel Generations," *Chem. Rev.*, vol. 114, no. 19, pp. 9987–10043, 2014.

[20] T. Tachikawa and T. Majima, "Photocatalytic oxidation surfaces on anatase TiO_2 crystals

revealed by single-particle chemiluminescence imaging," *Chem. Commun.*, vol. 48, no. 27, p. 3300, 2012.

[21] Y. Zhu, Q. Ling, Y. Liu, H. Wang, and Y. Zhu, "Photocatalytic H_2 evolution on MoS_2-TiO_2 catalysts synthesized via mechanochemmistry," *Phys. Chem. Chem. Phys.*, vol. 17, no. 2, pp. 933–940, 2015.

[22] M. F. Abid, "Desulfurization of Gas Oil Using a Solar Photocatalytic Microreactor," *Energy Procedia*, vol. 74, pp. 663–678, 2015.

[23] V. Etacheri, C. Di Valentin, J. Schneider, D. Bahnemann, and S. C. Pillai, "Visible-light activation of TiO_2 photocatalysts: Advances in theory and experiments," *J. Photochem. Photobiol. C Photochem. Rev.*, vol. 25, pp. 1–29, 2015.

[24] F. L. Toma, L. M. Berger, D. Jacquet, D. Wicky, I. Villaluenga, Y. R. de Miguel, J. S. Lindelov, "Comparative study on the photocatalytic behaviour of titanium oxide thermal sprayed coatings from powders and suspensions," *Surf. Coatings Technol.*, vol. 203, no. 15, pp. 2150–2156, 2009.

[26] M. Zarrabi, M. H. Entezari, and E. K. Goharshadi, "Photocatalytic oxidative desulfurization of dibenzothiophene by C/TiO_2 @MCM-41 nanoparticles under visible light and mild conditions," *RSC Adv.*, vol. 5, no. 44, pp. 34652–34662, 2015.

[27] C. Shen, Y. J. Wang, J. H. Xu, and G. S. Luo, "Oxidative desulfurization of DBT with H_2O_2 catalysed by TiO_2 / porous glass," *Green Chem.*, vol. 18, no. 3, pp. 771–781, 2016.

[28] T. H. T. Vu, T. T. T. Nguyen, P. H. T. Nguyen, M. H. Do, H. T. Au, T. B. Nguyen, D. L. Nguyen, J. S. Park, "Fabrication of photocatalytic composite of multi-walled carbon nanotubes/TiO_2 and its application for desulfurization of diesel," *Mater. Res. Bull.*, vol. 47, no. 2, pp. 308–314, 2012.

[29] C. L. Bianchi, S. Gatto, C. Pirola, M. Scavini, S. Vitali, and V. Capucci, "Micro-TiO2 as a starting material for new photocatalytic tiles," *Cem. Concr. Compos.*, vol. 36, no. 1, pp. 116–120, 2013.

[30] G. Dedual, M. J. Macdonald, A. Alshareef, Z. Wu, D. C. W. Tsang, and A. C. K. Yip, "Requirements for effective photocatalytic oxidative desulfurization of a thiophene-containing solution using TiO_2," *J. Environ. Chem. Eng.*, vol. 2, no. 4, pp. 1947–1955, 2014.

[31] I. Fenoglio, G. Greco, S. Livraghi, and B. Fubini, "Non-UV-induced radical reactions at the surface of TiO_2 nanoparticles that may trigger toxic responses," *Chem. - A Eur. J.*, vol. 15, no. 18, pp. 4614–4621, 2009.

[32] J. Ramirez, G. Macias, L. Cedejo, A. Gutierrez-Alejandre, R. Cuevas, and P. Castillo,

"The role of titania in supported Mo, CoMo, NiMo, and NiW hydrodesulfurization catalysts: Analysis of past and new evidences," *Catal. Today*, vol. 98, no. 1–2 SPEC. ISS., pp. 19–30, 2004.

[33] W. P. Zhang, X. Y. Xiao, L. L. Zheng, and C. X. Wan, "Fabrication of TiO_2/MoS_2 Composite Photocatalyst and Its Photocatalytic Mechanism for Degradation of Methyl Orange under Visible Light," *Can. J. Chem. Eng.*, vol. 93, no. 9, pp. 1594–1602, 2015.

[34] S. Bai, L. Wang, X. Chen, J. Du, and Y. Xiong, "Chemically exfoliated metallic MoS_2 nanosheets: A promising supporting co-catalyst for enhancing the photocatalytic performance of TiO_2 nanocrystals," *Nano Res.*, vol. 8, no. 1, pp. 175–183, 2014.

[35] K. H. Hu, X. G. Hu, Y. F. Xu, and J. D. Sun, "Synthesis of nano-MoS_2/TiO_2 composite and its catalytic degradation effect on methyl orange," *J. Mater. Sci.*, vol. 45, no. 10, pp. 2640–2648, 2010.

[36] M. Shen, Z. Yan, L. Yang, P. Du, J. Zhang, and B. Xiang, "MoS_2 nanosheet/TiO_2 nanowire hybrid nanostructures for enhanced visible-light photocatalytic activities," *Chem. Commun.*, vol. 50, no. 97, pp. 15447–15449, 2014.

[37] S. Ingole, A. Charanpahari, A. Kakade, S. S. Umare, D. V Bhatt, and J. Menghani, "Tribological behavior of nano TiO_2 as an additive in base oil," *Wear*, vol. 301, no. 1, pp. 776–785, 2013.

[38] B. S. Shenoy, K. G. Binu, R. Pai, D. S. Rao, and R. S. Pai, "Effect of nanoparticles additives on the performance of an externally adjustable fluid film bearing," *Tribol. Int.*, vol. 45, no. 1, pp. 38–42, 2012.

[39] M. De Feo, C. Minfray, M. I. De Barros Bouchet, Th. Le Mogne, B. Vacher, B. Thiebaut, J. M. Martin "Ageing impact on tribological properties of MoDTC-containing base oil," *Tribol. Int.*, vol. 92, pp. 126–135, 2015.

[40] M. I. De Barros'Bouchet, J. M. Martin, T. Le-Mogne, and B. Vacher, "Boundary lubrication mechanisms of carbon coatings by MoDTC and ZDDP additives," *Tribol. Int.*, vol. 38, no. 3, pp. 257–264, 2005.

[41] P. U. Aldana, F. Dassenoy, B. Vacher, T. Le Mogne, and B. Thiebaut, "WS_2 nanoparticles anti-wear and friction reducing properties on rough surfaces in the presence of ZDDP additive," *Tribol. Int.*, vol. 102, pp. 213–221, 2016.

Chapter 7

Discussion

The previous chapters dealt with the results obtained in case of steel / TiO_2 APS contact lubricated with MoDTC (Chapter 4 and 5) and steel / reference steel contact lubricated with TiO_2 anatase nanoparticles and MoDTC (Chapter 6). Both the contacts with their respective lubricants showed complete decomposition of MoDTC to form MoS_2 which was evident from the tribochemistry observed using XPS.

This chapter deals with the mechanisms proposed to explain the decomposition of MoDTC to form MoS_2 in contacts involving TiO_2 in the form of APS coating or nanoparticles.

Two mechanisms are discussed: photocatalysis and tribocatalysis. Different tests are carried out to prove / discard photocatalysis and tribocatalysis.

7.1 Summary of the previous results:

7.1.1 TiO_2 APS coating lubricated with base oil + MoDTC:

It was shown in chapters 4 and 5 that better friction behavior is obtained in case of steel / TiO_2 APS coating ($\mu \approx 0.040$) than with steel / reference steel ($\mu \approx 0.055$) contact lubricated with base oil + 0.5 % MoDTC. This low friction behavior in case of TiO_2 APS was attributed to the differences in tribochemistry and morphology of MoS_2 tribofilm formed on the coating. From the XPS results, it was shown that the tribofilm is composed of MoS_2 and MoO_3 on TiO_2 APS flats while, it is composed of Mo-oxysulphide, MoS_2 and MoO_3 on reference steel flats. From the FIB-TEM results, formation of long and crystalline MoS_2 flakes on the surface of TiO_2 APS coatings were observed compared to short flakes embedded in an amorphous matrix in case of reference steel [1]. It was also shown that wear resistant Magneli phases are formed on the surface of TiO_2 APS disc, decreasing wear when the contact was lubricated only with base oil. Addition of antiwear additive ZDDP had no further effect on wear reduction. This type of wear reduction had been previously observed in Ti-based materials [27-29] in tribological conditions at higher temperatures. Results obtained in case of TiO_2 APS coating are summarized in fig 7.1, highlighting the various compounds formed inside the tribofilm.

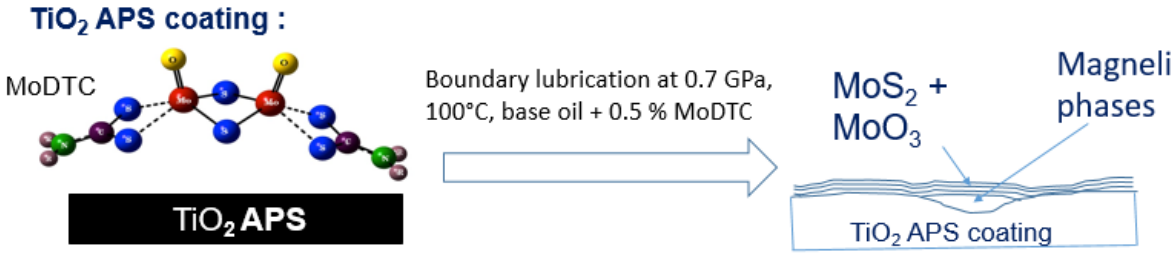

Fig 7.1. Schematic highlighting the compounds obtained after friction test under boundary lubrication conditions in presence of MoDTC and TiO_2 APS coating (0.7 GPa Hertzian maximum pressure, 100°C, 0.5 wt % MoDTC in base oil).

7.1.2 Steel / reference steel contact lubricated with a blend of TiO_2 anatase nanoparticles and MoDTC:

From the results obtained in chapter 6, it is clear that better friction behavior is obtained in case of steel / steel contact ($\mu \approx 0.039$) when it is lubricated with base oil + 0.5 wt % TiO_2 anatase nanoparticles + 0.5 wt % MoDTC than with base oil + 0.5 wt % MoDTC ($\mu \approx 0.055$). This low friction behavior was again attributed to the differences in tribochemistry and morphology of MoS_2 tribofilm formed on the reference steel surface. The tribochemistry was found to be exactly similar to that observed in case of TiO_2 APS coating by XPS. From the FIB-TEM results, formation of a thick tribofilm made up of layers of crystalline MoS_2 flakes and TiO_2

anatase nanoparticles were observed compared to short flakes embedded in an amorphous matrix on the surface of steel [1]. Results obtained in steel / steel when lubricated with TiO_2 nanoparticles and MoDTC in base oil are summarized in fig 7.2, highlighting the various compounds formed inside the tribofilm.

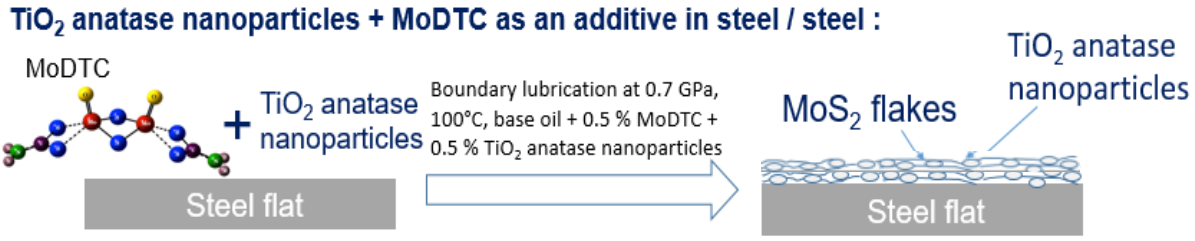

Fig 7.2. Schematic highlighting the compounds obtained after friction test under boundary lubrication conditions in presence of MoDTC and TiO_2 anatase nanoparticles on steel / steel contact (0.7 GPa Hertzian maximum pressure, 100°C, 0.5 wt % MoDTC + 0.5 wt % TiO_2 anatase nanoparticles in base oil).

7.2 Mechanisms for the decomposition of MoDTC:

To understand more about the mechanism for the decomposition of MoDTC in case of steel / TiO_2 APS and steel / steel contacts lubricated with TiO_2 anatase nanoparticles + MoDTC, some of the previous decomposition mechanisms proposed are discussed.

One of the essential requirements for decomposition of MoDTC is presence of **reducing agent** in the form of electrons or a compound like ZDDP which is also a sulphur donor. This was proved by studying the formation of MoS_2 from MoDTC by DFT (Density Functional Theory) technics [5]. Also, Grossiord *et al* [6] and De Barros Bouchet *et al* [7], showed that electron transfer occurs in a first step as shown in the fig 7.3. This transfer of electrons reduces Mo+5 atoms to Mo+4 and thereby reduces the energy barriers required to decompose MoDTC as studied by Cobian *et al* [5]. They found that the reduction of Mo atoms in the initial stages is essential otherwise the energy barriers involved in decomposition of MoDTC are too large to expect to reach them experimentally.

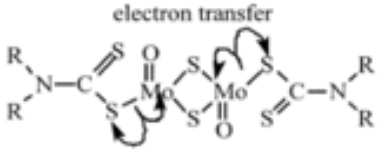

Fig 7.3 Initial electron transfer step in the decomposition of MoDTC [6].

De Barros Bouchet *et al* [8] also showed that presence of optimum concentration of ZDDP provides sulphur atoms for sulphuration of Mo-oxysulphide formed inside the tribofilm in case of steel / steel contacts to form pure MoS_2.

One of the previous studies showed that sufficient **energy** is also required for the decomposition of MoDTC [9]. Energy required to form MoS_2 from MoDTC could be obtained by high temperature and pressure conditions. This was shown by Khaemba *et al* [9] where they concluded that the decomposition of MoDTC is dependent on test conditions including the temperature, pressure and the concentration of MoDTC. Best set of parameters are required to ensure complete decomposition of MoDTC to MoS_2 otherwise incomplete decomposition occurs and leads to the formation of thick amorphous MoS_x tribofilm along with short crystalline MoS_2 flakes and $FeMoO_4$.

From this studies following conclusions can be drawn regarding the decomposition of MoDTC:

(a) Electron transfer occurs in the initial step to reduce some of the Mo+5 atoms to Mo+4. Therefore**, reducing agents in the form of electrons, anions or sulphur donors like ZDDP** are required to ensure complete decomposition of MoDTC to form MoS_2 or re-sulphuration of Mo-oxysulphide formed.

(b) **Sufficient energy** is required in the form of temperature, pressure etc.

In this study, from the results obtained in TiO_2 APS coating and TiO_2 anatase nanoparticles + MoDTC as a lubricant additive in steel / steel contact, it is clear that pure MoS_2 is obtained in both the cases with no oxidised sulphur compounds like MoO_xS_y and sulphate. This suggests that either complete decomposition of MoDTC occurs to form MoS_2 and / or the replacement of S with O is prevented on the TiO_2 surface to form any oxysulphides.

The decomposition of MoDTC to MoS_2 is not so effective in case of steel / reference steel contact. Considering the previous discussion on the mechanisms for the decomposition of MoDTC requiring electrons in the initial reduction step, the better decomposition behaviour in case of steel / TiO_2 APS contact could be attributed to the presence of negatively charged particles (electrons) generated from the ceramic TiO_2 surface (as shown by Nakayama *et al* [10] in case of ceramic oxides surfaces). For the complete decomposition of MoDTC in presence of negatively charged particles, two mechanisms are hypothesized and discussed:

(1) Photocatalysis - generation of negatively charged particles from the surface of TiO_2 in presence of UV or visible light leading to complete decomposition of MoDTC and

(2) Tribocatalysis - generation of negatively charged particles from the surface of TiO_2 in tribological conditions due to various phenomena occurring in the contact which help in initial reduction of Mo atoms as well as ensure the complete decomposition of MoDTC.

To further investigate the mechanisms for the complete decomposition of MoDTC, following hypotheses are discussed in detail:

7.2.1 Photocatalysis:

From the literature review carried out on photocatalysis in chapter 6, TiO_2 anatase as well as rutile nanoparticles are known to exhibit photocatalysis in presence of UV as well as in some cases in visible light. The surface of the nanoparticles gives out electrons and holes which in turn helps in oxidation and reduction of various components [11]. Previous studies also suggest photocatalytic behaviour from the coating material when the coating was manufactured using nano plus micro TiO_2 anatase particles [12-13]. On this basis, it is suggested that the negatively charged particles could be emitted in the contact due to photocatalytic activity which may help in complete decomposition of MoDTC to MoS_2 from the TiO_2 APS coating as well as in case of the TiO_2 anatase nanoparticles.

To verify this, various type of tests involving dark, normal and UV light were carried out in case of TiO_2 APS coating as well as the TiO_2 anatase nanoparticles and are discussed as follows:

7.2.1.1 TiO_2 APS coating:

To find out if the photocatalytic effect plays a role in case of steel / TiO_2 APS contact, reciprocating ball-on-flat tribotests were carried out in the dark and then compared to the ones carried out in normal light. Similar contact conditions as mentioned in chapter 3 are used. Friction curves obtained are compared in fig 7.4.

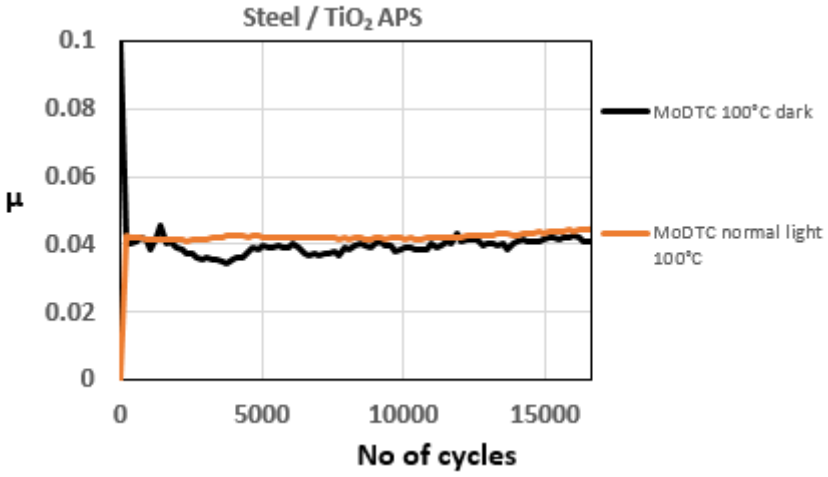

Fig 7.4 Friction curves showing the effect of light on the tribological behaviour of TiO_2 APS.

Friction behaviour shows that there is no change in the friction behaviour even if the test is carried out in dark compared to the test carried out in normal light. Therefore, it can be concluded that there is no photocatalytic effect observed in steel / TiO_2 APS contact where the TiO_2 coating is mainly composed of TiO_2 rutile phase. This is in agreement with the works done on photocatalysis where the authors show that it is observed mostly in nanoparticles of

anatase TiO_2 or coatings made up of anatase nanoparticles [12]. It is not observed in case of other TiO_2 coatings unless they are synthesized from anatase nanoparticles and the transformation to rutile is avoided [11]. Since these coatings were synthesized using micron sized particles of TiO_2 in rutile phase, the photocatalytic effect could be ruled out.

7.2.1.2 TiO_2 anatase nanoparticles:

To evaluate the presence of the photocatalytic behaviour in case of TiO_2 nanoparticles blended with MoDTC in base oil, various tests were carried out on the blend, before any tribotest. Blend of 0.5 % TiO_2 anatase nanoparticles + 0.5 % MoDTC in base oil was mixed using magnetic stirrers at 60°C for 2 hrs until a homogenous solution was obtained in presence of normal laboratory light. The solution obtained was green in colour with no sedimentation of the nanoparticles observed which suggested that the MoDTC has reacted with TiO_2 nanoparticles and formed a stable complex. Since liquid samples cannot be analysed using XPS, to investigate the blend before using it in tribotests, it was necessary to dry the blend. Few drops were taken in a test tube and mixed with *n*-heptane and then centrifuged at 3500 rpm to separate the complex of MoDTC and TiO_2 nanoparticles from base oil. Oil was removed along with *n*-heptane and the wet powder remained as a residue. This powder residue was subsequently dried in the furnace at 80°C to evaluate it using different techniques like XPS, Raman and TEM to observe if some reduction or oxidation occurred due to the photocatalytic phenomena.

(a) XPS analysis on the powder blend:

From the survey XPS spectrum on the dried anatase nanoparticles + MoDTC shown in fig 7.5 (a), it is clear that O, Ti, C, Mo and S are the elements observed. Ti and O observed come from the TiO_2 anatase nanoparticles and C, Mo and S come from the MoDTC molecule. High resolution spectra were carried out to find in which oxidation state the elements Ti and O are present. From the fig 7.5 (b), it is observed that Ti is present in TiO_2 form and the binding energy contribution of Ti2p for the oxide is assigned to be 458.5 eV from the literature [14]. Therefore, it can be confirmed that the contribution of the TiO_2 comes from the titanium dioxide anatase nanoparticles. From the fig 7.5 (c), it can be observed that the Mo3d spectra consists of two different contributions. One of them is assigned to Mo in +6 oxidation state at the binding energy of 231.8 eV, while the other one is assigned to Mo in +5 oxidation state which is similar to the one in MoDTC at the binding energy of 230.2 eV [15]. Mo is observed to be in +5 oxidation state which could be due to the adsorbed MoDTC on the surface of the nanoparticles. Mo+6 is also observed which could be due to oxidation of the MoDTC in air.

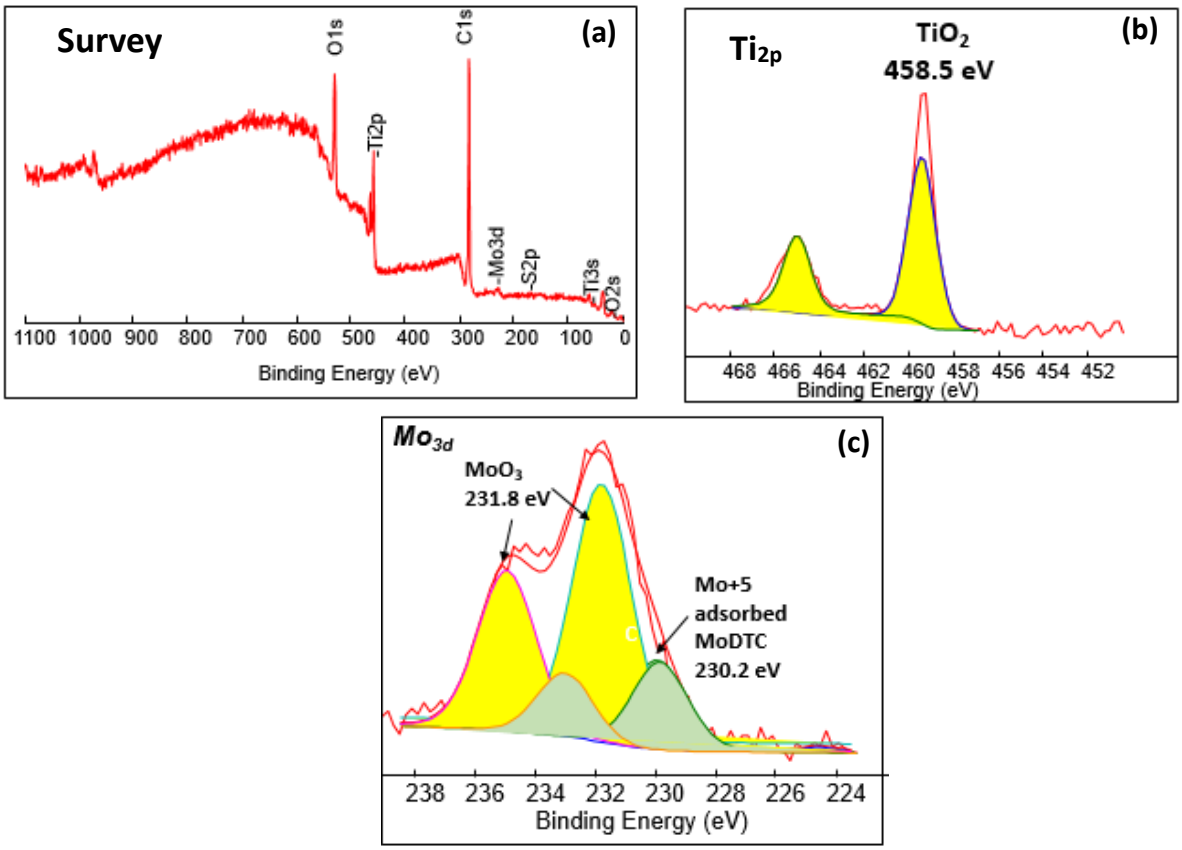

Fig 7.5 (a) General XPS survey spectra on the blend of dried TiO_2 anatase nanoparticles + MoDTC (b) High resolution spectra for Ti2p (c) High resolution spectra for Mo3d.

Considering the initial assumption about photocatalysis during blending of the nanoparticles with MoDTC, it can be concluded that no reduction of the Mo present in MoDTC is observed from the XPS results. Therefore, there is no direct evidence of photocatalysis taking place in case of TiO_2 anatase nanoparticles.

(b) TEM analysis on the dried powder residue:

To find out if the MoDTC molecule is reduced or oxidized in presence of TiO_2 anatase nanoparticles due to photocatalysis, TEM analysis was also carried out on the dried powder residue. To analyse the dried powder residue, some amount of powder was placed on the TEM copper grid for analysis.

TEM micrographs on the dried powder residue of the blend are shown in the fig 7.6. The nanoparticles are found to be agglomerated to each other with white patches on their surface which could be due to adsorbed MoDTC. No flakes or sheet like structures are observed on the surface of the particles which suggests that there is no MoS_2 formation taking place after blending. To confirm the presence of various elements and quantify them, TEM-EDS was carried out. The EDS spectra was carried out on the image shown alongside the spectra on the

right side. EDS spectra predominantly shows C, O, Mo, S, Ti and some contamination from other elements like Si, Fe, Cu (TEM grid). The quantification of the elements is shown in the table 7.1. From the quantification, it can be observed that Ti and O are the major elements which is justified as the powdered residue predominantly consists of TiO_2 nanoparticles with some amount of adsorbed MoDTC. Traces of Mo and S are observed with around 1 atomic % of both the elements which is extremely less to quantify and check the stoichiometry of MoS_2. Also, no flakes of MoS_2 are observed on the surface of nanoparticles. This suggests that there is no decomposition of MoDTC during blending and so no direct evidence of photocatalytic effect.

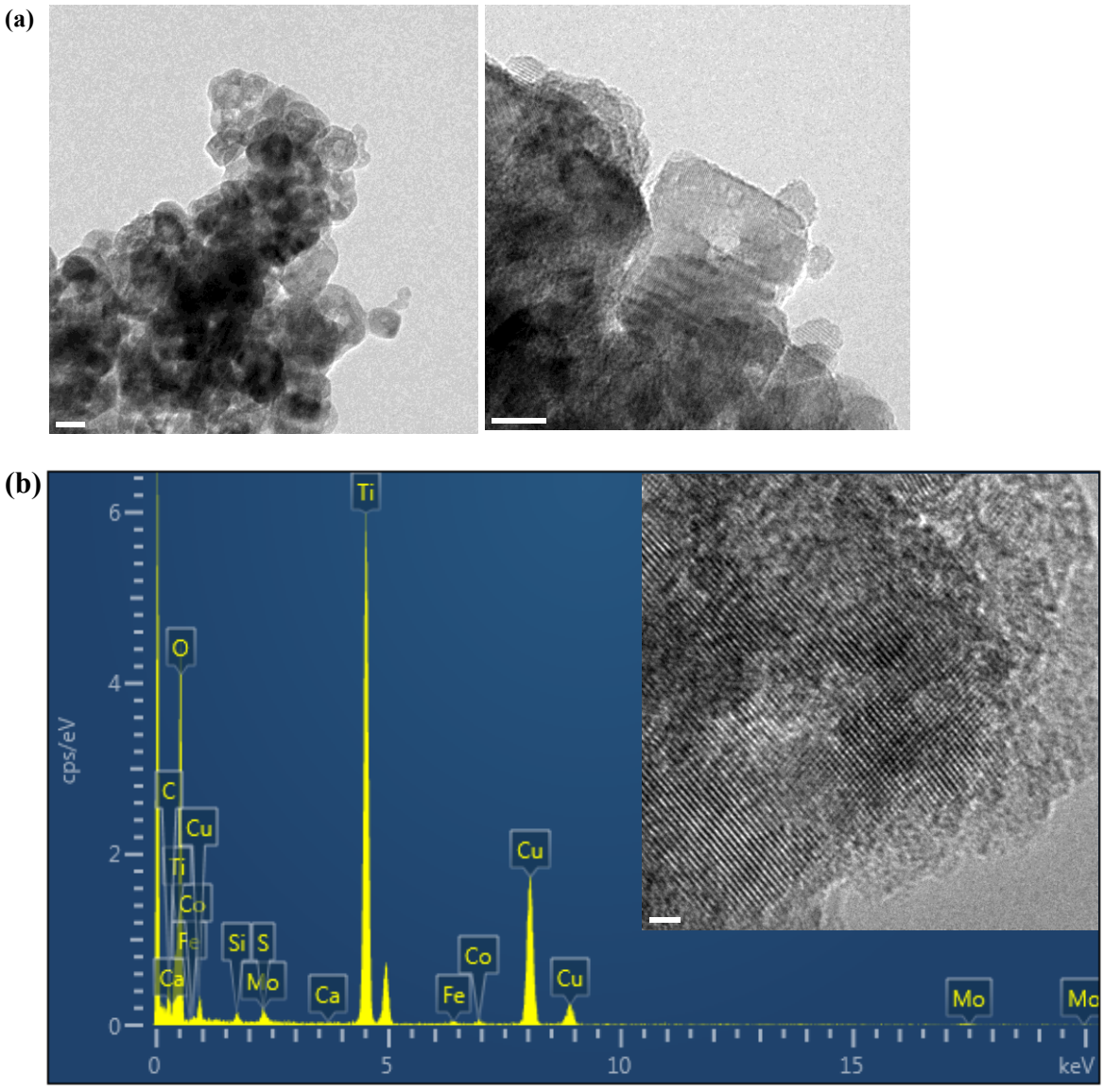

Fig 7.6 **(a)** TEM micrographs of the dried powder residue of the blend of TiO_2 anatase nanoparticles + MoDTC **(b)** TEM image on which the EDS analysis is carried out.

Table 7.1 Atomic % of all the elements present in the TEM EDS image shown in fig 7.6 (b).

Element	C	O	S	Ti	Mo	Total
Atomic %	8.8	41	1.4	47	1.8	100

(c) Raman analysis on the dried powder residue and the oil blend:

To confirm if the presence of Mo and S in the blend is due to the formation of MoS_2 or adsorbed MoDTC in the blend, Raman spectroscopy was carried out on the dried powder and the oil blend. Raman spectra obtained on both the dried powder residue (blue spectrum) and the oil blend (black spectrum) is shown in the fig 7.7. It can be observed in the blue spectrum that it consists of the peaks at 160 cm^{-1}, 419 cm^{-1}, 544 cm^{-1} and 662 cm^{-1} which are assigned to anatase TiO_2 [14]. In the other analysis of the oil blend containing anatase nanoparticles and MoDTC in base oil shown in the black spectrum, similar anatase peaks are observed but with low intensity as the higher intensity peaks at higher Raman shifts are assigned to base oil. Broad peaks at 867 cm^{-1}, 1089 cm^{-1} and 1171 cm^{-1} are assigned to C-C stretching which could come from base oil as well as MoDTC. Peaks at 1315 cm^{-1} and 1455 cm^{-1} are assigned to the stretching and bending of alkyl groups in mineral oil or MoDTC [14] to the peaks of base oil and MoDTC [14] on the surface of the TiO_2 nanoparticles. Primary MoS_2 peaks are not observed which are around 384 and 405 cm^{-1}. Thus it can be confirmed that there is no MoS_2 formation on the surface of the nanoparticles.

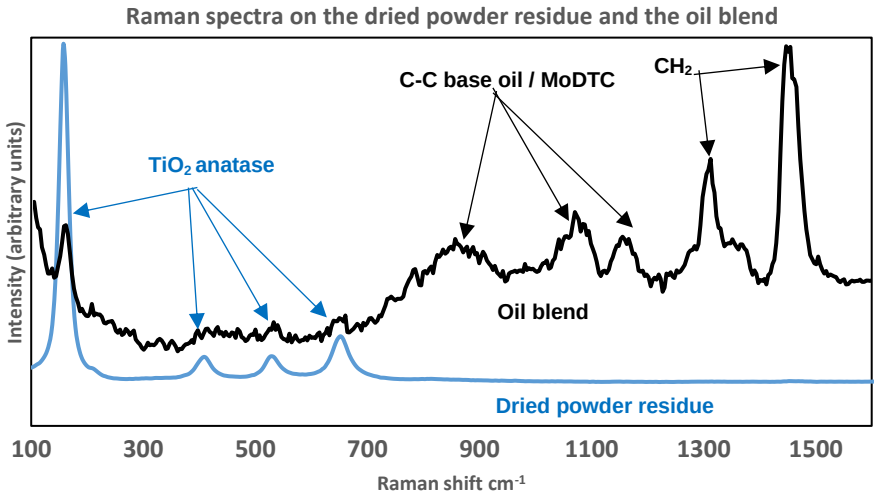

Fig 7.7 Raman spectra for the dried powder residue and the oil blend of TiO_2 anatase nanoparticles + MoDTC.

Taking into account the results obtained from XPS, TEM and Raman analysis, it can be confirmed that there is no MoS_2 formation observed in blends before tribotests. Therefore, it

can be concluded that there is no evidence of photocatalysis mechanism.

(d) Tribotests using blend irradiated with UV light:

It was confirmed from the above test results that MoDTC is not reduced before that any tribotests are carried out. To confirm the absence of photocatalytic effect during tribotesting, the blend was irradiated with long wave UV light (wavelength = 365 nm) using a portable UV light device Spectroline close to the band gap of TiO_2. The blend was kept in a bottle inside an enclosed box along with the portable UV light device on top of the box. Irradiation of UV light was done for 12 hours and tribotests were carried out under normal light using this blend. The results were compared to the previously obtained test results for blending carried out in normal light and dark in case of steel / steel and steel / steel APS as shown in fig 7.8. For both the contacts, the friction trends are found to be similar when the tribotests are lubricated with an oil blended in normal light, dark or after UV light exposure as the steady state friction coefficient remains to be around 0.04 in case of steel / reference steel and 0.033 in case of steel / steel APS contacts. This suggests that UV light exposure on the blend before tribotest has no effect on the friction behaviour of the contacts.

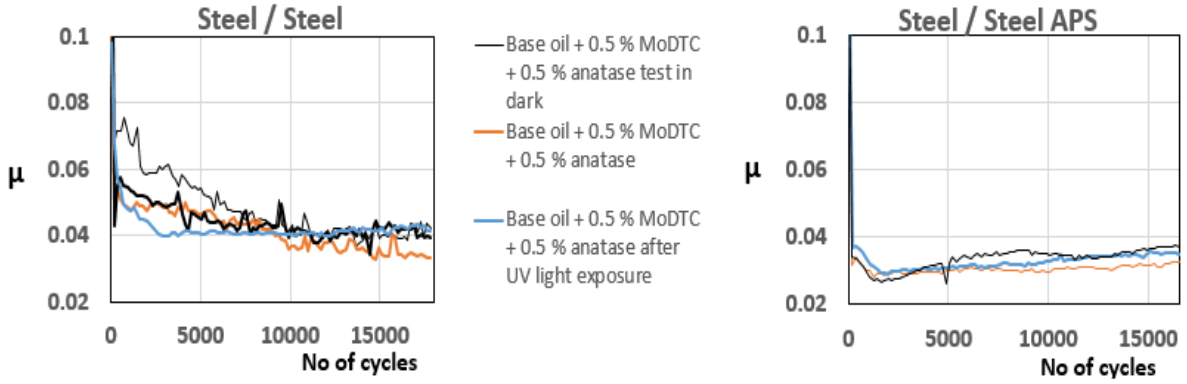

Fig 7.8 Friction behaviour for steel / steel and steel / steel APS after the blend was exposed to UV light for 12 hours.

From all the results presented in this section, it could be confirmed that our initial assumption concerning the existence of photocatalytic effect is incorrect. Therefore, the photocatalytic effect in the TiO_2 APS coating lubricated with MoDTC as well as the blend of TiO_2 anatase nanoparticles and MoDTC needs to be ruled out. Therefore, there exists some other similar mechanism which governs the complete decomposition of MoDTC to MoS_2 in case of TiO_2 APS coating as well as steel / steel contact lubricated with a blend of TiO_2 anatase nanoparticles + MoDTC in base oil.

7.2.2 Tribocatalysis:

The other mechanism proposed to explain the complete decomposition of MoDTC to MoS_2 in presence of TiO_2 is tribocatalysis. This involves catalytic behaviour of the material in contact to help in producing tribofilms with better antiwear and friction reducing properties compared to the reference materials lubricated with various additives like MoDTC and / or ZDDP. The catalytic material does not directly react with the additive but helps in its complete decomposition.

A lot of research has been carried out by both Hiratsuka *et al* [16-17] and Kajdas *et al* [18–21] on tribochemistry and tribocatalysis showing how the catalytic behaviour of different materials including ceramics, coatings influence the tribochemistry of the materials in contact. Erdemir *et al* [22] showed that catalytic nanocrystalline coatings composed of nitrides of either molybdenum or vanadium in severe tribological conditions, formed carbon based tribofilms structurally similar to DLC which reduce friction and wear. Hiratsuka *et al* [16] has previously shown that tribocatalytic effect was found in case of oxidation of ethylene when palladium was rubbed against Al_2O_3. They found that oxidation activity of ethylene was enhanced due to the tribological conditions generated between palladium and alumina. This led to complete oxidation of ethylene. Similar tribocatalytic behaviour was observed for complete oxidation of methane by Abe *et al* [17] and in case of carbon dioxide by Hiratsuka *et al* [23]. Molina *et al* [21] suggested that various emissions are observed from the ceramic materials in tribological conditions. These emissions generated due to tribological conditions help in accelerating the tribochemical reactions until completion [24]. Kajdas *et al* [21] suggested a mechanism for generation of electrons from the surface of ceramic oxides in tribological conditions. Similarly, Nakayama *et al* [25-26] observed different types of emission occurring in dry as well as lubricated tribological conditions in various ceramic oxide materials. Higher intensity of the negatively charged particles was observed in case of semiconducting materials than pure insulators.

In this study, tribocatalysis is the mechanism discussed in TiO_2 APS coating in boundary conditions based on the following results:

(a) TiO_2 APS coating does not directly react with the MoDTC additive but plays an important role in the reduction reaction to ensure complete decomposition of MoDTC to form pure MoS_2 tribofilms with no oxidised sulphur compounds. Therefore, TiO_2 acts as a catalyst in the reaction.

(b) Also, generation of wear resistant Magneli phases on the surface of TiO_2 APS coating is observed due to severe tribological conditions.

Since this catalytic effect of the TiO_2 APS coating is observed only in tribological conditions, it can be termed as tribocatalysis.

However, we believe that this effect includes emission of negatively charged particles like electrons, ions or free radicals from the semiconducting ceramic oxide (TiO_2) [10, 24-25] under severe boundary lubrication conditions and similarly from the TiO_2 anatase nanoparticles when they are used as one of the constituents of the oil blend used to lubricate steel / steel contact. These negatively charged particles in turn could help in initial reduction of MoDTC as well as ensure complete decomposition to MoS_2.

7.2.2.1 **Evidence of reduced Mo species in the tribofilms formed on TiO_2 APS**:

From the results and discussions for the effect of various parameters (chapter 5) in case of reference steel and TiO_2 APS flats on their tribological behaviour, it was previously concluded that complete decomposition of MoDTC occurs in case of TiO_2 APS to form pure MoS_2. As discussed in this chapter, it could be due to the generation of negatively charged particles from the surface of TiO_2 APS coating or TiO_2 anatase nanoparticles in the tribological conditions. To support that negatively charged particles are generated in steel / TiO_2 APS contact, following are some indirect evidences of negatively charged particles obtained in case of steel / TiO_2 APS coating from the previous results:

(1) Effect of temperature:

XPS results obtained for steel / TiO_2 APS contact suggested formation of pure MoS_2 at all temperatures. However, **more reduced contribution (Mo metal)** is observed at 100°C. At lower temperatures (20°C and 60°C), the contact is less severe and the reduced Mo metal species were not observed. This reduced Mo metal contribution is not observed at all in case of reference steel which could confirm the argument that negatively charged particles are generated in steel / TiO_2 APS contact.

(2) Effect of pressure:

Similar friction coefficients were observed at all pressures for steel / TiO_2 APS contacts which is in agreement with the XPS results where pure MoS_2 was observed in all cases. Also, **reduced species of Molybdenum (Mo metal)** was observed at higher pressures of 0.7 GPa and 1 GPa along with MoS_2 and MoO_3. This further reduction in Mo species is again observed only for steel / TiO_2 APS contacts which could be due to the presence of negatively charged particles.

(3) Effect of change of counterpart material:

Similar friction results were obtained when TiO_2 APS flats were tested against ceramic balls and steel balls which was in agreement with the XPS results where pure MoS_2 and reduced Mo

metal species formation was observed. However, replacing the steel ball counterpart with ceramic balls like ZrO_2 or Al_2O_3 led to even more reduction of Mo atoms in the tribofilm as Mo_xC (carbide) are found. These results clearly show evidence of reduced Mo species in tribological contacts involving TiO_2 APS flats and lubricated with MoDTC. Actually, molybdenum, initially in +5 oxidation state in the MoDTC molecule, is found to be reduced to species such as MoS_2 (+4), Mo metal (0) and also Mo_xC (+2) or Mo_2C (+4) in ceramic / TiO_2 APS contacts. Formation of even more reduced species in ceramic / TiO_2 APS contact than steel / TiO_2 APS contact at different pressures and temperatures could be due to generation of more negatively charged particles from the ceramic / ceramic contact than steel / ceramic contact. This is in agreement with the previous work carried out by Molina *et al* [24] and Nakayama *et al* [10; 25 - 26] where they showed that high amount of emission is observed in case of insulating ceramic oxides like alumina even in lubricated conditions. Since similar results are obtained in case of steel / steel contact when it was lubricated with a blend of TiO_2 anatase nanoparticles and MoDTC in base oil, it can be considered that there exists a similar type of mechanism like tribocatalytic effect responsible for the complete decomposition of MoDTC to form pure MoS_2 as observed from the XPS analysis.

7.2.2.2 Sources of negatively charged particles:

From the discussion in the previous section concerning indirect evidences of negatively charged particles, it can be considered that negatively charged particles could be generated under boundary lubricated tribological conditions in case of steel / TiO_2 and ceramic / TiO_2 APS contacts which help in complete decomposition of MoDTC to form MoS_2 as well as formation of more reduced Mo species inside the tribofilm. This is in agreement with the theoretical work on MoDTC decomposition pathway presented in the introduction [13], as it was shown that the reduction of Mo atom in MoDTC molecule is required to reduce the energy barriers experimentally to form MoS_2. However, it is necessary to find out the source of these negatively charged particles. They could come from different tribological processes occurring in the contact which are discussed as follows:

(a) Triboemission :

First source could be the generation of negatively charged particles (ions, electrons, free radicals) from ceramic oxides in lubricated tribological conditions as discussed above where Nakayama *et al* [10; 25 - 26], Kajdas *et al* [19; 20 - 24], Molina *et al* [21; 27 - 28] clearly suggested emission occurring in tribological conditions in the form of electrons, ions and radicals. This generation of negatively charged particles is a necessary step of the tribocatalytic behaviour observed in ceramic oxide coatings. Also, Puhan *et al* [29] experimentally suggested

that emission of negatively charged particles in the form of electrons or anions in a contact lubricated with ZDDP involving steel / aluminum oxide and help in additive degradation process. However, in this study, no direct evidence of triboemission is observed and only indirect evidences from the reduced Mo compounds were observed.

(b) Magneli phases:

The other source of negatively charged particles could be the generation of electrons from the vacancies generated due to the formation of wear resistant Magneli phases on the surface of TiO_2 APS coating in tribological conditions explained in chapter 4. Magneli phases are the oxygen deficient species with the general formula TiO_x, where x is between 1.75 and 1.83. Therefore, whenever the oxygen is lost from the TiO_2 rutile surface, an oxygen vacancy created at the site has two electrons to maintain the electrical charge neutrality as explained by Gardos *et al* [30]. The oxygen vacancies go on increasing as the oxygen is lost from the surface till a stage is reached where Magneli phases are formed. Electrons obtained at this vacancy site could be used for initial reduction of MoDTC to accelerate the reaction of forming MoS_2 and then also for reducing the TiO_2 structure to $TiO_{1.75}$. Also, these Magneli phases due to the presence of a mixture of corundum and rutile structure are known for their charge storage ability [31]. Therefore, whenever electrons are generated on the surface of the TiO_2 APS coating, these could be stored for a long period of time and this could ensure complete decomposition of MoDTC as well as avoid the formation of oxygen containing sulphur compounds formed in case of reference steel. As mentioned before, Magneli phase generation was confirmed by Raman spectroscopy in chapter 4 [32]. Even if we don't have any direct evidences, this could lead us to consider that electrons are generated in the contact through the Magneli phase sites which help in the complete decomposition of MoDTC to MoS_2.

Considering the fact that reduced Mo metal and carbide species are observed in case of steel / TiO_2 APS contact as well as ceramic / TiO_2 APS contacts, it can be due to the combination of both the sources of negatively charged particles, triboemission as well as Magneli phase formation that generate excess negatively charged particles in the contact and in turn help to form Mo metal as well as carbide species. However, it is true that there is no direct evidence of triboemission or negatively charged particles in the contact.

However, in case of TiO_2 anatase nanoparticles + MoDTC as an additive in steel / steel contact, since the Magneli phases are not found and similar tribochemistry is observed, it can be assumed that the first source of electrons (triboemission) is the most appropriate one.

7.2.3 Proposed mechanism for complete decomposition of MoDTC in presence of TiO_2 coating:

The proposed reaction mechanism for the decomposition of MoDTC in case of steel / TiO_2 APS contacts is summarized in fig 7.9. This mechanism shows that when a steel / TiO_2 APS contact is subjected to reciprocating sliding under boundary lubrication conditions in presence of base oil + 0.5 % MoDTC, it leads to complete decomposition of MoDTC to form MoS_2 and MoO_3 due to the negatively charged particles generated from the TiO_2 surface. Also, wear resistant Magneli phases are generated on the surface of TiO_2. Similar results are obtained in case of steel / reference steel contact lubricated with a blend of MoDTC and TiO_2 anatase nanoparticles except the formation of Magneli phases which is observed only in bulk TiO_2 materials. Due to the similarities in friction and tribochemistry results whenever TiO_2 is present in the contact in the form of coating or as anatase nanoparticles, it is assumed that even steel / steel contact when lubricated with a blend of TiO_2 anatase nanoparticles and MoDTC also exhibits similar kind of tribocatalytic behaviour. This type of tribocatalytic behaviour is unique to TiO_2 based materials and not observed in case of reference steel as it forms oxysulphides of Mo on the tribopair surfaces which generally shows higher friction than pure MoS_2 formation [1]. Also, the replacement of S by O occurs in case of reference steel flats as XPS always shows the formation of oxysulphides, sulphates (Fe-sulphates) which could lead to higher wear and corrosion [33].

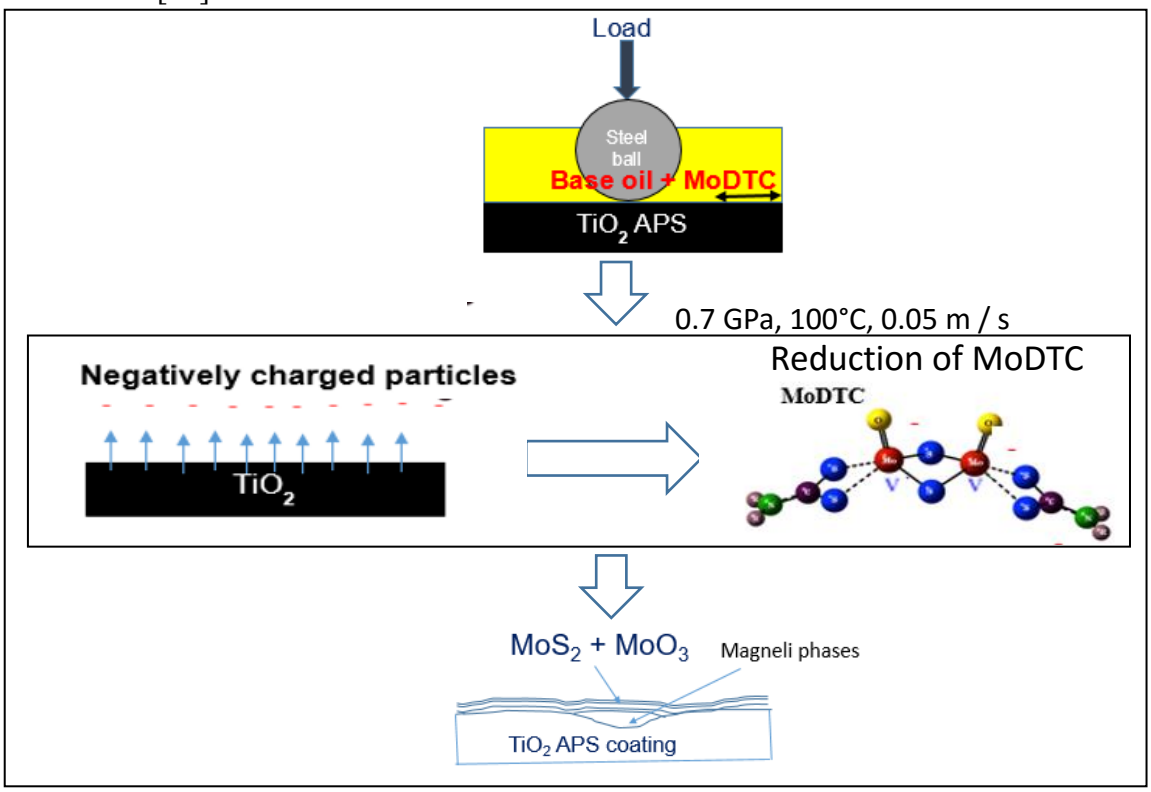

Fig 7.9 Schematic of the decomposition mechanism of MoDTC in steel / TiO_2 APS contact.

7.3 Conclusions

From the discussions on the two different hypothesized mechanisms for the complete decomposition of MoDTC in presence of TiO_2, photocatalysis and tribocatalysis, following conclusions are made:

(1) Various tests were carried out in case of steel / TiO_2 APS coating lubricated with MoDTC and steel / steel lubricated with an oil blend of TiO_2 anatase nanoparticles and MoDTC. No evidences were found in favour of photocatalytic behaviour and this mechanism was discarded.

(2) Tribocatalysis, the other proposed mechanism is considered to be the most appropriate mechanism responsible for complete decomposition of MoDTC in presence of TiO_2 coating or nanoparticles. This is because the coating / nanoparticles do not directly react with MoDTC but help in complete decomposition of the additive to MoS_2 with no oxidized sulphur compounds. Presence of reduced Mo species inside the tribofilm on TiO_2 APS contact strongly suggests the generation of negatively charged particles in the contact which is a necessary step in the overall tribocatalysis mechanism. In case of TiO_2 nanoparticles, only triboemission could be the source of generation of negatively charged particles whereas in case of steel / TiO_2 and ceramic / TiO_2 contact, source of negatively charged particles could be a combination of Magneli phases and triboemission.

7.4 References

[1] M. De Feo, C. Minfray, M. I. De Barros Bouchet, Th. Le Mogne, B. Vacher, B. Thiebaut, J. M. Martin, "Ageing impact on tribological properties of MoDTC-containing base oil," *Tribol. Int.*, vol. 92, pp. 126–135, 2015.

[2] J. Landa, I. Illarramendi, N. Kelling, M. Woydt, A. Skopp, and M. Hartelt, "Potential of thermal sprayed Ti_nO_{2n-1} coatings for substituting molybdenum-based ring coatings," *Ind. Lubr. Tribol.*, vol. 59, no. 5, pp. 217–229, 2007.

[3] A. Skopp, N. Kelling, M. Woydt, and L. M. Berger, "Thermally sprayed titanium suboxide coatings for piston ring/cylinder liners under mixed lubrication and dry-running conditions," *Wear*, vol. 262, no. 9–10, pp. 1061–1070, 2007.

[4] M. Woydt, "Tribological characteristics of polycrystalline Magnéli-type titanium dioxides," *Tribol. Lett.*, vol. 8, no. 2–3, pp. 117–130, 2000.

[5] M. Cobian. D.Jose, M. De Feo, C.Minfray, "Computational studies of reaction mechanism of MoDTC," *Leeds- Lyon Symp. Tribol.*, p. 2015, 2015.

[6] C. Grossiord, K. Varlot, J. M. Martin, T. Le Mogne, C. Esnouf, and K. Inoue, "MoS_2 single sheet lubrication by molybdenum dithiocarbamate," *Tribol. Int.*, vol. 31, no. 12, pp. 737–743, 1998.

[7] M. I. De Barros Bouchet, J. M. Martin, T. Le-Mogne, and B. Vacher, "Boundary lubrication mechanisms of carbon coatings by MoDTC and ZDDP additives," *Tribol. Int.*, vol. 38, no. 3, pp. 257–264, 2005.

[8] M. I. De Barros Bouchet, J. M. Martin, T. Le Mogne, P. Bilas, B. Vacher, and Y. Yamada, "Mechanisms of MoS_2 formation by MoDTC in presence of ZnDTP: Effect of oxidative degradation," *Wear*, vol. 258, no. 11–12, pp. 1643–1650, 2005.

[9] D. N. Khaemba, A. Neville, and A. Morina, "New insights on the decomposition mechanism of Molybdenum DialkyldiThioCarbamate (MoDTC): a Raman spectroscopic study," *RSC Adv.*, vol. 6, no. 45, pp. 38637–38646, 2016.

[10] K. Nakayama, "Triboemission of charged particles from various solids under boundary lubrication conditions," *Wear*, vol. 178, no. 1–2, pp. 61–67, 1994.

[11] F. L. Toma, L. M. Berger, D. Jacquet, D. Wicky, I. Villaluenga, Y. R. de Miguel, J. S. Lindelov, "Comparative study on the photocatalytic behaviour of titanium oxide thermal sprayed coatings from powders and suspensions," *Surf. Coatings Technol.*, vol. 203, no. 15, pp. 2150–2156, 2009.

[12] T. Tachikawa and T. Majima, "Photocatalytic oxidation surfaces on anatase TiO_2 crystals revealed by single-particle chemiluminescence imaging," *Chem. Commun.*, vol. 48, no.

27, p. 3300, 2012.

[13] "Photocatalytic activity assessment of micro-sized TiO_2 used as powders and as starting material for porcelain gres tiles production," 2014.

[14] J. A. Mejias, V. M. Jiménez, G. Lassaletta, A. Fernández, J. P. Espinós, and A. R. González-Elipe, "Interpretation of the binding energy and auger parameter shifts found by XPS for TiO_2 supported on different surfaces," *J. Phys. Chem.*, vol. 100, no. 40, pp. 16255–16262, 1996.

[15] M. De Feo, "Impact of thermo-oxidative degradation of MoDTC additive on its tribological performances for steel-steel and DLC-steel contacts." Ecole Centrale de Lyon, 2015.

[16] K. Hiratsuka, T. Abe, and C. Kajdas, "Tribocatalytic oxidation of ethylene in the rubbing of palladium against aluminum oxide," *Tribol. Int.*, vol. 43, no. 9, pp. 1659–1664, 2010.

[17] T. Abe, K. Hiratsuka, and C. Kajdas, "Tribocatalytic Enhancement of Methane Oxidation," in *World Tribology Congress III*, 2005, pp. 919–920.

[18] C. Kajdas, A. Kulczycki, and D. Ozimina, "A new concept of the mechanism of tribocatalytic reactions induced by mechanical forces," *Tribol. Int.*, 2016.

[19] C. Kajdas and K. Hiratsuka, "Tribochemistry, tribocatalysis, and the negative-ion-radical action mechanism," *Proc. Inst. Mech. Eng. Part J J. Eng. Tribol.*, vol. 223, no. 6, pp. 827–848, 2009.

[20] C. K. Kajdas, "Tribochemistry of selected ceramic materials," *Mechatron. Syst. Mater.*, vol. 113, pp. 339–347, 2006.

[21] G. Molina, M. Furey, C. Kajdas, and N. Steika, "on the Mechanism of Electron Triboemission From Ceramics," pp. 17–23, 2005.

[22] A. Erdemir, G. Ramirez, O. L. Eryilmaz, B. Narayanan, Y. Liao, G. Kamath, Subramanian K. R., S. Sankarnarayanan, "Carbon-based tribofilms from lubricating oils," *Nature*, vol. 536, no. 7614, pp. 67–71, Aug. 2016.

[23] K. Hiratsuka, C. Kajdas, and M. Yoshida, "Tribo-catalysis in the synthesis reaction of carbon dioxide," *Tribol. Trans.*, vol. 47, no. 1, pp. 86–93, 2004.

[24] C. K. Kajdas, "Importance of the triboemission process for tribochemical reaction," *Tribol. Int.*, vol. 38, no. 3, pp. 337–353, 2005.

[25] K. Nakayama and H. Hashimoto, "Triboemission from various materials in atmosphere," *Wear*, vol. 147, no. 2, pp. 335–343, 1991.

[26] K. Nakayama and H. Hashimoto, "Triboemission, tribochemical reaction, and friction and wear in ceramics under various n-butane gas pressures," *Tribol. Int.*, vol. 29, no. 5,

pp. 385–393, 1996.

[27] G. J. Molina, M. J. Furey, A. L. Ritter, and C. Kajdas, “Triboemission from alumina, single crystal sapphire, and aluminum,” *Wear*, vol. 249, no. 3–4, pp. 214–219, 2001.

[28] G. J. Molina, M. J. Furey, a L. Ritter, N. S. Eiss, and K. Triboemission, “Triboemission From Ceramics : Charge Intensity and Energy Distribution Characterizations,” 2000.

[29] C. Paper, “An experimental study into the possible effects of triboemission,” no. October, pp. 7–9, 2016.

[30] M. N. Gardos, “The effect of anion vacancies of the tribological properties of rutile ({$TiO_{\{2-x\}}$}),” *Tribol. Trans.*, vol. 31, no. 4, pp. 427–436, 1988.

[31] A. C. M. Padilha, H. Raebiger, A. R. Rocha, and G. M. Dalpian, “Charge storage in oxygen deficient phases of TiO_2: defect Physics without defects,” *Sci. Rep.*, vol. 6, p. 28871, 2016.

[32] P. Deshpande, C. Minfray, F. Dassenoy, B. Thiebaut, T. Le Mogne, B. Vacher, F. Jarnias, “Tribological behaviour of TiO_2 Atmospheric Plasma Spray (APS) coating under mixed and boundary lubrication conditions in presence of oil containing MoDTC,” *Tribol. Int.*

[33] F. H. Stott, J. E. Breakell, and R. C. Newman, “The corrosive wear of cast iron under potentiostatically-controlled conditions in sulphuric acid solutions,” *Corros. Sci.*, 1990.

General conclusion

MoDTC is used as a friction modifier additive in majority of the engine lubricants and has been extensively studied for various contacts. However, its interaction with APS coatings was not well studied. APS coatings are recently used as a replacement for the traditional iron based materials for cylinder liner. The main focus of this work was to study the interaction of MoDTC with various APS coatings and specifically TiO_2 APS coating and to find out how MoDTC behaves in presence of TiO_2 APS coating under boundary lubrication conditions.

Steel / TiO_2 APS contact showed the better tribological properties than any other contacts including other steel based APS and reference steel contacts. Various configurations were used for testing and it can be concluded that change in configuration did not considerably affect the tribological behaviour of steel / TiO_2 APS contact. Following are the conclusions deduced for the tribological behaviour as well as the detailed surface characterization of the tribofilms formed in case of steel / TiO_2 APS contact:

(a) Friction reduction was attributed to better tribochemistry and morphology of the tribofilms formed.

(b) Wear reduction was attributed to the tribologically induced formation of sub-stoichiometric wear resistant phases called Magneli phases.

Considering the better tribological behaviour of steel / TiO_2 APS contact, parametric study involving change of roughness of the counterparts, concentration of MoDTC, test temperature, contact pressure, counterpart material were carried out. From these parametric studies on contacts involving TiO_2 APS, it can be concluded that change of any parameter did not affect the friction behaviour as the decomposition of MoDTC to MoS_2 was observed in all cases and confirmed by XPS analysis. In fact, XPS analysis showed formation of more reduced species of Mo than MoS_2 like Mo metal and Mo-carbides in case of tribofilms present on TiO_2 APS coating.

Considering the better tribological results obtained for TiO_2 APS coating in presence of MoDTC as a lubricant, TiO_2 nanoparticles were blended with MoDTC. From the tribotests carried out on steel / reference steel contact in presence of this newly formulated lubricant consisting of MoDTC and TiO_2 nanoparticles, it was found that friction and involved tribochemistry is related to similar mechanism. This was concluded from the detailed characterization of the tribofilms carried out using XPS and FIB-TEM.

To discuss the interesting results obtained with TiO_2 based materials, two different mechanisms were hypothesized. It is concluded that photocatalysis does not exist owing to the different tests

carried out which were not in favour of photocatalytic process responsible for the decomposition of MoDTC in case of contacts involving presence of TiO_2 in coating or nanoparticle form. Similarity in friction results whenever TiO_2 based material is used in a tribological contact in presence of MoDTC led us to propose a similar mechanism for the decomposition of MoDTC in these contacts.

The most probable mechanism suggested for the complete decomposition of MoDTC in contacts involving TiO_2 coating or nanoparticles is the tribocatalytic behaviour. This is because the coating / nanoparticles do not directly react with MoDTC but help in complete decomposition of the additive to MoS_2 with no oxidized sulphur compounds. This mechanism probably involves formation of negatively charged particles in the contact which help in complete decomposition of MoDTC. Presence of reduced Mo species like Mo metal and Mo-carbide inside the tribofilm on TiO_2 APS contact are strong but indirect evidences of the generation of negatively charged particles in the contact which is a necessary step in the overall tribocatalysis mechanism.

This work has enabled us to understand better the interaction of MoDTC with APS coatings specifically TiO_2 based materials like TiO_2 APS coating as well as TiO_2 nanoparticles where the decomposition of MoDTC is governed by a tribocatalytic process. The tribocatalytic behaviour of APS coatings which leads to their better tribological behaviour will surely enhance the use of these kind of materials for cylinder liners in the near future. However, there is still a necessity to further understand the tribocatalytic behaviour of APS coatings in lubricated conditions.

Perspectives:

Although this study explains the possible tribocatalysis mechanism for the complete decomposition of MoDTC in presence of TiO_2 based materials like TiO_2 APS coating and TiO_2 nanoparticles, there is a further need to explore or prove the hypothesized mechanisms directly or indirectly by carrying out further tests. Following are the proposed tests to prove the tribocatalytic behaviour of TiO_2 based materials.

1. **Charge measurement using AFM:**

From our study, there was only indirect evidence of generation of negatively charged particles. Therefore, to gather direct evidences for the presence of charged particles like electrons on the ceramic oxide surface (TiO_2), surface charge measurement could be one of the methods used. To measure the charged particles or the negative charge generated on the TiO_2 surface, Electrostatic Force Microscopy (EFM) can be used. This EFM, which is a modified form of AFM, measures electrostatic force between the surface and a biased AFM cantilever. Images obtained can give information about the surface potential and charge distribution of a sample surface.

2. **Effect of change of additive combinations;**

Tribocatalytic behaviour of TiO_2 APS coatings could be used for decomposition of other kind of additives. Reciprocating ball-on-flat tribotests were so carried out using various combinations of additives like sulphur and molybdenum sources like DTC (Dithiocarbamate) or Polysulphide (PS) and Molyvan (Molybdenum amide) respectively to find out if they react with each other to achieve low friction by forming MoS_2 inside the tribofilm. Similar tribological conditions were used as mentioned in chapter 3 for ball-on-flat tribotests in case of steel / TiO_2 APS contact. To compare the results with a reference material, tests were also carried out with steel / reference steel contact in similar conditions. Following graphs in the figure 1 (a) and (b) show the results obtained in case of steel / TiO_2 APS and steel / reference steel contacts lubricated with base oil + 0.5 % DTC + 0.5 % Molyvan, base oil + 0.5 % PS + 0.5 % Molyvan and base oil + 0.5 % MoDTC. It can be observed that whatever the combination of additive low friction coefficient is still achieved in case of steel / TiO_2 APS contact. However, in case of steel / reference steel contact, steady state friction coefficient is always higher than steel / TiO_2 APS contact. In fact, when the contacts are lubricated with base oil + 0.5 % PS + 0.5 % Molyvan, steel / reference steel contact shown no friction reduction and the friction behaviour obtained resembles that of base oil as shown in chapter 3. On the contrary, steel /

TiO_2 APS contact clearly shows extremely low steady state friction coefficient. Even in case of base oil + 0.5 % DTC + 0.5 % Molyvan, steel / steel contact shows increase in friction coefficient compared to steel / TiO_2 APS contact where the friction coefficient is low from the beginning of the test and remains constant for the whole duration.

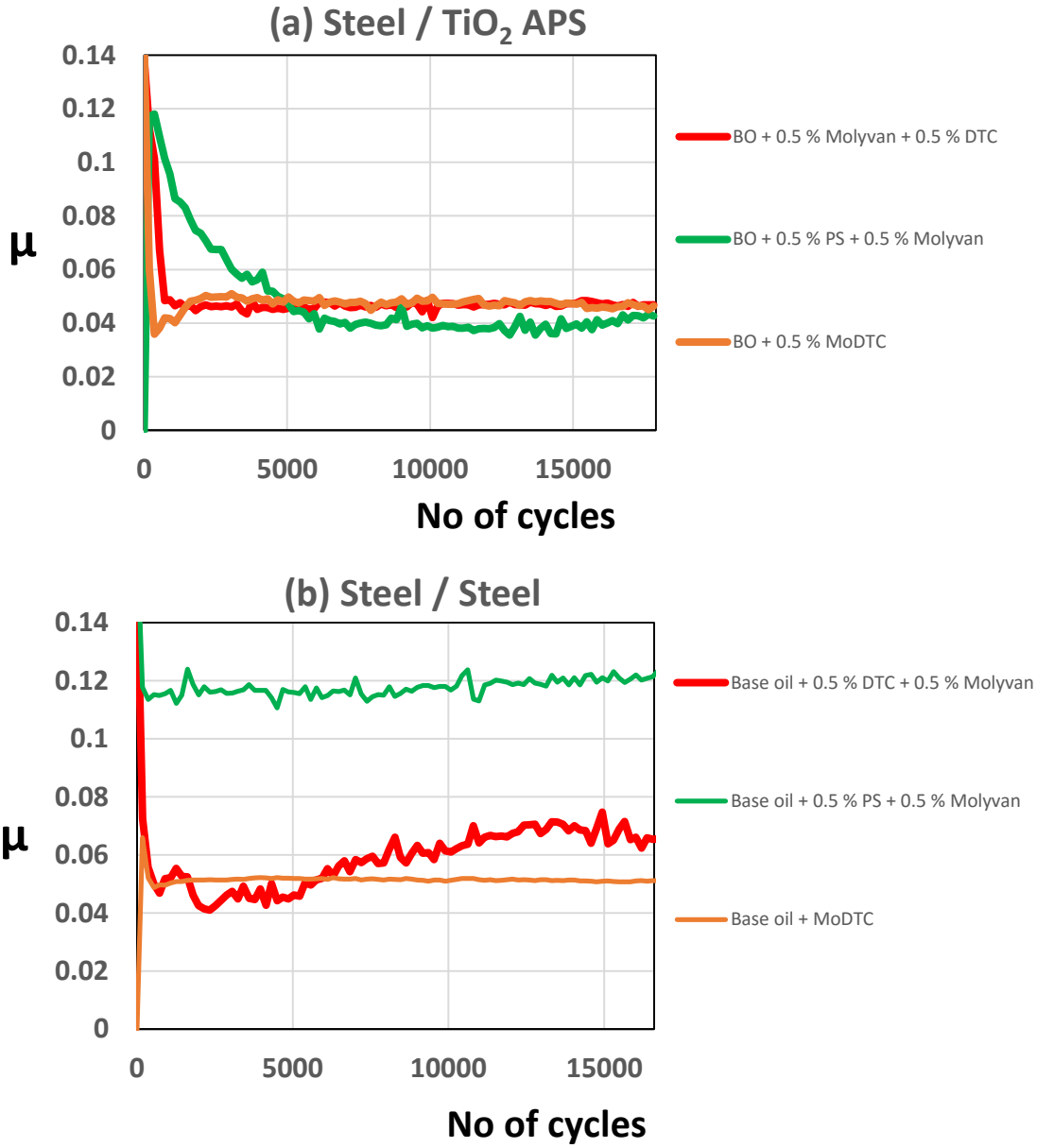

Fig.1 Friction behaviour for (a) steel / TiO_2 APS (b) steel / reference steel contact lubricated with Mo source (Molyvan) and S source (PS and DTC).

To investigate the reasons for low friction behaviour in case of different additive combinations in steel / TiO_2 APS contact, XPS was carried out. Fig.2 shows the high resolution Mo3d spectra obtained inside the tribofilm on the TiO_2 APS flat lubricated with base oil + 0.5 % PS + 0.5 % Molyvan and base oil + 0.5 % DTC + 0.5 % Molyvan. It is clearly observed that MoS_2 is

obtained for both the cases and this is in agreement with the low friction coefficients in both the cases.

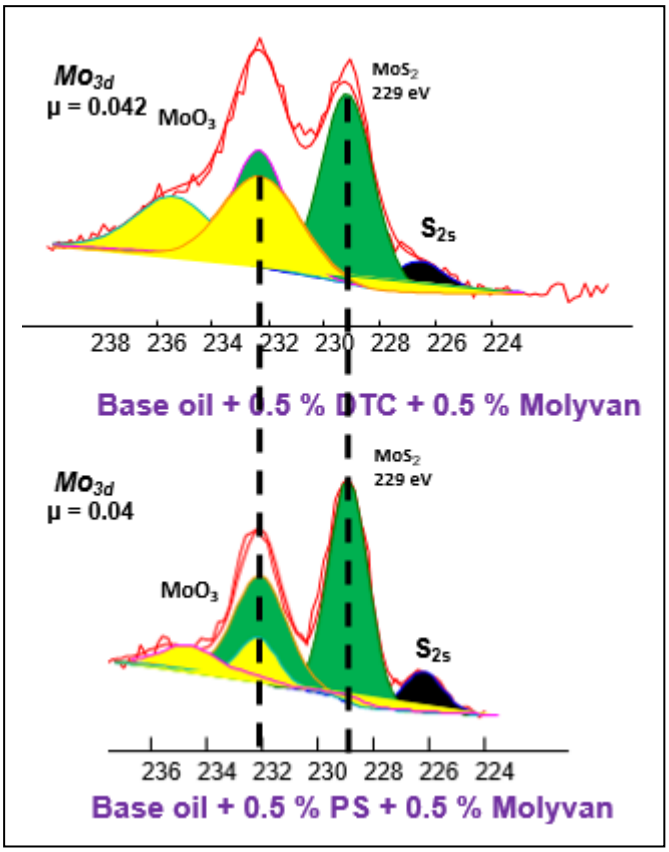

Fig.2 Mo3d high resolution XPS spectra on TiO_2 APS flats lubricated with base oil + 0.5 % DTC + 0.5 % Molyvan and base oil + 0.5 % PS + 0.5 % Molyvan.

This clearly suggests that the sources of molybdenum (Molyvan) and sulphur (PS and DTC) present in the lubricant help in formation of MoS_2 which leads to lower friction in case of steel / TiO_2 APS contact lubricated with base oil + 0.5 % PS + 0.5 % Molyvan and base oil + 0.5 % DTC + 0.5 % Molyvan. This improved friction behaviour compared to steel / reference steel could be related to the tribocatalytic behaviour of TiO_2 APS coating involved in the contact. However, there is clearly a need to further investigate tribocatalysis phenomenon for optimizing action mechanism of a wide range of lubricant additives.

Annex 1

Surface finishing processes:

Introduction

Various surface finishing processes are used to precisely remove material to get the desired shape, surface finish etc. Processes used include lapping, polishing, grinding and honing according to the desired requirements. Lapping and polishing can produce surface finishing in nanometer range compared to micrometer range finish in case of grinding and honing depending on the application.

1. **Polishing**

Polishing is the removal of material to produce a scratch free surface using (> 3 μm) abrasive particles. It is done at low speeds using polishing cloth on which the abrasive particles are suspended and can roll or slide across the cloth and the specimen [1]. Plate material and the cloth material are critical when polishing a particular sample [2]. The polishing process used in this study is manual polishing with 50 MPa pressure and four different emery papers followed by a polishing cloth with fine Al_2O_3 particles as abrasives.

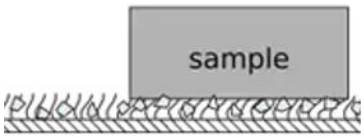

Fig.1 Schematic showing the polishing process with abrasive particles

2. **Grinding**

Grinding is defined as rapid removal of material from the sample to remove large surface irregularities. It is done either with a rigid grinding tool (wheel, disk) or an abrasive paper, backed by a rigid plate where the plate rotates at a high speed (200-1000 rpm). Coarse, bonded abrasive particles (> 40 μm) are used [2]. Generally, grinding causes deep sub surface damage in the materials [1]. The primary purpose of grinding is to remove the stock from the surface. Therefore, grinding uses fixed abrasives — the abrasive particles are bonded to the paper or platen for fast stock removal [1]. Manual grinding allows better control of grinding depth than automatic grinding, which could be important when the cross section is of extreme interest.

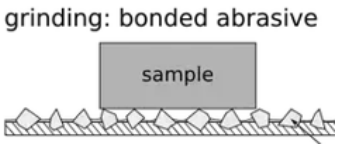

Fig.2 Schematic showing grinding process with coarse particles.

3. Lapping

Lapping is defined as removal of material to produce flat, smooth but unpolished and dimensionally accurate surface. It is done either with a hard lap (it can also be a second workpiece) or with a soft metal lap which is "charged" with the abrasive grains. Speed used in lapping for rotating the lapping plate is low (< 80 rpm) [2]. Mid-range abrasive particles (5- 20 µm) are used [1]. In this study two different sizes of abrasive particles are used – 15 micron and 6 micron. 15 min 15 micron mentioned in the report suggests that lapping is carried out using 15 micron particles for 15 minutes.

Lapping removes sub surface damage caused by sawing or grinding and produces the required thickness and flatness. Lapping is of two types – fixed abrasive and free abrasive lapping.

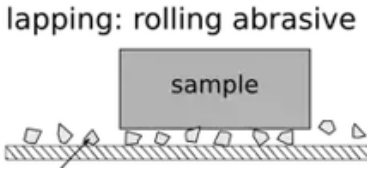

Fig.3 Schematic showing lapping process.

4. Surface and flat honing

Surface honing is defined as removal of the material by using geometrically undefined cutting edges (grain bound) that are held together in large working wheels. The workpieces are held in toothed carriers (plastic, steel) that are driven by two horizontal pin rings as shown in fig.4 below. Honing combines the high speed stock removal rates of grinding with the slower, more precise finishing of conventional lapping. It is generally done for

specific industrial purposes like cylinder liner applications. Two types generally exist including flat honing and surface honing [3]. Flat honing is carried out for flat samples like flat discs and coupons in this study and surface honing is carried out for rounded samples like cylinder liner in this study for ring-on-liner tests.

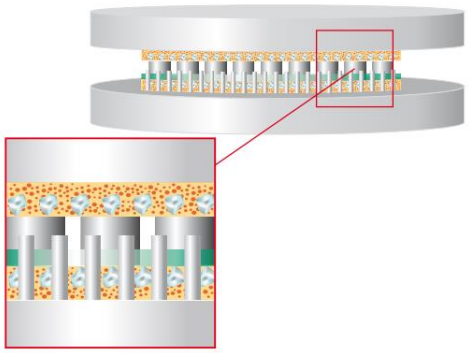

Fig.4 Schematic showing flat honing process.

References:

[1] R. and J. B. Ltd., "Grinding and polishing machine," *J. Sci. Instrum.*, vol. 34, no. 11, pp. 468–469, 2002.

[2] "Lapping and polishing machines," *Vacuum*, vol. 18, no. 8, p. 481, 1968.

[3] P. Ernst and K. Fletcher, "SUMEBore – thermally sprayed protective coatings for cylinder liner surfaces," pp. 1–12, 2011.

Annex 2

Principles for characterisation techniques

1. Interferometry

Principle:

Light is passed towards a beam splitter and then splits into two different beams: the reference and the objective beam. The reference beam is directed towards an internal reference mirror and is reflected back to the beam splitter while the objective beam is directed towards the sample being analysed and is reflected back at a different distance. Reflected light from the sample is later recombined with the reference beam and the objective beams are directed to a detector.

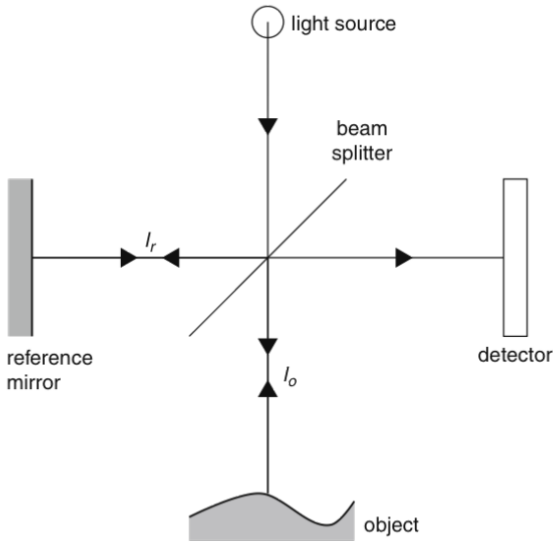

Fig. 1 Principle of an optical white light interferometer.

Interference fringes are obtained as the two beams travel different distances and they form interferometric images when they recombine. The principle is explained schematically in fig 1. The images obtained are analysed to generate different topographic information on the samples using various features available in the Vision 64 software.

2. Microindenter

Principle:

Hardness and elastic modulus are calculated from indentation load-displacement data obtained during one cycle of loading and unloading. During the test, load is applied using a pyramidal diamond indenter and increases exponentially versus time, in order to keep a constant strain rate throughout indentation.

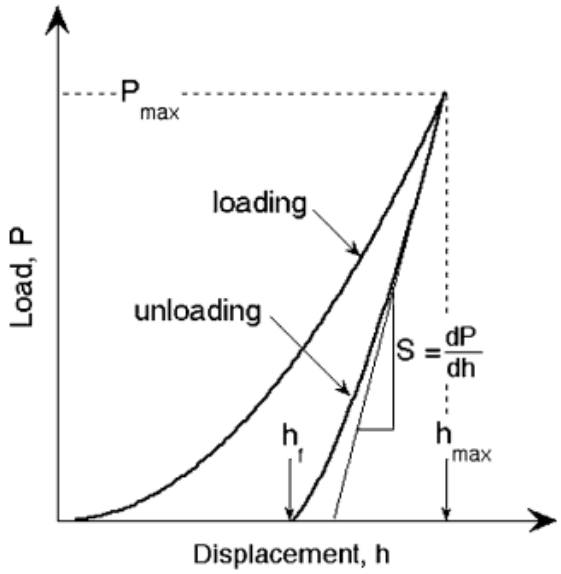

Fig. 2 Schematic illustration of indentation load-displacement data showing important measured parameters**.**

Locations of number of points on a sample can be set by setting the difference in width so as to carry out number of indentations in one go.

3. Scanning Electron Microscope

Principle

This type of microscope produces images of samples by scanning it with a focused beam of electrons. The electrons interact with the atoms in the sample and then by using separate detectors for secondary electrons and back scattered electrons, produce signals to get information about the topography as well as the composition of the surface. High voltages such as 30 kV are used to get good quality images. However, for insulating samples like ceramics and non-metals, charging effect reduces the quality of images and so low voltages or metallic coating on the top surface should be used to analyse them.

4. Raman Spectroscopy

Principle:

Intensity of inelastically scattered light from a material is measured as a function of the wavelength. Shifts in the wavelength of the scattered light occur due to interactions of the incident light with the specific vibrational modes of the material. Raman scattering occurs when a lattice vibrational mode causes a deformation in the electron cloud, thus affecting the polarizability (ability to form dipoles). The polarizability changes as the molecular bonds are altered by their vibrational motion. The principle of Raman spectroscopy is schematically explained in fig 3.

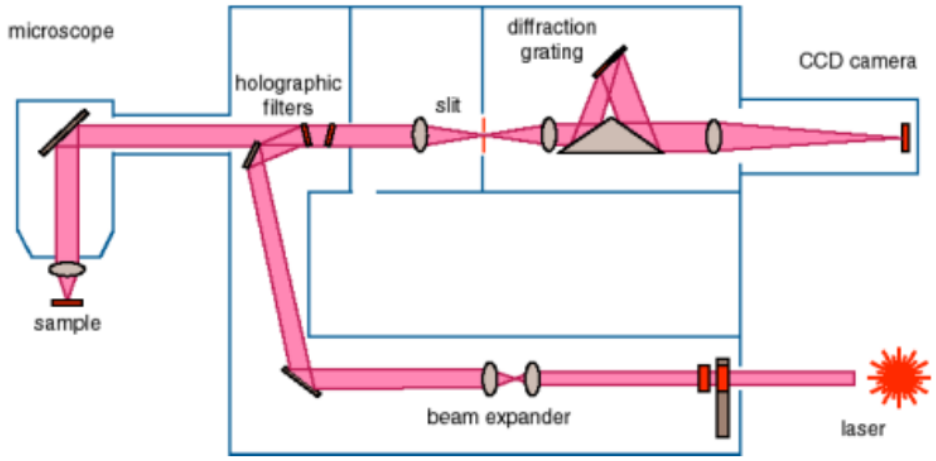

Fig. 3 Principle of Raman spectroscopy**.**

Raman equipment consists of the following: Laser sources, lenses, filters microscope, diffraction grating and a detector (CCD camera). The lenses are used to focus the light beam from the laser source to the sample. Scattered light is collected from the sample at 180° by the same lenses used to radiate the samples. The holographic filters are used to separate reflected light from the laser source and scattered light from the sample. The filters block the light reflected from the laser source and allows scattered light from the sample to pass to the diffraction grating. At the diffraction grating, the scattered light is split into different colours before being focused on the CCD camera. Objective lenses used increase the energy density of the light delivered to the sample. It is recommended to use objective lenses with high magnification as the energy density increases with magnification.

Raman spectra consists of Raman shift (cm^{-1}) on X-axis which is the difference in wavenumber between the incident light and Raman scattered light. Intensity of the scattered light is labelled on Y-axis.

5. X-ray Photoelectron Spectroscopy

Principle:

XPS is based on photoelectric effect. When a solid surface is irradiated with photons, an incident photon of energy hv is absorbed by an electron with binding energy E_b below the vacuum level; the entire photon energy is transferred to the electron which occupies a state above the vacuum level. Thus, the photoelectron is ejected in the vacuum with kinetic energy $E_{kin} = hv - E_b$. Schematic of the principle of XPS is shown in fig 2.11.

This kinetic energy of the electron can be detected by an electron energy analyser. Each element is known to have different binding energies for their different oxidation states.

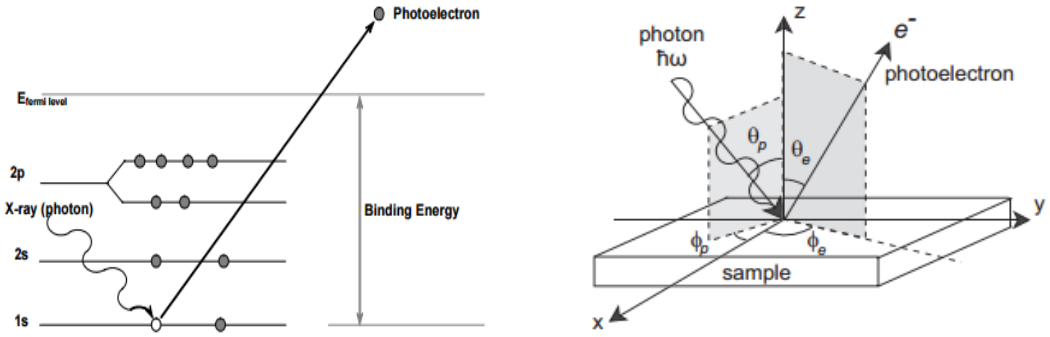

Fig.4 Schematic view of photoemission process: a photon of energy hv impinged on the surface ejects an electron in the given direction with some kinetic energy**.**

6. Transmission Electron Microscopy

Principle

A beam of electrons is transmitted through an ultra-thin specimen or less than 100 nm thickness or a suspension or a grid to form an image. The image is formed from the electron interaction with the specimen as the beam is transmitted through it. This image is then magnified and focused onto an imaging device such as a fluoroscent screen or a camera.

Annex 3

Equation for Hertzian contact pressure:

When load is applied between two bodies, they either deform plastically or elastically depending on the value of the stresses. From the Hertzian theory of contact dynamics, when the material is elastically deformed, the maximum Hertzian pressure at the centre of the contact is given by the equation 1.1

$$p_{max} = \frac{3F}{2\pi a^2} \quad \ldots\ldots\ldots\ldots\ldots\ldots (1.1)$$

Where P_{max} is the maximum Hertzian pressure, F is the applied normal load and a is the effective radius given by

$$a = \sqrt[3]{\frac{3F}{8}\frac{(1-\nu_1^2)/E_1 + (1-\nu_2^2)/E_2}{1/d_1 + 1/d_2}} \quad \ldots\ldots\ldots\ldots\ldots (1.2)$$

Where ν_1 and ν_2 are the Poisson's ratios for the solids 1 and 2, E_1 and E_2 are the elastic moduli of solids 1 and 2, d_1 and d_2 are the diameters of the solids 1 and 2 respectively.

Equation for lambda ratio:

Lambda ratio in a specific contact is given by the ratio of minimum film thickness to the effective roughness of the contact materials.

$$\Lambda = \frac{h_{min}}{(Ra_1^2 + Ra_2^2)^{1/2}}$$

Where h_{min} is the minimum lubricant film thickness, Ra_1 and Ra_2 are the average surface roughness values of the contact materials.

h_{min} for ball-on-plate contacts was calculated using the equation proposed by Hamrock and Dawson [1].

References:

[1] B. J. Hamrock and D. Dowson, "Isothermal Elastohydrodynamic Lubrication of Point Contacts: Part IV—Starvation Results," *J. Lubr. Technol.*, vol. 99, no. October, p. 15, 1976.

[2] R. Budnyas, K. Nisbett (2014) Shigley's Mechanical Engineering Design, 10th edition, Mc-Graw Hill.

ÉCOLE
CENTRALE LYON

dernière page de la thèse

AUTORISATION DE SOUTENANCE

Vu les dispositions de l'arrêté du 25 mai 2016,

Vu la demande du directeur de thèse

Madame C. MINFRAY et Monsieur F. DASSENOY

et les rapports de

M. P. MONTMITONNET
Directeur de Recherche CNRS -CEMEF Mines-ParisTech - UMR CNRS 7635
1 rue Claude Daunesse - CS 10207 - 06904 Sophia-Antipolis cedex

et de

Mme A. ROSSI
Professeure - Università degli Studi di Cagliari - Dipartimento di Scienze Chimiche e Geologiche - S.S. 554 bivio per Sestu - I-09042 Monserrato (Cagiari) - Italie

Monsieur DESHPANDE Pushkar

est autorisé à soutenir une thèse pour l'obtention du grade de **DOCTEUR**

Ecole doctorale MATERIAUX

Fait à Ecully, le 22 novembre 2017

P/Le directeur de l'E.C.L.
La directrice des Etudes

ECOLE CENTRALE DE LYON
Service Scolarité
ECULLY

M-A. GALLAND

36, avenue Guy-de-Collongue - 69134 Écully Cedex - France
T +33 (0) 4 72 18 60 00
www.ec-lyon.fr
SIRET : 196 901 870 000 10 - APE 8542Z